Using an Ecohydrology Model to Explore the Role of Biological Soil Crusts on Soil Hydrologic Conditions at the Canyonlands Research Station, Utah

by

Kristen M. Whitney

A Thesis Presented in Partial Fulfillment
of the Requirements for Degree
Master of Science

Approved July 2015 by the
Graduate Supervisory Committee:

Enrique R. Vivoni, Chair
Jack D. Farmer
Ferran Garcia-Pichel

ARIZONA STATE UNIVERSITY

August 2015

ABSTRACT

Biological soil crusts (BSCs) dominate the soil surface of drylands in the western United States and possess properties thought to influence local hydrology. Little agreement exists, however, on the effects of BSCs on runoff, infiltration, and evaporative rates. This study aims to improve the predictive capability of an ecohydrology model in order to understand how BSCs affect the storage, retention, and infiltration of water into soils characteristic of the Colorado Plateau.

A set of soil moisture measurements obtained at a climate manipulation experiment near Moab, Utah, are used for model development and testing. Over five years, different rainfall treatments over experimental plots resulted in the development of BSC cover with different properties that influence soil moisture differently. This study used numerical simulations to isolate the relative roles of different BSC properties on the hydrologic response at the plot-scale.

On-site meteorological, soil texture and vegetation property datasets are utilized as inputs into a ecohydrology model, modified to include local processes: (1) temperature-dependent precipitation partitioning, snow accumulation and melt, (2) seasonally-variable potential evapotranspiration, (3) plant species-specific transpiration factors, and (4) a new module to account for the water balance of the BSC. Soil, BSC and vegetation parameters were determined from field measurements or through model calibration to the soil moisture observations using the Shuffled Complex Evolution algorithm.

Model performance is assessed against five years of soil moisture measurements at each experimental site, representing a wide range of crust cover properties. Simulation experiments were then carried out using the calibrated ecohydrology model in which

BSC parameters were varied according to the level of development of the BSC, as represented by the BSC roughness.

These results indicate that BSCs act to both buffer against evaporative soil moisture losses by enhancing BSC moisture evaporation and significantly alter the rates of soil water infiltration by reducing moisture storage and increasing conductivity in the BSC. The simulation results for soil water infiltration, storage and retention across a wide range of meteorological events help explain the conflicting hydrologic outcomes present in the literature on BSCs. In addition, identifying how BSCs mediate infiltration and evaporation processes has implications for dryland ecosystem function in the western United States.

DEDICATION

This thesis is dedicated to my mom, Kimberly, and my dad, Ralph Jr., for their tireless support, patience, and love, and for serving as true examples of what it means to commit and work towards great and worthy goals.

ACKNOWLEDGMENTS

I would like to thank Dr. Enrique Vivoni for the opportunity to work on this research and for his patience, guidance, and motivation, and for serving as an inspiring educator, researcher, and advisor who is always available to provide guidance and support. Thanks also for the research support provided by Michael Duniway, John Bradford, Sasha C. Reed, and Jayne Belnap of the U.S. Geological Survey, Southwest Biological Science Center. Funding is acknowledged from the U.S. Geological Survey (Grant number G13AC00207). For field assistance, I would like to thank Hilda Smith and technicians at the USGS Southwest Biological Science Center in Moab, UT, as well as Gina Rivera of Arizona State University. Lastly, I would like to thank Dr. Vivoni's entire hydrology research group for all assistance throughout this research, and for their support and encouragement.

TABLE OF CONTENTS

Page

LIST OF TABLES……..ix

LIST OF FIGURES……...….xi

CHAPTER

1. INTRODUCTION……...1

1.1. Colorado Plateau: Background and Management History…….....…….....3

1.2. Biological Soil Crusts: Physiology and Recent Research…….....6

1.3. Research Motivation…….....12

2. METHODS…….....15

2.1. Site and Experiment Description…….....15

2.2. Field Measurements…….....…….....….....18

2.3. Ecohydrology Model…….....…….....24

2.3.1. Simulated Surface Moisture Budget…….....……26

2.3.2. Simulated BSC Moisture Budget…….....……36

2.3.3. Simulated Soil Moisture Budget…….....….……41

2.4. Model Calibration Testing……..…….…….....47

2.4.1. General Approach…….……..…….…….....47

2.4.2. Calibration of Soil Layer and RI Class I Parameters…….....…49

2.4.3. Calibration of RI Class II-IV Parameters ……..…54

2.5. Biological Soil Crust Layer Simulations: Experiment Descriptions…….…56

2.6. Biological Soil Crust Layer Simulations: Statistical Analyses.....……..58

3. RESULTS AND DISCUSSION……..……..61

CHAPTER Page

3.1. Model Calibrations and Parameter Line Fits……..……..…61

3.2. Experiment Simulations…….....…...70

3.2.1. Water Balance Comparison……..…..……..…..…….74

3.2.2. Statistical Analyses of Moisture Infiltration and Drying Rates.....83

3.2.2.1. Soil Moisture Infiltration and Drying Rates.....83

3.2.2.2. BSC Moisture Infiltration and Drying Rates.....89

3.3. Discussion.....94

4. CONCLUSIONS AND FUTURE WORK……..……100

4.1. Conclusions.....100

4.2. Future Work.....…….....….101

REFERENCES…….…….....104

APPENDIX

A. FIELD DATA COLLECTION…….…….....113

A.1. Field Site Map.....114

A.2. Soil Moisture Data.....117

A.3. Meteorological Data.....119

A.4. Soil Depth Measurements.....119

A.4.1. Soil Depth: Materials.....120

A.4.2. Soil Depth: Standard Procedure and Rules.....120

A.4.3. Soil Depth: Results.....120

A.5. Percent Cover Measurements.....123

A.5.1. Percent Cover: Materials.....123

APPENDIX Page

A.5.2. Percent Cover: Standard Procedures and Rules.....124

A.5.3. Percent Cover: Calculations and Results.....125

A.6. Roughness Index Measurements.....126

A.6.1. Roughness Index: Materials.....127

A.6.2. Roughness Index: Standard Procedures and Rules.....127

A.7. Leaf Area Index Measurements.....129

A.7.1. Leaf Area Index: Materials.....130

A.7.2. Leaf Area Index: Standard Procedures and Rules.....131

B. UNMANNED AERIAL VEHICLE IMAGERY……..…….....138

C. SOIL MOISTURE AND METEOROLOGICAL DATA.....141

C.1. Processing Soil Moisture Observations.....142

C.2. Processing Meteorological Observations.....143

D. ECOHYDROLOGY MODEL SCRIPTS.....146

D.1. Verification Figures.....147

D.2. Comparison Metrics.....153

D.2.1. Observations vs. Discrete BSC Parameters.....154

D.2.2. Observations vs. Continuous BSC Parameters.....155

D.2.3. Discrete BSC Parameters vs. Continuous BSC Parameters.....156

D.3. Simulated Experiments.....157

D.4. Fitting Lines to Calibrated Parameters.....160

D.5. Visualizing Observation Time Series.....161

APPENDIX Page

E. CALIBRATION PROCEDURES AND RESULTS.....163

E.1. Shuffled Complex Evolution Alogorithm.....164

E.2. General Calibration Procedure.....166

E.3. Soil and BSC RI Class I – Dry Parameter Calibration.....171

E.4. Soil and BSC RI Class I – Wet Parameter Calibration.....174

E.5. BSC RI Class IV – Wet Parameter Calibration.....180

E.6. BSC RI Class IV – Dry Parameter Calibration.....181

E.7. BSC RI Class III – Wet Parameter Calibration.....182

E.8. BSC RI Class III – Dry Parameter Calibration.....183

E.9. BSC RI Class II – Wet Parameter Calibration.....184

E.10. BSC RI Class II – Dry Parameter Calibration.....186

F. MOISTURE INPUT RATE PER STORM AND RESIDENCE TIME SCRIPTS.....188

F.1. Model Metric Analysis.....189

F.2. Observation Metrics and Analayis.....191

G. MOISTURE BALANCE AND EVAPORATIVE DEMAND PARTITIONING 193

G.1. Surface Moisture Balance Inputs and Partitioning.....194

G.2. BSC Moisture Balance Inputs and Partitioning.....199

G.3. Soil Moisture Balance Inputs and Partitioning.....204

G.4. Total Evaporative Demand and Partitioning.....209

H. THESIS FIGURES……..…….....215

LIST OF TABLES

Table Page

1. Field Measurement Results Including Soil Texture, Roughness Index, and Percent Cover Over All Quads…….....….....……..22
2. Summary of Calibrated Parameter Subsets for Each Parameter Group and Corresponding Calibration Time Period …….....…..50
3. Summary of Value and Range Utilized for Parameter Space Limits during Calibration of Each RI Class I Parameter…….....……52
4. Summary of Value and Range Utilized for Parameter Space Limits during Calibration of Each RI Class IV Parameter…….....…55
5. Summary of Final Calibrated Parameter Values for Soil and BSC Classes.....62
6. Summary of R^2 values for Equation Fits to BSC Parameters….....…..64
7. Summary of Comparison Metrics Used to Verify Fit of Model….....…….....66
8. Summary of Results of Assumptions Tests for Statistical Analyses of Soil Infiltration and Drying Rates for Each Experiment Dataset…….....86
9. Summary of Results of Assumptions Tests for Statistical Analyses of Soil Infiltration and Drying Rates for Each RI Class Dataset…….....…..86
10. Summary of Results from Multi-Way Comparisons for Significance Between Soil Infiltration and Drying Rates for Each Experiment Dataset…….....87
11. Summary of Results from Multi-Way Comparisons for Significance Between Soil Infiltration and Drying Rates for Each RI Class Dataset…….....…..88
12. Summary of Results of Assumptions Tests for Statistical Analyses of BSC Infiltration and Drying Rates for Each Experiment Dataset…….....91

Table Page

13. Summary of Results of Assumptions Tests for Statistical Analyses of BSC Infiltration and Drying Rates for Each RI Class Dataset…….....…..91

14. Summary of Results from Multi-Way Comparisons for Significance Between BSC Infiltration and Drying Rates for Each Experiment Dataset…….....92

15. Summary of Results from Multi-Way Comparisons for Significance Between BSC Infiltration and Drying Rates for Each RI Class Dataset……...…..93

LIST OF FIGURES

Figure Page

1. Photograph Showing Biological Soil Crust Cover.....2
2. Map of Colorado Plateau Province from Foos (1999).....4
3. Cartoon Block of a Biological Soil Crust Surface and Subsurface Layer with Common Colonizers from Belnap *et al.* (2001).....7
4. Microscopic Subsurface View of Cyanobacteria Exopolysaccharide Filament Wrapped Around Soil Particle from Belnap (2006).....7
5. Field Site Location, Photographs, and Google Earth© Aerial Image.....16
6. Profile Diagram of the Soil Moisture Sensors and the Relative Sensed Depth Ranges Used for the Depth-Weighting Calculation.....20
7. Time Series of Field Site Meteorological and Soil Moisture Observations.....20
8. Photographs Taken during Field Measurements.....21
9. Plot of All Roughness Index (RI) Measurements, Color-Coded According to RI Class.....25
10. Conceptual Schematic of Modeled System with Lines Showing Modeled Interactions.....25
11. Modeled Cartoon Showing Precipitation Partitioning, and Surface, Soil, and BSC Layer Moisture Balance.....27
12. Conceptual Plot of BSC Losses Verses Relative BSC Moisture.....41
13. Conceptual Plot of Soil Losses Verses Relative Soil Moisture.....43
14. Example Storm Event and Drying Period Used for Estimation Change in Relative Moisture and Residence Time.....60

Figure Page

15. BSC Parameters as a Function of Increasing Roughness Index Using Equations Fit to DOE Calibrated Parameters....63

16. Time Series and Frequency Diagram of Modeled Verses Observed Soil Moisture during the Entire Study Period for Two Quads Using Discrete Calibrated Parameter Sets....67

17. Time Series of Modeled Verses Observed Soil Moisture during the Entire Study Period for Two Quads Using Parameters Estimated as a Function of Roughness Index....69

18. Altered BSC Parameter Values Used For Each Experiment....72

19. Temporal Average of Relative Moisture Across Simulation Plots for Each Simulation Experiment....75

20. Water Partitioning in the BSC Layer Across Simulation Plots for Each Simulation Experiment....76

21. Water Partitioning in the Soil Layer Across Simulation Plots for Each Simulation Experiment....79

22. Total Potential Evapotranspiration Demand Partitioning Across Simulation Plots for Each Simulation....80

23. Temporal Standard Deviation of Relative Moisture Across Simulation Plots for Each Simulation Experiment....82

24. Average Relative Soil Moisture Change Per Storm and Residence Time for Each Roughness Index Class for All Experiments....85

Figure Page

25. Average Relative BSC Moisture Change Per Storm and Residence Time for Each Roughness Index Class for All Experiments.....90

1 INTRODUCTION

In the 21st century, the arid Southwest U.S. has experienced intense, widespread, and prolonged drought with precipitation averaging up to 22-40% below the 20th century annual mean (data from NDMC and NOAA via MacDonald 2010). These periods have been exacerbated by high temperatures, with increases in average annual temperatures up to 0.8°C warmer than the 20th century mean (data from NDMC and NOAA via MacDonald 2010). Despite such intense aridity, for centuries humans have migrated into the region afforded by the high-appropriation of water resources irrigated from the Colorado River Basin (CRB) within the Colorado Plateau (Woodhouse *et al*. 2006). Models project future climate scenarios for this region with even higher temperatures and possibly more frequent and intense drought and flood events (Seager *et al*. 2007). Combined with the increase in freshwater demands associated with projected population growth, climate change could have major consequences on society's ability to secure and maintain adequate amounts of quality water supplies in the already water-stressed, arid region (Garfin *et al*. 2013; Graf *et al*. 2010).

Utilizing accurate ecohydrology models that account for all factors affecting the partitioning of precipitation and evapotranspiration will prove key to sustainable management of these limited resources under such exacerbated conditions within the region. It is well recognized that many soil factors influence local hydrologic regimes including soil texture, degree of soil aggregation, structure, vegetation cover, and physical crusting. More recently, scientists have attempted to understand how the presence of biological soil crusts (BSCs), or communities of cyanobacteria, lichens, and mosses, influence local hydrologic regimes (Figure 1; reviewed in Belnap 2006). By

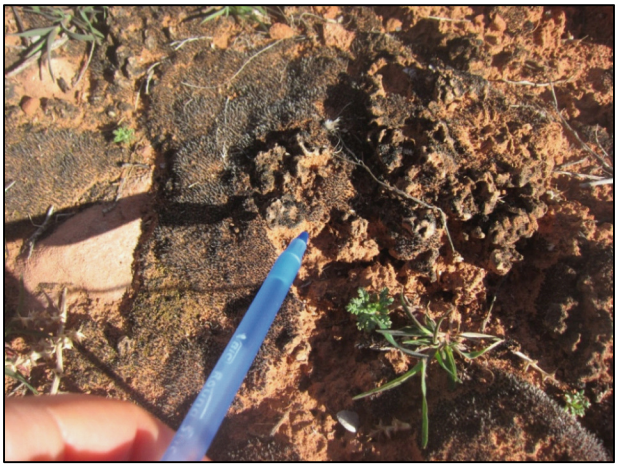

Figure 1: Photograph showing biological soil crust (BSC) cover.

connecting soil particles together, these organisms and their associated extracellular polysaccharide (EPS) materials create coherent living crusts that are abundant on the surface of the world's dryland regions (Belnap *et al.* 2001; Belnap 1995). Developed BSC layers have microstructural properties unique from the underlying soil layers that could influence the local hydrologic cycle, including a unique porosity, hydrophobicity and absorptivity, and other textural properties, as well as added surface roughness, and aggregate stability (Felde *et al*. 2014; Rossi *et. al.* 2012; Lichner *et al*. 2013; Rodriguez-Caballero *et al*. 2012; Verrecchia *et al*. 1995; Eldridge and Greene 1994). Recent investigations into the potential role of BSCs in mediating infiltration and evaporation processes have yielded apparently contradictory, site-specific conclusions, and are therefore, difficult to translate to larger scales for regional resource management (reviewed in Belnap 2006). In response, this study aims to explore the competing processes potentially underlying these paradoxical conclusions through use of an ecohydrology model modified for use with areas affected by BSCs and climate regimes with both snow and precipitation. After calibrating the model to site-specific field conditions, a simulation experiment is utilized to understand how the relative rates of

infiltration and evaporation could change given alternative field site conditions. Through these efforts, this study aims to improve predicative capabilities of ecohydrology models with results that are translatable to larger modeling scales applicable for water resource management.

1.1 Colorado Plateau: Background and management history

The Colorado (CO) Plateau encompasses 340,000 km^2 of land centered on the Four Corners Intermountain region of the United States (southeast Utah, southwest Colorado, northwest New Mexico, and northeast Arizona; Figure 2) where large pre-Cenozoic aged sandstone rocks have been uplifted into a broad series of plateaus, and subsequently weathered and eroded to form steep canyon landscapes (Powell *et al*. 2002; Nicholas and Dixon 1986; Howard and Kochel 1988; Thornbury 1965). The dominant canyons of this region compose a large portion of the Colorado River Basin (CRB; Figure 1; Thornbury 1965).

The Colorado Plateau experiences strong seasonal temperature contrasts, with mean annual temperatures ranging between 4 to 17^{o}C (Bailey 1994). Due to the presence of the high-elevations of the Sierra Nevada to the west and the resulting rain shadow effect, the plateau is one of the driest regions in the country with low annual precipitation, averaging between 130-250 mm/yr (Dixon 2010; Hereford *et al*. 2002). Tree ring studies suggest that throughout history, the region has experience highly variable drought and non-drought conditions (reviewed in Schwinning *et al*. 2008). Despite these highly variable and arid conditions, the CRB has been a water source for

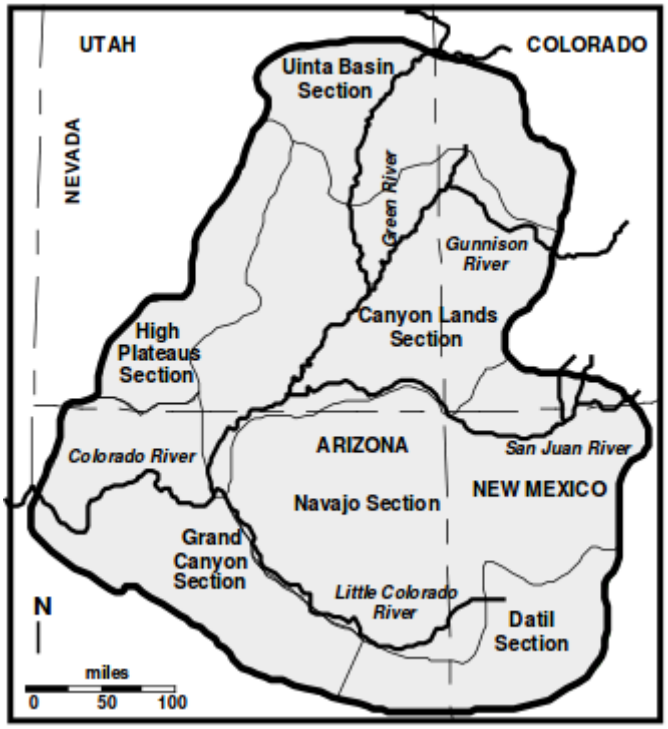

Figure 2: Map of Colorado Plateau province showing major drainages of Upper Colorado River Basin; image sourced from Foos (1999).

human populations since 800 A.D. due to progressive improvements in irrigation techonologies and storage capacities (reviewed in Schwinning *et al*. 2008).

The first humans to migrate to and settle within the CO plateau were the Ancestral Pueblo People around 800 AD (Petersen 1994). During this time, the Medieval Warm Period (800-1300 AD) extended the growing season and increased precipitation, allowing the Pueblo People to introduce dry farming to the region (Axtell *et al*. 2002). Records indicate the abrupt disappearance of the Pueblan society in 1253 AD, coinciding with the final peak in several megadroughts occurring at the tail end of this warm period (Petersen 1994; Cook *et al*. 2007). A small ice age soon followed and ended in the 1800s, ushering in the first Anglo human settlers, as well as, their sheep, cattle, dry farming, and ore mining practices (Petersen 1994; Cook *et al*. 2007).

The period from 1905 to 1922 was an unusually and persistently wet period for the plateau, resulting in the highest long-term annual Colorado River discharges recorded in the 20th century (U.S.G.S. 2004). These flow volumes served as the basis for estimating water production for the 1922 Colorado River Compact, an agreement among seven states surrounding and nearby the basin that serves as the foundation for the numerous compacts and laws governing the allocation of water rights collectively known as the "Law of the River" (U.S.G.S. 2004). These exceptionally high estimates of "normal" flow volumes resulted in unsustainably high river allocations (Woodhouse *et al*. 2006). This combined with external government subsidies during drought years (e.g. financial support for fencing, water developments, roads, and animal feed), improved irrigation technologies, and climate-independent industries (e.g. service and tourist sectors) encouraged more to settle and maintain constant and high cattle numbers on the plateau, despite extended drought periods within the last century (reviewed in Schwinning *et al.* 2008). As a result, a large majority of the plateau is used by the ranching industry today, and the CRB supplies water to nearly 40 million people across the four corner states, as well as California, Wyoming, and Mexico (Schwinning *et al.* 2008; Bureau of Reclamation 2012).

These ranching activities have caused extensive disturbances to soils and their sensitive BSC communities, and which has in turn been linked to widespread negative impacts to ecosystem resource reserves used for drought recovery (Neff et al. 2005; Evans and Belnap 1999; Belnap and Eldridge 2001; Le Houérou 1984; reviewed in Belnap 2001a). The reduced health of the ecosystem can in turn have negative impacts to certain provisioning and regulating services that benefit the quality and quantity of

human water resources (reviewed in Brauman *et al*. 2007). In the water limited arid and semiarid regions, sustainable water resource management in the face of forecasted extreme climates will thus depend upon having a thorough understanding of how the development of BSCs produces modifications to the hydrologic processes affecting water resources for human and ecosystem use.

1.2 Biological Soil Crusts: Physiology and Recent Research

Due to their low moisture requirements, and extreme temperature and light tolerances, biological soil crusts (BSCs) can exist in a wide variety of environments and are especially dominant in low-productivity, dryland regions (Büdel 2001; Belnap *et al.* 2001). The composition and micro-topography of a given BSC depends upon their inhabited climate, soil type, and disturbance history but generally include various cyanobacteria, lichen, and moss species (Figure 3; reviewed in Belnap 2006). Studies of BSC growth following disturbance have found that development occurs in a sequence of characteristics all indicative of the level of development (LOD; Belnap *et al,* 2008; Belnap and Eldridge 2001). These characteristics include an increase in successional species types, increased percent species cover, biomass, species diversity, and color (Belnap *et al,* 2008; Belnap and Eldridge 2001). Generally, cyanobacteria first colonize and weave a network of exopolysaccharide (EPS) filaments through the top few centimeters (reviewed in Belnap 2006). These filaments wrap around soil particles and secrete binding agents as a metabolism byproduct, forming dense cemented horizons of soil aggregates in the sub-surface (Figure 4; reviewed in Belnap and Eldridge 2001). In

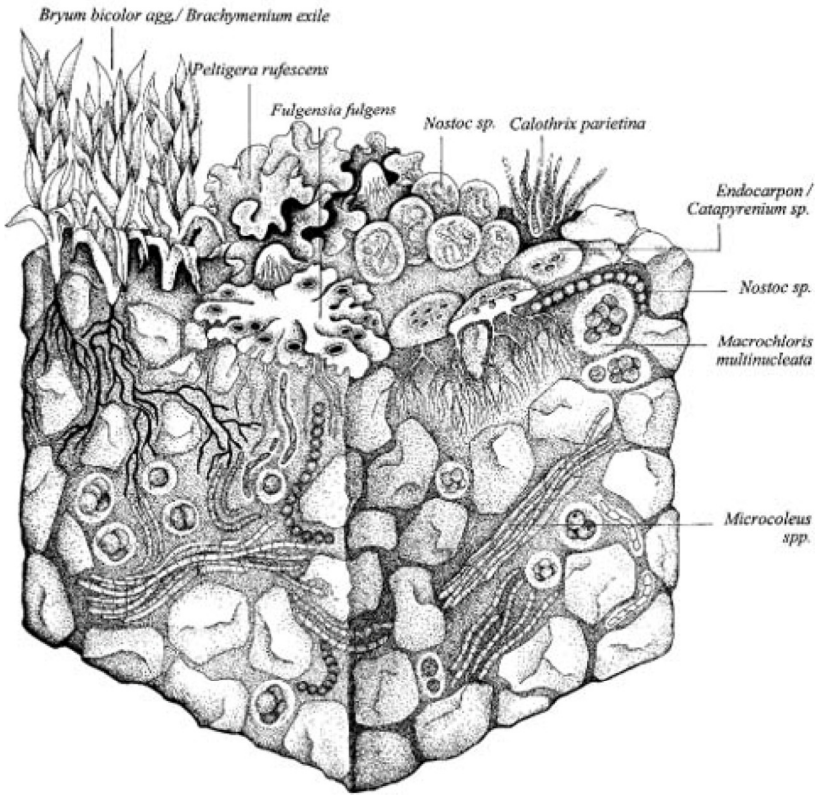

Figure 3: Cartoon block of a biological soil crust surface and subsurface layer with common colonizers; thickness of the layer about 3mm; organisms not drawn to scale; Illustration renate: Klein-Rüdder; image sourced from Belnap *et al.* (2001).

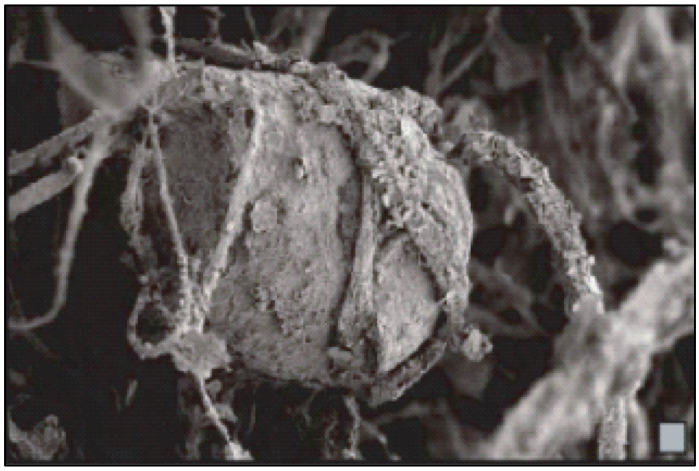

Figure 4: Microscopic subsurface view of cyanobacteria exopolysaccharide filament wrapped around soil particle. Scale bar is 10µm. Imaged sourced from Belnap (2006).

cooler climates, lichens and mosses and their associated anchoring structures (e.g. stems, rhizoids, and rhizines) can develop on and within the surface of undisturbed BSC areas (reviewed in Belnap 2006). These later successional species darken the surface color, adding UV protection, and also increase the nutrient fixation in the subsurface (Bowker *et al*. 2002; reviewed in Barger *et al.* 2003; Belnap *et al*. 2003; reviewed in Belnap 2001a). Together these cyanobacteria soil aggregates and lichen-moss anchoring structures increase soil stability and protect against erosion (reviewed in Belnap 2001c; reviewed in Warren 2001a).

BSCs within the lower-elevations of the Colorado Plateau and other mid-latitude, cool desert regions of the world (e.g. mid-latitude China deserts, high-elevation Sonoran and Mojave deserts) are generally dominated by cyanobacteria (reviewed in Rosentreter and Belnap 2001). Within these elevations, seasonal temperature variations can induce freeze-thaw processes that cause soil uplift and the formation of pedicelled mounds up to 15 cm high, with thin tips 4-10 mm across (reviewed in Belnap 2001b). In higher elevations where temperatures are colder and potential evapotranspiration is lower, lichens and mosses heavily dominate the species composition of BSCs, and form thick, cohesive mats that counteract frost heaving and provide surface armoring against erosion (reviewed in Belnap 2001b).

In all elevations of the Colorado Plateau, surface roughness can increase significantly with BSC development resulting from both the frost-heaving processes affecting cyanobacteria-dominated surfaces and the increase in surface biomass associated with lichen-moss dominated BSCs (reviewed in Belnap 2001b). The added roughness has been shown to significantly decrease runoff and wind velocities, thereby

increasing nutrient capture and dust entrapment (Barger *et al.* 2006; Danin and Gaynor 1991). As dust is added to the surface, algae migrate upwards to meet the depth of light penetration, and form new soil aggregates on top of the deeper abandoned cemented horizons, thickening the BSC sub-surface (Belnap and Gardner 1993; Tchan and Whitehouse 1953; Garcia-Pichel and Pringault 2001; Hu *et al*. 2002; Felde *et al.* 2014). Comparisons of the organic and inorganic matter content within BSC samples further indicates that much of the entrapped fine particles are incorporated into the soil aggregates bound below the surface (Hu *et al*. 2002). Studies indicate that the increases in fine particles and their associated textures can affect the microstructure of BSC by increasing the water holding capacity and adding to the pore size distribution of BSC layers (Verrecchia *et al.* 1995; Menon *et al.* 2011; Felde *et al*. 2014).

The impacts of biological soil crusts on infiltration capacity have been studied in a wide range of environments with different precipitation regimes and BSC species type compositions. Studies indicate that certain hydraulic properties defining the infiltration capacity of a soil system are altered with the development of BSCs. For instance, the sheaths surrounding cyanobacteria EPS filaments can absorb moisture, swelling up to 12 times their dry weight and increase their volume up to 10 times, thus further increasing the retention capacity of BSC layers (Wang *et al.* 1981; Campbell 1979; Verrecchia *et al.* 1995; Yair 2001). Studies examining the microporosity of developed BSC samples indicate that the swollen EPS filaments reach a diameter sufficient in size to fill the void space of between particle spheres and can thus, “clog pores”, or decrease the effective pore space available for water storage and movement (Verrecchia *et al.* 1995; Menon *et al.* 2011).

Field and laboratory studies suggest that this "pore clogging" can potentially increase runoff generation by either creating hydrophobic surface conditions or decreasing the subsurface saturation capacities, depending upon the climate and given antecedent moisture conditions (Verrecchia *et al*. 1995; Rutin 1983; Yair 1990; Lange *et al*. 1992; Kidron 1995; Kidron and Yair 1997; Kidron *et al.* 1999). For example, rainfall simulation experiments conducted in humid conditions where the soils remain wet for long periods of time observed that water repulsion increased across more developed cyanobacteria-dominated surfaces and attributed this apparent hydrophobicity to the high-density of pre-swollen EPS filaments (Verrecchia *et al*. 1995; Rutin 1983; Yair 1990). Similar experiments, but under hot desert ecosystem conditions, concluded that runoff generation increased along more developed BSC surfaces due to enhanced rates of sub-surface saturation and excess (Yair 1990; Lange *et al.* 1992; Kidron 1995; Kidron and Yair 1997). For example, Kidron and Kidron (1997) found that thicker more developed BSC layers could absorb lower intensity rains, whereas the thinner, less developed layers saturated must faster, producing runoff.

These experiments were conducted in warmer desert regions where cyanobacteria tend to dominate and surfaces remain smoother in the absence of strong seasonal frost-heaving (reviewed in Barger *et al*. 2006). Other rainfall simulations conducted over highly roughened BSC surfaces, however, indicate that infiltration rates can increase due to decreased velocity and increased ponding (Warren 2001; Belnap et. al. 2005). Similarly, recent micro-tomography studies examining the microstructure of BSC samples have suggested that infiltration rates can increase with the development of lichen-moss species and their associated anchoring structures (Felde et al. 2014).

Simulated velocities through the measured microstructures suggest infiltration rates are lower within the least developed samples due to the presence of a pre-existing vesicular horizon, or a disconnected pore system created by abiotic processes when gas bubbles are trapped by moisture wetting fronts (Felde et. al 2014). Increased infiltration rates simulated through the most developed samples were attributed to increased channelization, or increased pore connectivity, along shrinkage cracks and macro-pore channels connected along the stems and rhizoids of bryophytes and rhizines of lichens (Felde *et al*. 2014).

The studies of how BSC development alters drying rates are fewer and yield contrasting conclusions based on evidence from relative BSC moisture levels. In their review of these studies, Belnap (2006) suggests that observed increased drying rates could be due to increases in the evaporative demands associated with the increased soil temperatures under the darker cover of developed surfaces (Harper and Marble 1988; Belnap *et al*. 2008). Contrasting these conclusions, other studies have observed that the presence of BSCs buffered fluctuations in soil moisture more efficiently than bare soil, and that BSCs act to preserve moisture in the subsurface by increasing water flux resistance (Veluci *et al.* 2006; Verrecchia *et al.* 1995; Booth 1941; Rushforth and Brotherson 1982; George *et al*. 2003; Belnap 2006). Some of these studies have concluded that the pore clogging of more developed BSCs can add to this buffer effect by sealing the surface against moisture-loss (Verreccia *et al.* 1995; George *et al.* 2003). In the absence of direct precipitation, other studies have attributed observed moisture increases below BSC-encrusted surfaces to vapor condensation via direct atmospheric

capture or dew rise from lower sub-surface layers (Jacobs *et al.* 2000; Agam and Berliner 2004).

Furthermore, studies indicate that different BSC species dominate hot and cold deserts due to differential temperature tolerances, and predicted climate change scenarios will likely shift these dominance patterns (Garcia-Pichel *et al*. 2013). However, the consequences of such shifts are unknown and more studies are needed that address both cold and warm season components in assessing the influence of BSCs on soil moisture dynamics (Garcia-Pichel *et al*. 2013).

1.3 Research Motivation

Thus, the effect of BSCs on soil infiltration and loss rates is not uniform with development within and across environments. Infiltration capacities and the potential for runoff generation appears influenced by two competing effects: (1) the enhanced percentages of subsurface filaments serving to clog pores and (2) the increase in subsurface anchoring structures than can potentially induce channelization and increased connectivity of pores. Soil drying rates may be increased by an increased evaporative demand due to surface darkening of more developed surfaces. These underlying soil layers could potentially be buffered from experiencing evaporation by the added BSC biomass at the surface. Furthermore, moisture replenishment by adsorption and dew rise can occur between precipitation events, further complicating soil drying rates.

One approach for studying soil moisture dynamics in arid and semiarid regions is through the application of numerical models (Laio *et al.* 2001, Vivoni *et al.* 2010, Pierini *et al.* 2014). For this purpose, ecohydrology models have been shown to capture the

essential physical interactions between climate, soil and vegetation under natural or irrigated conditions (e.g., Porporato *et al*. 2001, Volo *et al*. 2014). Prior studies that utilize a point-scale model by Laio *et al*. (2001) have explored these soil moisture dynamics in hot desert climates, utilizing long-term soil moisture and meteorological datasets for calibration and validation (e.g. Volo *et al.*2014). To date, however, this model does not consider the effects of either snowmelt or BSC cover on soil moisture. Furthermore, while these and many similar ecohydrology studies use physically-based models, comparatively few have coupled empirical and modeling approaches, and even fewer have included manipulative experimental designs (King and Caylor 2011). This combined approach is important for building more robust ecohydrological models based on experimental studies, which directly discriminate between hypotheses of underlying system functions, rather than traditional models based on functions indirectly predicted from state variable observations (King and Caylor 2011).

This work takes advantage of a manipulative experiment conducted in the Colorado Plateau, near Moab, Utah, within a site of naturally-abundant BSCs adapted to cold winters and warm summer conditions. This investigation consisted of a five-year factorial warming and supplemental rainfall experiment conducted by US Geological Survey and referred to as the Department of Energy (DOE) experiment. Aimed at assessing the effects of climate change on dryland ecosystems, summer monsoon rainfall events were enhanced with additional irrigation at varying frequencies and volumes across the DOE experimental plots (Reed *et al.* 2012; Wertin *et al.* 2015). Soil moisture and temperature was monitored hourly at each of the twenty-five DOE plots containing paired control and treatment areas. Experimental manipulations caused differential

damage to BSCs in the plots, and thus, allow for comparisons of plot soil moisture measurements along a landscape mosaic of BSC cover (Reed *et al.* 2012).

Previously published measurements and interpretations of BSC microstructural properties and proportional changes occurring within developing BSC subsurface layers are used to modify the ecohydrology model with processes related to BSCs and snowmelt, and to inform the calibration procedure (Felde *et al.* 2014; Verrecchia *et al.* 1995; Menon *et al.* 2011; DeWalle and Rango 2008). After calibrating the model to soil moisture observations at the experimental site, a series of BSC infiltration and evaporation scenarios are conducted and analyzed in terms of soil moisture dynamics and water balance partitioning. Further simulation experiments are conducted under alternative conditions to explore the isolated effects of potential increases in pore clogging and channelization on moisture infiltration rates, and subsurface storage and retention capacities.

Based on the above, this study aims to provide a more complete understanding of the soil water balance under the influence of BSCs in climates of rainfall and snow precipitation through the use of datasets from the DOE experiment.

2 METHODS

A quantitative model of soil moisture dynamics was modified to include a BSC layer and calibrated to soil moisture data from an experimental site under a spectrum of BSC cover at various stages of development, with data from an on-site meteorological station as model forcing. To capture the effects of the given climate, the model was also modified to include precipitation partitioning, and snowmelt simulation. This chapter discusses the site, the field observations, the model, and method of calibration, then describes a series of simulations conducted to test the effects of a developing BSC on water balance partitioning under the site hydraulic conditions, and then under altered conditions to explore any potentially competing effects to the moisture fluxes.

2.1 Site and Experiment Description

The DOE experiment is located in southeast Utah, 30 km northwest of Moab (Figure 5), on a 300 m long, 50 m wide plateau at 1330 m in elevation. Mean daily temperatures ranges from 4 to 22 ^{o}C, while the long-term mean annual rainfall and snowfall is 230 and 250 mm (data collected by the NWS Cooperative Network; Western Regional Climate Center 2009). Soils across this plateau are classified as sandy-loam. The area is moderately vegetated (~60%) with C_3 and C_4 grasses and shrubs, dominated by *Achnatherum hymenoides* (indian ricegrass), *Pleuraphis jamesii* (galleta grass), and *Atriplex confertifolia* (saltbrush), and *Bromus tectorum* (cheatgrass). Vascular plant interspaces contain BSCs populated with varying amounts of cyanobacteria (*Microcoleus vaginatus*, *Nostoc commune*, and *Scytonema hyalinum*), lichen (*Collema tenax* and *C.*

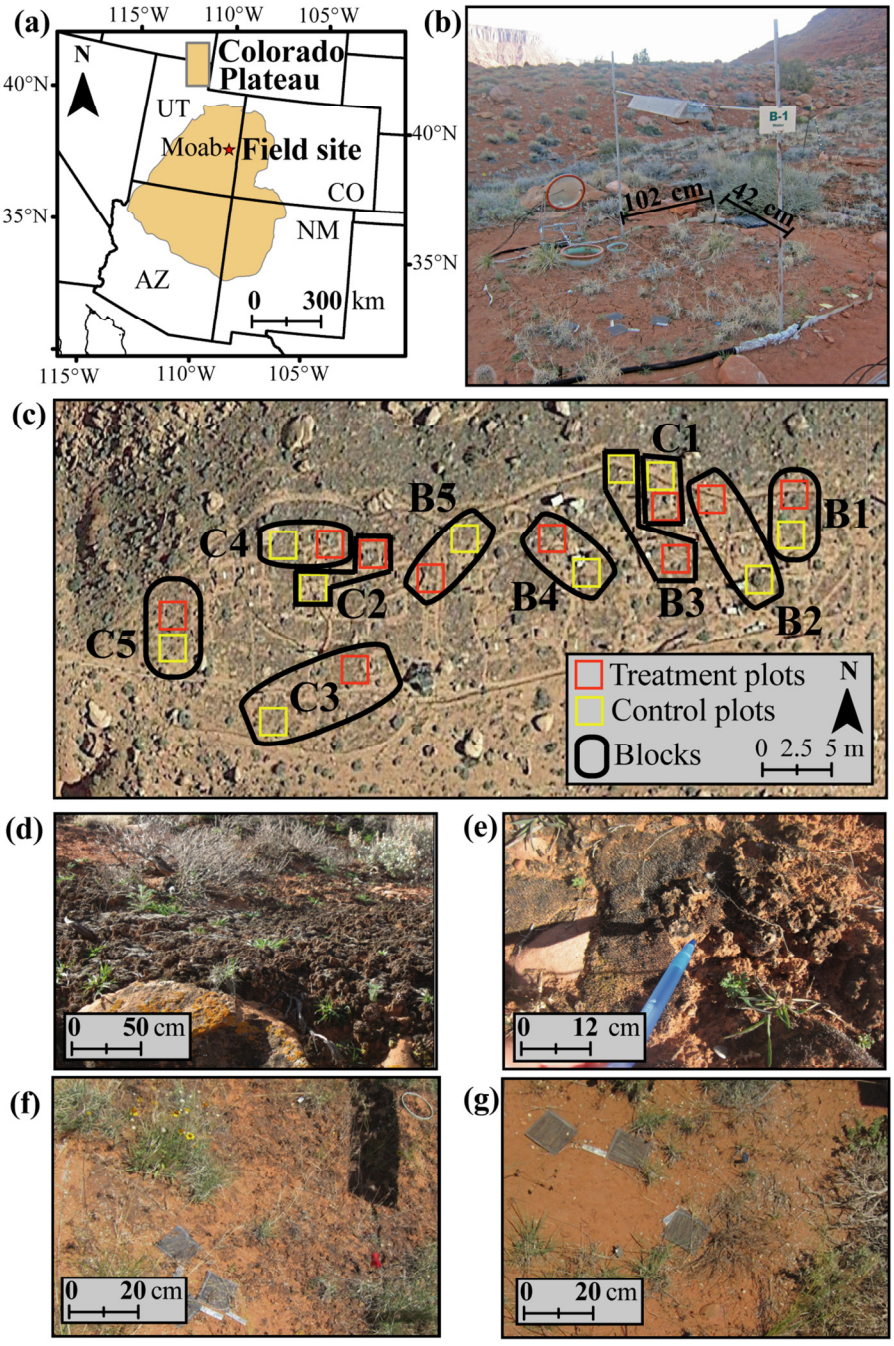

Figure 5: (a) Location of the DOE experiment with respect to the Colorado Plateau. (b) Photograph of treatment plot at block B1 showing approximate scale bars of w-treatment quad dimensions. (c) Google Earth© aerial image showing the approximate plot and block locations. Images of cyanobacteria- (d) and moss-lichen- (e) dominated BSCs at DOE site. Images of example control quad (C3-c) with intact BSCs (f) and w-treated quad (B3-w) with damaged BSCs (g).

coccophorum), and moss (*Syntrichia caninervis*) species. These BSC surfaces contain variable levels of roughness, depending upon the level of development (LOD) and freeze-thaw action (Belnap 2006).

The site has a total of 10 blocks, or 10 pairs of 5x5 m fenced plot areas, each split into four quadrants (quads) for various treatments (Figure 5). Half of these blocks (B1 through B5), were established in 2004, each with one control plot (c treatment) and one treatment plot. During summer seasons, 1.2 mm depth of water was applied twice weekly (w treatments) to the southeast quad of the B blocks. In 2008, 5 new blocks (C1 through C5) were established each with control and treatment plots. A higher-volume water treatment (x treatment) was applied once a week in summer months to the northwest quads of all B- and C-block treatment plots, which increased the precipitation amount over these quads to the 30 year summer average. Across the field site, there are therefore a total of 10 control quads (1 for each of the control plots of all 10 blocks), 5 w treatment quads (1 for each treatment plot of the 5 B type blocks), and 10 x treatment quads (1 for all treatment plots of all 10 blocks), and thus, a grand total of 25 quads used in this study.

Both treatments continued until 2013, except for a 1 year break from irrigation in 2012. Throughout this time-period, a widespread mortality of BSC populations was noted over w treated quads and relatively intact BSCs over c- and x- treated areas (Reed *et al.* 2012; Figure 5). Laboratory measurements indicate that the small, frequent w treatments caused a negative mass carbon balance in mosses that decreased the biomass of these hard-to-recover BSC species, and thus, enhanced long-lasting contrasts in BSC cover across the DOE quads (Reed *et al.* 2012).

2.2 Field Measurements

At the time of block establishment, three water content reflectometers (CS-616, Campbell Sci.) were installed at 2 cm depths under all c and w quads to measure volumetric water content θ [L^3 L^{-3}] using time domain reflectometry. Six additional soil moisture sensors (EC-5, Decagon Devices) were installed at both 5 and 10 cm depths under all treatments (c, w and x quads) to measure θ using the capacitance technique. All devices were calibrated using field-site soil samples and manual stock equations. Together, these sensors recorded triple-replicated profiles (either 5 and 10 cm, or 2, 5, and 10 cm depths) of hourly θ below all quads throughout the experiment period. A meteorological station was also installed at the site to measure hourly air temperature $T_{a,h}$ [^{o}C], total precipitation $P_{T,h}$ [L], relative humidity RH [%] among other variables. The daily average of $T_{a,h}$ (T_a in [^{o}C]) and $P_{T,h}$ (P_T in [L]) were estimated to match the timestep of the ecohydrology model. Hamon's (1963; via Dingman 2002) temperature-based approach was used to estimate PET as a function of the day length D_d [T] of the given Julian day, the saturated vapor pressure e_s [kPa], and the air temperature ($T_{a,h}$):

$$e_s = 0.6108e^{\left(\frac{17.27T_{a,h}}{23.73+T_{a,h}}\right)} \quad (1)$$

$$PET = 29.8VD\frac{e_s}{T_a + 273.2} \quad (2)$$

This study utilizes datasets taken from 2008 to 2013, after w treatments had caused disturbances to BSC cover, and thereby, established a BSC mosaic across the field site. In order to smooth out any residual variations from individual moisture sensors, a spatial average was taken of the three replicate θ measurements at each probe depth (i.e.

2, 5, or10 cm) for each hour. The daily average of θ was then taken to aggregate at the time step of the model (θ_{daily} in [L^3 L^{-3}]). Finally, the depth-weighted average of θ_{daily} was calculated across all probe depths of a given profile for a given day, yielding a single time series at each quad for statistical analysis and model calibration (θ_w in [L^3 L^{-3}]). The depth weighted average was estimated by multiplying a θ_{daily} value by the sensed depth range *dr* of a given sensor (2.5, 7.5 and 12.5 cm for the 2, 5 and 10 cm depth sensors), dividing by the total sensed depth (12.5 cm), and summing these weighted averages together according to the following equation:

$$\theta_w = \theta_{daily} \frac{dr}{12.5} \tag{3}$$

Figure 6 shows a profile diagram of the soil moisture sensors positioned at depth below the surface and the relative sensed depth ranges used for the depth-weighting calculation. Figure 7 shows an example θ_w time series calculated from the soil moisture observations under the B5 quad at DOE site, and also includes the daily average air temperature (T_a) and total precipitation (P_T) measurements from DOE meteorological station, and estimates of daily potential evapotranspiration (*PET*).

Field measurements were taken in 2014 to quantify the amount and type of BSCs and vascular plant species (Figure 8). A grid-point intercept method (Herrick *et al.* 2005) was used to quantify species-specific percent cover *p* [%] of BSCs and plants over each quad. The species type intercepted at each point of a grid frame was counted and used to estimate *p* of a given species (p_{sp} in %) as:

$$p_{sp} = 100\% \cdot \frac{N_{sp}}{N_T} \tag{4}$$

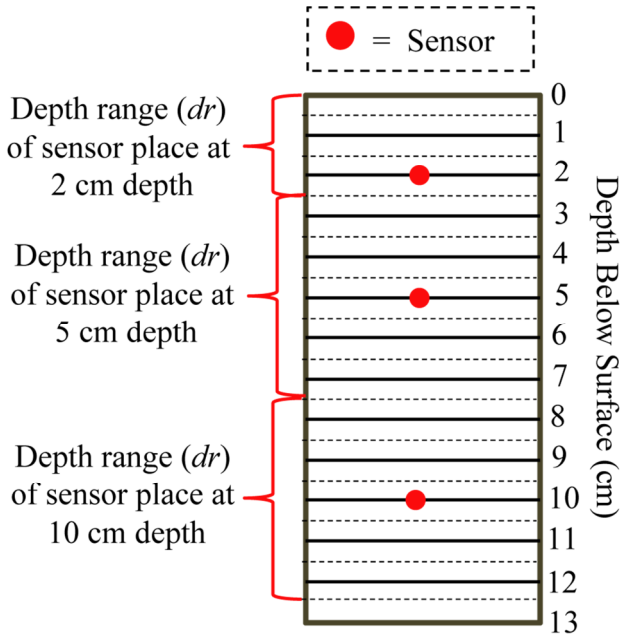

Figure 6: Profile diagram of the soil moisture sensors (red dots) positioned at depth below the surface and the relative sensed depth ranges (red brackets) used for the depth-weighting calculation.

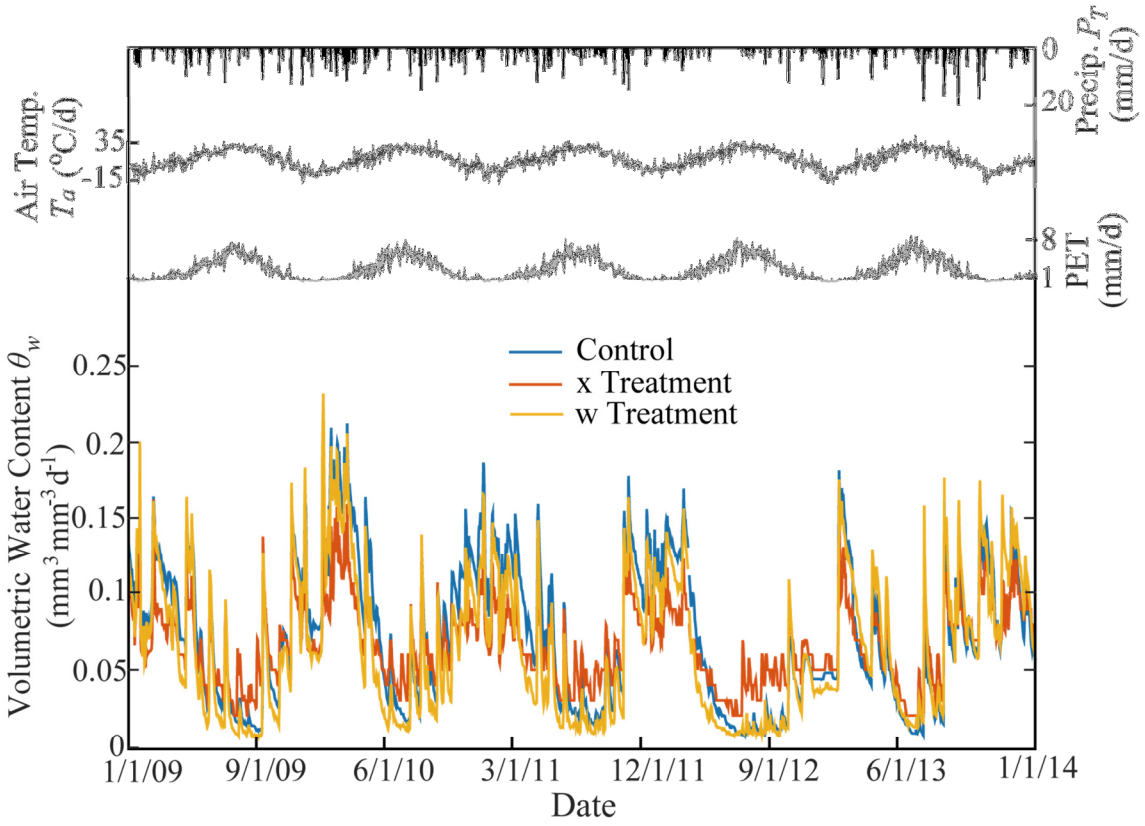

Figure 7: Time series of daily average air temperature (T_a), total precipitation (P_T), and daily total potential evapotranspiration (PET), and daily depth-weighted average volumetric water content (θ_w) of the observations taken under the B5 quad.

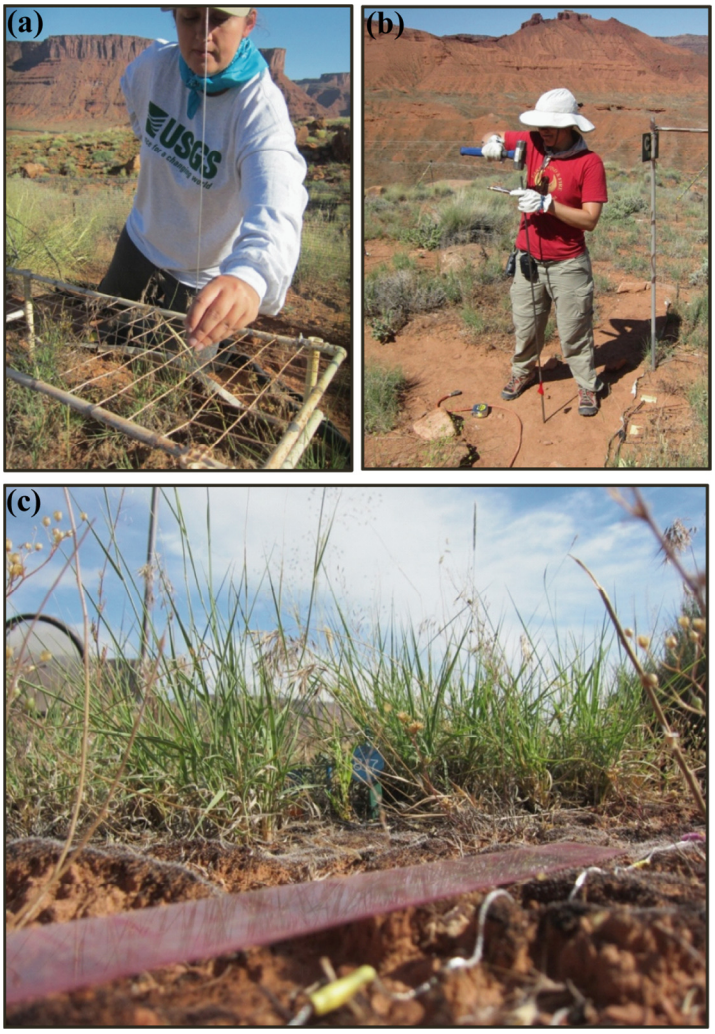

Figure 8: Photographs taken during field measurements of (a) percent cover, (b) soil depth, and (c) roughness index (RI). Grid frame and rod shown for percent cover measure (a). Hammer and rod shown for soil depth measure (b). Ruler and jewelry chain shown for RI measure (c).

where N_{sp} is the number of species-specific counts per total number of grid points (N_T = 96 points). The percent cover of cyanobacteria $p_{Cya}$was calculated individually (Table 1). Since lichens and mosses co-develop if left undisturbed and were both strongly affected by the watering treatments (Belnap *et al*. 2005; Reed *et al.* 2012), the percent cover of these two species were calculated as a combined percentage (p_{LM}, Table 1). The percent cover of total vegetation (p_{Veg}; Table 1), for each of the dominant perennial plant

Table 1: Field measurement results including soil texture, roughness index, and percent cover over all quads.

Block	Treatment	Soil Texture	Roughness Index, $RI\ (cm\ cm^{-1})$	Percent Cover, p (%)						
				LM	Cya	Veg	Ac	Pj	Ah	Ann
B1	c	Loam	7.79	0.43	0.55	0.82	0.00	0.54	0.04	0.43
	w	Sandy-Loam	5.94	0.01	0.99	0.76	0.00	0.74	0.05	0.21
	x	Sandy-Loam	7.50	0.36	0.64	0.41	0.00	0.14	0.32	0.54
B2	c	Loam	6.10	0.33	0.66	0.79	0.10	0.00	0.39	0.51
	w	Sandy-Loam	5.70	0.03	0.97	0.60	0.00	0.45	0.00	0.55
	x	Sandy-Loam	NA	0.47	0.53	0.79	0.00	0.25	0.21	0.54
B3	c	Sandy-Loam	5.50	0.14	0.86	0.63	0.00	0.00	0.63	0.37
	w	Sandy-Loam	2.42	0.00	1.00	0.63	0.00	0.30	0.51	0.19
	x	Sandy-Loam	4.17	0.06	0.94	0.53	0.12	0.22	0.24	0.42
B4	c	Sandy-Loam	11.83	0.43	0.57	0.57	0.00	0.20	0.49	0.31
	w	Sandy-Loam	4.90	0.00	1.00	0.55	0.00	0.64	0.12	0.24
	x	Sandy-Loam	5.33	0.27	0.73	0.51	0.00	0.27	0.02	0.71
B5	c	Sandy-Loam	15.00	0.51	0.49	0.41	0.00	0.07	0.00	0.93
	w	Sandy-Loam	1.75	0.00	1.00	0.79	0.00	0.48	0.00	0.53
	x	Sandy-Loam	4.67	0.00	1.00	0.71	0.00	0.53	0.01	0.46
C1	c	Sandy-Loam	9.75	0.34	0.66	0.70	0.00	0.23	0.17	0.59
	x	Sandy-Loam	7.22	0.31	0.69	0.86	0.00	0.51	0.27	0.22
C2	c	Sandy-Loam	21.75	0.39	0.61	0.81	0.00	0.22	0.00	0.78
	x	Sandy-Loam	9.92	0.19	0.81	0.90	0.00	0.17	0.39	0.44
C3	c	Sandy-Loam	9.69	0.30	0.70	0.49	0.00	0.00	0.00	1.00
	x	Sandy-Loam	17.00	0.23	0.77	0.25	0.00	0.21	0.00	0.79
C4	c	Sandy-Loam	8.13	0.09	0.91	0.79	0.10	0.07	0.30	0.53
	x	Sandy-Loam	12.00	0.29	0.71	0.95	0.01	0.29	0.19	0.51
C5	c	Sandy-Loam	6.39	0.11	0.89	0.03	0.00	0.00	0.00	1.00
	x	Sandy-Loam	13.13	0.20	0.80	0.56	0.00	0.43	0.00	0.57

Species (p_{Ah}, p_{Pj}, , and p_{Ac}, for *A. hymenoides*, *P. jamesii*, *A. confertifolia*, and *B. tectorum*, Table 1) and for the annuals p_{Ann} were all calculated for additional model

parameterization. The fraction of total vegetative cover f_v was also estimated for each plot as the total number of vegetation counts N_V per total number of grid points N_T:

$$f_v = \frac{N_v}{N_T} \tag{5}$$

The chain method originally proposed by Saleh (1993) was utilized as a quick and easy method for measuring the roughness of soil crust surfaces through an estimate of the roughness index RI [L L^{-1}]. In this method, a jewelry chain of known stretched length L_s [L] was (1) draped across the ground surface; (2) the horizontal distance from end to end of the draped chain was measured; (3) this measurement was repeated three times for each plot; (4) the average draped length measurement of each quad L_d [L] was measured; and (5) RI calculated as:

$$RI = 1 - \left(100 \cdot \frac{L_s}{L_d} \right) \tag{6}$$

Additionally, depth to bedrock Z_b in [L] was measured using a rod and hammer, and leaf area index LAI_{sp} [L^2 L^{-2}] was measured for each plant species (sp), or a measure of one-sided leaf surface area of a given plant per ground area, using a LAI-2200 Plant Canopy Analyzer (LI-COR Environmental) for each quad to aid in model parameterization. Since strong correlation exists between the measures of RI and p_{LM} (Spearman's r^2 = 0.71), and since degree of freeze-thaw also affects surface roughness (reviewed in Belnap 2006), RI is evaluated as a as a metric for the LOD of each quad throughout model parameterization. Since the vegetative cover at one of the given quads (B2-x) was too dense for RI measurement (Table 1).and the RI was evaluated as the

predictor variable for much of the analyses and experiments, observations from the B2-x quad are not utilized in this thesis.

Four RI ranges, RI Class I through IV, were defined and set by the 25th, 50th, and 75th percentiles of the RI measurements (5.5, 7.3, 10.9, respectively). All quad specific observations (*pc* and θ_w) were subsampled and assigned into an RI class based off of the given RI measure. Each class thus contains six quads and their corresponding observations. Figure 9 shows all observed RI measures at the field quads, each color coded according to their respective RI class. The range of all RI measurements, as listed in Table 1 and represented in Figure 9, is between 1.75 for the smoothest, least developed BSC cover (quad B5-w) to 21.75 for the roughest, most developed BSC cover (quad C2-c). For reference, the two photographs of quads shown in Figure 5f and g (C3-c and B3-w), have RI measurements of values of 9.68 and 2.42, respectively.

2.3 Ecohydrology Model

As illustrated in Figure 10, the conceptual model used is centered on the interactions affecting the moisture status of a three-layered system including at the surface and within the BSC and soil layers. BSC characteristics control the impact of irrigation and meteorological forcing on water fluxes at the surface and BSC layer, which in turn affects the rate of inputs into the underlying soil layer. Vegetative and soil characteristics control the impact of inputs from the BSC layer on the water fluxes within the soil. Soil moisture dynamics are simulated mathematically using a point-scale model proposed by Laio *et al*. (2001), but modified to receive inputs filtered through the overlying BSC layer. An altered version of the model is used as the basis for simulating

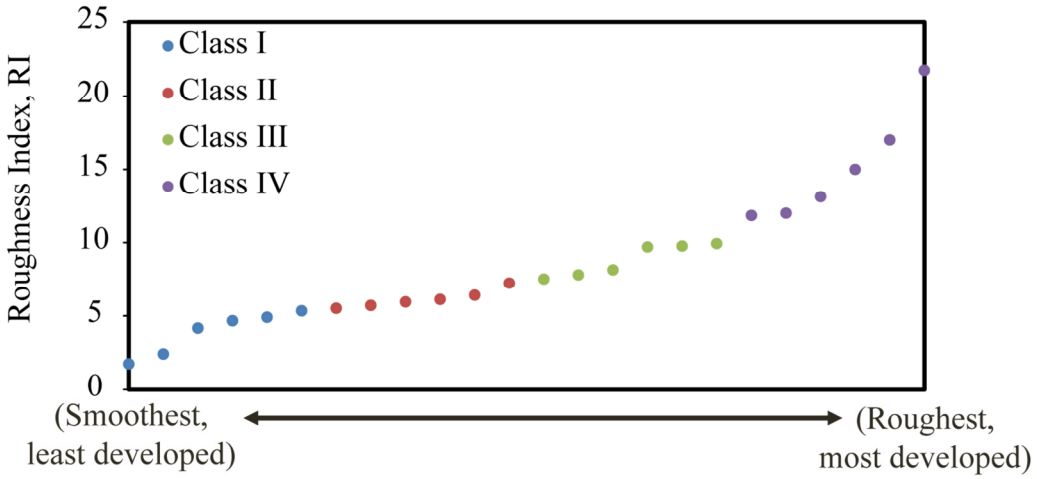

Figure 9: Plot of all roughness index (RI) measurements from smoothest to roughest, color-coded according to RI Class.

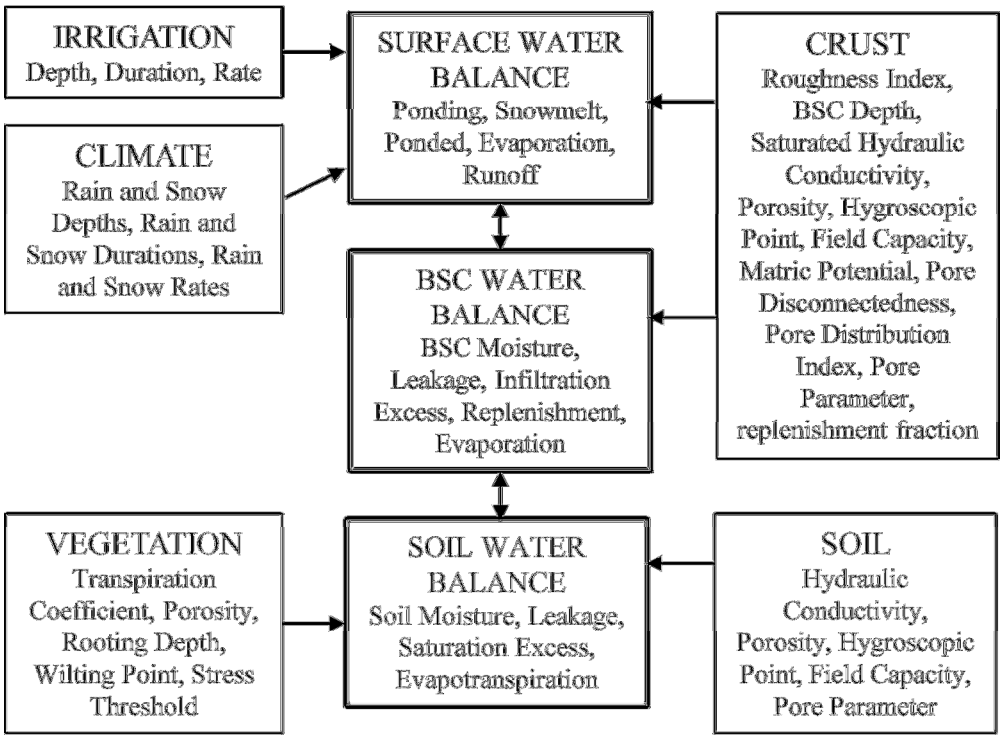

Figure 10: Conceptual schematic of modeled system with lines showing modeled interactions.

the moisture dynamics within the BSC layer, which includes a modified input scheme that considers the impact of storm intensity on the infiltration capacity, an additional flux

to recycle moisture upward from the soil, and hydraulic properties modified to reflect previously published studies of BSC microstructures.

Rather than using the probabilistic approach of the original authors, partitioned precipitation and soil moisture observations are respectively used for model forcing and testing. Precipitation observations are partitioned according to a multi-stage temperature-threshold function. Irrigated inputs of the DOE water experiments are added to the total liquid water inputs according to the rate and time of application over the observation time period. Furthermore, the surface has been modeled as an additional layer where liquid water can be held in excess at an amount dependent upon the relative roughness of the underlying BSC. Snow is also potentially held and melted at the surface, and inputted to the BSC layer at a rate depending upon temperature-based estimates of the snowpack energy budget, following DeWalle and Rango (2008). The calculations involved for the model are discussed in three sections, one for each layer. Each flux and associated layer is represented in a cartoon model depiction in Figure 11.

2.3.1 Simulated Surface Moisture Budget

The algorithm employed at the simulated surface partitions total precipitation P_T, estimating snowmelt M, and total liquid water inputs X (all [L T^{-1}]) from the surface to the underlying BSC layer (Figure 11). The snowmelt estimation uses the degree-day method proposed by DeWalle and Rango (2008) to estimate the liquid and snow storage capacity of a given surface snowpack and estimate the total melt and outflow. A degree-day is defined here as the difference between the air temperature T_a and some base temperature T_b (T_a - T_b; all [^{o}C]), with T_b defined at the temperature of freezing

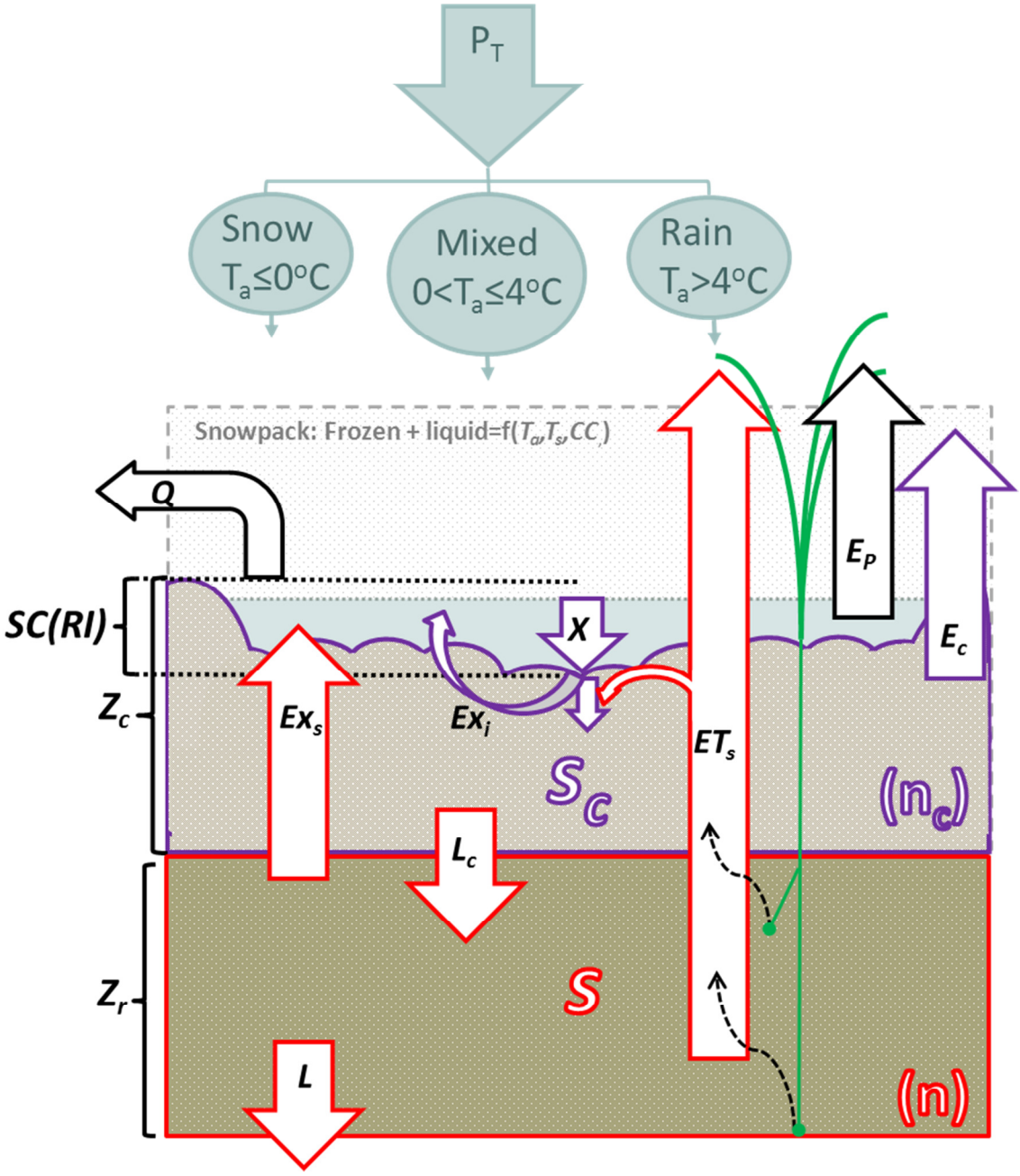

Figure 11: Model cartoon showing total precipitation (P_T) partitioned as a function of air temperature (T_a); snowpack content as function of T_a, snow temperature (T_s) and cold content (CC); surface ponding held to surface capacity (sc) as a function of roughness index (RI); surface runoff (Q) and ponded evaporation losses (E_p); total water inputs (X) infiltrating to BSC layer (purple), with relative BSC moisture (s_c), BSC depth (Z_c), BSC porosity (n_c) and losses of excess infiltration (Ex_i), BSC evaporation (E_c) and BSC leakage (L_c). L_c infiltrating to soil layer (red), with relative soil moisture (s), depth (Z_r), soil porosity (n), and losses of excess saturation (Ex_s), soil evapotranspiration (ET_s), and soil leakage (L_s).

(T_b = 0°C). An iterative process is used to estimate the daily status of three snowpack storage components: (1) the snowpack water equivalent *SWE* [L T^{-1}] that reflects the absence (*SWE* = 0) or presence (*SWE* > 0) of snow and is initially set to 0 (i.e. no snow); (2) the cold-content of the snowpack *CC* [L T^{-1}], representing snow "ripeness", or the amount of energy needed to raise a dry snowpack to T_b, and thus, how close the snowpack is to producing melt; and (3) the liquid-water storage holding capacity *WHC* [L T^{-1}], representing the amount of liquid water held within the snowpack (Figure 11).

Using a daily timestep *t* [days], *SWE* is incrementally updated with each addition of P_r, and P_s, changes in *WHC* (ΔWHC; [L T^{-1}]), and reductions as *M* and P_r become outflow, according to the following budget:

$$SWE_t = SWE_{t-1} + P_{r,t} + P_{s,t} + \Delta WHC - \Delta(M_t + P_{r,t}) \quad (6)$$

Assuming no initial snowpack, SWE was first set to 0 ($SWE_{t=0} = 0$). The model was forced with air temperature T_a [°C] and total precipitation P_T [L T^{-1}] observed at the DOE site. T_a is used to estimate the degree-day factor *DDF* [L °C^{-1} T^{-1}], which dictates the amount *M* occurring for a given degree-day (T_a - T_b), according to a linear function:

$$M = DDF(T_a - T_b) \quad (7)$$

Any errors associated in assuming *M* varies linearly with a degree-day is approximately corrected by varying *DDF* seasonally between a minimum and maximum *DDF* value for the given Julian day (*d*) according to a sinusoidal-wave function (Anderson 1973 via DeWalle and Rango 2008):

$$P_{S,WRCC}(s) = \begin{cases} d = 0 \\ DDF_{\min} + \left[DDF_{\max} \cdot \sin\left(\frac{\pi d}{365}\right) \right] & d > 0 \end{cases} \quad (8)$$

DDF is in turn used to estimate the cold content factor *CCF* [L ^{o}C T^{-1}], which dictates the rate of change in *CC* as a function of how far snowpack temperature T_s [^{o}C] is above T_a:

$$CCF = \tfrac{1}{10} DDF \tag{9}$$

$$\Delta CC = CCF(T_s - T_a) \tag{10}$$

CCF is estimated as a fraction of *DDF* since heat exchange occurs at a much faster rate through heat conduction than through melt, per degree-day. Since no snow is assumed present at the initial timestep ($SWE_0 = 0$), T_s is initialized at the base temperate (T_b) and does not change until snow is present ($SWE_t > 0$) and at which point a temperature-index approach is employed to estimate T_s following Anderson (1973) and Marks *et al*. (1992; via DeWalle and Rango 2008):

$$T_{S,t} = \begin{cases} T_b, & SWE_t = 0 \\ T_{s,t-1} + TSF(T_{a,t} - T_{s,t-1}), & SWE_t > 0 \end{cases} \tag{11}$$

where the surface temperature factor *TSF* employed was 1, and thus, assumes that the snowpack surface temperature tracks air temperatures.

After the estimation of *DDF*, *CCF*, and T_s, the model partitions P_T according to a multi-stage function dependent upon T_a relative to both a critical air temperature where partial freezing commences T_c [^{o}C], assumed equal to 4^{o}C, and to freezing temperature (T_b; Figure 11). If T_a is less than or equal to T_b, all P_T was assumed to fall as snow ($P_S = P_T$); if T_a was greater than or equal to T_c all P_T was assumed to occur as rain ($P_R = P_T$); and if T_a was between these two threshold temperatures, P_T was assumed mixed, falling as both P_R and P_S based upon daily rain and snow fractions, f_R and f_S respectively:

$$P_R = \begin{cases} 0, & T_a \le 0^o C \\ f_R P_{T,} & 0^o C < T_a < 4^o C \\ P_{T,} & T_a \ge 4^o C \end{cases} \quad (12)$$

$$P_S = \begin{cases} P_T, & T_a \le 0^o C \\ f_s P_{T,} & 0^o C < T_a < 4^o C \\ 0, & T_a \ge 4^o C \end{cases} \quad (13)$$

where f_R and f_S were estimated from meteorological observations made by the Western Regional Climate Center (WRCC) at a nearby site in Moab, UT (Figure 3). The WRCC database reports daily observations of total snowfall $P_{S,WRCC}$ [L], total snow depth $Z_{S,WRCC}$ [L], and total precipitation $P_{T,WRCC}$ [LL] that represents the non-partitioned sum of daily liquid rain $P_{R,WRCC}$ [mm] and the snow water equivalent SWE_{WRCC} [mm] estimated by melting snowpack cores collected daily. The snow to liquid ratio can vary for a given storm and here a 10:1 ratio is assumed, and $Z_{S,WRCC}$ was multiplied by a factor of 0.1 to obtain estimations of the daily SWE_{WRCC}:

$$SWE_{WRCC} = 0.1 \cdot Z_{S,WRCC} \quad (14)$$

On days where this conversion produced overestimations in SWE_{WRCC} greater than $P_{T,WRCC}$, all precipitation was assumed to have fallen as snow, otherwise $P_{R,WRCC}$ was assumed to be the difference between $P_{T,WRCC}$ and SWE_{WRCC}.:

$$P_{R,WRCC} = \begin{cases} 0, & SWE_{WRCC} > P_{T,WRCC} \\ P_{T,WRCC} - SWE_{WRCC}, & SWE_{WRCC} \le P_{T,WRCC} \end{cases} \quad (15)$$

$$P_{S,WRCC} = \begin{cases} P_{T,WRCC}, & SWE_{WRCC} > P_{T,WRCC} \\ SWE_{WRCC}, & SWE_{WRCC} \le P_{T,WRCC} \end{cases} \quad (16)$$

The ratio of $P_{S,WRCC}$ and $P_{R,WRCC}$ to $P_{T,WRCC}$ were then used as estimates of f_r and f_s, respectively:

$$f_s = \frac{P_{s,WRCC}}{P_{T,WRCC}} \tag{17a}$$

$$f_r = \frac{P_{R,WRCC}}{P_{T,WRCC}} \tag{18a}$$

Alternatively if such observations are not available, f_r and f_s could be computed as a function of the relative differences T_a and T_c above freezing T_b:

$$f_s = \frac{T_a - T_b}{T_c - T_b} \tag{17b}$$

$$f_r = 1 - f_s \tag{18b}$$

When a large enough snow event occurs to produce P_s greater than or equal to some critical depth $P_{s\text{-}c}$ ([L]; $P_S > P_{S\text{-}c}$) T_s is updated to a value equal to T_a:

$$T_s = T_a, \quad P_S > P_{S-c} \tag{19}$$

where value of 10mm was assumed for $P_{S\text{-}c}$.

Relative T_a and precipitation type are also used to distinguish between melt-producing and no-melt events. On a given day t when T_a is above T_b ($T_a > T_b$), melt is produced at a value set by the minimum of either (1) the potential M as estimated from equation 7 or (2) the amount of snowpack available summed from the initial SWE remaining after the previous day ($SWE_{t\text{-}1}$) and P_S of the current day ($P_{S,t}$). In freezing ambient conditions ($T_a \leq T_b$), however, temperatures are assumed low enough such that no melt is produced ($M = 0$):

$$M = \begin{cases} \begin{cases} DDF(T_a - T_b), & SWE_{t-1} + P_{s,t} > DDF(T_a - T_b) \\ SWE_{t-1} + P_{s,t}, & DDF(T_a - T_b) > SWE_{t-1} + P_{s,t} \end{cases} & T_a > T_b \\ 0 \quad Ta \le T_b \end{cases} \quad (20)$$

At this point, the model computes the *CC* status of the pack according to T_s. If T_s is greater than T_b ($T_s > T_b$), the *CC* is updated via equation 10 to reflect the changing capacity to freeze and hold liquid within the snowpack. Otherwise, the snowpack is assumed isothermal, with a relatively stable *CC* at maximum capacity (*CC* = 0):

$$CC = \begin{cases} CC + \Delta CC, & T_s > T_b \\ 0, & T_b > T_S \end{cases} \quad (21)$$

An interval outflow *Out* [L T^{-1}] is then computed as the sum of *M* and P_r:

$$Out = M + P_r \quad (22)$$

If *Out* produces an equal or greater amount of liquid than the *CC* demand (*Out* > *CC*), all of *Out* is frozen and T_s is brought to T_b to reflect the supplied demand (eq. 23a). Otherwise, only a portion of *Out* is frozen as dictated by the value of the *CC* demand and T_s remains the same:

$$Out \ge CC \begin{cases} Out = Out - CC \\ CC = 0 \\ T_s = 0 \end{cases} \quad (23a)$$

$$Out < CC \begin{cases} CC = CC - Out \\ Out = 0 \end{cases} \quad (23b)$$

The status of *SWE* of the current timestep (*t*) is then updated to include all inputs (P_T) reduced by *Out*:

$$SWE_t = SWE_{t-1} + P_{T,t} - Out_t \quad (24)$$

If no snow remains after the outputs have been extracted ($SWE_t = 0$) then T_s is reset back to the initial base value T_b (0°C) assumed when no snowpack remains on the surface. If the surface still has a snowpack after extractions ($SWE_t > 0$), the *WHC* status is updated with increases from some fraction f_{WHC} of the total inputs (P_T) and reductions from *Out*:

$$WHC_t = WHC_{t-1} + \left(f_{WHC} \cdot P_{T,t}\right) - Out_t \tag{25}$$

Following the original authors, a value of 0.3 was assumed for $f_{WHC.}$ Since initially there is no snowpack ($SWE_{t=0} = 0$), *WHC* was initialized to 0 ($WHC_{t=0} = 0$). This intermediate value of *Out* is then used to satisfy the *WHC* (eqs. 26a,26b). If *Out* produces an equal or greater amount of liquid than the *WHC* demand (*Out* > *WHC*), all of *Out* is locked as liquid in the snowpack and *WHC* is brought to *0* to reflect the supplied demand (eq. 26a). Otherwise, only a portion of *Out* remains locked in the snowpack per *WHC* demand:

$$Out \geq WHC \begin{cases} Out = Out - WHC \\ WHC = 0 \end{cases} \tag{26a}$$

$$Out < WHC \begin{cases} WHC = WHC - Out \\ Out = 0 \end{cases} \tag{26b}$$

Following these extractions, SWC is updated via equation 24 and a final snowpack estimated for the day.

In order to capture the effect of the increased roughness with BSC development, the surface is able to pond water that was exhumed in excess of the capacity of the underlying BSC and soil (Figure 11). The depth of this surface capacity *SC* [L] is proportional to the measured roughness index *RI* of the simulated quad relative to a

maximum capacity SC_{max} associated with a potential roughness RI_{max}, set equal to the maximum RI observed at the DOE site (21.75):

$$SC(RI) = SC_{\max} \cdot \frac{RI}{RI_{\max}} \tag{27}$$

$$RI_{\max} = 21.75 \tag{28}$$

Through this relative RI approach, model calibration efficiency is improved, requiring calibration of a single parameter SC_{max} to estimate SC for any simulated quad.

Estimation of the water exhumed in excess of the BSC and soil layers is discussed below in relation to the respective layer moisture balance sequence (Figure 11). Both are used to estimate a total excess depth Ex_T [L T^{-1}], which in turn generates runoff Q [L T^{-1}] and/or is held at the surface as a ponded depth *pond* [L T^{-1}] as dependent upon SC:

$$Q = \begin{cases} SC - Ex_T & SC > Ex_T \\ Ex_T - SC & Ex_T > SC \end{cases} \tag{29}$$

Ex_T retained within surface capacity by the surface is evaporated at a rate Ep [L T^{-1}] dependent upon the potential evapotranspiration demand PET:

$$E_p = \begin{cases} PET & Ex_T - SC > PET \\ Ex_T - SC & PET > Ex_T - SC \end{cases} \tag{30}$$

Ex_T retained against runoff and evaporation remains as a ponded surface layer *pond* [L T^{-1}]:

$$pond = Ex_T - Q \tag{31}$$

Initially, no water is assumed held on the surface ($pond_{t=0} = 0$), and on any given day thereafter, *pond* estimated and held after the extractions of the previous day ($pond_{t-1}$) are added to Out for infiltration into the BSC layer.

$$Out_t = Out_t + pond_{t-1} \tag{32}$$

In order to estimate the intensity outflow i_O ([L T-1]; eq. 34) at a resolution relevant for the modified BSC infiltration scheme, the duration of outflow D_o [T] from the surface layer is estimated at the hourly timescale. This scheme approximates D_o acknowledging the rates relevant to the specific outflow source. If any portion of outflow occurs as melt from a snow layer (M > 0, Out >0), the rate of outflow is assumed delayed by the rate of melting as regulated by the length of daylight D_d of the given Julian day [T] in hours. Otherwise, D_o is assumed to have occurred without any significant delay and set equal to the total hours h [T] where hourly precipitation observations were greater than 0 ($P_{T,h} > 0$) for the given day (t):

$$D_{o,t} = \begin{cases} D_{d,t} & M > 0; Out > 0 \\ h & M = 0; Out > 0 \end{cases} \tag{33}$$

$$i_o = \frac{Out}{D_O} \tag{34}$$

The intensity of irrigation inputs i_I [L T^{-1}] was estimated from the depth I [L] and duration D_I [L] of applications according the experiment schedule during the five-year observation period:

$$i_I = \frac{I}{D_I} \tag{35}$$

Since irrigations took place during the summer, I, D_I , and i_I were added directly to the total BSC input depth X [L], duration D [T], and intensity i [L T^{-1}]) of surface water inputs:

$$X = Out + I \tag{36}$$

$$D = D_O + D_I \tag{37}$$

$$i = i_O + i_I \tag{38}$$

2.3.2 Simulated BSC Moisture Budget

The change in time of relative BSC moisture s_c (0 for perfectly dry BSC and 1 at saturation) is expressed as the inputs from the surface (X) reduced by applicable losses, averaged over a BSC depth Z_c ([L]; Figure 11):

$$n_c Z_c \frac{ds_c}{dt} = X - Ex_i(s_c) - L_c(s_c) - E_c(s_c) \tag{39}$$

with BSC porosity n_c [L^3_{voids}/L^3_{total}], infiltration excess Ex_i, leakage L_c, and evaporation E_c (all [$L\ T^{-1}$]). Relative BSC moisture s_c is defined as the fraction of porosity n_c that is occupied by the volumetric BSC moisture θ_c [L^3_{water}/L^3_{total}]:

$$s_c = \frac{\theta_c}{n_c}. \tag{40}$$

The modeled BSC layer has an active depth Z_c that is functionally defined to contain all horizons once cemented and abandoned by the microorganisms (Figure 11). In this manner, the BSC layer contains all sheath materials, active and inactive, which are capable of binding soil particles together and increasing the moisture retention (reviewed in Belnap 2001b). Since both sub-surface thickness and soil aggregation increases with fine particle entrapment, which in turn increases with roughness (Belnap and Gardner 1993; Tchan and Whitehouse 1953; Hu *et al.* 2002; Felde *et al.* 2014; reviewed in Belnap 2001b), Z_c is assumed proportional to the LOD metric of roughness index (RI) of the simulated quad relative to a maximum depth $Z_{c,max}$ [L], associated with RI_{max} (21.75):

$$Z_c(RI) = Z_{c,\max} \cdot \frac{RI}{RI_{\max}} \tag{41}$$

This relative RI approach not only improves modeling efficiency by reducing the number of parameters calibrated, but also avoids the need to employ more invasive methods to estimated Z_c of fragile BSC layers.

In order to explore the potential effects of BSC of decreasing porosity on hydrophobicity and saturation excess, an alternative infiltration scheme was added following Eagleson (1978 via Manfreda *et al*. 2001) that accounts for the effects of antecedent moisture conditions and high intensity storm events relative to the infiltration capacity. Infiltration is modeled using numerically and infiltration excess is generated when the intensity of water inputs i [L T^{-1}] exceeds the infiltration capacity of the BSC layer, defined by two system parameters: (1) the infiltration sorptivity S [L T^{-1}], or capacity of the BSC to absorb water by capillary action, and (2) the gravitational infiltration rate A [L T^{-1}]. These two parameters are expressed as a function of the initial moisture condition ($s_{c,t-1}$) relative to saturation (1- $s_{c,t-1}$) and certain hydraulic properties of the system:

$$A(s_{c,t-1}) = \frac{1}{2} K_{s,c} \left[1 - s_{c,t-1}^{c}\right] \tag{42}$$

$$S(s_{c,t-1}) = 2\left(1 - s_{c,t-1}^{c}\right)\left(\frac{5 n_c K_{s,c} \Psi_1 \phi(m, s_{c,t-1})}{3m\pi}\right)^{1/2} \tag{43}$$

where $K_{s,c}$ is the BSC saturated hydraulic conductivity [L T-1], c is the dimensionless BSC pore disconnectedness, m is the dimensionless BSC pore size distribution index, and Ψ_1 is the BSC matric potential at saturation [L T^{-1}], and ϕ is the dimensionless effective diffusivity expressed as a function of m and initial moisture condition relative to saturation (1- $s_{c,t-1}$; Bras 1990 via Manfreda *et al*. 2010):

$$\phi(m, s_{c,t-1}) = \frac{3\pi}{10(1-s_{c,t-1})}\left(\begin{array}{l}\dfrac{m}{1+4m} \\ +\dfrac{m^2 s_{c,t-1}^{1/m+4}}{(1+4m)(1+3m)} - \dfrac{m^2 s_{c,t-1}}{1+3m}\end{array}\right) \quad (44)$$

Together, A and S are used to estimate the time until pond ponding t_0 [T], or the length of time it would take for the intensity of the given inputs X_i [L T^{-1}] to exceed the given infiltration capacity (A and S). If ponding remains on the surface after the previous days extractions ($pond_{t-1} > 0$), t_0 is assumed to occur immediately ($t_0 = 0$). Otherwise, t_0 is assumed to occur at a time dictated by A and S:

$$t_{0,t} = \begin{cases} 0 & t_{0t-1} > 0 \\ \dfrac{S(s_{c,t-1})^2}{4(i - A(s_{c,t-1}))^2} & t_{0t-1} = 0 \end{cases} \quad (45)$$

Following the original author's approach, the actual ponding time is assumed greater than t_0 since the rainfall intensity is lower than the infiltration rate prior to ponding (i.e. when $t < t_0$), and thus, the actual infiltration capacity decreases slower than estimated. Under the assumption that i is much greater than A ($i >> A$), the actual ponding time can be assumed equal to twice that of the estimated t_0 ($2t_0$; Eagleson 1978 via Manfreda *et al.* 2010). The relationship between this actual ponding time $2t_0$ and total duration of inputs D is used to estimate the proportion of X returned to the surface layer as infiltration excess E_{xi} [L T^{-1}] and the portion infiltrated into the BSC layer in ([L T^{-1}]; Figure 11). If $2t_0$ is greater than or equal to D ($2t_0 \geq D$), no excess moisture occurs by the end of input duration ($E_{xi} = 0$) and all available water is infiltrated into the BSC layer ($in = X$). Otherwise, in is the minimum of either the amount available water for infiltration

(X), or the infiltration capacity of the BSC (I_c) computed from the integral solution of the Philip's equation for infiltration (eq. 46; Eagleson 1978 via Manfreda *et al.* 2019):

$$I_c = 2it_0 + A(s_{c,t-1})(D - 2t_0) + S(s_{c,t-1})\sqrt{D - t_0} - S(s_{c,t-1})\sqrt{t_0} \quad (46)$$

$$in = \begin{cases} X & 2t_0 \geq D \\ \begin{cases} X_t & X < I_c \\ I_{c,t} & X > I_c \end{cases} & D_t > 2t_0 \end{cases} \quad (47)$$

Any excess water inputs not infiltrated are treated as infiltration excess E_{xi} and are added to the estimation of total excess losses E_{xT}, *pond* and associated surface fluxes, and potentially added to the surface outflow *Out* (eqs. 29-32) of the next timestep (Figure 11):

$$E_{xi} = X - in \quad (48)$$

In the original approach, any infiltration in excess of saturation (E_{xs}) is also accounted for in this computation of X. In this multi-layered approach, however, E_{xs} is assumed more dependent upon the saturation capacity of the lower soil layer given the larger proportional depth of the soil relative to that of the BSC layer, and thus, E_{xs} is calculated with the soil moisture budget below. Due to previous observations of increased BSC moisture in the absence of direct precipitation (Jacobs *et al.* 2000; Agam and Berliner 2004), an additional moisture supply is added as a fraction f_R of the potential bare soil evaporation ($f_R E_w$) to account for potential recycled replenishment via direct adsorption or dew rise. Since such processes would potentially occur at the end of the day pending the temperature gradient between soil and atmosphere, the replenished amount is taken from the previous day's estimation of vapor ($f_R E_{w,t-1}$). An initial value of the relative BSC moisture level prior to losses s_c is then estimated to reflect the additions of

the estimated infiltration (X) and recycled moisture ($f_R E_{w,t-1}$) to the antecedent moisture conditions ($s_{c,t-1}$):

$$s_{c,t} = s_{c,t-1} + frE_{w,t-1} + X_t \tag{49}$$

As shown in Figure 12, BSC leakage and evaporation losses occur in stages defined by certain relative moisture thresholds that are dependent upon the BSC defining properties. BSC leakage, or infiltration from the BSC to the underlying soil layer, is assumed to only occur when s_c surpasses the BSC field capacity $s_{fc,c.}$ Under these conditions ($s_c > s_{fc,c}$) leakage rate L_c is modeled as a fraction of the saturated BSC hydraulic conductivity $K_{s,c}$ [L T-1] in the following:

$$L_c = K_{s,c} \frac{e^{\beta_c (s_c - sf_{c,c})} - 1}{e^{\beta_c (1 - sf_{c,c})} - 1} \tag{50}$$

where $\beta_c = 2b_c + 4$ and b_c [-] is a BSC pore parameter related to the pore size distribution index c and pore disconnectedness m by the following:

$$c = 2b_c + 3 \tag{51}$$

$$c = (2 + 3m)/m \tag{52}$$

Thus, the hydraulic conductivity of the BSC layer is a function of these BSC parameters and this hydraulic conductivity decays exponentially from the maximum ($K_{s,c}$) under saturated conditions (when $s_c = 1$) to zero (when $s_c < s_{fc,c}$).

If PET still remains after extractions from E_p (eq. 30), and if s_c is greater than the BSC hygroscopic point $s_{h,c}$, BSC evaporation (E_c) occurs at a rate dictated by the PET and weighted by the BSC demand-weighting factor k_c (Figure 12):

$$E_c(s_c) = \begin{cases} 0 & s_c \le s_{h,c} \\ k_c PET & s_c > s_{h,c} \end{cases} \tag{53}$$

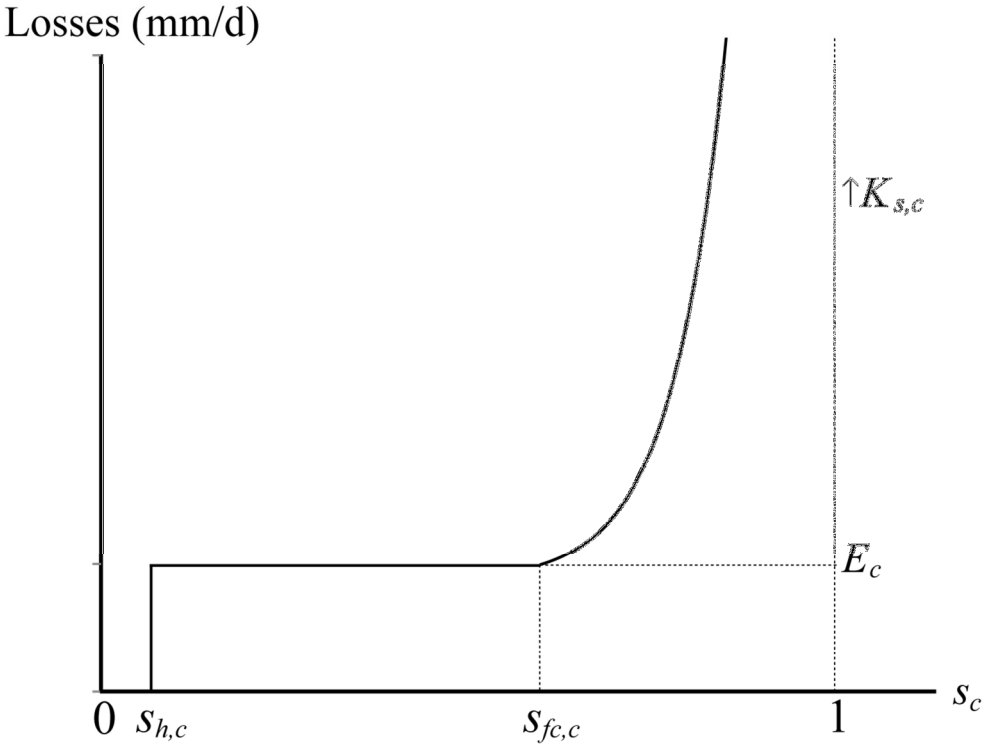

Figure 12: Conceptual plot of BSC losses (black line) verses relative BSC moisture (s_c) showing location of all relative BSC moisture thresholds including hygroscopic point ($s_{h,c}$) and field capacity ($s_{fc,c}$).

where k_c is calibrated according to the LOD to explore the potential increases in demand associated with darker biomass (reviewed in Belnap 2006).

2.3.3 Simulated Soil Moisture Budget

The change in time of relative soil moisture *s* (0 for perfectly dry soil and 1 at saturation) is similarly expressed as the inputs from the BSC layer (L_c) reduced by applicable losses, averaged over the active soil rooting depth Z_r [L] (Laio *et al.* 2001):

$$nZ_r \frac{ds}{dt} = L_c - E_{x_s}(s) - L(s) - ET_s(s) \tag{54}$$

with soil porosity n [L^3_{voids}/L^3_{total}], saturation excess E_{xs}, leakage L, and evapotranspiration ET_s (all [$L\ T^{-1}$]). Relative soil moisture s is defined as the fraction of soil porosity n that is occupied by the volumetric soil moisture θ [L^3_{water}/L^3_{total}]:

$$s = \frac{\theta}{n} \tag{55}$$

Again, the same numerical approach is utilized, discretizing the above differential equation at a daily time scale. When the inputs (L_C) added to the initial moisture conditions causes values of s greater than 1, saturation excess E_{xs} is produced to restore s back to the storage capacity (nZ_r):

$$E_{xs}(s) = \begin{cases} 0 & \left(s_{t-1} + \frac{L_c}{nZ_r}\right) > 1 \\ \left(nZ_r s_{t-1} + L_c\right) - nZ_r & \left(s_{t-1} + \frac{L_c}{nZ_r}\right) \le 1 \end{cases} \tag{56}$$

As shown in Figure 13, soil evaporative and leakage losses occur as a multi-stage function defined by upon certain relative moisture thresholds that are dependent upon the properties of the soil texture and vegetation. Soil leakage to deeper layers beyond the active rooting zone, occurs only when s is greater than soil field capacity (s_{fc}). Under these conditions, the soil leakage rate L occurs as a fraction of the saturated hydraulic conductivity K_s, and is dependent upon soil parameters dictating the exponential rate of decay of hydraulic conductivity from saturated conditions (when $s = 1$), to zero (when $s < s_{fc}$) (Figure 13):

$$L(s) = K_s \frac{e^{\beta(s - s_{fc})} - 1}{e^{\beta(1 - s_{fc})} - 1} \tag{57}$$

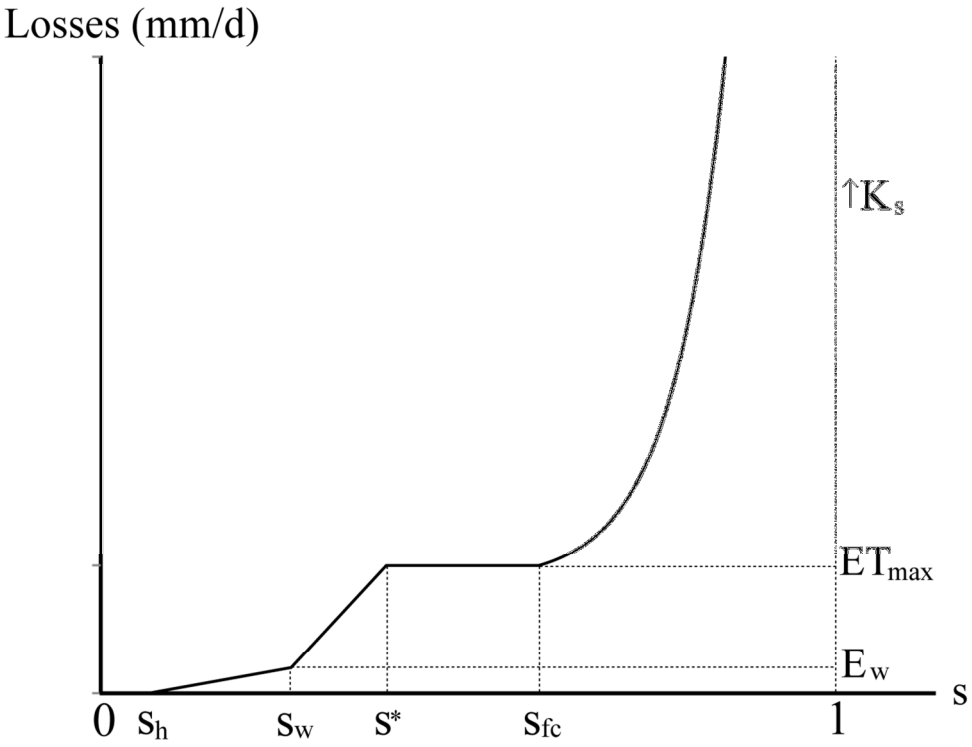

Figure 13: Conceptual plot of soil losses (black line) verses relative soil moisture (s) showing location of all relative soil moisture thresholds including hygroscopic point (s_h) and field capacity (s_{fc}).

where $\beta = 2b + 4$ and b [-] is an empirical soil pore parameter related to the pore size distribution and disconnectedness of the soil.

Evapotranspiration is simulated as a multi-ramp function of relative soil moisture s that accounts for four different behaviors conditional to the moisture state relative to soil and vegetative thresholds (Figure 13):

$$ET(s) = \begin{cases} 0 & s \le s_h \\ E_w \dfrac{s - s_h}{s_W - s_h} & s_h \le s \le s_w \\ E_W + \dfrac{s - s_w}{s^* - s_w}\left(ET_{\max} - E_W\right) & s_w \le s \le s^* \\ ET_{\max} & s \ge s^* \end{cases} \quad (58)$$

where s_h is the soil hygroscopic point at which *ET* reaches zero. Both s_h and s_{fc} are soil dependent characteristics related to matric potentials through soil moisture retention curves (Clapp *et al.* 1978). E_w is the evapotranspiration at the plant wilting point s_w. $ET_{\max}$ is the maximum evapotranspiration rate occurring at the plant stress threshold s^*, and is dependent upon the PET demand remaining after accounting for ponded evaporation and BSC evaporation. Field observations were utilized to more accurately represent the partitioning of ET and relative seasonal changes in the transpiration rates specific to the dominant species of the DOE site:

$$ET_{\max} = E_w + f_v k_v(se) PET \tag{59}$$

where total vegetation fraction of a given plot f_v was estimated via equation 5 and the average vegetation coefficient $k_v(se)$ [%PET] represents the average maximum transpiration estimated from the dominant plant species during the given season *se* (growth or non-growth). The growing season was designated as occurring from April to September and non-growth from October to March based off of the timing of leaf greening as interpreted from the LAI field measures and by observations made by Wertin *et al.* (2015). E_w was similarly estimated from a weighted PET term k_e to account for the maximum potential loss occurring from bare soil below s_w:

$$E_w = k_e PET \tag{60}$$

The average vegetation coefficient $k_{v,sp}(se)$ provides an estimate similar to the concept of a crop coefficient, which factors in differences in evaporation and transpiration between field crops and reference grass surfaces into a single factor used to estimate the crop evapotranspiration under standard evapotranspiration conditions (Allen *et al.* 1988).

In this study, the average vegetation coefficient $k_{v,sp}(se)$ factors in the species-specific vegetation coefficients $k_{v,sp}(se)$ of each dominant perennial plant over a given simulated plot, weighted by their respective percent cover (P_{sp}), and all expressed as a fraction of the total PET demand:

$$k_v(se) = \frac{1}{PET}\sum_{sp} P_{sp} k_{v,sp}(se) \tag{61}$$

The species-specific vegetation coefficient is estimated as the ratio of a seasonal-average species-specific maximum evapotranspiration $\overline{ET}_{\max,sp}$ [L T^{-1}] relative to the potential demand of a given day (PET):

$$k_{v,sp} = \frac{\overline{ET}_{\max,sp}}{PET} \tag{62}$$

In maximum conditions, species-specific evapotranspiration $ET_{\max,sp}$ [L T^{-1}] can be assumed equal to species-specific transpiration $T_{\max,sp}$ [L T^{-1}], under the assumption that the rate of evaporation from bare soil is comparatively small in such conditions (i.e. supplies and demand are maximized):

$$ET_{\max,sp} \approx T_{\max,sp}, \quad T_{\max,sp} >> E_{w,\max} \tag{63}$$

The maximum conductance $g_{\max}$ [mol L^{-2} T^{-1}] and the maximum rate of transpiration $T_{\max}$ [mmol L^{-2} T^{-1}], are both shown to be functions of temperature, CO^2 concentration, and soil water content, and thus, can be used to describe the relation between canopy conductance g_c [mol L^{-2} T^{-1}] and the rate of transpiration T [mmol L^{-2} T^{-1}] (Monteith 1995 via Pataki *et al.* 1996). A re-arranged form of this relationship is used to solve for maximum species-specific transpiration $T_{\max,sp}$ [mmol L^{-2} T^{-1}]:

$$T_{\max,sp} = \frac{-g_{c,\max} VD}{1 - g_{c,\max} / g_c} \quad (64)$$

where *VD* is the vapor pressure deficit [mmol mol^{-1}]. This study utilizes the DOE field measurements of stomatal conductance ($g_{s,sp}$) taken by Wertin *et al*. (2015) from the three main species (sp) at the DOE site, *Achnatherum hymenoides* (*AH*), *Pleuraphis jamesii* (*PJ*), *Atriplex confertifolia* (*AC*), using a portable photosynthesis system (Li-6400, LiCor Biosciences, Lincoln, NE, USA) at 9:00, 12:00, 15:00, and 18:00 h in the early-, mid-, and late-season growth periods of 2011 and 2012 (Wertin *et al.* 2015). Growth periods were designated as occurring in the months of April, May and June for 2011, and March, April, and May for 2012, and were based on the phenologic timing of vegetation green-up and growth observed in each year (Wertin *et al.* 2015). These measures were up-scaled to the plant-scale ($g_{c,sp}$) using the average leaf area index of each species ($\overline{LAI}_{sp}$) and a shade factor (f_s) assumed at a maximum value of 1 to reflect a minimum reduction of conductance by shade provided by these relatively sparse desert canopies:

$$g_{c,sp} = f_{s,sp} g_{s,sp} \overline{LAI}_{sp} \quad (65)$$

Daily actual and saturated vapor pressures e_a ([kPa]; estimated from relative humidity *RH*) and e_s were used to estimate *VD* with the actual vapor pressure estimates:

$$e_a = e_s \frac{RH}{100} \quad (66)$$

$$VD = (e_a - e_s) f_{mf} \quad (67)$$

where f_{mf} is the vapor pressure [kPa] to mole fraction [mmol mol^{-1}] conversion factor equal to 10 ([mmol mol^{-1} kPa^{-1}]; i.e. the vapor pressure in millibars; via Campbell and Norman 1988).

The maximum canopy conductance (g_m) was assumed equal to the maximum value of each hourly species canopy conductance estimate (g_c in hours). The hourly canopy conductance estimates were average to the daily timescale for each species ($g_{c,sp}$ in days) and utilized to estimate the daily average maximum species-specific transpiration $T_{\max,sp}$ (eq. 64). The average non-growth and growth maximum-species specific transpiration were respectively estimated as the minimum and maximum of the daily estimates ($T_{\max,ng} = \min(T_{\max,sp})$ and $T_{\max,g} = mean(T_{\max,sp})$) and then used to estimate the species-specific vegetation coefficient $k_{v,sp}$ for each season (eq. 62).

The average of the vegetation coefficient values ($k_{v,sp}$) for the two monocot species (*AH* and *PJ*) was taken and assumed for the value of the annual monocot grasses and herbs measured at the DOE site ($k_{v,ann}$). Finally, the seasonal average species-weighted vegetation coefficient (k_v) was then estimated taking into account the estimated coefficients species and annuals (and percent cover of the three dominant eq. 61).

2.4 Model Calibration and Testing

2.4.1 General Approach

The values for soil, vegetation, and crust parameters were estimated using an approach that combined both automated and manual optimization routines, with meteorological data collected from the on-site as model forcing. The automated routine

employed the Shuffle Complex Evolution (SCE) method developed by Duan *et al*. (1993), which searches for the optimal parameter value set found within multi-dimensional spaces through cluster, shuffled complex, and competitive evolution optimization strategies. The objective used for this method was the minimization of the root mean square error (RMSE) between the observed and simulated soil moisture values. The model calibration was repeated multiple times to find four groups of optimal BSC parameter values that produce time series fit to observations from four quad locations representative of the four RI classes. The selection criteria for these four quad locations are described detail below in sections 2.42. and 2.43. Further details of the procedure are also provided in Appendix E.

Two sets of observation time series were selected for calibration corresponding to the wettest and driest average precipitation six-month time periods of the entire five years of observations (10/1/2009 to 3/3/2010 and 4/1/2012 to 9/30/2012, respectively). The wet and dry calibration time series were centered on the defined growth and non-growth seasons (April-September and October-March, respectively) and selected from the periods with the greatest and lowest average of water inputs into the BSC layer (X). Each parameter set was sub-divided into two groups of parameters corresponding to those parameters best suited for optimization under the wet or dry conditions. For example, the field capacity was calibrated during the wet time period using the time series corresponding to the given parameter set (soil or specific RI group set). In this manner, the number of parameters calibrated for within each SCE procedure was minimized, increasing the computational efficiency.

Table 2 outlines the calibration scheme used to sequentially optimize the parameter sets of the soil layer and each function BSC group. Within each parameter set sequence, two calibration procedures were performed for each of the parameter subsets during the corresponding time period (wet or dry). For each procedure, optimal values were determined within a range of reasonable values determined from published literature. When quantitative measures of BSC parameters were not available from literature, calibration ranges were set relative to calibrated soil values based upon the proportional changes known to occur within soil matrices as BSC develop.

After all calibrations were complete, model fitness was verified both spatially and temporally for each parameter set combination (soil parameters + one RI class parameter set). The calibrated model was forced using meteorological data from (1) a 1.5 year period different from the calibration procedure (10/15/2012 to 3/23/2014) and (2) from the entire five year study period (12/2/2008 to 3/23/2014), and the simulated results were compared to (A) observations from the representative calibration quads and (B) observations at different quad locations of the same RI class for the given parameter set.

2.4.2 Calibration of Soil Layer and RI Class I Parameters

Since the soil texture is similar across the entire field site (Table 1), the soil parameter values were calibrated first at one representative time series and assumed equal for all other parameter groups. The soil parameter values were calibrated within a range of values known for sandy loam textures from previously published literature (e.g. Caylor *et al*. 2005; Laio *et al*. 2001; Manfreda *et al*. 2010; Porporato *et al*. 2003). The initial soil

Table 2: Summary of calibrated parameter subsets (wet or dry) for each parameter group (soil, or specific BSC RI class) and corresponding calibration time period (wet or dry) for each calibration step showing arrows indicating parameter group range across which the given calibrated parameter set was assumed valid and dashed lines to separate RI Class parameter ranges.

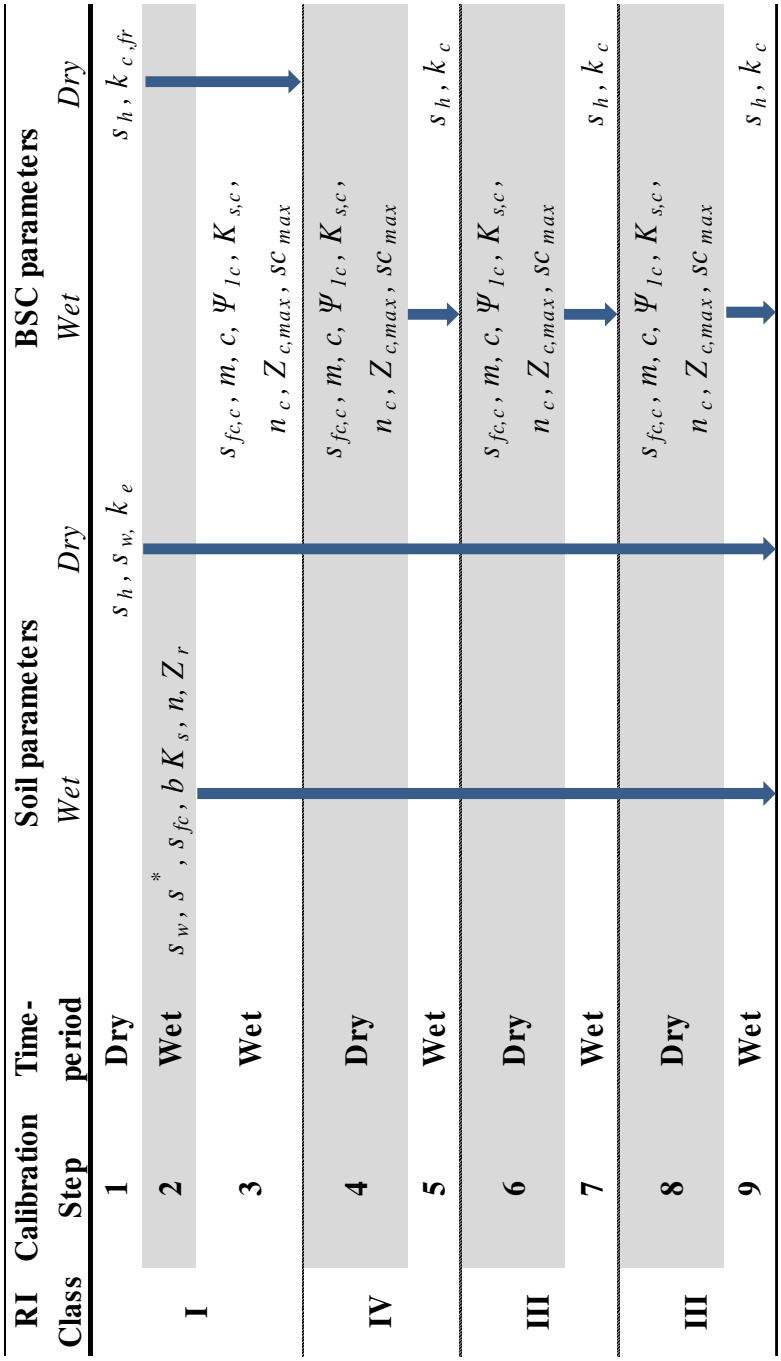

moisture value (s_0) was assumed equal to the average moisture measure observed on the day just previous to the start of the given calibration time period. The rooting depth Z_r was calibrated within the range of depth to bedrock (Z_b) measurements obtained at the DOE site (Appendix A).

The disturbances caused by the experimental watering to certain BSC plots were not mechanical in nature, and therefore, are assumed to not have caused direct damage to the underlying microstructure (Reed *et al*. 2012). Furthermore, since the main agents of stabilization (i.e. lichen-mosses and associated sub-surface anchoring structures) were most damaged by these experiments, the sites of the most damage have an increased chance of surface erosion, and sub-surface particle mixing from vegetative root and burrowing critters (Warren *et al.* 2001b). Similarly, these sites are assumed to have decreased connectivity between newly formed vesicular pores in the absence of channelization agents (Felde *et al*. 2014). The RI class I sites are, therefore, assumed as the least developed, with the most crustal damage, the thinnest BSC layers, and an increased potential reversion back to soil conditions. Thus, the quad with the lowest RI (B5-w) was selected as representative quad for soil calibration and for RI class I calibration.

Since the same quad was used to calibrate for the soil and RI Class I parameters, the calibration of their corresponding parameters occurred in sequence together. Table 3 lists the RI class I parameter spaces ranges, and a brief description of the literature review supporting their central assumed value. The central range value of $Z_{c,\max}$ was assumed equal to the average of reported measures for BSC sub-surface layers (Lan *et al.* 2012; Li *et al.* 2000). Assuming that the amount held at the surface is proportional in height to the

Table 3: Summary of value and range utilized for parameter space limits during calibration of each RI Class I parameter showing brief assumption descriptions.

BSC RI I class parameter	Assumed calibration value & range	Reasoning behind assumed calibration value
Porosity n_c $[mm^3\ mm^{-3}]$	$\approx n$ (0.3 - 0.5)	Least developed RI class renders a val.ue close to that of soil
Max BSC depth Zc,max *[mm]*	221 (74 - 360)	Average of depth of sub-BSC layers measured by Lan *et al*. (2012) and Li *et al*. (2000)
Max water surface capacity sc_{max} *[mm]*	2 (1 - 4)	Above-ground height of moss stem-leaf layer measured by Lan *et al*. (2012)
Sat. Hydraulic Conductivity $K_{s,c}$ $[mm\ d^{-1}]$	141 (104 - 178)	Average of hydraulic conductivity measured by Rossi *et al*. (2012) for sandy loam BSC
Pore distribution parameter b_c *[-]*	$\approx b$ (1 - 5)	Least developed RI class renders a val.ue close to that of soil
Pore disconnectedness c [-] *Pore size distribution index m [-]*	$= 2b_c + 3$ $= 2/(c-3)$	Equation from Laio *et al*. (2001) via Manfreda *et al*. (2010)
Saturated matric potential $\Psi 1c$ *[mm]*	132 (120 - 310)	Value associated with sandy loam (Cosby *et al*. 1984 via Manfreda *et al*. 2010)
Field Capcity $s_{fc,c}$ *Hygroscopic point* $s_{h,c}$	$\approx s_{fc}$ (0.2 - 0.6) $\approx s_h$ (0.01 - 0.35)	Least developed RI class renders a value close to that of soil
Replenishment factor fr	(0.005 - 0.4)	Moisture change due to adsorption measured by *Agam and Berliner* (2004) was very low
PET weighting factor kc	(0.1 - 0.9)	Wide range to account for lack of data

surface dwelling species, central range value of maximum surface capacity ($SC_{\max}$) set equal to measurements of above-ground height of moss stem-leafs (Lan *et al*. 2012). Given the dominance in percent cover by cyanobacteria, the central range value for saturated hydraulic conductivity ($K_{s,c}$) was assumed equal to the average of all hydraulic conductivity measurements from cyanobacteria-dominated, sandy loam textured samples reported by Rossi *et al*. (2012).

The central range values for the RI class I parameters lacking in literature reported values were iteratively set equal to the values of parallel soil parameters during the soil parameter calibration sequence (n_c, b_c, $s_{fc,c}$, and $s_{h,c}$ Table 3). For example, as the value of soil pore distribution parameter (b) was alternated within the given space, the value of the equivalent BSC parameter (b_c) equaled b for each iterative step. The values of pore disconnectedness (c) and pore size distribution index (m) were determined by the original equations defining their empirical relationship to the value b_c (eqs. 51-52). Similarly, the central range value of the BSC saturated matric potential (Ψ_1) was set equal to the value empirically determined for sandy-loam textures (Cosby *et al*. 1994 via Manfreda *et al.* 2010). For the newly defined BSC factors f_r and k_c with no soil parameter equivalent the parameter space range was set to a wide limit (0.1 to 0.9). Calibration began by optimizing for the dry soil and RI 1 parameters (k_e, s_h, s_w, s_h, f_r) within the defined ranges (Table 3) with wet parameters set to the central value of their calibration range ($s*$, s_{fc}, b, K_s and n;Table 3). In this manner, the resulting values could be used to set the lower limit threshold for the wet parameters during the subsequent wet calibration period.

2.4.3 Calibration of RI Class II-IV Parameters

The quad locations with RI measures close to the median values of their respective RI classes were chosen as the representative calibration quads for RI Classes II, III, and IV (C5-c, C3-c, and C5-x, respectively). Since the RI Class IV display the most developed features (e.g. RI, P_{LM}), the parameter values can be assumed greater or smaller relative to the values of the lower developed classes (Classes I-III). Thus RI Class IV parameters were optimized after the calibration of RI Class I in order to discover the limit of these relative parameter values ranges. Table 4 lists the relative parameter value ranges utilized for calibration of wet and dry parameters, and a brief description of the logic behind their selected values. BSC Class IV wet parameters (n_c,$K_{s,c}$,b_c,Ψ_1,$s_{fc,c}$) were calibrated first prior to the dry parameters ($s_{h,c}$, k_c) to increase computational efficiency relative to the number of parameters needed to be calibrated.

The value of the calibrated RI Class I parameters were utilized as the lower limit for the calibrated RI Class IV parameter space range. BSC porosity (n_c) was calibrated within a range lower than that of RI Class I to reflect the decrease in porosity with EPS enrichment (reviewed in Belnap 2006; Menon *et al*. 2011). Under the assumption that as more lichen-moss develop and create channels along their anchoring structures (Felde *et al.* 2014), saturated hydraulic conductivity ($K_{s,c}$; Table 4) was assumed to increase. The pore parameter (b_c) was calibrated within a lower range than the RI I calibrated value to yield lower *c* and higher *m* values, reflecting studies that show pore connectedness increases with lichen-moss channelization and that the pore size distribution increases with the entrapment of fine particles (Felde *et al.* 2014; Menon *et al.* 2011; Verrecchia *et*

Table 4: Summary of value and range utilized for parameter space limits during calibration of each RI Class IV parameter showing brief assumption descriptions.

BSC RI Class IV parameter	Value relative to lower RI Classes	Reasoning behind assumed relative value
Porosity n_c $[mm^3\ mm^{-3}]$	Decrease	Porosity decrease with EPS clogging (Verrecchia *et al.* 1995; Menon *et al.* 2011).
Max BSC depth $Z_{c,max}$ *[mm]*	No Change	$Z_{c,max}$ applies to entire field site (no change in value across RIs).
Max water surface capacity sc_{max} *[mm]*	No Change	sc_{max} applies to entire field site (no change in value across RIs).
Sat. Hydraulic Conductivity $K_{s,c}$ $[mm\ d^{-1}]$	Increase	Macropore channelization increases conductivity (Felde *et al.* 2014), potentially to values greater than those in Laio et al. (2001b)
Pore distribution parameter b_c *[-]*	Decrease	Decrease b_c to reflect decreasing disconnectedness (lower c) from macropore channelization and increaseing pore size distribution (higher m) with fine particle entrapment (Felde *et al.* 2014; Menon *et al.* 2011; Verrecchia *et al.* 1995).
Pore disconnectedness c [-]	$= 2b_c + 3$	
Pore size distribution index m [-]	$= 2/(c-3)$	
Saturated matric potential $\Psi 1c$ *[mm]*	Increase	Increased sorptivity with biomass (Felde *et al.* 2014; Menon *et al.* 2011).
Field Capcity $s_{fc,c}$ *Hygroscopic point* $s_{h,c}$	Increase	Higher water retention capaicty with increase in organic matter and entrapped fine particles (Wang *et al.* 1981; Campbell 1979; Verrecchia *et al.* 1995; Yair 2001; Felde *et al.* 2014; Menon *et al.* 2011).
Replenishment factor fr	Wider Range	Allowing wider range since literature does not list measured values
PET weighting factor kc	Wider Range	Evaporation could increase with darker mass or decrease with an increase in flux resistance (reviewed in Belnap 2006).

al. 1995; Table 4). The saturated matric potential (Ψ_1), field capacity ($s_{fc,c}$), and hygroscopic point ($s_{h,c}$) were assumed to increase with development to reflect the increased sorptivity and water retention capacity with higher amounts of biomass, organic matter, and fine particles (Wang *et al.* 1981; Campbell 1979; Verrecchia *et al.* 1995;Yair 2001; Felde *et al.* 2014; Menon *et al.* 2011). Finally, the parameter space range was again set to a wide limit (0.1 to 0.9) for the newly defined BSC factors f_r and k_c with no soil parameter equivalent.

The wet and dry RI Class III parameter subsets were calibrated next against the observations from quad C3c, again during the wet and dry time periods. Since crust roughness is known to progressively increase with crust development (Belnap *et al.* 2008), it is expected that the underlying crust parameters progressive increase or decrease with RI. By this reasoning, the values of RI III crust parameters were calibrated within ranges set by the values of RI II and IV. Lastly, RI Class II parameters were calibrated in the same manner as Class II with value ranges set by the calibrated values for Class I and III.

2.5 Biological Soil Crust Layer Simulations: Experiment Descriptions

In order to explore the isolated effects of the BSC level of development on the soil moisture balance, the modeled output was analyzed from four sets of experiment simulations, each involving multiple simulations over a number of plots displaying a spectrum of RI values. Since the lowest RI measured at the DOE site was 1.75 and the model was not parameterized to reproduce measurements obtained from sites completely devoid of BSC, the lowest RI value assigned to a simulation plot was 1. The highest RI

value assigned to a simulation plot was 21.75, or the maximum value observed at the field site. Within each RI class range, RI was incrementally increased so that each class includes 20 simulated sites for each of the experiments. Thus for each experiment, a total 80 simulated sites were analyzed each with a unique RI value and set of BSC parameters. At each experimental site, the model was forced with the precipitation and temperature observations from the entire five-year study period.

A control experiment (experiment 0) was first conducted to explore the moisture balance under the unaltered-calibrated conditions of the DOE site. In this base case scenario, the BSC parameter values for each site were estimated as a function of RI using equations derived from lines fit to the calibrated values of the six crust parameters that vary for each discrete class type (b_c, $K_{s,c}$, Ψ_1, n_c, $s_{fc,c}$, $s_{h,c}$, f_r, kc). Data points were added to the fit for $s_{fc,c}$ and $s_{h,c}$, at the maximum RI value (21.75) where $s_{fc,c}$ was set equal to 0.9, and $s_{h,c}$ set equal to 0.8 to ensure that the fitted lines respected the relative unit ranges of these two parameters. Both linear and exponential fits for each of the parameters types were tested.

A series of experiments (Experiments 1-3) were then performed to explore the relative dominance certain development characteristics thought to greatly affect infiltration and evaporation rates. This set of simulation experiments again involved using the entire five years of meteorological data as forcing over a spectrum of 80 simulated plots with a range of RI values between RI of 1 and the maximum (21.75), and a corresponding set of unique parameter values determined from the fit equations. For these three experiments, however, the rate of change r for selected BSC parameters with increasing RI was altered to test the relative dominance of each effect on the simulated

water balance outcome. This study acknowledges that numerous changes simultaneously occur within the development of BSC microstructures to affect the water balance, but chose to narrow the scope and examine two of the main effects reviewed in the literature: the clogging and channelization effects.

The rates of developmental changes for parameters (r) underlying these effects were altered in ways hypothesized to cause diminished infiltration and evaporation rates. Since the channelization effect and porosity effects are hypothesized to have opposite effects on the rate of infiltration and evaporation (i.e. channelization enhances and clogging diminishes; Felde *et al.* 2014; Verrecchia *et al.* 1995; Rutin 1983; Yair 1990; Lange *et al.* 1992; Kidron 1995; Kidron and Yair 1997; Kidron *et al.* 1999; Booth 1941; Rushforth and Brotherson 1982; George *et al.* 2003; Belnap 2006), opposite changes were applied to the rates of development for the associated parameters. In Experiment 1, the relative effect of clogging on the system was explored by increasing the rate of decrease in porosity n_c by 10% (r_{nc} multiplied by 10), thereby enhancing the clogging effect. In Experiment 2, the relative effect of channelization was explored by diminishing the rate of increase in saturated hydraulic conductivity $K_{s,c}$ by 10% (r_{Ksc} divided by 10), thereby diminishing the channelization effect. Finally, the combined effect of both of these changes (r_{nc} multiplied by 10 and) was explored in Experiment 3.

2.6 Biological Soil Crust Layer Simulations: Statistical Analyses

The main statistical analyses goals were to identify relative differences in BSC parameters that have significant effects on the soil moisture response during and after storm events, testing for differences in infiltration and loss rates produced under the given simulation experiments. A total of 86 storm periods were identified from the 2008-2013

DOE precipitation time series based on the following criteria: (1) storm event starts when $P_T \geq 3.5$ mm, and (2) soil moisture recessions either end seven days later or when another storm event of $P_T \geq 3.5$ mm begins. To compare drying rates across sites, the soil moisture residence time (τ in days) and BSC moisture residence time (τ_c in days) was calculated from the equation fit to the simulated relative moisture (s or s_c) during drying events following each (Figure 14):

$$s(t) = a \cdot e^{-t/\tau} \tag{68}$$

where t is time in days and a is a dimensionless constant. Some post-storm instances (<1% of events) were excluded where s (or s_c) decreased by < 1 % and τ estimates exceeded 200 days. The change in relative moisture Δs (or Δs_c) between the maximum s (or s_c) simulated in a storm period on a given day $s_{\max}$ and the antecedent moisture of day prior s_a was also calculated for each storm (Figure 14):

$$\Delta s(t) = s_{\max} - s_a \tag{69}$$

By quantifying increases in soil moisture following inputs, Δs (or Δs_c) is a metric for comparing parameters affecting infiltration rates across simulated plots. Negative Δs (or Δs_c) values (<3% of events) were excluded from the analyses.

Since the model accounts for the previous soil moisture status when estimating the current value, it intrinsically incorporates correlations of soil moisture across time. Thus, the given response metric of each storm event, either $\Delta\theta$ or τ, was considered independent, and significant differences were tested across experiment quads due to relative differences in BSC cover. RI class was evaluated as the predictor variable and the Δs (or Δs_c) and τ (or τ_c) datasets were subsampled into four sets based upon the

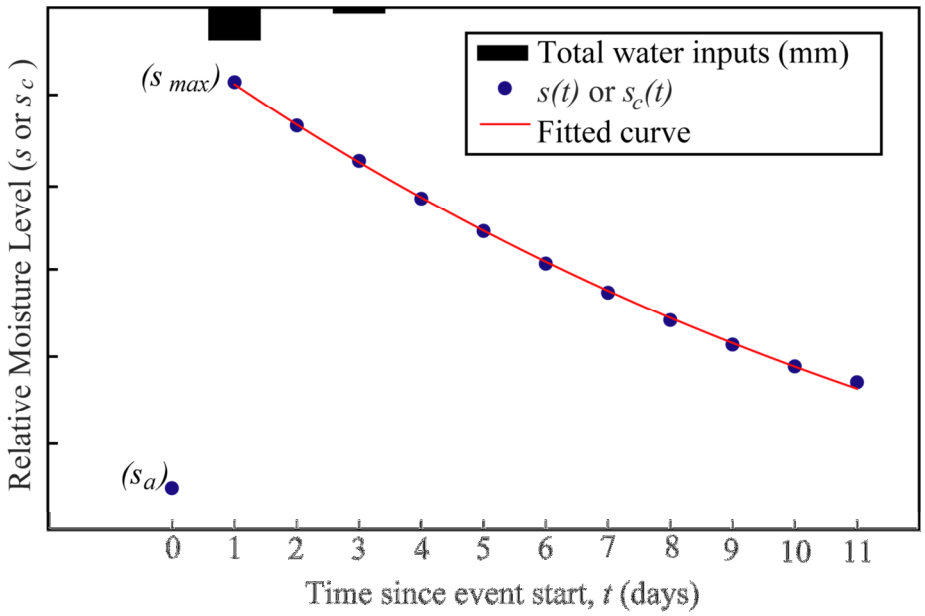

Figure 14: Example storm event and drying period showing simulate relative moisture (s or s_c) with italicized labels of maximum relative moisture (s_{max}) and antecedent moisture (s_a) used for the estimation of change in relative moisture (Δs or Δs_c) and fitted moisture decay curve used for estimation of moisture residence time (τ or τ_c).

corresponding *RI* class of the quad for the given RI measure. Two linear models were fit with RI class as a predictor of (1) Δs (or Δs_c) or (2) τ (or τ_c). Significance levels of $p < 0.05$ (i.e. $\alpha = 0.05$) are discussed for assumptions tests. Due to unmet assumptions, Kruskal-Wallace one-way analyses of variance and non-parametric multiple-comparisons were performed on the raw τ (or τ_c) and Δs (or Δs_c) datasets. Multiple Mann-Whitney tests of significance were performed between the raw τ (or τ_c) and Δs (or Δs_c) values of each class, applying a Bonferoni correction to account for the multiple-comparisons. Given this Bonferoni correction, α was divided by the number of comparisons (6) and significance levels of $p < 0.008$ are discussed for the Mann-Whitney multiple comparisons. The results of these multiple-comparisons tests are also used to distinguish significance visually in the figures displaying the results through indices.

3 RESULTS AND DISCUSSION

3.1 Model Calibrations and Parameter Line Fits

The sequence of optimization runs performed for the calibration of each RI Class subgroup resulted in high convergence of values within the specified ranges, as indicated by low standard deviation of calibration output. Table 5 shows the calibrated values for all soil layer and RI Class parameters. Figure 15 shows the parameter values for the base case conditions (Experiment 0), calculated from the equation fits to the calibrated values. Due to the higher R^2 values (table 6), $s_{fc,c}$ was estimated from RI using a linear fit equation (eq. 73) and all other parameters were estimated from RI using exponential equations:

$$b_c = 3.266 \cdot e^{-0.0266 \cdot RI} \tag{70}$$

$$K_{sc} = 82.6206 \cdot e^{0.1348 \cdot RI} \tag{71}$$

$$n_c = 0.3388 \cdot e^{-0.0171 \cdot RI} \tag{72}$$

$$s_{fc,c} = 0.1665 - 0.0366 \cdot RI \tag{73}$$

$$s_{h,c} = 0.0698 \cdot e^{0.1131 \cdot RI} \tag{74}$$

$$\Psi_1 = 117.87 \cdot e^{0.0624 \cdot RI} \tag{75}$$

$$f_r = 0.4565 \cdot e^{0.0360 \cdot RI} \tag{76}$$

$$k_c = 0.4788 \cdot e^{0.0209 \cdot RI} \tag{77}$$

Table 5: Summary of final calibrated parameter values for soil and BSC classes.

Parameter	Calibrated value			
	RI Class			
BSC	**I**	**II**	**III**	**IV**
Porosity n_c $[mm^3\ mm^{-3}]$	0.33	0.3	0.29	0.27
Max BSC depth Zc,max *[mm]*	79	79	79	79
Max water surface capacity sc_{max} *[mm]*	2	2	2	2
Sat. Hydraulic Conductivity $K_{s,c}$ $[mm\ d^{-1}]$	163	176	263	506
Pore distribution parameter b_c	3.1	2.8	2.5	2.3
Pore disconnectedness c	$= 2b_c + 3$	$= 2b_c + 3$	$= 2b_c + 3$	$= 2b_c + 3$
Pore size distribution m	= 2/(c-3)	$= 2b_c + 3$	= 2/(c-3)	= 2/(c-3)
Saturated matric potential Ψ_{1c} $[mm\ d^{-1}]$	131	176	216	267
Field Capcity $s_{fc,c}$	0.27	0.28	0.47	0.84
Hygroscopic point $s_{h,c}$	0.08	0.09	0.12	0.44
BSC replenishment factor fr	0.51	0.51	0.7	0.72
BSC PET weighting factor kc	0.5	0.54	0.59	0.63
Soil				
Porosity n $[mm^3\ mm^{-3}]$	0.44			
Rooting depth Z_r *[mm]*	303			
Sat. Hydraulic Conductivity K_s $[mm\ d^{-1}]$	125			
Pore distribution parameter b	1.4			
Hygroscopic point s_h	0.017			
Wilting point s_w	0.15			
Stress threshold s^*	0.17			
Field Capcity $s_{fc,c}$	0.2			
Bare soil PET weighting factor k_e	0.68			

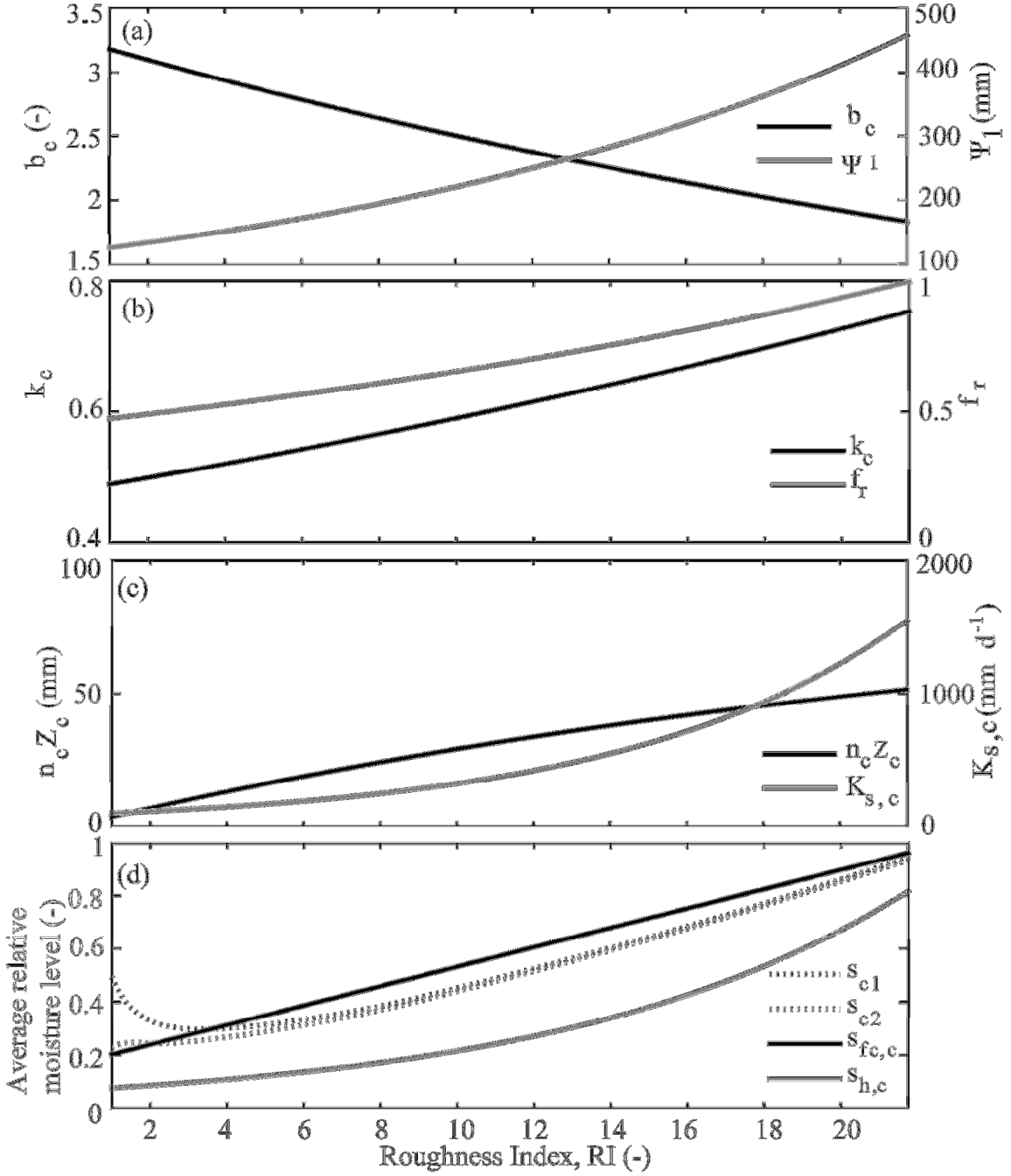

Figure 15: BSC parameter values utilized in experiment 0 for each simulated quad across a range of RI (1 to 21.75). Parameters include (a) the BSC pore parameter b_c, (a) matric potential at saturation Ψ_1 (mm), (b) PET weighting factor k_c, (b) replenishment factor f_r, (c) BSC storage capacity n_cZ_c (mm), (c) saturated hydraulic conductivity $K_{s,c}$ (mm d^{-1}), and (d) field capacity $s_{fc,c}$ and hygroscopic point $s_{h,c}$.

Table 6: Summary of R2 values for linear and exponential equation fits to BSC parameters.

	R^2 value	
	Linear	*Exponential*
b_c	0.994	0.992
$K_{s,c}$	0.767	0.921
Ψ_1	0.99	0.999
n_c	0.985	0.987
$s_{fc,c}$	0.836	0.772
$s_{h,c}$	0.888	0.928
f_r	0.796	0.809
k_c	0.988	0.992

Model performance was assessed using three metrics to compare the observations (O) and simulations (S) of soil moisture over the number of time steps (N). The first metric, the root mean square error (RMSE) describes the sample standard deviation of the differences between O and S, using the following equation:

$$RMSE = \sqrt{\frac{\sum_{i=1}^{N}(O_i - S_i)^2}{N}} \tag{78}$$

The second metric, the correlation coefficient (CC), measures the linear relation between S and O, using the following equation:

$$CC = \frac{\sum_{i=1}^{N}(O_i - \overline{O})(S_i - \overline{S})}{\left[\sum_{i=1}^{N}\left(O_i - \overline{O}\right)^2\right]^{0.5}\left[\sum_{i=1}^{N}\left(S_i - \overline{S}\right)^2\right]^{0.5}} \tag{79}$$

where the overbar denotes a temporal mean value. CC varies from -1 (negative correlation) to 1 (positive correlation), with CC = 0 indicating no correlation. The third

metric, the dimensionless bias (*bias*) is obtained as the ratio of temporal mean of the simulated and observed variables, as:

$$bias = \frac{\overline{S}}{\overline{O}} \tag{80}$$

Table 7 shows the root mean square error (RMSE), correlation coefficients (CC), and bias of fit for three different moisture time series comparisons: (A) Observed moisture vs. simulated moisture from the calibrated model using the four discrete RI class parameter (i.e. discrete model), (B) Observed moisture vs. simulated moisture from the calibrated model using the continuous RI Class parameters derived from the equation fits made to the calibrated values (i.e. continuous model), and (C) simulated moisture from the discrete vs. simulated model. In each case, the model was forced by meteorological observations from one of the two verification periods (1.5-year and entire study period) and tested against the moisture observations from the corresponding verification period. These six comparisons (A, B, and C in two different time periods) were made with soil moisture observations taken from the four representative calibration quad locations and from one verification plot for each RI class. These comparison metrics suggest that the model adequately simulates the observations (Table 7).

Figure 16 shows example time series comparisons used to verify the ability of the model to reproduce the observations using the discrete RI Class calibrated parameters

Table 7: Root mean square error (RMSE), correlation coefficient (CC) and bias of fits between (A) observations vs. discrete BSC parameter simulations, (B) observations vs. continuous BSC parameter simulations, and (C) discrete vs continuous BSC parameter simulations for soil moisture observations taken from all representative calibration quad locations (with asterisk) and from one verification plot for each RI class during the six-month verification period and the entire study period. Simulations were forced with meteorological data of corresponding verification time period.

RI class	Quad	Comparison	Entire study period			1.5 year verification period		
			RMSE	*CC*	*bias*	*RMSE*	*CC*	*bias*
1	B5w *	*A*	0.021388	0.896	1.031	0.016776	0.923	1.017
		B	0.020913	0.898	0.994	0.016705	0.921	0.982
		C	0.003204	0.999	0.964	0.003506	0.998	0.966
	B5x	*A*	0.025149	0.834	0.829	0.015791	0.915	0.911
		B	0.023953	0.84	0.864	0.014705	0.92	0.953
		C	0.002992	0.999	1.043	0.00356	0.998	1.045
2	B2w	*A*	0.025321	0.845	0.937	0.02724	0.867	0.822
		B	0.024718	0.85	1.019	0.024522	0.872	0.889
		C	0.006088	0.996	1.087	0.005793	0.997	1.082
	C5c *	*A*	0.022027	0.899	0.834	0.015205	0.923	0.961
		B	0.018027	0.918	0.934	0.016458	0.917	1.064
		C	0.008484	0.991	1.12	0.00767	0.995	1.107
3	B1x	*A*	0.027361	0.829	0.853	0.017767	0.885	0.954
		B	0.031975	0.827	0.733	0.02212	0.882	0.828
		C	0.012251	0.986	0.859	0.011979	0.988	0.868
	C3c *	*A*	0.020256	0.9	0.913	0.023704	0.829	1.116
		B	0.022461	0.901	0.826	0.02057	0.85	1.028
		C	0.007824	0.995	0.905	0.007269	0.994	0.922
4	B4c	*A*	0.027421	0.816	1.154	0.020576	0.887	1.027
		B	0.026571	0.826	1.151	0.019917	0.894	1.018
		C	0.00221	0.999	0.998	0.001744	0.999	0.991
	C5x *	*A*	0.025287	0.851	0.887	0.022328	0.86	0.917
		B	0.023946	0.858	0.928	0.021202	0.866	0.951
		C	0.003702	0.999	1.046	0.003511	0.998	1.037

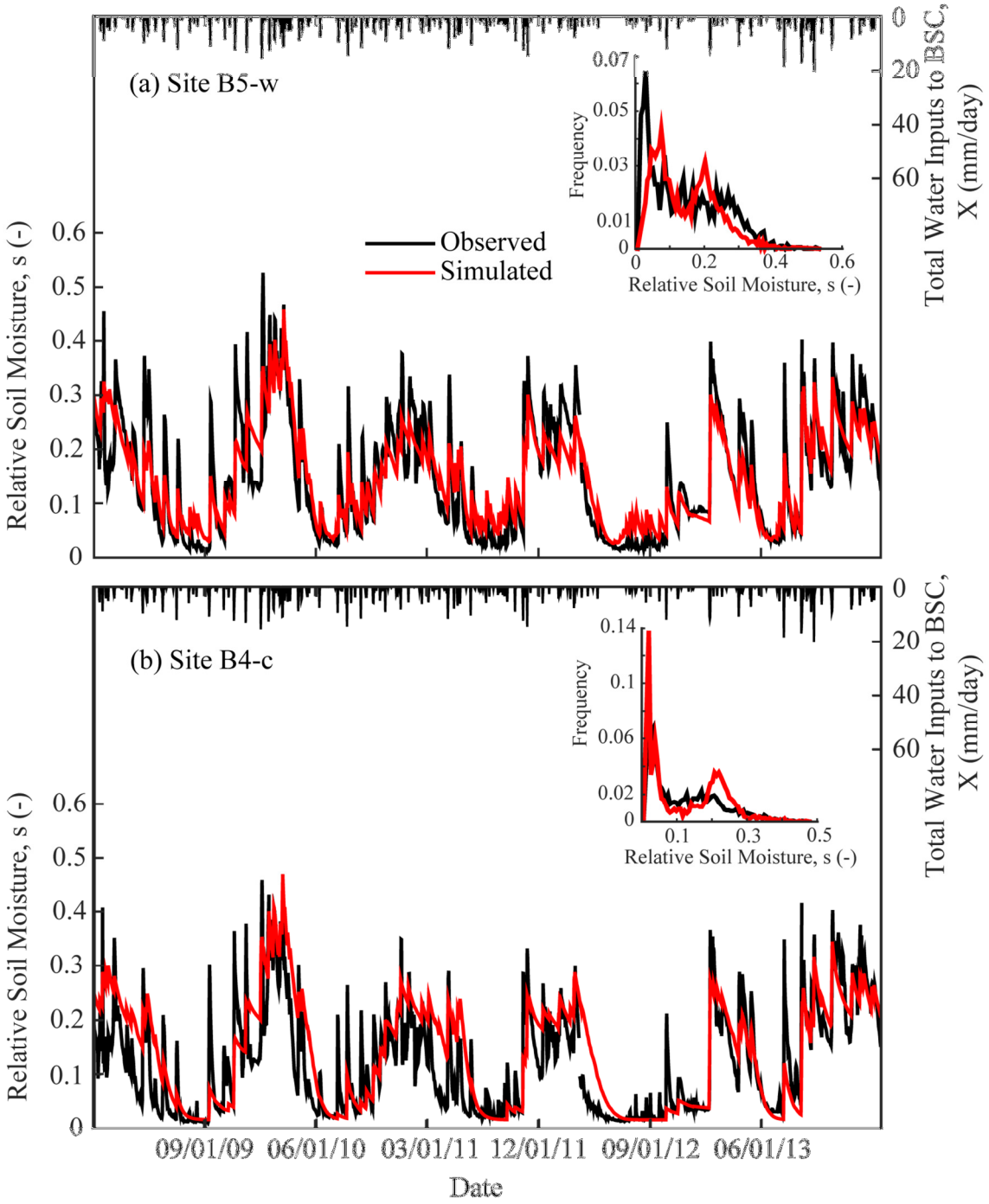

Figure 16: Time series and frequency diagram of modeled and observed relative soil moisture at (a) representative calibration quad for RI Class I (B5-w) and (b) RI Class IV verification quad location (B4-c) during the entire study period. Simulations utilized discrete calibrated parameter sets for (a) RI Class I and (b) RI Class IV. Inset shows frequency distribution in which ordinate values represent frequency of *s* within a bin interval of 0.01, relative to the total number of soil moisture values.

during the entire timeperiod (i.e. temporal verification). In Figure 16a, the simulated fit was tested against the observations of the representative RI Class I calibration quad (B5-w). In Figure 16b, the simulated fit was also tested spatially against the observations of a representative RI Class IV calibration quad (B4-c).

Within these time series, the simulated moisture values match the seasonal variations displayed in the observations. These minimal seasonal differences are also exemplified by the relatively low RMSE estimates for the time series compared in each figure (0.0225, and 0.0247, for Figures 16a, 16b, respectively; Table 7). Furthermore, their respective CC values (0.0896 and 0.816, respectively; Table 7) are relatively high, indicating high correlation. The model was unable to reproduce the peak moisture values resulting from certain storm inputs, as exemplified by the probability distribution functions (insets in Figure 16). This is attributed to a slight underestimation of the moisture inputs in certain instances. The observed moisture decay curves, however, are matched almost exactly by the simulation, suggesting that the loss rates are captured nearly accurately by the model. Due to the success of capturing the moisture decays, which dominate the composition of the moisture time series, the simulated values are on average a close match to the average observation. This is indicated by the near 1 to 1 ratio of the *bias* (1.031 and 1.154, Figures 16a, 16b, respectively; Table 7).

Figure 17 simulations utilize the continuous parameters estimated from equations 70-19 as a function of the RI for two plots from different RI Classes (Table 2) during the entire timeperiod (i.e. temporal verification). In Figure 17a, the simulated fit was tested against the observations of the representative RI Class III calibration quad (C3-c; RI = 5.7). In Figure 17b, the simulated fit was also tested spatially against the observations of

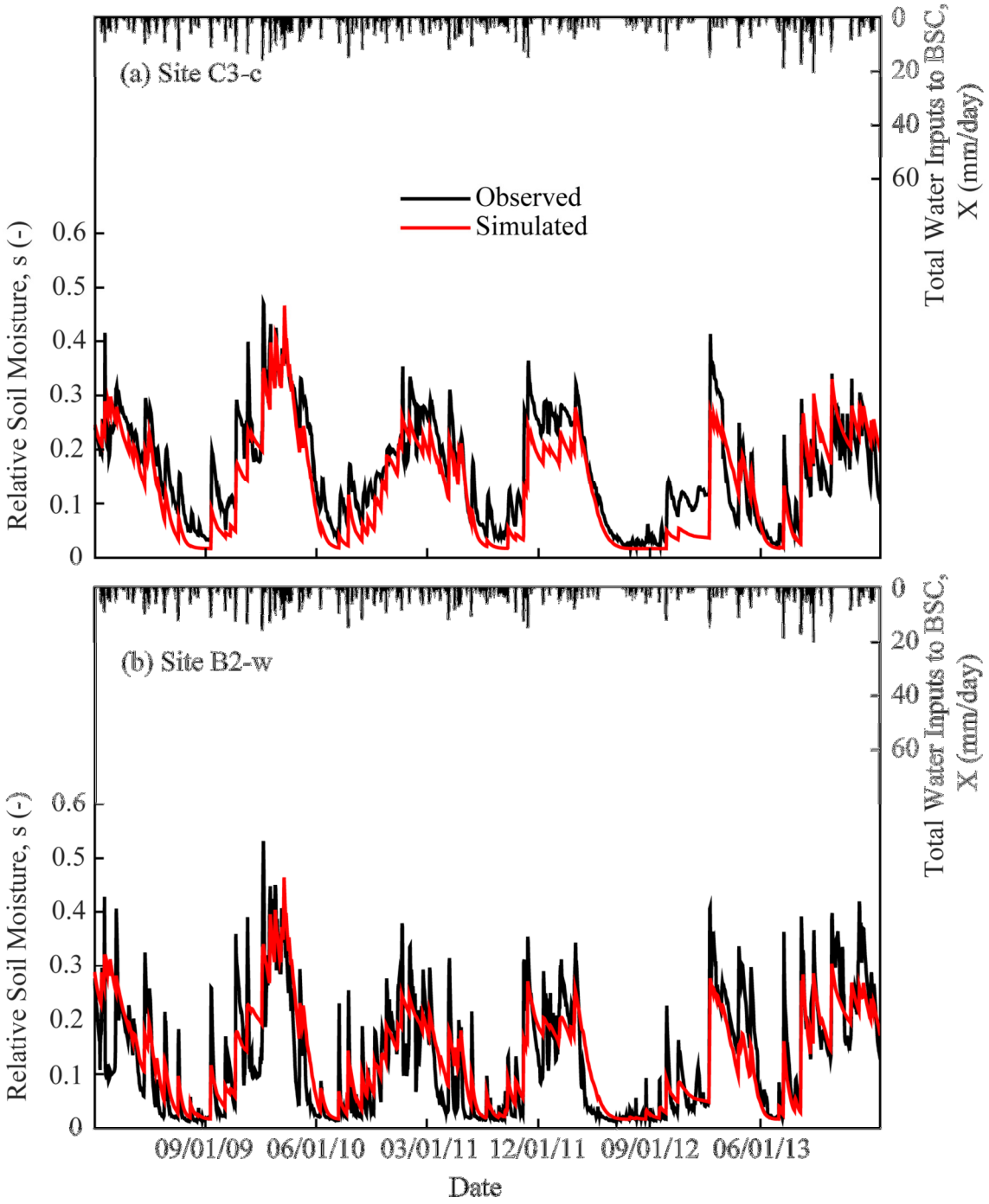

Figure 17: Time series and frequency diagram of modeled and observed relative soil moisture at (a) representative calibration quad for RI Class III (C3-c) and (b) RI Class II verification quad location (B2-w) during the entire study period. Simulations utilized parameters estimated as a function of quad RI (eqs. 70 – 77).

a representative RI Class II calibration quad (B2-w; RI = 9.69). The simulation in Figure 17a slightly underestimates the observations as indicated by the slightly lower *bias* (0.826 and 1.1019, for Figures 17a and 17b, respectively), and is attributed to a slight over estimation of the losses. Again, however, the simulations in both Figures 17a and 17b produced optimal fits to the seasonal variations in observations, with optimally minimized RMSE values (0.0225 and 0.0247, respectively, Table 7) and high CC values (0.901 and 0.85, respectively).

The verification results (Figures 16, 17; Table 7) support the assumption that each parameter increases or decreases progressively with development such that the value of each parameter can be estimated as a function of RI (eqs. 70-77). These results also support the assumptions used to define these parameter trends with development (Table 4). Furthermore, the calibration results (Table 5) reveal that applying an increasing value trend is optimal for the newly defined parameters f_r and k_c, which were allowed to vary within a wide parameter space range (Table 4). The increase in f_r with RI suggests that replenishment increases with development perhaps due to the increases in biomass and roughness that could cause an increase in surface area and adsorption (reviewed in Agam and Berliner 2005). This increase in k_c with RI suggests that the evaporation demand placed on the BSC surface increases with development perhaps due to the increases in surface temperature associated with darker surface colors (reviewed in Belnap 2006).

3.2 Experiment Simulations

Based on the ability of the calibrated model to reproduce soil moisture conditions across a range of development, simulations were run under enhanced clogging and/or

diminished channelization conditions through the alteration of the rate of change in BSC porosity (r_{nc}) and saturated hydraulic conductivity (r_{Ksc}) with RI. Figure 18 shows the BSC storage capacity (n_cZ_c) and $K_{s,c}$ as a function of RI for each experiment simulation set. Due to BSC thickening (increasing Z_c; eq. 41), n_cZ_c increases under Experiment 0 and 2 conditions, but at a de-accelerating rate due to BSC clogging (decreasing n_c). In Experiments 1 and 3, the rate of decrease in n_c gathered from equation 70 was enhanced by a factor of 10 (r_{nc} changed from -0.0171 to -0.171) to explore the hypothetical situation where clogging results in BSC storage capacity decreases despite BSC thickening (lower n_cZ_c despite higher Z_c). In Experiments 2 and 3, the rate of decrease in $K_{s,c}$ gathered from equation 69 was decreased by a factor of 10 (r_{Ksc} changed from 0.1348 to 0.01348) to explore the hypothetical situation where channelization is almost constant across development. By exploring these extreme situations, this study is able to distinguish the potential mechanisms underlying the given phenomenon (clogging and/or channelization) that alter the hydrologic balance and are perhaps too subtle to detect under less accentuated conditions.

The results of these experiments are presented in two sections below. The first section explores the water balance within the BSC layer and within the soil layer resulting from each experimental condition. In this section, the temporal average and standard deviation of relative soil and BSC moisture (average and standard deviation of s and s_c) are computed for each simulated plot under each experimental condition and compared within and between experiments (0 through 3). The total water balance of a given layer is also computed for each simulated plot by (1) totaling all values of a given layer loss and totaling all values of a given layer input across the entire five-year

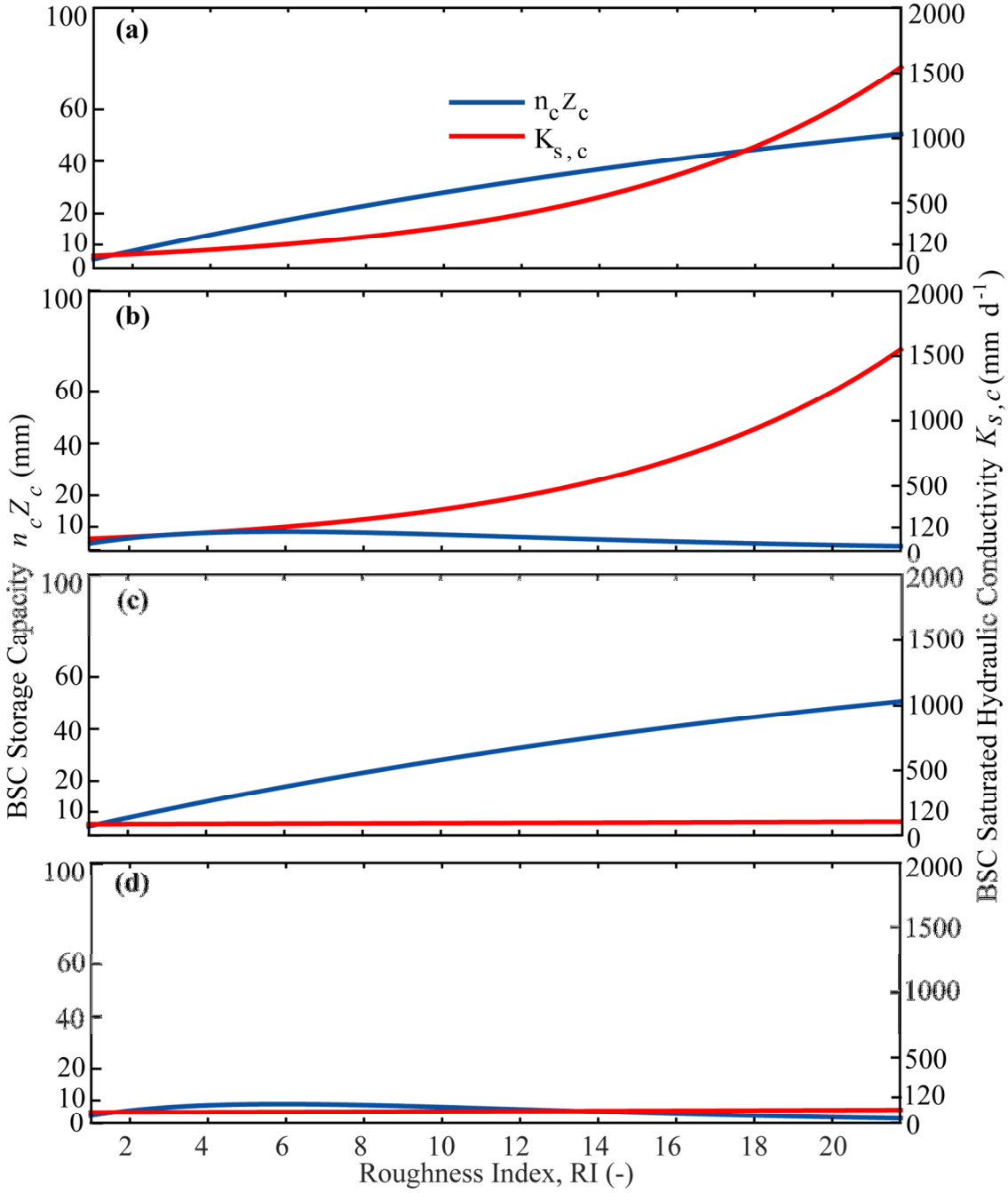

Figure 18: Parameter values utilized to BSC storage capacity n_cZ_c (mm) and saturated hydraulic conductivity $K_{s,c}$ (mm d^{-1}) as a function of RI for (a) calibrated-base case conditions (Experiment 0), (b) enhanced decrease in n_c (i.e. enhanced clogging in Experiment 1), (c) diminished increase in $K_{s,c}$ (i.e. diminished channelization in Experiment 2), and (d) both added rate changes (i.e. enhance clogging with diminished channelization in Experiment 3).

simulation period, (2) dividing each of the total loss components by the total input, and (3) multiplying by 100 to obtain a percentage of the total loss for each component. All of the computed loss component percentages for each simulated plot of a given experiment are then plotted against the RI of the given simulated plot. In this way, a plot of the partitioning of inputs across the spectrum of simulated RI is created for each of the soil and BSC layers of each of the experiments. This same procedure and plotting was repeated to compare the partitioning of the total potential evaporation (*PET*) between the ponded evaporation (E*p*), BSC evaporation (E_c), and total soil evapotranspiration ($ET_{s,t}$) for each experiment. Appendix G contains the roughness index (RI), total inputs, and partitioning of inputs in the BSC and soil layers, as well as the surface layer, for each simulated plot for each experiment in tabular form. This appendix also contains a table for the *PET* partitioning listed as fractions of the total *PET*.

The second section below explores and compares the infiltration and loss rates of each storm and subsequent decay period (i.e. Δs, Δs_c, τ, and τ_c) as estimated from the procedure and equations outlined in section 3.2.2. The average of each of these metrics is compared from each RI Class of each experiment and compared statistically according to the methods outlined in section 3.2.2. This section is in turn divided into two sub-sections; one for presenting the results of the metrics computed using the soil layer moisture, and the other for the BSC layer.

Also included below is a third section devoted to reflection and discussion of the implications of the presented results in general and in the context of previous studies.

3.2.1 Water Balance Comparisons

The average moisture within the BSC and soil layers exhibit different trends with development. Under all experiment conditions, for example, the average relative BSC moisture (s_c) increases with BSC development (increasing RI; Figure 19). This increase in average s_c is attributed to both the increase in BSC retention capabilities against leakage and evaporation (increasing $s_{fc,c}$ and $s_{h,c}$; Figure 15d), and the enhanced recycling of moisture within the system adding replenishment to the BSC layer (increasing f_r; Figure 15b). The trend in average relative soil moisture s, however, appears to vary across development and experimental conditions (Figure 19). These variations can be explored through comparisons of the experimental conditions and water balance partitioning in the BSC and soil layers (e.g. Volo *et al*., 2014; Laio *et al*., 2001) across development.

Figure 20 shows how the total water inputs into the BSC layer (X) across the five-year time period is partitioned into BSC evaporation (E_c), leakage from BSC to soil (L_c), and excess infiltration (E_{xi}), for each experiment with increasing RI. The trend in average s with development (Figure 19) appears proportional to the trend in the total percentage of BSC inputs (X) lost to L_c for all experiments (Figure 20), suggesting that average s is greatly influenced by the amount of soil inputs (L_c). At the lowest RI, for example, the low retention capacity against leakage (i.e. low $s_{fc,c}$; Figure 15d) results in a greater proportion of X lost to L_c (Figure 20) and relatively high average s (Figure 19). As RI increases in these earliest stages of development (RI equal to 1 to 3.5), the rates of L_c and resulting average s decrease exponentially reflecting the increase in $s_{fc,c}$(Figures 20,19,15d). Past this early development stage, the increase in average s_c heightens the

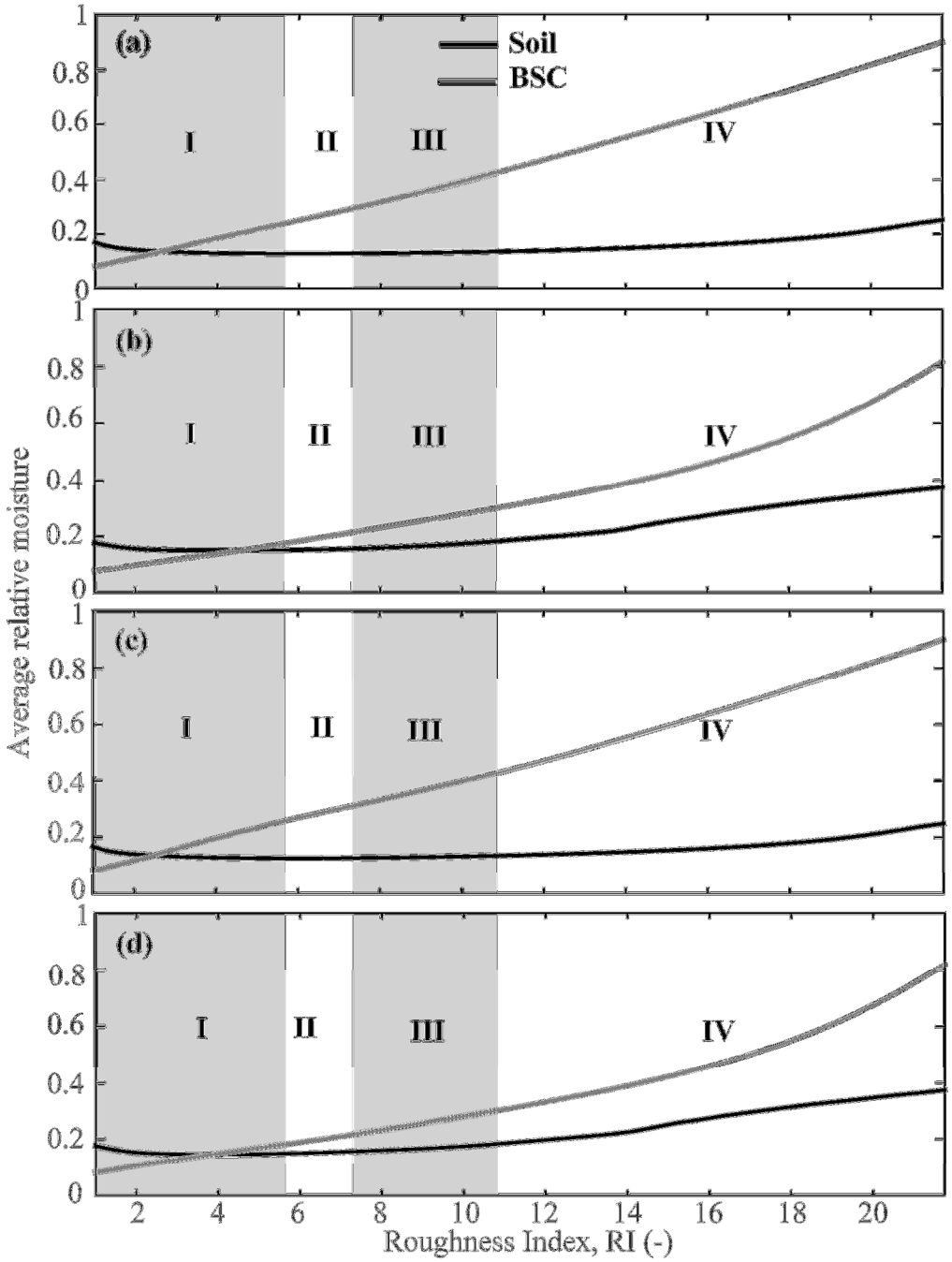

Figure 19: Temporal average of relative moisture simulated in the soil and BSC layers across a range of roughness indices (RI) values (1 - 21.75) using BSC parameters under (a) DOE conditions (Experiment 0), (b) diminished clogging (Experiment 1), (c) diminished clogging (Experiment 2), and (d) enhanced clogging and diminished channelization (Experiment 3). Greyed and white areas highlight RI classes, labeled with roman numerals (I - IV).

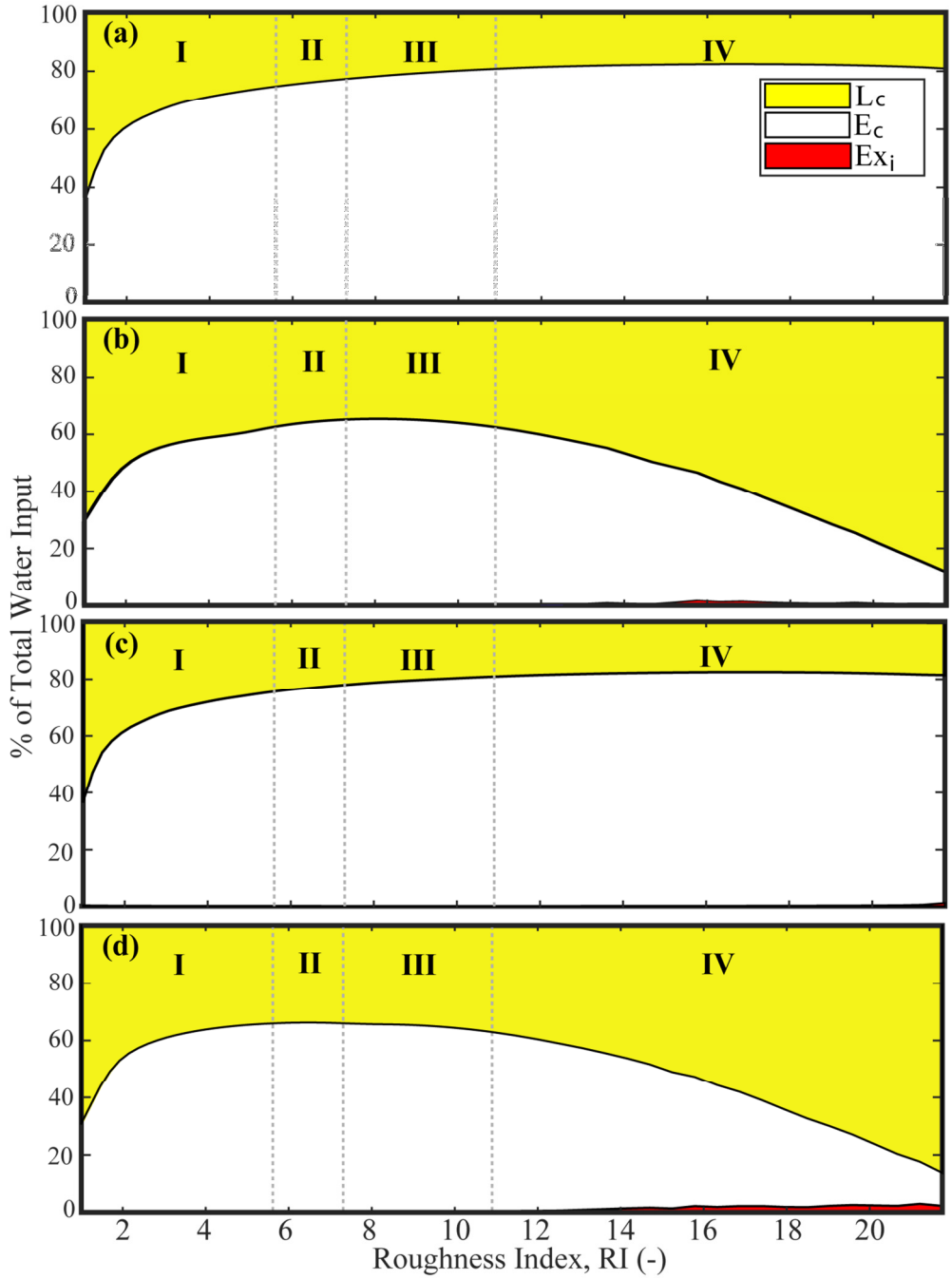

Figure 20: BSC water balance partitioning for varying roughness index (RI) using BSC parameters under (a) DOE conditions (Experiment 0), (b) diminished clogging (Experiment 1), (c) diminished clogging (Experiment 2), and (d) enhanced clogging and diminished channelization (Experiment 3). L_c is leakage from the crust layer, E_c is evaporation from the crust, and Ex_{inf} is infiltration excess, all represented as percentage of total inputs (X). Dotted lines separate RI classes, labeled with roman numerals (I - IV).

chance of exceeding $s_{fc,c}$ and diminishes the rates of decrease in total L_c and average s with increasing RI (Figures 19, 20).

Under all experiment conditions, the total L_c losses and average s increase beyond certain RI thresholds (Figure 20). Comparisons across experiments suggests that the that reversed trend in L_c and resulting average s is due to an increased chance of exceeding $s_{fc,c}$ after a certain level of clogging has significantly reduced the storage space for s_c. In base case conditions (Experiment 0), for example, average s and total L_c increase beyond RI thresholds of about 11 and 19 (Figures 19a, 20a). Enhancement of the clogging effect (Experiment 1) appears to not only accelerate the rate of increase in average s and total L_c for later development, but also lowers the RI thresholds that define the reversed trends of average s and total L_c to about 7 and 8, respectively (Figures 19b, 20b). The diminished channelization (Experiment 2) appears to slightly lower the rate of increase in average s and total L_c past slightly higher RI thresholds of development equal to about 12 and 20, respectively (Figures 19c, 20c). When both experimental alterations are applied (Experiment 3), the resulting trend in average s resembles that of Experiment 1 (Figures 19, 20), suggesting that the total L_c and average s for any LOD is more affected by changes in n_c (Experiment 1) than $K_{s,c}$ (Experiment 2), and/or the parameter rates with development (r_{nc} and r_{Ksc}) require different magnitude changes to produce proportionally equal and opposite effects. In either case, the reduced storage capacity by the clogging effect appears to significantly reduce the BSC storage capacities such that more moisture is sent out of the BSC layer via leakage.

Although the BSC leakage rates (L_c) are enhanced under these more developed and clogged conditions, the accelerated soil inputs do not appear to exceed the saturation

capacity of the soil system. Figure 21 shows how the total L_c across the five-year time period is partitioned into soil evaporation below the wilting point ($E_{s,b}$), stressed soil evapotranspiration ($ET_{s,s}$), unstressed soil evapotranspiration ($ET_{s,u}$), and soil leakage (L_s), for each experiment with increasing RI. Under all experiment conditions, none of s is lost to excess saturation (Ex_s) since the soil capacity (nZ_r) is great enough to hold all inputs before reaching saturation (Figure 21; Table 5).The experimental effects, however, do appear to significantly lower the infiltration capacity of the surface and impede moisture entry into the BSC layer. At the lowest RI values under all experimental conditions, for example, less than 1% of BSC moisture is lost to Ex_i due to the relatively low pore connectedness (higher c), low pore size distribution (lower m), decreased sorptivity (i.e. decreased saturated matric potential, Ψ1), and low saturated hydraulic conductivity (lower $K_{s,c}$) (Figures 15,Appendix G). When either the BSC storage capacity is reduced further by the clogging effect (lower n_c) or the $K_{s,c}$ is reduced by a diminishment in channelization, additional moisture added to the surface lost by Ex_i at both the lowest and most developed RI (Experiments 1-2 Figure 21; Appendix G).These two effects compounded together cause even larger increases in Ex_i , and produce large increases in runoff (Q) generation (Experiment 3; Appendix G). Given the increase in surface capacity accompanying the increase in RI (SC; eq. 40), however, runoff (Q) decreases with development (Appendix G).

Furthermore, the trends in BSC leakage (L_c) directly affect the rates of BSC evaporation and the partitioning of evaporative demand amongst the system. Figure 22 shows how total potential evapotranspiration (total PET) is partitioned between the evaporative losses of the surface (E_p) and BSC (E_c), and the total soil evapotranspiration

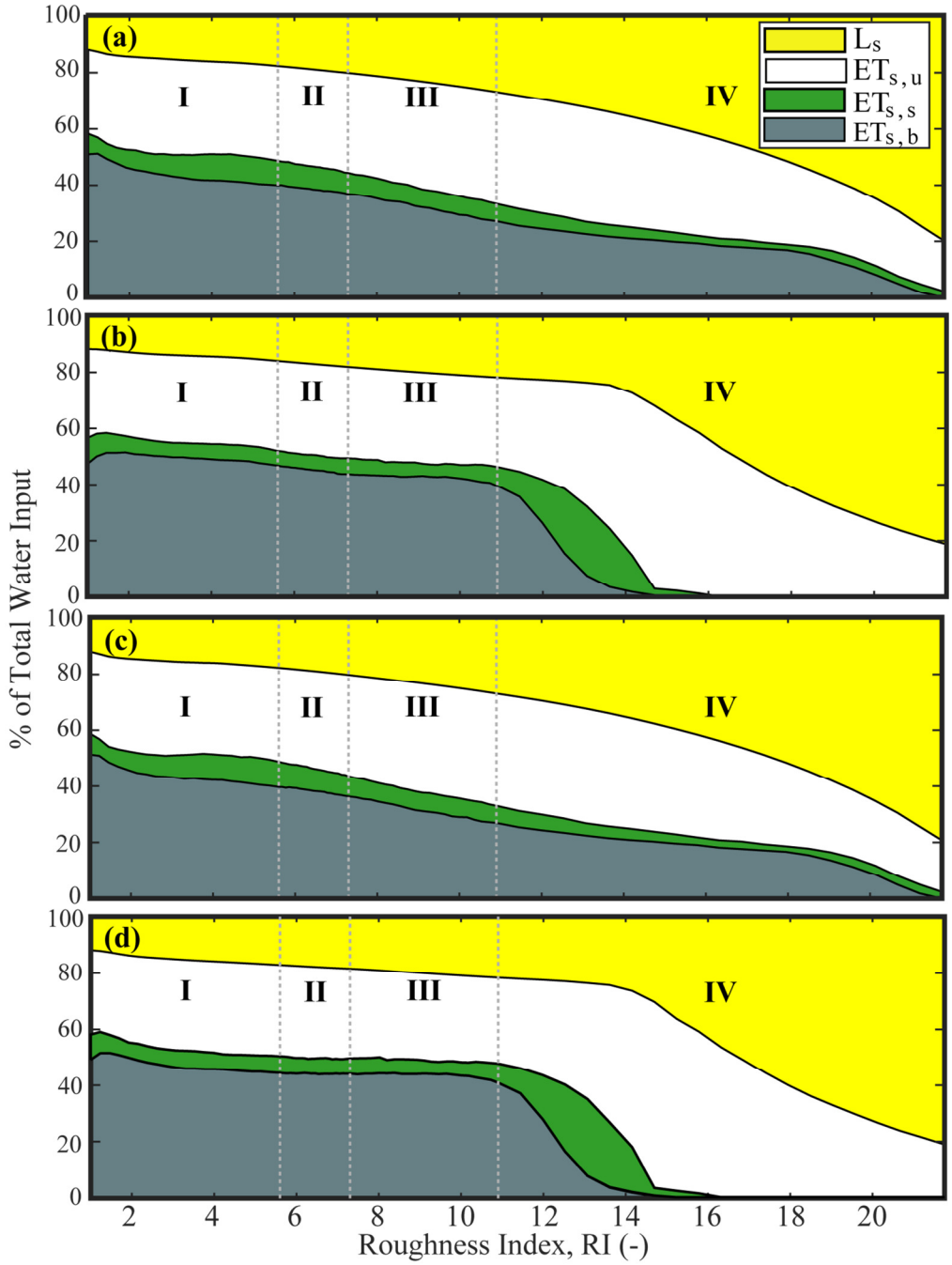

Figure 21: Soil water balance partitioning for varying roughness index (RI) using BSC parameters under (a) DOE conditions (Experiment 0), (b) diminished clogging (Experiment 1), (c) diminished clogging (Experiment 2), and (d) enhanced clogging and diminished channelization (Experiment 3). $ETs_{,u}$ is unstressed soil evapotranspiration ($s^* < s \leq s_{fc}$), $ET_{s,s}$ is stressed soil evapotranspiration ($s_w < s \leq s^*$), $E_{s,b}$ is bare soil evaporation ($s \leq s_w$), L_s is leakage from the soil layer, all represented as percentage of total inputs (L_c). Saturation excess (Ex_{sat}) is not shown since none occurred for any experiment. Dotted lines separate RI classes, labeled with roman numerals (I - IV).

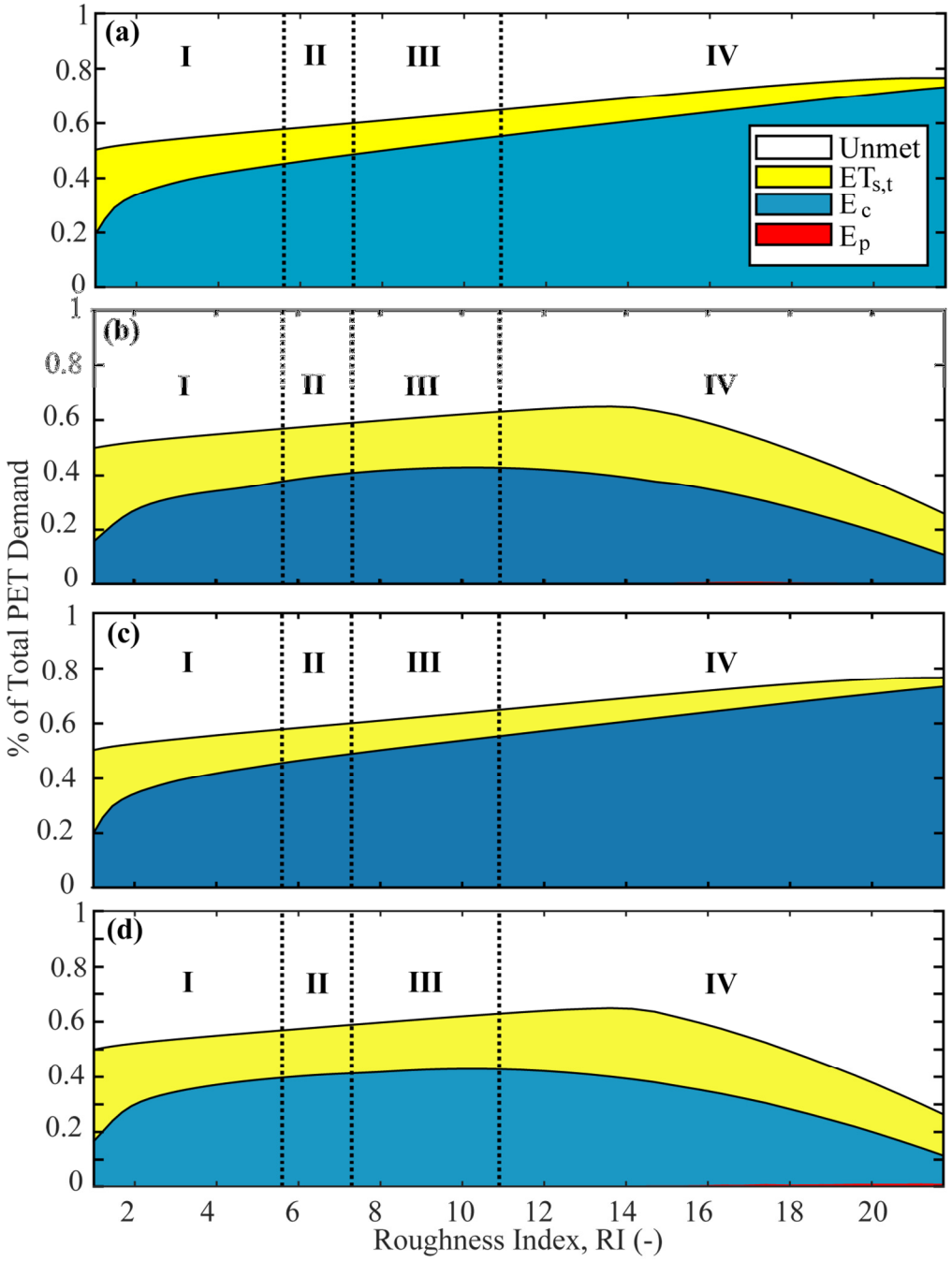

Figure 22: Total potential evapotranspiration demand partitioning for varying roughness index (RI) using BSC parameters under (a) DOE conditions (Experiment 0), (b) diminished clogging (Experiment 1), (c) diminished clogging (Experiment 2), and (d) enhanced clogging and diminished channelization (Experiment 3). $ET_{s,t}$ is total soil evapotranspiration, E_c is BSC evaporation, E_p is ponded evaporation, and "unmet" is the total *PET* demand remaining after accounting for the evaporative losses from the three layers. Dotted lines separate RI classes, labeled with roman numerals (I - IV).

($ET_{s,t}$). As the amount of moisture held within the BSC against leakage increases (lower L_c), the supplies available for BSC evaporation E_c increase, resulting in increases in total losses to E_c for much of development under base case conditions (Figure 20). The increases in E_c result in a decreased evaporative demand placed on the soil and decrease the total soil losses through any component of evaporation and transpiration (Figures 20,21,22;Appendix G; $ET_{s,t} = ET_{s,u} + ET_{s,s} + ET_{s,b}$). Under enhanced clogging, the enhanced total *Lc* serves to decrease the BSC evaporation supplies, and decrease the total E_c losses as compared to base case conditions (Figures 20, 22; Appendix G). The added inputs to the soil layer under these conditions produces an increase in the supplies available for soil evapotranspiration, and a resulting increase the total losses to unstressed evapotranspiration ($ET_{s,u}$; Figure 21). Under diminished channelization, the further decreases in BSC leakage L_c enhance the supply and rates of BSC evaporation (E_c) in the middle RI Class range (II-III; Figure 20c). As a result, the evaporative demands placed on the soil are further decreased, and total soil evapotranspiration is reduced even more across these ranges of development (RI Classes II and III of Experiment 2 vs. Experiment 0; Figure 21,22).

Lastly, the supply and demand for E_c and $ET_{s,t}$ appear to directly affect the variability of moisture within the system. The trend in standard deviation of relative moisture for both the soil and BSC across development, shown in Figure 23 for example, appears proportional to the trend in Ec. This suggests that the variability of moisture is dependent upon the rates of evaporative losses from either layer. This could be due to the fact that these loss rates depend upon the supply relative to the demand, which are both variable on any given day.

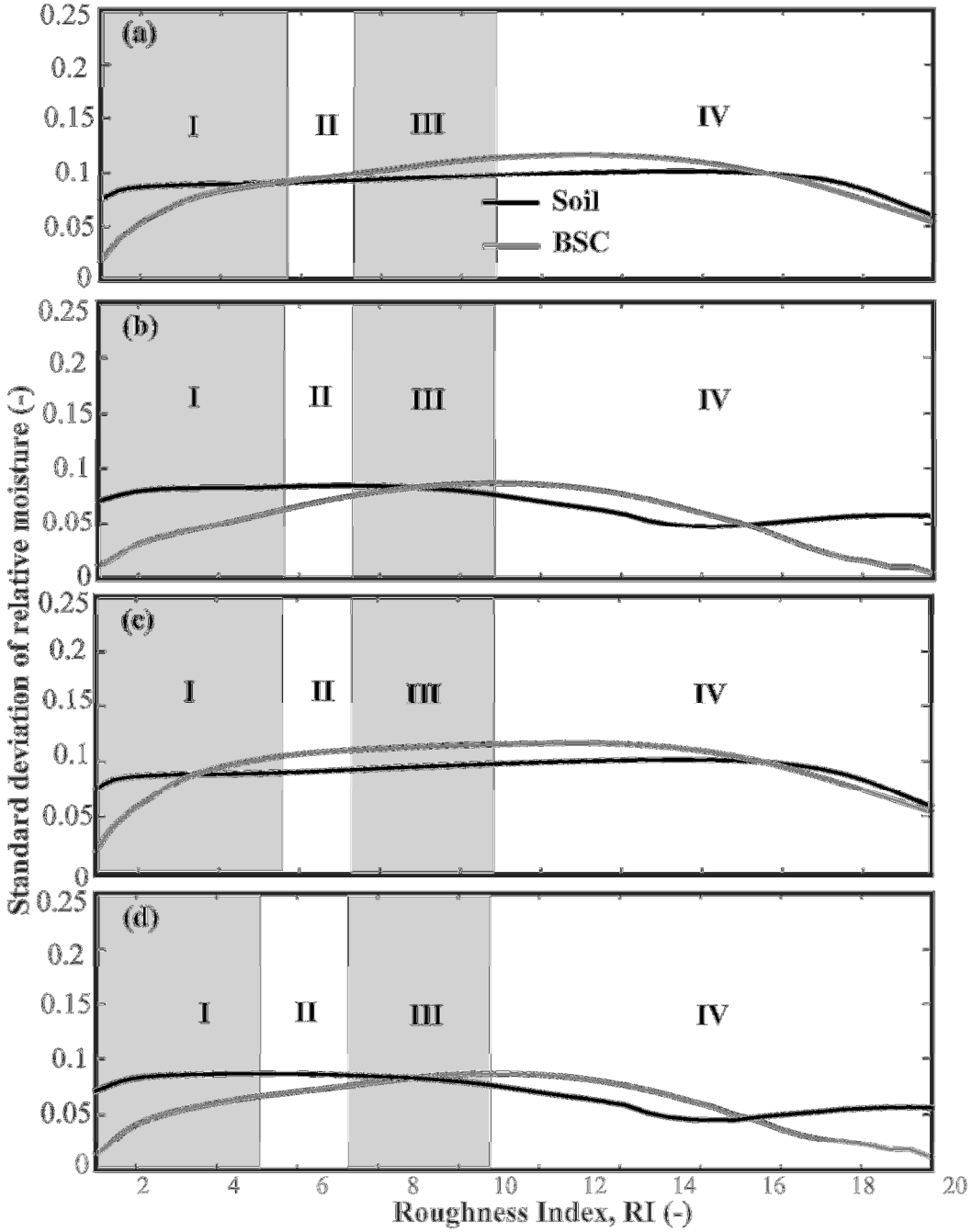

Figure 23: Temporal standard deviation of relative moisture simulated in the soil and BSC layers across a range of roughness indices (RI) values (1 - 21.75) using BSC parameters under (a) DOE conditions (Experiment 0), (b) diminished clogging (Experiment 1), (c) diminished clogging (Experiment 2), and (d) enhanced clogging and diminished channelization (Experiment 3). Greyed and white areas highlight RI classes, labeled with roman numerals (I - IV).

3.2.2 Statistical Analyses of Moisture Infiltration and Drying Rates

Since the soil moisture residence time (τ or τ_c) is indirectly proportional to the drying rate, and since the moisture input per storm (Δs or Δs_c) is directly proportional to the infiltration rate, comparisons of these two metrics to the experimental water balance dynamics are useful for understanding the infiltration and drying rates across BSC development. The averages of these two metrics across the entire simulation period for each RI Class were also statistically analyzed for significant differences between RI Class within each experimental dataset and between experiments within each RI Class dataset. These statistical differences are discussed below in two separate sections for the soil and BSC layer. Each section contains a figure (Figure 24 or 25) used to compare the average change in relative moisture per storm input (average Δs or Δs_c) and the average relative soil moisture residence time (average τ or τ_c) across all storm and subsequent drying events of each RI Class of each experiment. Each metric average shown in their respective figure contains a lower case and upper case letter to distinguish significant differences detected between RI Classes of the same experiment and between experiments of the same RI class, respectively. Thus, averages with different letters denote significant differences. Each section contains two tables that summarize the assumptions test results and two tables that summarize the multi-way comparison test results.

3.2.2.1 Soil Moisture Infiltration and Drying Rates

In the soil layer, the average infiltration rate for each RI Class appears directly linked to total BSC leakage (L_c). Across all experiment conditions, for example, the

average Δs for each RI Class appears to decrease across RI Classes I to III and increase from RI III to IV with the associated changes in soil moisture inputs (i.e. changes in L_c; Figures 24a and 20). Under DOE conditions, the change in average Δs is only significant between RI Classes I to II across which the L_c decreases exponentially (Table 10). Furthermore, the applied experimental affects appear to have opposite effects on the trend in average Δs, similar to the opposite effects on to the trends in L_c with development.

When the clogging effect is enhanced across development, the overall increase in L_c rates for any given LOD increases average Δs significantly for moderate and highly developed BSC layers as compared to the base case conditions (RI I-IV of Experiment 1 compared to Experiment 0; Figure 22a; Table 11). Also under these conditions (Experiment 1), the change in average Δs between RI Class I and IV are insignificant; suggesting that the clogging effect enhances the overall infiltration rates but diminishes the differences observed across development (Tables 10,11). Under diminished channelization, the decrease in average L_c rates for moderately developed BSC layers (RI Classes II and III; Figure 20) appears to significantly decrease the average Δs as compared to base case conditions (RI Classes II and III of Experiment 2 vs. Experiment 0 Figure 22a; Table 11). This effect appears to enhance the general trend in average Δs with development, causing significant changes the average Δs with each RI Class (Figure 22a, lower case letters of Experiment 2).

The average residence time in the soil (τ) appears significantly affected by the relative trends in E_c across experimental treatments and resulting evaporative demands place on the soil water. Under all experimental cases, for example, the development of BSC (increasing RI) appears to cause significant increases in the average τ for each RI

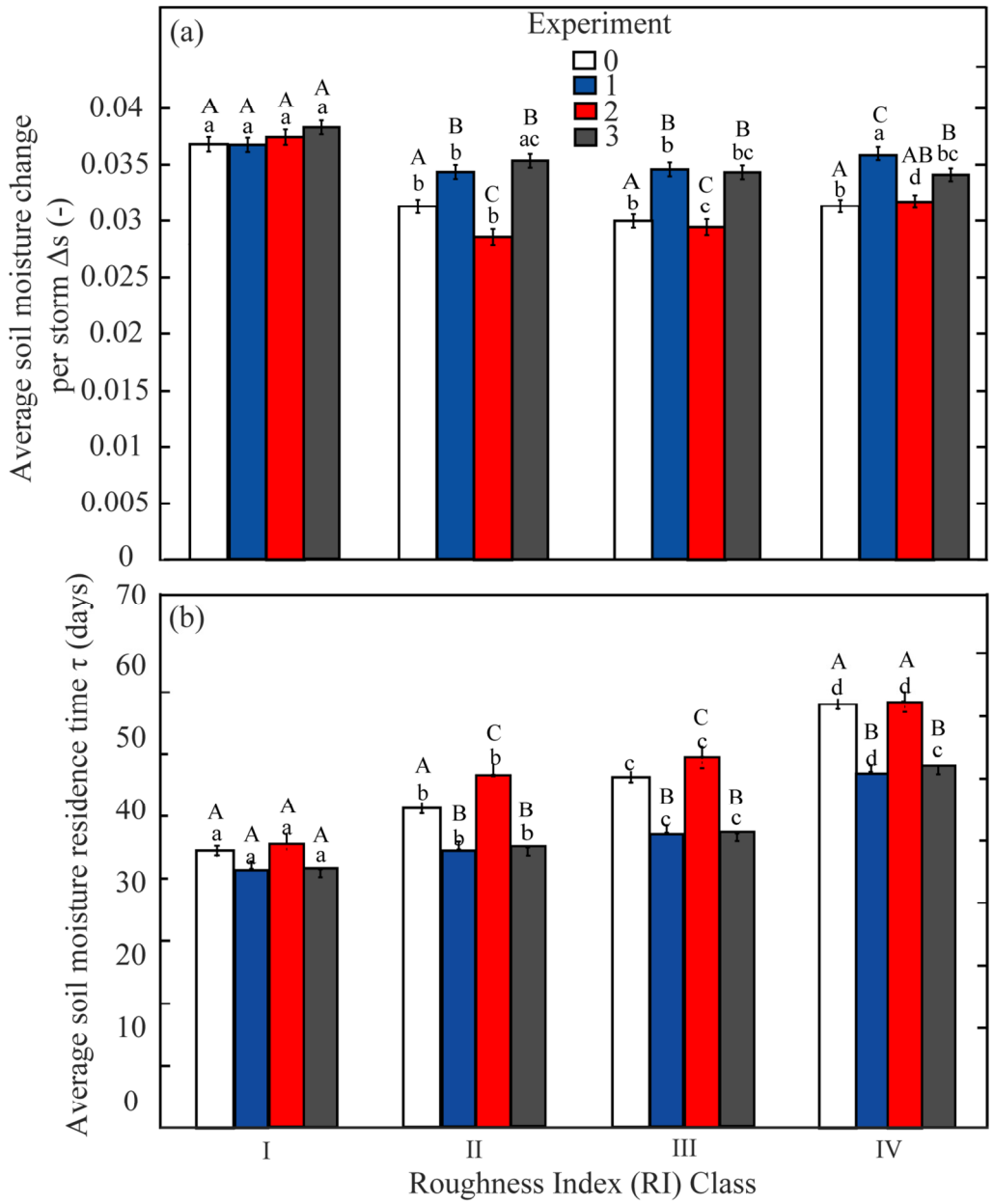

Figure 24: Average (a) relative soil moisture change per storm Δs and (b) soil moisture residence time residence time τ (days) for each roughness index class (I – IV) for all experiments. Different lower case letters indicate significant difference between RI Class averages within each experiment. Different upper case letters indicate significant difference between experiment averages within each RI Class.

Table 8: Summary of results for assumptions and significance tests between average soil moisture residence time τ and relative soil moisture change per storm Δs for each experiment dataset. Tests include Kolmogorov-Smirnov for normality, Bartlett's for equal variance, Kruskal-Wallace for significant variation across RI Classes. Significant p-values (<0.05) are indicated with asterisk.

Test	Experiment	Δs Results		τ Results	
		Statistic (df = 3)	*p-value*	*Statistic (df = 3)*	*p-value*
Kolmogorov-Smirnov	*0*	1	< 2.2E-16 *	1	< 2.2E-16 *
	1	1	< 2.2E-16 *	1	< 2.2E-16 *
	2	1	< 2.2E-16 *	1	< 2.2E-16 *
	3	1	< 2.2E-16 *	1	< 2.2E-16 *
Bartlett's	*0*	12.6 (3)	0.00551 *	29.7 (3)	1.63E-6 *
	1	10.6 (3)	0.01404 *	59.5 (3)	7.44E-13 *
	2	7.42 (3)	0.05969 *	48.2 (3)	1.945E-10 *
	3	81.9 (3)	< 2.2E-16 *	73.1 (3)	9.162E-16 *
Kruskal-Wallace	*0*	101 (3)	< 2.2E-16 *	627 (3)	< 2.2E-16 *
	1	48.8 (3)	1.43E-10 *	536 (3)	< 2.2E-16 *
	2	24.8 (3)	1.698E-5 *	509 (3)	< 2.2E-16 *
	3	178 (3)	< 2.2E-16 *	558 (3)	< 2.2E-16 *

Table 9: Summary of results for assumptions and significant variance tests for average soil moisture residence time τ and relative soil moisture change per storm Δs for each RI class dataset. Tests include Kolmogorov-Smirnov for normality, Bartlett's for equal variance, Kruskal-Wallace for significant variation across experiments. Significant p-values (<0.05) are indicated with asterisk.

Test	Class	Δs Results		τ Results	
		Statistic (df = 3)	*p-value*	*Statistic (df = 3)*	*p-value*
Kolmogorov-Smirnov	*1*	1	< 2.2E-16 *	1	< 2.2E-16 *
	2	1	< 2.2E-16 *	1	< 2.2E-16 *
	3	1	< 2.2E-16 *	1	< 2.2E-16 *
	4	1	< 2.2E-16 *	1	< 2.2E-16 *
Bartlett's	*1*	12.7	0.00543 *	202	< 2.2E-16 *
	2	52.7	2.1E-11 *	390	< 2.2E-16 *
	3	58.4	1.31E-11 *	406	< 2.2E-16 *
	4	1.23	0.7457	539	< 2.2E-16 *
Kruskal-Wallace	*1*	24.8	1.698E-05 *	509.3	< 2.2E-16 *
	2	135	< 2.2E-16 *	92.5	< 2.2E-16 *
	3	102	< 2.2E-16 *	130	< 2.2E-16 *
	4	56.6	3.20E-16 *	142	< 2.2E-16 *

Table 10: Summary of results from multi-way comparisons for significance between average soil moisture residence time τ and relative soil moisture change per storm Δs between RI classes within each experiment. Significant p-values (<0.008) are indicated with asterisk.

Experiment	RI Class Comparison	Δs Results		τ Results	
		Statistic (df = 3)	*p-value*	*Statistic (df = 3)*	*p-value*
0: DOE Conditions	*1 vs. 2*	1.60E+06	1.0524E-11 *	1.22E+06	5.098E-11 *
	1 vs. 3	1.69E+06	1.37E-21 *	1.08E+06	4.94E-33 *
	1 vs. 4	1.67E+06	3.04E-14 *	7.86E+05	4.58E-119 *
	2 vs. 3	1.53E+06	0.0712	1.31E+06	7.32E-09 *
	2 vs. 4	1.51E+06	0.852	9.85E+05	1.73E-71 *
	3 vs. 4	1.45E+06	9.36E-03	1.13E+06	8.89E-40 *
1: Stengthened clogging	*1 vs. 2*	1.55E+06	1.07E-06	1.30E+06	9.41E-05 *
	1 vs. 3	1.59E+06	1.04E-10 *	1.18E+06	9.02E-17 *
	1 vs. 4	1.53E+06	1.22E-07 *	8.05E+05	1.66E-97 *
	2 vs. 3	1.53E+06	0.0637	1.34E+06	2.47E-06 *
	2 vs. 4	1.47E+06	0.506	9.45E+05	1.17E-68 *
	3 vs. 4	1.42E+06	0.315	1.02E+06	4.59E-51 *
2: Diminshed channelization	*1 vs. 2*	1.51E+06	9.66E-05 *	1.31E+06	1.76E-03 *
	1 vs. 3	1.50E+06	4.23E-04 *	1.19E+06	1.91E-14 *
	1 vs. 4	1.43E+06	0.638	8.35E+05	3.48E-94 *
	2 vs. 3	1.46E+06	0.675	1.34E+06	3.85E-06 *
	2 vs. 4	1.38E+06	4.73E-04 *	9.76E+05	3.45E-67 *
	3 vs. 4	1.39E+06	2.13E-03 *	1.07E+06	3.03E-46 *
3: Strengthened clogging and diminished channelization	*1 vs. 2*	1.71E+06	2.78E-27 *	1.14E+06	2.19E-21 *
	1 vs. 3	1.68E+06	5.57E-25 *	1.01E+06	8.72E-42 *
	1 vs. 4	1.64E+06	6.05E-13 *	7.83E+05	3.62E-116 *
	2 vs. 3	1.43E+06	0.157 *	1.34E+06	1.21E05 *
	2 vs. 4	1.31E+06	6.33E-13 *	1.11E+06	1.36E-43 *
	3 vs. 4	1.33E+06	4.57E-09 *	1.19E+06	1.56E-25 *

Table 11: Summary of results from multi-way comparisons for significance between average soil moisture residence time τ and relative soil moisture change per storm Δs between experiments within each RI class. Significant p-values (<0.008) are indicated with asterisk.

RI	Experiment	Δs Results		τ Results	
Class	Comparison	*Statistic (df = 3)*	*p-value*	*Statistic (df = 3)*	*p-value*
1	*0 vs. 1*	1318882	0.244	1.37E+06	0.382
	0 vs. 2	1372844	0.301	1.34E+06	0.896
	0 vs. 3	1320756	0.499	1.33E+06	0.630
	1 vs. 2	1417749	0.008	1.31E+06	0.217
	1 vs. 3	1351883	0.657	1.30E+06	0.173
	2 vs. 3	1292301	0.121	1.32E+06	0.653
2	*0 vs. 1*	1.34E+06	4.04E-06 *	1.60E+06	1.20E-05 *
	0 vs. 2	1.38E+06	1.68E-03 *	1.59E+06	1.33E-05 *
	0 vs. 3	1.64E+06	6.14E-08 *	1.36E+06	7.16E-5 *
	1 vs. 2	1.53E+06	2.99E-02	1.47E+06	0.871
	1 vs. 3	1.79E+06	1.31E-26 *	1.25E+06	1.05E-15 *
	2 vs. 3	1.76E+06	9.48E-22 *	1.24E+06	3.31E-16 *
3	*0 vs. 1*	1.33E+06	7.38E-08 *	1.67E+06	1.37E-10 *
	0 vs. 2	1.32E+06	2.43E-08 *	1.67E+06	7.06 E-11 *
	0 vs. 3	1.59E+06	7.24E-0.5 *	1.39E+06	4.904-03 *
	1 vs. 2	1.47E+06	0.896	1.48E+06	0.886
	1 vs. 3	1.69E+06	2.51E-15 *	1.20E+06	6.32E-20 *
	2 vs. 3	1.70E+06	4.98E-16 *	1.20E+06	2.76E-20 *
4	*0 vs. 1*	1.37E+06	1.71E-05 *	1.71E+06	2.46E-14 *
	0 vs. 2	1.33E+06	4.02E-11 *	1.79E+06	2.14E-18 *
	0 vs. 3	1.53E+06	0.402	1.55E+06	0.709
	1 vs. 2	1.39E+06	2.76E-02 *	1.50E+06	0.184
	1 vs. 3	1.59E-06	4.46E-04 *	1.25E+06	9.70E-16 *
	2 vs. 3	1.69E+06	9.78E-09 *	1.25E+06	5.70E-20 *

Class (Figure 22b; Table 10). This could be related to the general decrease in evaporative demand placed on the soil and subsequent decreases in soil drying rates as BSC evaporation decreases with development (Figures 22). Under diminished channelized conditions, for example, the increased E_c rates decreases the demand on the soil and causes significant increases in average τ in moderately developed sites as compared to base case conditions (RI II and III in Experiment 2 vs. Experiment 0; Figures 20,21,22n;

Table 11). Under enhanced clogging conditions, the increased soil evaporative demand and increased rates of $ET_{s,u}$ appears to accelerate drying rates, or decrease the average τ in moderately and highly developed BSC sites (RI Classes II and III) as compared to the base case conditions (Figures 20,21,22b,Table 10).

3.2.2.2 BSC Moisture Infiltration and Drying Rates

In the BSC layer, the average moisture residence time (τ_c) appears to also increase significantly with development (increasing RI Class) under all experimental conditions (Figure 23b; Table 14), and reflects the increased moisture retention capacity (higher $s_{fc,c}$ and $s_{h,c}$; Figure 15d) and the increased BSC thickness (increased Z_c; eq.41). As compared to the residence times in the soil layer below, however, the added experimental effects appear to cause opposite effects on the drying rates and resulting τ_c. Under enhanced clogging, for example, the increased of total L_c losses (Figure 20) appears to diminish the average τ_c across all RI Classes as compared to base case conditions (Experiment 1 vs. Experiment 0; Figure 23b; Table 14). Under diminished channelization, the decrease in L_c (Figure 20) appears to significantly diminish drying rates and increase the average τ_c for low to moderately developed BSC sites (RI Classes I, II, and III) as compared to base case conditions (Experiment 2 vs. Experiment 0; Figure 23b; Table 15). After the BSC has reached a high level of development (RI Class IV), however, a reduction in the channelization produces significant decreases in the average τ_c and perhaps could be associated with the increase in excess infiltration (Ex_i; Figure 20) as compared to base case conditions (RI Class IV Experiment 2 vs. Experiment 0; Figure 23b; Table 15).

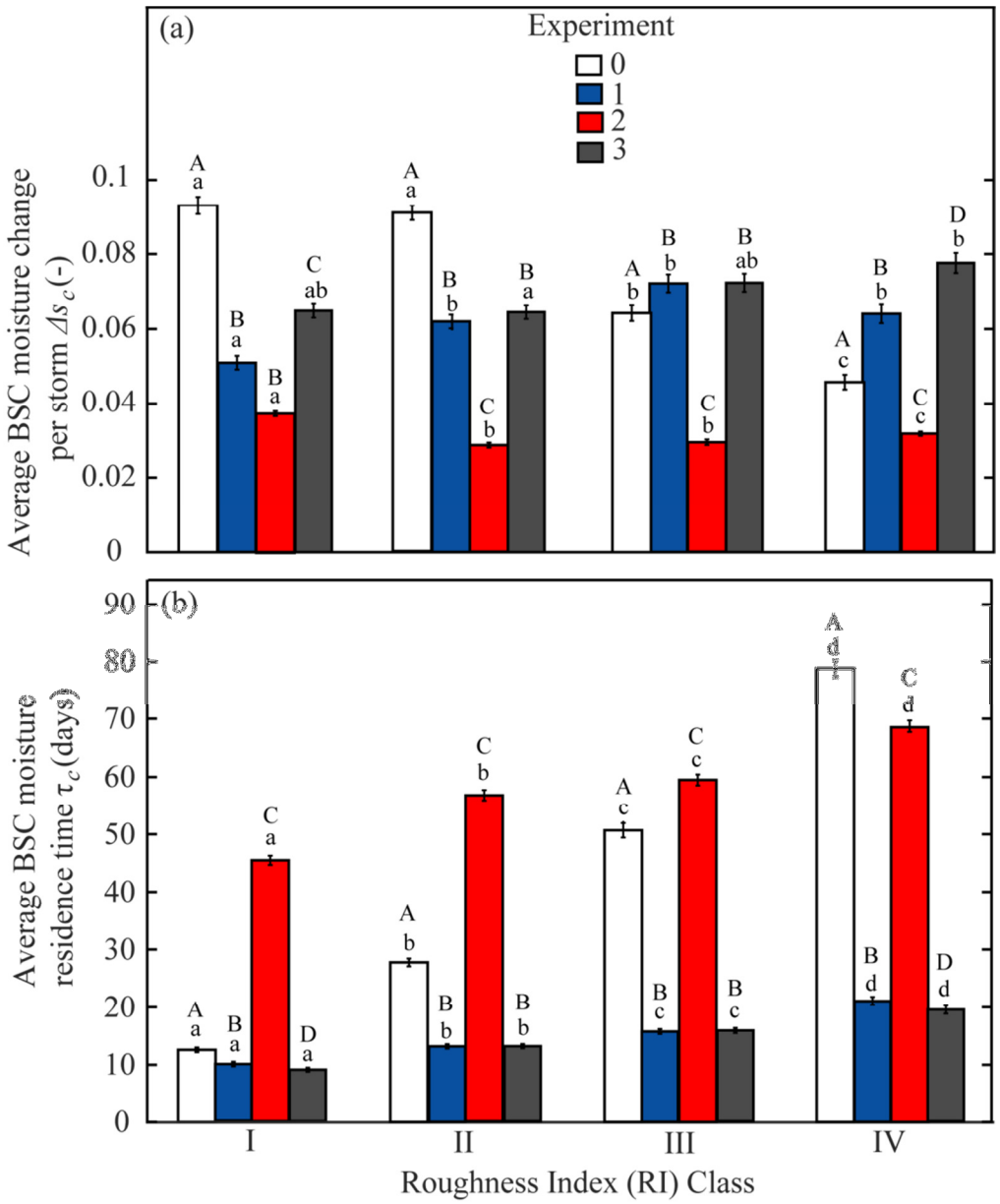

Figure 25: Average (a) relative BSC moisture change per storm Δs_c and (b) BSC moisture residence time residence time τ_c (days) for each roughness index class (I – IV) for all experiments. Different lower case letters indicate significant difference between RI Class averages within each experiment. Different upper case letters indicate significant difference between experiment averages within each RI Class.

Table 12: Summary of results for assumptions and significant variance tests for average BSC moisture residence time τ_c and relative BSC moisture change per storm Δs_c for each experiment dataset. Tests include Kolmogorov-Smirnov test for normality, Bartlett's test for equal variance, Kruskal-Wallace test for significant variation across RI classes. Significant p-values (<0.05) are indicated with asterisks.

Test	Experiment	Δs_c Results		τ_c Results	
		Statistic (df = 3)	*p-value*	*Statistic (df = 3)*	*p-value*
Kolmogorov-Smirnov	*0*	1	< 2.2E-16	0.9637	< 2.2E-16
	1	1	< 2.2E-16	0.9637	< 2.2E-16
	2	1	< 2.2E-16	1	< 2.2E-16
	3	1	< 2.2E-16	1	< 2.2E-16
Bartlett's	*0*	42.6	2.986 *	1819	< 2.2E-16
	1	42.6	2.986 *	1819	< 2.2E-16
	2	82.4	< 2.2E-16	75.5	2.844E-16
	3	120	< 2.2E-16	441	< 2.2E-16
Kruskal-Wallace	*0*	671.4	< 2.2E-16	2504	< 2.2E-16
	1	671.4	< 2.2E-16	2504	< 2.2E-16
	2	671.4	< 2.2E-16	2504	< 2.2E-16
	3	671.4	< 2.2E-16	2504	< 2.2E-16

Table 13: Summary of results for assumptions and significant variance tests for average BSC moisture residence time τ_c and relative BSC moisture change per storm Δs_c for each RI class dataset. Tests include Kolmogorov-Smirnov for normality, Bartlett's for equal variance, Kruskal-Wallace for significant variation across experiments. Significant p-values (<0.05) are indicated with asterisks.

Test	Class	Δs_c Results		τ_c Results	
		Statistic (df = 3)	*p-value*	*Statistic (df = 3)*	*p-value*
Kolmogorov-Smirnov	*1*	1	< 2.2E-16 *	1	< 2.2E-16 *
	2	1	< 2.2E-16 *	0.959	< 2.2E-16 *
	3	1	< 2.2E-16 *	0.989	< 2.2E-16 *
	4	1	< 2.2E-16 *	0.989	< 2.2E-16 *
Bartlett's	*1*	1358	0.00543 *	2152	< 2.2E-16 *
	2	1500	< 2.2E-16 *	2344	< 2.2E-16 *
	3	1374	< 2.2E-16 *	2254	< 2.2E-16 *
	4	1811	< 2.2E-16 *	948.5	< 2.2E-16 *
Kruskal-Wallace	*1*	348	< 2.2E-16 *	92.5	< 2.2E-16 *
	2	671	< 2.2E-16 *	2504	< 2.2E-16 *
	3	671	< 2.2E-16 *	2504	< 2.2E-16 *
	4	671	< 2.2E-16 *	2504	< 2.2E-16 *

Table 14: Summary of results from multi-way comparisons for significance between average BSC moisture residence time τ_c and relative BSC moisture change per storm Δs_c between RI classes within each experiment. Significant p-values (<0.008) are indicated with asterisks.

Experiment	RI Class Comparison	Δs_c Results		τ_c Results	
		Statistic (df = 3	*p-value*	*Statistic (df = 3)*	*p-value*
0: DOE Conditions	*1 vs. 2*	858690	0.211	434955	8.15E-97 *
	1 vs. 3	889881	2.03E-28	193519	2.03E-204
	1 vs. 4	812546	6.23E-62	41927	2.68E-302
	2 vs. 3	1288662	7.40E-28	677477	1.35E-59 *
	2 vs. 4	1167707	4.07E-60	239254	7.08E-218
	3 vs. 4	813082	2.09E-08	424991	1.13E-66 *
1: Stengthened clogging	*1 vs. 2*	394879	3.63E-3	343421	2.42E-13 *
	1 vs. 3	292735	2.75E-06	221222	1.13E-33 *
	1 vs. 4	234079	4.50E-04	117341	6.78E-74 *
	2 vs. 3	497588	1.08E-02	449534	1.15E-09 *
	2 vs. 4	396874	0.168	260288	4.99E-41 *
	3 vs. 4	329617	0.637	250003	1.19E-15 *
2: Diminshed channelization	*1 vs. 2*	1867810	4.45E-28	1242128	6.87E-23 *
	1 vs. 3	1517028	5.70E-24	909968	3.04E-41 *
	1 vs. 4	1640285	6.05E-13	782608	3.62E-116
	2 vs. 3	1416577	0.184	1327428	9.90E-06 *
	2 vs. 4	1428943	2.55E-13	1216027	1.28E-44 *
	3 vs. 4	1204003	1.89E-08	1084399	1.58E-23 *
3: Strengthened clogging and diminished channelization	*1 vs. 2*	476639	0.419	346235	1.77E-22 *
	1 vs. 3	366637	0.704	221466	2.72E-47 *
	1 vs. 4	303002	0.034	167637	2.02E-62 *
	2 vs. 3	499516	0.191	433758	3.91E-10 *
	2 vs. 4	408563	5.54E-04	336804	4.72E-21 *
	3 vs. 4	331814	1.09E-02	316869	5.48E-05 *

Table 15: Summary of results from multi-way comparisons for significance between average BSC moisture residence time τ_c and relative BSC moisture change per storm Δs_c between experiments within each RI class. Significant p-values (<0.008) are indicated with asterisk.

Experiment	Δs_c Results		τ_c Results	
Comparison	*Statistic (df = 3)*	*p-value*	*Statistic (df = 3)*	*p-value*
0 vs. 1	514055	1.95E-29 *	446480	4.79E-07 *
0 vs. 2	1221063	9.75E-73 *	163728	1.11E-277 *
0 vs. 3	515981	2.66-12 *	521102	1.06E-13 *
1 vs. 2	634383	3.27E-02	68329	2.89E-262 *
1 vs. 3	258609	1.04E-06 *	322147	2.18E-02 *
2 vs. 3	504769	9.74E-23 *	1271375	3.41E-294 *
0 vs. 1	1103603	1.11E-20 *	1318759	7.42E-88 *
0 vs. 2	2199211	2.22E-132 *	656620	9.90E-176 *
0 vs. 3	1055291	3.61E-15 *	1295044	5.25E-87 *
1 vs. 2	1430186	2.11E-45 *	156825	0 *
1 vs. 3	643268	0.218	663234	0.984
2 vs. 3	702179	5.01E-58 *	2001415	0 *
0 vs. 1	542193	1.37E-05 *	986024	6.56E-139 *
0 vs. 2	1211088	1.95E-17 *	762961	6.28E-32 *
0 vs. 3	537608	2.18E-05 *	973352	1.23E-136 *
1 vs. 2	922210	6.33E-37 *	110206	6.844E-269 *
1 vs. 3	415569	0.956	412777	0.85
2 vs. 3	487126	5.82E-36 *	1286830	5.81E-266 *
0 vs. 1	277996	3.98E-23 *	700902	3.78E-192 *
0 vs. 2	791718	3.58E-14 *	1033298	1.49E-04 *
0 vs. 3	281760	2.99E-36 *	786474	3.42E-213 *
1 vs. 2	742353	2.82E-13 *	88386	2.94E-245 *
1 vs. 3	254901	2.61E-03 *	307714	9.65E-04 *
2 vs. 3	500168	1.05E-29 *	1301160	9.47E-273 *

The average change in BSC relative moisture input for each RI Class (Δs_c; Figure 23a) appears affected by a complex interaction of the trend in storage capacity affected by the relative rates of clogging and thickening (Figure 18), as well as the average BSC moisture residence time (Figure 19). Under base conditions, the average Δs_c decreases significantly past a certain level of development (Experiment 0 in Figure 23a; Table 14), and is potentially due to the relative increases in the storage depth with BSC development

(increasing Z_c with RI; Eq. 41; Figure 18). Under diminished channelization (Experiment 2), perhaps the increased average amount and residence time of relative moisture (average s and τ_c; Figures 19 and 15) reduces the potential changes that can occur in average moisture inputs for any given storm, and thus, causes significant decreases in average Δs_c as compared to base case conditions (Figure 23a; Table 15).

The clogging effect, however, appears to change both the trend across development and the average Δs_c as compared to base case conditions. Within RI Classes I and II, the added clogging effect significantly reduces the average Δs_c below that of base conditions (Figure 23a; Table 15), and is potentially because the added moisture is distributed across a reduced storage volume (lower $n_c Z_c$; Figure 18). Under these conditions, the average Δs_c increases with the decrease in storage volume across RI Classes I to III, causing significantly higher average Δs_c in Class III than under base conditions (RI Class III of Experiment 1 vs. Experiment 0 Figure 23a; Table 15). After a certain level of development, however, the average Δs_c decreases significantly from RI Class III to IV under the enhanced clogging conditions (Figure 23a; Table 14). This is perhaps related to the increase in excess infiltration (Ex_i; Figure 20).

3.3 Discussion

In this study, the total BSC leakage (average L_c) and average change in relative soil moisture (Δs) for simulated plots serve as two metrics of soil infiltration rates for any level of development. The two metrics indicate that infiltration rates decrease across the earliest stages of BSC development and increase after a certain threshold of development. These results suggest that comparisons of infiltration rates across differently developed

BSC systems could yield contrasting results depending upon the range of development considered. Under situations where clogging is less enhanced or channelization less diminished (i.e. base case conditions), the contrasting infiltration rate trends across development are potentially augmented by an increased potential to store moisture within the BSC layer. This suggests that in order to truly compare infiltration trends across BSC surfaces, the widest range of development possible should be considered within any given system.

The enhancement added to the clogging effect in this study produced profound increases excess infiltration (Ex_i), and thus, captures the increases in hydrophobicity accompanying clogging as concluded by previous studies (Verrecchia et al. 1995; Rutin 1983; Yair 1990). Furthermore, the modeled clogging effect under base case and enhanced conditions appears to greatly limit the BSC storage capacity such that less infiltrated moisture can be held in the BSC layer. Rather than produce excess saturation moisture (Ex_s), however, the reduction in BSC porosity (n_c) and resulting limited BSC storage capacity (n_cZ_c) modeled in this study actually increases infiltration rates to the lower soil layers. Since the modeled saturation excess component is dependent upon the soil storage capacity (nZ_r), the reduced storage capacity of the BSC layer (n_cZ_c) has no direct effect on the saturation excess mechanism.

Some of the studies which found that pore clogging enhanced saturation excess analyzed field areas and samples affected by frequent sandstorms (Yair 1990; Lange *et al.* 1992; Kidron 1995; Kidron and Yair 1997; Goldreich 2003). As Felde *et al.* (2014) demonstrated, the coarse grain deposits by these frequent sandstorms can create sharp texture horizons that produce a capillary barrier effect and isolates moisture within the

upper BSC layers. Thus, in these studies, saturation excess could be directly dependent upon the storage capacity of the BSC layers due to the potential presence of this capillary barrier effect. Under the DOE field site conditions where the high intensity sandstorms are non-existent, however, the contrasting soil texture layers necessary to produce the capillary barrier effect is absent. As modeled in this study, subsurface moisture can presumably leak from the BSC to the soil layer uninhibited by any sandstorm-created capillary barrier effect. The modeled clogging effect, thus, increases flow in the downward direction to the soil layers where a high relative storage capacity prevents excess saturation.

Felde *et al.* (2014), also concluded that excess infiltration should decrease with development due to the increases in channelization with development and that the importance of pore clogging might have been overestimated in previous research. In the present thesis, excess infiltration (Ex_i) was indeed produced in the least developed simulations and decreased as channelization increased with development. Furthermore, this pulse of Ex_i in the least developed sites was also enhanced when channelization was diminished. Under these diminished channelization conditions (Experiment 2), however, a greater pulse of Ex_i was produced in the most developed BSC sites due to the reductions in the infiltration capacity accompanying the combined effect of lower conductivity ($K_{s,c}$) and reduced BSC porosity (n_c). Whether Ex_i is greater in the least or most developed conditions, thus appears dependent upon both the level of channelization, as Felde *et al.* (2014) concluded, as wells as the level of clogging present at a given site

The results of this study also indicate that the development of the BSC can cause significant increases in the moisture levels within the BSC and soil system. Across all

experimental conditions for example, the average relative BSC moisture level and residence time increase significantly with development as retention and recycling of moisture increases within the system. Furthermore, the evaporative demand placed on the soil was directly affected by the evaporation of the upper BSC layer. Thus as BSC evaporation accelerated, the average relative soil moisture residence time was increased with development. Similar to the conclusions of previous studies, these development trends suggest that the BSC layer acts as a buffer to lower evaporation from lower soil layers (Verrecchia *et al.* 1995; Booth 1941; Rushforth and Brotherson 1982; George *et al*. 2003; Belnap 2006; Veluci *et al.* 2006). In this manner, the developing BSC layers can potentially cause significant increases in the moisture available for both vascular and microbiological process.

Previous studies have concluded that the added cap of the pore clogged BSC layer would serve to increase this buffering effect by increasing the water flux resistance in the subsurface system (Verrecchia *et al.* 1995; George *et al.* 2003). As the BSC storage capacity decreased under the modeled clogging effect, however, more moisture was sent out of the BSC layer, decreasing the evaporation from the BSC layer, increasing the demand on the soil, reducing the moisture residence times within both layers. Thus, these trends indicate that the clogging effect can actually decrease the water flux resistance and reduce the buffering effect.

In this study, diminishments in channelization appeared to increase the buffering effect by decreasing the flow from moisture out of the BSC layer to the lower soil layers. The differences in the conclusions of the clogging effects on the buffering trends in this and other studies could, therefore, be due to differences in the relative level of

channelization accompanying the type of BSCs present. George *et al.* (2003), for example, analyzed BSC areas and samples composed of cyanobacteria and moss species different from those of this study (*Psora decipiens, Placidium squamulosum*), which could have completely different amounts of channelization, especially since these samples did not include any lichen-type species. Verrecchia *et al.* (1995) examined cyanobacteria-dominated samples, which presumably have little to no added channelization with development due to the absence of the lichen-moss anchoring structures (Felde *et al.* 2014). Furthermore, Rossi *et al*. (2012) found that that hydraulic conductivity decreased with EPS and biomass concentrations in cyanobacteria-dominated samples, which suggests that the samples analyzed by Verrecchia *et al*. (1995) might even display negative channelization ($K_{s,c}$ reduces with development). Perhaps in the absence of high rates of channelization associated with certain lichen and moss species, the added EPS biomass within in the samples of these other studies could therefore have acted to not only clog pores, but also increase the flux resistance and decrease the amount subsurface channels with development.

Furthermore, the modeled increase in surface roughness appeared to decrease runoff generation with development by increasing the ponding capacity of the system. These results confirm previous findings that simulated livestock trampling and destruction of roughened BSC surfaces can significantly decrease infiltration capacities and increase runoff rates (Fierer and Gabet 2002). Some studies in warmer field site conditions, however, have concluded that runoff generation increased with development (Rutin 1983; Yair 1990; Lange *et al.* 1992; Kidron 1995; Kidron and Yair 1997; Kidron *et al.* 1999). In these warmer climates, there is a lower potential for freeze-thaw and

development of surface dwelling species (i.e. lichens-mosses), which causes less dramatic surface roughness expressions with development. Thus, the differences in runoff trends are most likely due to the difference in the expression of surface roughness with development.

4 CONCLUSIONS AND FUTURE WORK

4.1 **Conclusions**

In this study, a point-scale ecohydrology model was modified to simulate biological soil crust (BSC) moisture dynamics under mixed precipitation regimes. This model was used to reproduce a set of moisture observations from sites displaying various amounts of BSC development in a cool desert climate. A manual and automated routine for parameter calibration was implemented to identify the optimal soil, vegetation, and BSC conditions that best matched the observed records under different levels of development. The calibrated model fit the observations well with accurate precision as evidenced by a low RMSE, high CC, and near 1-to-1 *bias* ratios, as well as optimal visual fit of simulated moisture to observed moisture timeseries. A set of simulation experiments were conducted to explore the isolated effects of two mechanisms presented in previous studies of BSC development thought to significantly alter infiltration dynamics. Due to the controlled conditions inherent in modeled situations, the results of these simulation experiments can aid in clarifying apparent contrasting conclusions of previous BSC development studies.

Only in the most developed conditions did the modeled clogging effect appear to significantly increase surface hydrophobicity such that the surface infiltration capacity was reduced enough to produce excess moisture. This effect was enhanced by a significant decrease in the rate of channelization with development. Therefore, this study concludes that BSC pore clogging will not always generate moisture to the surface in excess of infiltration capacities. This is especially true when the BSC cover does not contain a high density of EPS filaments due to the species type or LOD and/or if the

subsurface does not display a high level of channelization. In the absence of the capillary barrier effect and under high channelization conditions, the clogging effect reduced the flux resistance to flow, increasing leakage to the lower soil layers, and decreasing the BSC buffer effect. Thus, BSC pore clogging does not always directly affect the saturation capacity of the system, especially in areas without frequent sandstorms and associated subsurface capillary barriers and/or across areas lacking predominant amounts of lichen-moss surface anchoring structures. Furthermore, the results of this study confirm that the trend in runoff generation across any system is tightly coupled to the level of roughness and how that roughness increases with development.

4.2 **Future Work**

In general, this study proposes that the range and relative roughness of BSC sites compared will greatly affect the trend observed in relative subsurface infiltration and drying rates with BSC development, and thus, future moisture flux studies should attempt to consider the widest range possible of BSC development. Given high precision and accuracy of the simulated moisture to the observations, the model appears to be a reliable method for understanding the fluxes relevant to moisture dynamics present in dryland areas affected by BSC cover and with climates of snow and/or rain. Therefore, the current results and experiments can serve a basis for numerous additional avenues of further research.

One possibility is to adjust the precipitation partitioning and snowmelt balance to investigate the effects of climate change on the moisture balance within these previously established BSC surfaces. These climate forcing alterations might also be combined with

an alternative method to explore the moisture dynamics under smoother-cyanobacteria dominated surfaces that are more prevalent in warmer climates. Since these surfaces do not display a high degree of increased roughness with development, such modeling efforts could utilize different metrics of development. Belnap *et al.* 2008, for example, outlines a fairly easy, highly repeatable, and non-destructive method for visually assessing the level of development (LOD) of cyanobacteria-dominated areas based on soil surface darkness. In this study, the method was confirmed as an accurate predictor of the chlorophyll *a* soil concentrations, EPS concentrations, and soil aggregate stability of a given field site location. Future studies might therefore examine the water balance dynamics under BSC development in warmer climates using the soil surface darkness rather than the roughness index as an LOD metric. Furthermore, such studies should consider calibrating the parameters of the more developed sites to reflect a decrease in the connectivity and channelization of the subsurface due to the abundance of EPS materials and lack of lichen-moss anchoring structures (Rossi *et al.* 2012; Felde *et al.* 2014). This might include increasing the pore distribution parameter (b_c), increasing the pore disconnectedness (c), and decreasing the saturated hydraulic conductivity ($K_{s,c}$).

Another experimental approach might be to test the effects of changing underlying soil layer parameters on the BSC subsurface moisture dynamics with different soil texture conditions calibrated to using empirical results (e.g. Laio *et al.* 2001). Such an approach could be used to explore sandy soil textures and combined with a method for exploring the capillary barrier effect of field sites prone to frequent sandstorms. In these examinations, the studies might include an excess saturation scheme within the BSC layer that is similar to the scheme utilized in the soil layer of this study but dependent

upon the BSC storage capacity. Such a study might also explore the possibilities of decreasing the effect of excess saturation with development of BSCs to reflect the increases in subsurface channelization by lichen-moss anchoring structures that serves to increase the connections between the BSC and sub-surface soil layer, thereby diminishing the capillary barrier effect (Felde *et al*. 2014).

This thesis represents an important step forward in understanding the impact of BSC development on hydrologic conditions in dryland systems. The results provided indicate that the relative moisture retained and available within the system for vascular plant and microorganism health and maintenance is significantly affected by the development of BSCs within the Colorado Plateau and across alternative hypothetical field conditions. Given the wide range of environments in which BSCs can dominate, the ability to isolate for variables such as BSC and vegetative species type and percent coverage, surface condition, climate, and soil texture is crucial to understanding the impacts that these small, yet influential, organisms have on soil moisture dynamics. The model, methods, and results of this study can serve as a powerful tool to further explore the role of BSCs on hydrologic processes in a time when such understanding is crucial for developing sustainable water management strategies in the face of future climate changes.

REFERENCES

Agam N, Berliner PR. 2004. Diurnal water content changes in the bare soil of a coastal desert. *Journal of Hydrometeorology* 5(5): 922. DOI: http://dx.doi.org/10.1175/1525-7541(2004)005<0922:DWCCIT>2.9.C0:2.

Agam N, Berliner PR. 2005. Dew formation and water vapor adsorption in semi-arid environments- A review. *Journal of Arid Environments* 65: 572-590. DOI: 10.1016/J.JARIDENV.2005.09.004.

Allen RG, Pereira LS, Raes D, Smith M. 1998. Single crop coefficient (K_c). In: *Crop evapotranspiration: guidelines for computing crop water requirements* ; FAO Irrigation and drainage paper 56. *Food and Agriculture Organization of the United Nations.* Rome. ISBN 92-5-104219-5. Retrieved from: www.fao.org/docrep/x0490e/x0490e/x0490e0b.htm#crop_coefficients

Anderson, EA. 1973. National Weather Service River Forecast System-Snow accumulation and Ablation Model NOAA Tech. Memo, NWS-HYDRO-17. *US Dept. Commerce, NOAA, NWS.*61 pp. Retrieved from: http://www.nws.noaa.gov/oh/hrl/nwsrfs/users_manual/part2/_pdf/22snow17.pdf

Axtell, RL, Epstein JM, Dean JS, Gumerman GJ, Swedlund AC, Harburger J, Chakravarty S, Hammond R, Parker J, Parker M. 2002. Population growth and collapse in multiagen model of the Kayenta Anasazi in Long House Valley. *Proceedings of the National Academy of Science* 99: 7275-7279. DOI: 10.1073/pnas.092080799.

Bailey RG. 1994. Description of the ecoregions of the US. *USDA Forest Service.* Washington DC. Retrieved from: http://www.fs.fed.us/land/ecosysmgmt/index.html

Barger NN, Herrick JE, Zee JV, Belnap J. 2006. Impacts of biological soil crust disturbance and composition on C and N loss from water erosion. *Biogeochemistry*. 77: 247-263. DOI: 10.1007/s10533-005-1424-7.

Belnap J. 1995. Surface disturbances: Their role in accelerating desertification. *Environmental Monitoring and Assessment* 37: 39-57. DOI: 10/1007/BF00546879.

Belnap J. 2001a. Microbes and microfauna associated with biological soil crusts. In *Biological soil crusts: structure, function, and Management*, Belnap J, Lange OL (eds). *Springer-Verlag*. Berlin, Germany; 167-174. ISBN: 3-540-41075-9.

Belnap J. 2001b. Comparative structure of physical and biological soil crusts. In *Biological soil crusts: structure, function, and Management*, Belnap J, Lange OL (eds). *Springer-Verlag*. Berlin, Germany; 177-191. ISBN: 3-540-41075-9.

Belnap J. 2001c. Biological soil crusts and wind Erosion. In *Biological soil crusts: structure, function, and Management*, Belnap J, Lange OL (eds). *Springer-Verlag*. Berlin, Germany; 339-347. ISBN: 3-540-41075-9.

Belnap, J. 2006. The potential roles of biological soil crusts in dryland hydrologic cycles. *Hydrological Processes* 20: 3159–3178. DOI: 10.1002/hyp.6325.

Belnap J, Büdel B, Lange OL. 2001. An introduction to Biological Soil Crusts Characteristics and Distribution. In *Biological soil crusts: structure, function, and Management*, Belnap J, Lange OL (eds). *Springer-Verlag*. Berlin, Germany; 3-30. ISBN: 3-540-41075-9.

Belnap J, Eldridge DJ. 2001. Disturbance and Recovery of Biological Soil Crusts. In *Biological soil crusts: structure, function, and Management*, Belnap J, Lange OL (eds). *Springer-Verlag*. Berlin, Germany; 363-383. ISBN: 3-540-41075-9.

Belnap J, Gardner JS. 1993. Soil microstructure in soils of the Colorado Plateau: the role of cyanobacterium Microcoleus vaginatus. *Great Basin Naturalist*. 53: 40-47.

Belnap J., Hawkes CV, Firestone MK. 2003. Boundaries in miniature: two examples from soils. *Bioscience* 53: 739-749. DOI: 10.1641/0006-3568(2003)053[0739:BIMTEF]2.0.CO;2

Belnap J, Phillips SL, Witwicki DL, Miller ME. 2008. Visually assessing the level of development and soil surface stability of cyanobacterially dominated biological soil crusts. *Journal of Arid Environments*. 72: 1257-1264. DOI: 10.1016/j.jaridenv.2008.02.019.

Bras RL. 1990. Hydrology: An introduction to the hydrologic science. *Addison Wesley*. Redding, MA. ISBN: 0201059223. 643 pp.

Booth WE. 1941. Algae as pioneers in plant succession and their importance in erosion control. *Ecology* 22: 38-46. ISSN: 0012-9658.

Bowker M, Reed SC, Belnap J, Phillips SL. 2002. Temporal variation in community composition, pigmentation, and F_v/F_m of desert cyanobacterial soil crusts. *Microbrobial Ecology* 43: 13-25. DOI: 10.1007/s00248-001-10139.

Büdel B. 2001. Synopsis: Comparative Biogeography of Soil-Crust Biota. In *Biological soil crusts: structure, function, and Management*, Belnap J, Lange OL (eds). *Springer-Verlag*. Berlin, Germany; 141-154. ISBN: 3-540-41075-9.

Bureau of Reclamation. 2012. Reclamation, Managing water in the west, Colorado River Basin Water Supply and Demand Study, Executive Summary. 34 pp. Retrieved from http://www.usbr.gov/lc/region/programs/crbstudy.html

Campbell SE. 1979. Soil stabilization by a prokaryotic desert crust: implications for Precambrian land biota. *Origins of Life*. 9: 33-348. DOI: 10/1007/978-94-009-9085-2_8.

Campbell GS, Norman JM. 1988. Water Vapor and Other Gases. In *An Introduction to Environmental Biophysics: second edition. Springer-Verlag*. New York; 42. ISBN: 0-387-94937-2.

Caylor KK, Manfreda S, Rodríguez-Iturbe I. 2005. On the coupled geomorphological and ecohydrological organization of river basins. *Advances in Water Resources* 28: 69-86. DOI: 10.1016/j.advwatres.2004.08.013.

Clapp RB, Hornberger GM. 1978. Empirical equations for some soil hydraulic properties. *Water Resources Research* 14: 601-604.

Cook ER, Seager R, Cane MA, Stahle DW. 2007. North American drought: reconstructions, causes, and consequences. *Earth-Science Reviews* 81: 93-134.

Danin A, Gaynor E. 1991. Trapping airbourne dust by mosses in Negev Desert, Israel. *Earth Surface Processes Landforms* 16: 153-162. DOI: 10.1002/ESP.3290160206.

DeWalle DR, Rango A. 2008. Modelling snowmelt runoff. In *Principles of Snow Hydrology*. *Cambridge University Press.* Cambridge, United Kingdom; 266-305. ISBN: 978-0-521-82362-3.

Dingman, SL. 2002. Evapotranspiration. In *Physical Hydrology, second edition. Waveland Press, Inc.* Long Grove, IL; 272-324. ISBN: 1-57766-561-9.

Dixon JC. 2010. Canyonlands and Arches: Windows on Landscapes in the American Southwest. In *Geomorphological Landscapes of the World*, Mignon P (ed.). *Springer*. Netherlands; 39-47. ISBN: 978-90-481-3054-2.

Duan QY, Gupta VK, Sorooshian S. 1993. Shuffled complex evolution approach for effective and efficient global minimization. *Journal of Optimization Theory and Applications* 76: 501-521. DOI: 10.1007/BG00939380.

Eagleson PS. 1978. Climate, soil and vegetation 5. A derived distribution of storm surface runoff. *Water Resources Research* 14(5): 740-748. DOI: 10.1029/WR014i005p00741.

Eldridge DJ. 2001. Biological soil crusts and water relations in Australian Deserts. In *Biological soil crusts: structure, function, and Management*, Belnap J, Lange OL (eds). *Springer-Verlag*. Berlin, Germany; 315-325. ISBN: 3-540-41075-9.

Eldridge DJ, Greene RSB. 1994. Assessment of sediment yield by splash erosion on a semi-arid soil with varying cryptogram cover. *Journal of Arid Environments* 26: 221-232. DOI: 10.1006/jare.1994.1025.

Evans RD, Belnap J. 1999. Long-term consequences of disturbance on nitrogen dynamics in an arid ecosystem. *Ecology*. 80:150-160.

Felde VJMNL, Peth S, Uteau-Puschmann, Drahorad S, Felix-Henningsen P. 2014. Soil microstructure as an under-explored feature of biological soil crust hydrological properties: case study from the NW Negev Desert. *Biodiversity and Conservation* 23 (7): 1687-1708. DOI: 10.1007/s10531-014-0693-7.

Foos A. 1999. Figure 1. In Geology of the Colorado Plateau. Geology Department, University of Akron. *Copyright by author.*6 pp. Retrieved from: https://www.nature.nps.gov/geology/education/Foos/plateau.pdf

Garcia-Pichel F, Loza V, Marusenko Y, Mateo P, Potrafka RM. 2013. Temperature drives the continental-scale distribution of key microbes in topsoil communities. *Science* 340(6140): 1574-1577. DOI: 10.1126/science.1236404.

Garcia-Pichel F, Pringault O. 2001. Cyanobacteria track water in desert soils. *Nature* 412: 380-381. DOI: 10.1038/35096640.

Garfin GA, Jardine A, Merideth R, Black M, LeRoy S. 2013. Assessment of Climate Change in the Southwest United States: A Report Prepared for the National Climate Assessment. *Island Press*. Washington, D.C.; 531 pp.

George DB, Roundy BA, St. Clair LL, Johansen JR, Schaalje GB, Webb BL. 2003. The effects of microbiotic soil crusts on soil water loss. *Arid Land Research and Management* 17: 113-125. DOI: 10/1080/15324980301588.

Goldreich Y. 2003. The climate of Israel: Observation, research, and application. *Springer.* 270 pp. ISBN: 030647445X,

Graf WL, Wohl E, Sinha T, Sabo JL. 2010. Sedimentation and sustainability of western American reservoirs. *Water Resources Research* 46: W12535. DOI 10.1029/2009WR008836.

Hamon, RW. 1963. Computation of direct runoff amounts from storm rainfall. *International Association of Scientific Hydrology.* Wallingford, Oxenfordshire, United Kingdom. 32 pp/

Harper KT, Marble JR. 1988. A role for nonvascular plants in management of arid and semiarid rangelands. In *Vegetational Science Applications for Rangeland Analysis and Management*. Teller PT (eds). *Kluwer Academic Press*. Dordrecht, Netherlands; 135-169.

Hereford, R. Webb RH, and Graham S. 2002. Precipitation history of the Colorado Plateau Region, 1900-2000. *U.S. Geological Survey Fact Sheet 119-02.*

Herrick JE, Van Zee JW, Havstad KM, Burkett LM, and Whitford WG. 2005. Monitoring manual for grassland, shrubland and savanna ecosystems. Volume I: Quick start. *Jornada Experimental Range*. The University of Arizona press, Tucson, Arizona, USA, p. 236.

Howard AD, Kochel RC. 1988. Introduction to cuesta landforms and sapping processes on the Colorado Plateau. In: *Sapping Features of the Colorado Plateau: a comparative planetary Geology field guide*. Howard AD, Kochel RC (eds.). *NASA.* Washington D.C.; 6-59.

Hu C, Zhang D, Huang Z, Liu Y. 2003. The vertical microdistribution of cyanobacteria and green algae within desert crusts and the development of algal crusts. *Plant and Soil* 257: 97-111. DOI: 10.1023/A:1026253307432.

Jacobs AFG, Heusinkveld BG, Berkowicz SM. 2000. Dew measurements along a longitudinal sand dune transect, Negev Desert. *International Journal of Biometeorology* 43(4) 184-190. DOI: 10/1007/s0048400500007.

Kidron GJ, Yair A. 1997. Rainfall-runoff relationship over encrusted dune surfaces, Nizzana, western Negev, Israel. *Earth Surface Processes Landforms* 22: 1169-1184. DOI. 10.1002/(SICI)1096-9837(199712)22:1<1169::AID-ESP812>3.0.CO;2-C.

Kidron GJ, Yaalon DH, Vonshak A. 1999. Two causes for runoff initiation on microbiotic crusts: hydrophobicity and pore clogging. *Soil Science* 164(1): 18-27. DOI: 10.1097/00010694-1999901000-00004.

King EG, Caylor KK. 2011. Ecohydrology Bearings- Invited commentary. Ecohydrology in practice: strengths, conveniances, and opportunities. *Ecohydrology* 4: 608-612. DOI: 10.1002/eco.248.

Laio F, Porporato A, Ridolfi L, Rodríguez-Iturbe I. 2001. Plants in water-controlled ecosystems: active role in hydrologic processes and response to water stress II. Probabilistic soil moisture dynamics. *Advances in Water Resources* 24: 707-723.

Lan S, Wu L, Zhang D, Hu C. 2012. Successional stages of biological soil crusts and their microstructure variability in Shapotou region (China). *Environmental Earth Earth Sciences* 65: 77-88. DOI: 10.1007/s12665-011-1066-0.

Lange OL, Kidron GJ, Büdel B, Meyer A, Kilian E, Abeliovitch A. 1992. Taxonomic composition and photosynthetic characteristics of the biological soil crusts covering sand dunes in the Western Negev Desert. *Functional Ecology.* 6 (5): 519-527. DOI: 10.2307/2390048.

Le Houérou, HN. 1984. Rain use efficiency: a unifying concept in arid-land ecology. *Journal of Arid Environment* 7: 213-247

Li XR, Zhang JG, Wang XP, Liu LC, Xiao HL. 2007. Study on soil microbiotic crust and its influences on sand-fixing vegetation in arid desert region. *Journal of Integrative Plant Biology* 42(9): 965-970.

Lichner L, Hallet PD, Drongová Z, Czachor H, Kovacik L, Mataix-Solera J, Homolák M. 2012. Algae Influence the hydrophysical parameters of a sandy soil. *Catena* 108: 58-68. DOI: 10.1016/j.catena.2012.02.016.

MacDonald, GM. 2010. Water, climate change, and sustainability in the southwest. *Proceeding of the National Academy of Sciences of the United States of America* 107 (50): 2156-21262. DOI: 10.1073/pnas.0909651107.

Manfreda S, Scanlon TM, Caylor KK. 2010. On the importance of accurate depiction of infiltration processes on modelled soil moisture and vegetation water stress. *Ecohydrology* 3: 155-165. DOI: 10.1002/eco.79.

Marks D, Domingo J, Suson S, Link T, Garen D. 1999. A spatially distributed energy balance snowmelt model for application in mountain basins. *Hydrological Processes* 13: 1935-59. DOI: 10.1002/(SICI)1099-1085(199909)13:12/13<1935::AID-HYP868>3.0.CO;2-C.

Menon M, Yuan Q, Jia X, Dougill AJ, Hoon SR, Thomas AD, Williams RA. 2011. Assessment of physical and hydrological properties of biological soil crusts using X-ray microtomography and modeling. *Journal of Hydrology* 397: 47-54. DOI: 10.1016/j.jhydrol.2010.11.021.

Monteith JL. 1995. A reinterpretation of stomatal responses to humidity. *Plant, Cell, and Environment* 18: 357-364. DOI: 10.1111/j.1365-3040.1995.tb00371.x.

Neff JC, Reynolds RL, Belnap J, Lamothe P. 2005. Multi-decadal impacts of grazing on soil physical and biogeochemical properties in southeast Utah. *Ecological Applications* 15: 87-95. DOI: 10.1890/04-0268.

Nicholas RM, Dixon JC. 1986. Sandstone scarp form and retreat in the land of standing Rocks, Canyonlands National Park. *Canyonlands Research Bibliography*. 30: 167-187.

Pataki DE, Oren R, Katul G, Sigmon J. Canopy conductance of *Pinus taeda, Liquidambar styraciflua* and *Quercus phellos* under varying atmospheric and soil water conditions. *Tree Physiology* 18: 307-315. DOI: 10.1093/treephys/18.5.307.

Petersen KL. 1994. A warm and wet little climatic optimum and cold and dry little ice age in the southern Rocky Mountains, USA. *Climate Change* 26: 243-269. DOI: 10.1007/BF1092417.

Philip JR. 1960. General method of exact solution of the concentration dependent diffusion equation. *Australian Journal of Physics* 13: 1-12. DOI: 10.1071/PH600001.

Pierini, N.A., Vivoni, E.R., Robles-Morua, A., Scott, R.L., and Nearing, M.A. 2014. Using observations and a distributed hydrologic model to explore runoff threshold processes linked with mesquite encroachment in the sonoran desert. *Water Resources Research* 50(10): 8191–8215. DOI:10.1002/2014WR015781.

Porporato A, Laio F, Ridolfi L, Rodríguez-Iturbe I. 2001. Plants in water-controlled ecosystems: active role in hydrological processes and response to water stress III. Vegetation water stress. *Advances in Water Resources* 24(7): 725-744.

Powell S, Smiley FE. 2002. Prehistoric Culture Change on the Colorado Plateau:Ten thousand years on Black Mesa. *University of Arizona Press.* Tucson, Arizona. 221 pp. ISBN: 0816514399

Reed, SC, Coe KK, Sparks JP, Houseman DC, Zelikova TJ, Belnap J. 2012. Changes to dryland rainfall result in rapid moss mortality and altered soil fertility. *Nature*. 2: 752-755. DOI: 10.1038/NCLIMATE1596.

Rodríguez-Caballero E, Cantón Y, Chamizo S, Afana A, Solé-Benet A. 2012. Effects of biological soil crusts on surface roughness and implications for runoff and erosion. *Geomorphology* 145-146: 81-90. DOI: 10.1016/j.geomorph.2011.12.042.

Rosentreter R, Belnap J. 2001. Biological soil crusts of North America. In *Biological soil crusts: structure, function, and Management*, Belnap J, Lange OL (eds). *Springer-Verlag*. Berlin, Germany; 31-50. ISBN: 3-540-41075-9.

Rossi F, Potrafka RM, Garcia-Pichel F, Philippis RD. 2012. The role of expolysaccharides in enhancing hydraulic conductivity of biological soil crusts. *Soil Biology and Biochemistry* 46: 33-40. DOI: 10.1016/j.soilbio.2011.10.016.

Rushforth SR, Brotherson JD. 1982. Cryptogamic soil crusts in the deserts of North America. *American Biology Teacher* 44: 471-475. DOI: 10.2307/4447572.

Rutin J. 1983. Erosional processes on a coastal sand dune, De Blink, Noordwijkerhout. *Physical Geography and Soils Laboratory*. University of Amsterdam, the Netherlands. 144 pp.

Saleh, A. 1993. Soil roughness measurement: Chain method. *Journal of Soil and Water Conservation* 48(6):527-529

Seager R, Ting M, Held I, Kushnir Y, Lu J, Vecchi G, Huan H-P, Harnik N, Leetmaa A, Lau N-C, Li C, Velez J, Naik N. 2007. Model projections of an imminent transition to a more arid climate in southwestern North America. *Science* 316 (5828): 1181-1184. DOI: 10.1126/science.1139601.

Schwinning S, Belnap J, Bowling DR, Ehleringer JR. 2008. Sensitivity of the Colorado Plateau to Change: Climate, Ecosystems, and Society. *Ecology and Society* 13(2).20 pp.

Tchan YT, Whitehouse JA. 1953. Study of soil algae. II. The variation of the algal populations in sandy soil. *Proceedings of The Linnean Society of New South Wales* 78: 160-170.

Thornbury, WD. 1965. Regional geomorphology of the United States. *Wiley & Sons Inc*. New York. 609 pp. ISBN: 0471862002.

U.S. Geologic Survey. 2004. Climatic Fluctuations, Drought, and Flow in the Colorado River Basin. *U.S.G.S Fact Sheet 2004-3042*. 4 pp. Retrieved from: http://pubs.water.usgs.gov/fs20043062

Veluci RM, Neher DA, Weicht TR. 2006. Nitrogen fixation and leaching of biological soil crust communities in mesic temperate soils. *Microbial Ecology* 51: 189-196. DOI: 10.1007/s00248-005-0121-3.

Verrecchia E, Yair A, Kidron GJ, Verrecchia K. 1995. Physical properties of the psammophile cryptogamic crust and their consequences to the water regime of sandy soils, north-western Negev Desert, Israel. *Journal of Arid Environmenst* 4: 427–437. DOI: 10.1016/S01400-1963(95)80015-8.

Vivoni, E.R., Rodríguez, J.C. and Watts, C.J. 2010. On the spatiotemporal variability of soil moisture and evapotranspiration in a mountainous basin within the North American monsoon region. *Water Resources Research*. 46: W02509, DOI:10.1029/2009WR008240.

Volo TJ. 2013. Modeling soil moisture dynamics of landscape irrigation in desert cities (Master's thesis). *Arizona State University*. Retrieved at: https://repository.asu.edu/attachments/114534/content/Volo_asu_0010N_13274.pdf

Volo TJ, Vivoni ER, Martin CA, Earl S, Ruddell BL. 2014. Modelling soil moisture, water portioning, and plant water stress under irrigated conditions in desert urban areas. *Ecohydrology* 7 (5): 1297-1313. DOI: 10.1002/eco.1457

Wang F, Zhung Z, Hu Z. 1981. Nitrogen fixation by an edible terrestrial blue-green algae. In: *Current Perspective in Nitrogen Fixation,* Gibson AH, Newton WE (eds.). *Elsevier-North Holland.* Amsterdam; 455

Warren SD. 2001a. Biological soil crusts and hydrology in North American Deserts. In *Biological soil crusts: structure, function, and Management*, Belnap J, Lange OL (eds). *Springer-Verlag*. Berlin, Germany; 328-347. ISBN: 3-540-41075-9.

Warren SD. 2001b. Synopsis: Influence of biological soil crusts on arid land hydrology and soil stability. In *Biological soil crusts: structure, function, and Management*, Belnap J, Lange OL (eds). *Springer-Verlag*. Berlin, Germany; 350-360. ISBN: 3-540-41075-9.

Wertin TM, Reed SC, Belnap J. 2015. C_3 and C_4 plant responses to increased temperatures and altered monsoonal precipitation in a cool desert on the Colorado Plateau, USA. *Oecologia* 177: 997-1013. DOI: 10.1007/s00442-015-3235-4.

Western Regional Climate Center. 2009. *Moab, UTAH (425733): Period of Record Monthly Climate Summary*. Retrieved from http://www.wrcc.dri.edu/cgi-bin/cliMAIN.pl?utmoab

Woodhouse CA, Gray ST, Meko DM. 2006. Updated streamflow reconstructions for the Upper Colorado River Basin. *Water Resources Research* 42: W05415. DOI: 10.1029/2005WR004455.

Yair A. 2001. Effects of biological soil crusts on water redistribution in the Negev Desert, Israel: a case study in Longitudinal Dunes. In *Biological soil crusts: structure, function, and Management*, Belnap J, Lange OL (eds). *Springer-Verlag*. Berlin, Germany; 304-313. ISBN: 3-540-41075-9.

APPENDIX A

FIELD DATA COLLECTION

This appendix contains descriptions of the datasets collected at the experimental plots during two, one week-long, field work campaigns during summer and fall 2014. The first section contains a field map for referencing the location of all field sites, or plot quadrants (quads), where the following field methods were used to quantify the cover conditions near and over each location where soil moisture measures were taken at depth. The method materials, standard procedure, and rules are then discussed and listed for each of the following field measures: soil depth to bedrock (Z_b), percent species cover (p), roughness index (RI), and leaf area index (LAI). Tables of the results for Z_b and LAI measures are also provided below. The data of the pc and RI measures can be found in Table 1.

A.1 **Field Site Map**

Below is a map of the DOE field site showing all plots contained within the fenced perimeter (thick black line). Note that the map is not drawn to scale. A map key is provided on the right outlined with a thin black dashed line. The five blocks of each B or C block type (B1 though B5 and C1 through C5), outlined in brown, and all plots contained within each block. The water treatment plots of each block contain colored boxes over the treated quadrants (quads) where measurements were taken. Red boxes correspond to the quads that received the w-treatments (i.e. quads B1w through B5w). Blue blocks correspond to the quads that received the x-treatments (i.e. quads B1-x through B5-x and C1-x through C5-x). Control plots of each block contain black boxes over the control quads (i.e. quads B1-c through B5-c and C1-c through C5-c) where measurements were taken. Additional plots are also shown in this map that received some

heated lamp treatments (grey outlined boxes with italicized labels) and were used in other studies besides this thesis (Reed *et al.* 2012; Wertin *et al.* 2015). This map was saved as FieldMap.ai in the AppendixA folder and can be opened and edited in adobe acrobat.

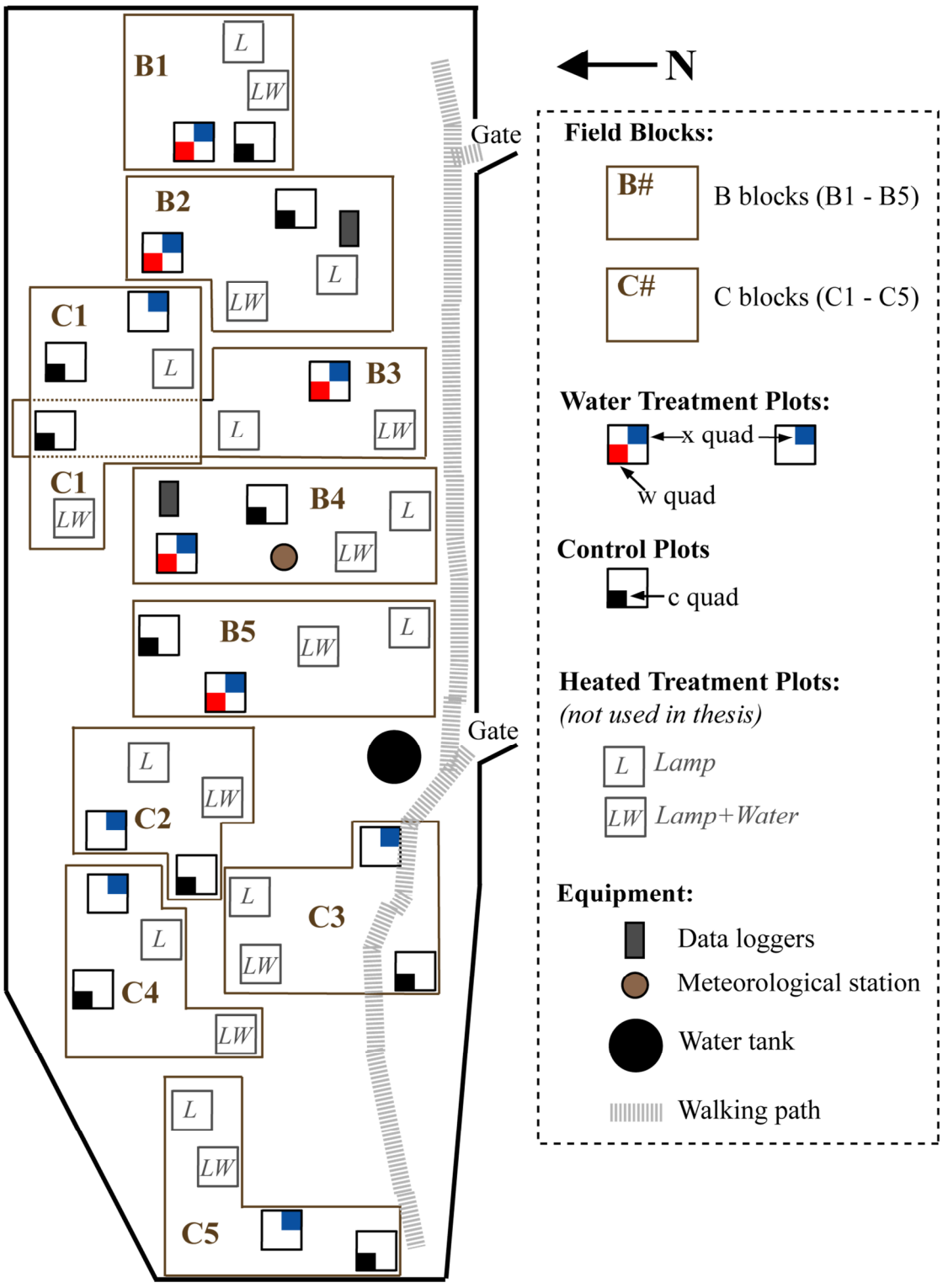
B1
L
LW
B2
L
LW
C1
L
B3
L
LW
C1
LW
B4
L
LW
B5
LW
L
Gate
Gate
L
LW
C2
L
C3
LW
L
C4
LW
L
LW
C5
N
Field Blocks:
B#
B blocks (B1 - B5)
C#
C blocks (C1 - C5)
Water Treatment Plots:
x quad
w quad
Control Plots
c quad
Heated Treatment Plots:
(not used in thesis)
L
Lamp
LW
Lamp+Water
Equipment:
Data loggers
Meteorological station
Water tank
Walking path

A.2 Soil Moisture Data

All quads except for the x-treated quads were equipped with three repetitions, or "reps", of soil moisture probe profiles. The x-treated quads were equipped with just one soil moisture probe profile rep. Each profile was equipped with the soil moisture probes described in section 2.2. The B1, B2, and B5 blocks had a "short" Campbell Scientific 616 probe at 2 cm depths. This "short" probe is a shortened Campbell Scientific probe that was calibrated to the long probes using a range of soil moistures from dry to wet using soil collected from the site and an equation created so that the output volumetric water content of the shortened probes would read the same as the long probes for a given water content.

Volumetric water content was recorded hourly from each sensor throughout the entire study period. Soil temperature was also recorded but was not utilized in this study. Whitney_Thesis/AppendixC/RawSoilObservations.txt contains the raw moisture and temperature observations at each site (note the file is saved under the AppendixC file since Appendix C describes the data processing). Each row contains the measurements made at one sensor with the comma-separated values for the following fields arranged in the following order with units in parenthesis where applicable:

Timestamp (MM/DD/YYYY hh:mm:ss),

Block Type (B or C),

Treatment (c, w, or x),

Soil moisture instrument ("CSVW" for "short" Campbell, "CVW" for Campbell, or "DVW" for Decagon),

Depth of measure (2, 5, or 10; in cm),

Rep (1, 2, or 3),

Temperature (C),

Original volumetric water content,

Manufacturer ("CS" for Campbell Scientific, or "DC" for Decagon),

Original mV or period recorded (depending on probe manufacturer),

Temperature corrected mV or period (depending on probe manufacturer),

Temperature corrected volumetric water content.

Note that in this spreadsheet, all watering treatments over C type blocks are called "w" treatments, not "x" treatments, according to the naming convention originally used at the DOE site. This C type watering treatment, however, consisted of the same irrigation amounts and frequencies as the x treatment for B type blocks (not the w treatments for the B type blocks). In these early soil moisture processing scripts and data files, this original naming convention is utilized (i.e. C block water treatments are called "w" treatments). In later modeling and analysis scripts (see Appendices D-F) and in the written thesis report, C type irrigations are called "x" not "w" treatments. This new naming convention was utilized to maintain consistency with the types of treatments utilized and named at the B type blocks.

Appendix C below describes how these raw soil moisture datasets were processed for use in this study.

A.3 Meteorological Data

The meteorological data was collected from an onsite weather station that has been known by the names “Uhura”, “Lisa”, and “Lisa2”. The station collects data of incident radiance, wind speed and direction, total precipitation from a tipping bucket rain gauge, net radiation, air temperature, relative humidity, and Barometric pressure (absolute). Whitney_Thesis/AppendixC/Meteorology.xlsx contains the data collected from Uhura and used in this study. This file contains the raw data and worksheets used to process the raw data for use with the model. Below is a description of the worksheet *raw* with the raw data. Appendix C describes the other worksheets and processing methods.

The *raw* worksheet contains the hourly measurements taken from Uhura used for this study during the study time period. This worksheet contains the following headers with descriptions separated by a colon and units in parentheses where appropriate:

DOY: day of year

Date/time: Timestamp (MM/DD/YYY hh:mm)

AirTemp: Average air temperature (C)

RH%: Average relative humidity (%)

Precip_mm: Total Precipitation for the hour (mm)

A.4 Soil Depth Measurements

Soil depth to bedrock was measured next to every control and water treatment quad (i.e. B1c through B5c, C1c through C5c, B1w through B5w, B1x through B5x, and C1x through C5x) using a rod and hammer approach. Below are outlined lists of the materials, standard procedure, and specific rules used for this approach. Also provided

are the field measurement results that were recorded on the Soil Depth Field form. This field form is stored as an excel spreadsheet found on the hard drive under the filename path AppendixA/DataForms/SoilDepthForm.xls.

A.4.1. Soil Depth: Materials

1. Metal mallet(s).
2. Workers gloves.
3. One stainless steel rod with a diameter of 10 mm, a beveled edge, and a total length Z_{rod} of 1.5 m.
4. Small magnetic level.
5. Measuring tape.
6. Clipboard, Soil Depth Data Form (AppendixA/DataForms/SoilDepthForm.xls)
7. Pencil(s).

A.4.2. Soil Depth: Standard Procedure and Rules

1. Starting at the uphill side of the most uphill plot in the pathway and working around one side of every plot.
2. Use the measuring tape to measure the length of the rod L_r before every depth measure and record in the L_r column of the data form.
3. While wearing gloves, hold rod on top (non-bevel side), place bevel side over measurement location (in pathway).
4. Use level to ensure rod is vertical.

5. Use other hand to hammer rod into ground until rod hits bedrock. Bedrock is reached once there is a drastic increase in resistance to hammering the rod deeper.
6. Use measuring tape to measure the distance from ground to top of rod Z_g and record this number in the Z_g column of data sheet.
7. Pull rod out of ground.
8. Calculate soil depth (Z_b) utilizing the following equation and record number in Z_b column of data sheet.

$$Z_b = L_r - Z_g .$$

9. Repeat on one side each quad location.

A.4.3. Soil Depth: Results

The following table shows the recorded results of the soil depth Z_b measurements. These measures have been stored as an excel spreadsheet found on the hard drive under the filename path AppendixA/Data/SoilDepthData.xlsx. Since the soil across the site mantles a field of boulders, which were weathered from the canyon walls at higher elevations, the Z_b measurements show high variability. Thus the standard deviation around the mean value (303 to 850 mm) was used for calibration of rooting depth Z_r.

Quad	Length of rod L_r [cm]	Height above ground Z_g [cm]	Soil Depth Z_b (L_r-Z_g) [cm]
C5c	150	104.8	55.2
C5x	150	94.5	69.5
C4c	150	60.5	91.5
C1x	150.1	71.2	78.9
B5c	152.8	112.6	49.2
B5w	152.6	117	43.6
B5X	152.5	91.4	71.1
C2x	153.7	73.8	90.3
C2c	152.3	132.1	34.2
C3x	152.6	133.1	28.5
C4x	149.8	89.5	65.3
C3c	152.2	89.6	71.6
B4w	153.3	84.5	80.4
B4x	152.6	144.4	17.2
B4c	152.1	88.1	79
B3x	152.4	131	31.4
C1c	152.5	38	122.5
B3w	152.1	81.4	76.7
B3c	152.2	126.7	17.5
B2w	149.9	125.5	38.4
B2x	153.3	136.5	33.4
B2c	152.2	127	34.2
B1w	149.8	115	39.8
B1x	152.1	132.9	32.2
B1x	153.1	62.5	88.6
		Average Z_b:	57.6
		Standard deviation :	27.3

A.5 Percent Cover Measurements

The grid-point intercept is adapted from the line-point intercept method (Herrick *et al.*2005) and quantifies the soil cover, including vegetation, litter, rocks and BSC species. The grid-point intercept involves totaling the number of times each species is present at each intersection point of a grid and dividing that total by the total number of grid intersection points. The following includes lists of the materials, and standard procedures and rules, and results description. The percent cover data form used to record the field measurements, is stored as an excel file found on the hard drive under the filename path AppendixA/DataForms/PercentCoverForm.xls.This form contains three spreadsheets. The first spreadsheet *Codes* contains all code names for each cover and species type. The second spreadsheet *Form* contains the data form that can be printed and used to record the field measurements according to the procedure below. The third spreadsheet *Photos* contains example photos of the species present at the field site used as reference for the percent cover measurement method.

A.5.1. Percent Cover: Materials

1. A 102 cm by 42 cm grid frame with 6 cm by 6 cm cell size.
2. One pointer, which consists of a straight piece of wire or rod, such as a long pin flag, at least 75 cm long and less than 1mm in diameter.
3. Clipboard, Grid-Point Intercept Data Form (see below) and pencil(s).

A.5.2. Percent Cover: Standard Procedures and Rules

1. Record the quad location on the data form (refer to section A.1 for quad names and map).
2. Lay grid down frame to line up with the edge of the quad, and center over soil moisture sensors, while observing these rules:
    a. The quad boundaries are outlined with wire, and the location of the three subsurface soil moisture sensor profiles of each quad are indicated by the presence of three groups of wires that feed from the surface to the subsurface.
    b. Begin at the outermost corner of cell 1, which is universally located on the northwest side of the grid frame at all quad location.
    c. Always stand on the same side of the grid.
3. Drop a pin flag to the ground from a standard height (100 cm) next to the tape, while observing these rules:
    a. The pin should be vertical.
    b. The pin should be dropped form the same height each time. A low drop height minimizes “bounces” off of vegetation but increases the possibility for bias.
    c. Do not guide the pin all the way to the ground. It is more important for the pin to fall freely to the ground than to fall precisely on the mark.
4. Once the pin flag is flush with the ground, record every plant species it intercepts on the data form within the row of the given cell , while observing these rules

a. For any species present in the top layer, record an “L” to indicate living or “D” to indicate dead under the appropriate code column (see *Code* worksheet of PercentCoverForm.xls)
b. Record the present of any materials in the lower and surface layers by recording the appropriate code within the “Lower” and “Surface” columns of the data form.

5. Repeat steps 3 and 4 at all intersection points of cells until measurements have been taken/recorded at all 96 intersection points once, while observing the following rules:
    a. When moving to the next cell, move from downhill to uphill (or west to east) for each row.
    b. When you have reached the last cell in the row, move to the next row located southward.
6. Repeat for all quadrants of all 25 quads (see section A.1 for measured quads and locations).

A.5.3. Percent Cover: Calculations and Results

The measurements obtained from this procedure can be used to estimate percent cover and fractional vegetation of each quad according the description and equations presented in section 2.2. The field measurements and results presented in Table 1 are stored on the external hard drive under the filename path AppendixA/Data/PercentCover.xls. This excel file contains multiple spreadsheets for all measurements used for estimating percent cover. Each of these spreadsheets contains the

measurements of a given quad organized such that each row corresponds to a grid point and each column corresponds to a species or material code. A value of "1" was placed in the cell if the given species or material was present at the grid interception point, otherwise a value of "0" is present. The last column of each quad spreadsheet records the results for an additional code *V* that indicates the general count of vegetation. Each row of the *V* column contains a "1" if vegetation was present at the given grid interception, and a "0" if not vegetation was present

Each of these spreadsheets are labeled by the quad name. The second to last spreadsheet *CountTotals* contains the total number of counts for each of the codes and for the total number of vegetation counts (*Nv*) for each of the quad locations. The final spreadsheet of the file *results* contains the percent cover and vegetation fractions presented in Table 1, with live links to the other worksheets to estimate the results according the equations 4 and 5.

A.6 **Roughness Index Measurements**

The Chain Method was proposed by Saleh 1993, as a quick and easy method for measuring the roughness index (RI) of BSC surfaces proposed. This method and the equation for estimating the final RI value for each quad is discussed and presented in section 2.2 (eq. 6). The following includes lists of the materials, and standard procedures and rules. The roughness index data form used to record the field measurements, is stored as an excel file found on the hard drive under the filename path AppendixA/DataForms/RoughnessIndexForm.xls. The results are stored as an excel file found on the hard drive under the filename path

AppendixA/Results/RoughnessIndices.xls. This excel file has two worksheets. The first *FieldMeasures* contains all RI values estimated in the field and the second *Results* contains the results presented in Table 1, as estimated from equation 6.

A.6.1. Roughness Index: Materials

1. One 30-cm length jewelry chain with 2 mm chain links.
2. One measuring tape with units of centimeters.
3. Clipboard, Jewelry Chain Data Form and pencil(s).
4. A 102 cm by 42 cm grid frame with 6 cm by 6 cm cell size.

A.6.2. Roughness Index: Standard Procedures and Rules

1. Starting in the first quad of measure, look to see if biological soil crust is present over sensors.
    1.1. Sensor locations are indicated by the presence of wires.
    1.2. If there is biological soil crust present on top of the area over soil moisture sensors move onto step 2.
    1.3. If no biological soil crust is present, mark “NC” in the “Measured length” column of data sheet and move onto step
2. Lay grid down frame to line up with the edge of the quad, and center over soil moisture sensors, while observing these rules:
    2.1. The quad boundaries are outlined with wire, and the location of the three subsurface soil moisture sensor profiles of each quad are indicated by the presence of three groups of wires that feed from the surface to the subsurface.

2.2. Always stand on the same side of the grid.

3. Take visual notes of the approximate location of the edges and midpoints of the short edge of the grid (i.e. the sides that are perpendicular your position).
4. Remove the grid and CAREFULLY drape the jewelry chain across biological soil crust over the area above soil moisture along a transect that is parallel to the quad edge and runs along the location of the grid edge furthest away from your position (locations visually noted in step 3).
    4.1. Quickly brush away loose litter or unembedded small rocks that lie along the chain path and may influence its length.
    4.2. Leave embedded litter and rocks in place.
    4.3. Take care to ensure that the links of the chain are fully extended (not bunched) and that the chain is in full contact with the surface along its entire length—following the rise and dip of each micro-topographic feature as closely as possible.
5. Using the measuring tape, measure the horizontal distance between the ends of the chain in centimeters.
6. Record this measurement in the "Draped length" column of data sheet.
7. Carefully pick up chain and repeat above steps two more times along two transect that are parallel to the quad edge and run along the location of the grid midpoints and grid edge closest to your position (locations visually noted in step 3).
8. Once all 3 grid transects have been analyzed, move to next step.
9. Repeat for all quadrants of all 25 quads (see section A.1 for measured quads and locations).

A.7 **Leaf Area Index Measurements**

The following description and method of measuring Leaf Area Index (LAI) is detailed according to the guidelines and descriptions provided in the LI-COR LAI-2200 Instruction Manual. The Leaf Area Index (LAI) is a measure of one-sided leaf surface area per ground area. The amount of foliage in a canopy can be indirectly measured from measurements of the radiation attenuation rate through the canopy. This study used the LAI-2200 Plant Canopy analyzer to calculate LAI from light measurements made with a "fish-eye" optical sensor. This instrument calculates LAI from the transmittance estimated from five zenith angles by comparing readings made with the sensor above and below the canopy.

Assumptions of this method include: (1) Since foliage typically reflects and transmits little radiation in spectrums >490nm, the optical filter rejects radiation in this portion, and thus, foliage is assumed black (i.e. below-canopy readings do not include any light that is reflected or transmitted in spectrums >490nm); (2) Foliage is randomly distributed within any foliage-containing envelope; (3) Foliage elements are small compared to the area of view of each ring (distance between sensors and nearest leaf above is at least 4x the leaf width); (4) Foliage has random azimuthally orientations. The plant canopies over the DOE field site are contained within small heterogeneous plots (i.e. multiple species per plot), and therefore, a careful protocol must be designed and implemented to minimize the influence of neighboring plants on LAI measures. Furthermore, the amount of sunlight measured is sensitive to the sun angle and measurements made in direct sunlight can result in overestimation of canopy gaps and

underestimates of LAI. Thus, this study conducted measurements during sunset when the light was not directly overhead.

The following lists the materials and standard procedures and rules utilized for the LAI measurements. The LAI data form used to record the field measurements, is stored as an excel file found on the hard drive under the filename path AppendixA/DataForms/LAIForm.xls. This file contains two worksheets. The first spreadsheet *Form* contains the data form. The second spreadsheet *Photos* contains example photos of the species present at the field site. The results are stored as an excel file found on the hard drive under the filename path AppendixA/Results/LAI.xls. This excel file has two worksheets. The first *FieldMeasures* contains all LAI values estimated and recorded in the field and the second *Results* contains the average LAI values for the three main species used to upscale the species-specific stomatal conductance ($g_{s,sp}$) measurements taken by Wertin *et al.* 2015 (eq. 65).

A.7.1. Leaf Area Index: Materials

1. LAI Control Unit with 4 fresh AA batteries.
2. LAI optical sensor.
3. View caps.
4. 9-pin female to female RS-232 cable.
5. LAI-2200 Instruction Manual.
6. Clipboard, LAI Data Form (see AppendixA/DataForms/LAIForm.xls.) and pencil(s).

7. Field photos of three species (see AppendixA/DataForms/LAIForm.xls.) to be analyzed.
8. Extra AA batteries and screwdriver
9. Field marker flags.

A.7.2. Leaf Area Index: Standard Procedures and Rules

1. Before the day of measurement, locate 4-8 ideal measurement locations for each of the three species and place a field marker flag, while observing the following rules:
   1.1. Look for an area where the species considered is prevalent in high densities and is somewhat isolated from other species/obstructions (i.e. fencing, lamps, posts, etc).
   1.2. Try to get as close to an ideal of location flagged and consider using lens caps if the location is not ideal (see step 4 for more info on lens cap guidelines).
2. Before the day of measurement, set up basic configurations of equipment and obtain gate code for field site, while observing the following rules:
   2.1. Define A readings as above canopy and B readings as below canopy on the control unit by navigating to main menu > log setup >transcomp.
   2.2. Define prompts, “plant type” and “location” (to be filled out during field measurements) on the control unit by navigating to main menu > log setup > Prompts.
   2.3. Set time to Mountain Time Zone on control unit by navigating to main menu > console setup > set time

3. Arrive at field location before sunset to set up equipment, while observing the following rules:
    3.1. Attach the 3-pin wire to bulkhead connectors on control unit and sensor wand.
    3.2. Press the power button on the control unit. The on/off indicator should light up on the sensor wand.
    3.3. Scan field to refresh your memory of the marker flag locations (remember, time is of the essence with this measurement!).
4. Go to first measurement location with instrument, clip board, pencils, and lens caps of different viewing angles.
5. At measurement location determine the necessary number of B readings (i.e. below canopy readings) and lens cap for use on sensor, while observing the following guidelines:
    5.1. The proper number of B readings depends upon the ground area over which the compute LAI is to be valid, what fraction of this area that one B reading represents, and the variability of the density of the foliage in the plot (a homogenous canopy requires fewer B readings than a heterogenous one). The following procedure is used to determining the number of B readings necessary for 95% confidence that the true LAI mean is within +/-10% of the measured LAI (from instruction manual):
6. Make an LAI reading based on 6 B readings (see step 10 for how to make a reading). Be sure to include both the thinnest and densest parts of the canopy.
7. Divide the Standard Error of LAI by the LAI (SEL/LAI). SEL and LAI can be viewed in the console by navigating to menu > data >consoled data > select data field > view)

8. Use the photographed table below (table 4.1 from manual, page 4-4) to determine the number of B readings and record this value in the appropriate column of the datasheet:

SEL/LAI	# B Readings	SEL/LAI	# B Readings
0.01	2	0.06	11
0.02	3	0.07	13
0.03	5	0.08	16
0.04	6	0.09	19
0.05	8	0.1	23

9. Determine the proper lens cap for use with the given canopy area. The following guidelines were selected from the manual as appropriate for our plot area, additional guidelines from the manual may be more useful once in the field, however (see Chapter 5 of manual) to determine the proper lens cap for the given canopy area:

    9.1. For small plot areas:

        9.1.1. "In a canopy that is 1m high, the sensor should be at least 3m from the edge (i.e. the edge between species canopy of interest and anything else such as another species type or bare ground areas) in any direction that it can "see". In a plot so small that the sensor will "see" outside the plot area if measured form the middle, once could use a 90^{o} view cap and make readings form the corners looking into the plot. Alternatively, a 180^{o} view cap could be used if the measurement were taken near the center of the plot." (Manual pages 5-1 to 5-2)

9.1.2. The following photographed figure (from Manual page 5-2) contains diagrams of the suggested lens cap orientation in small plot area:

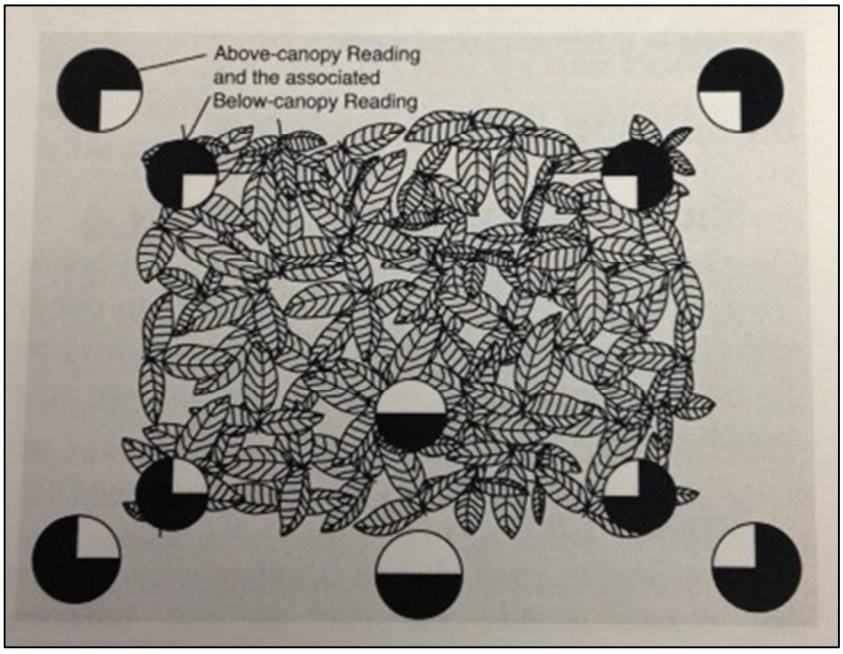

9.1.3. "In dense canopies, the minimum plot size may be reduced if foliage blocks enough of the sensor's view. This is easily tested by getting down on the ground and looking up at about 30o elevation angle. If you are unable to see the edge of the plot from this vantage point, then the plot is large enough regardless of its actual dimensions." (Manual pages 5-1 to 5-2)

9.2. For canopies with large gaps, "Use a view cap to restrict the sensor's field of view, so that dense and sparse regions of the canopy are included in separate B readings. [The figure] below illustrates how a 45^{o} view cap can help isolate a gap near a transect" (Manual page 5-8 to 5-9)

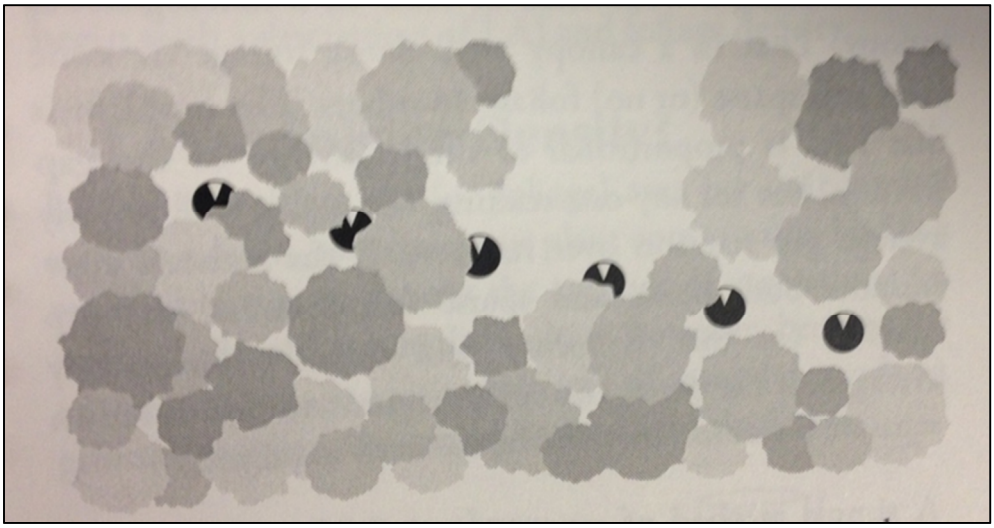

9.3. For canopies next to obstructions (e.g. fencing, posts, heatlamps), the 90^{o} or 45^{o} view cap can be used so that the viewing range of the sensor is blocked from viewing the obstruction(s).

9.4. Record the estimated # of B measures and angle of the appropriate lens cap on the data sheet along with the plot type (i.e. B or C plot, block #, treatment, and quad) and species abbreviation (Ac for *A. confertifolia*, Pj for *P. jamesii*, and Ah for *A. hymenoides*).

10. Place appropriate lens cap on sensor (determined in step 4 above) and take one A measurement (i.e. above canopy) and appropriate number of B measurements (i.e. below canopy; determined in step 9 above), according to these guidelines:

10.1. Place desired view cap on the sensor with the opening pointing away from the handle.

10.2. Press the START|STOP button on the control unit and choose New File. Enter file name (e.g. MoabDay1)

10.3. Enter responses to the prompts (set in step 2 above; e.g. species abbreviation and plot or GPS location)

10.4. Position the optical sensor above the canopy. Be sure it is parallel to the ground (i.e. if ground is sloped, hold sensor parallel to the slope not level) and that no foreign objects are in view of the sensor (use lens caps to accomplish this; see lens cap guidelines in step 4 above or in manual chapter 5). Verify that the Above LED is illuminated (press the A/B button on the wand if it is not). Press Log button on the wand or control unit to record an above reading

10.5. Press the A/B button (the above LED will turn off). Hold the optical sensor below the canopy (parallel to slope and oriented in the same direction as the above-canopy reading was) and press the Log button to record a Below reading.

10.6. Continue making B readings, moving the sensor to a new location each time (use guidelines in step 4 above or chapter 5 in the manual to decide on appropriate measurement location within the canopy). Typically, the distance between B readings is on the order of the canopy height. However, our plots are small so may need to restrict these measures according to guidelines in step 4 above. You can intersperse a readings as necessary, if sky conditions or the view direction changes.

10.7. When you are finished, LAI, MTA, SEL, and SEM values will be visible in Logging mode (use the arrow keys to change what is displayed). Record these values on the datasheet.

10.8. Press START|STOP button to close the file and exit the logging mode.

11. As long as the sun is not directly overhead, continue taking measurements at all flagged locations until 4 -8 LAI measures are made for each species, and be mindful of the following:

    11.1. If measurements are not completed before the sun is directly set, come back the next day to complete the measurements.

    11.2. Make all A and B readings with your back to the sun, with a view cap blocking the sensor's vie of you and the sun.

    11.3. Make sure your head or another object shades the sensor whenever an A or B reading is made. Even though the view cap prevents the detector form seeing direct sun, shading the optics prevents reflected sunlight from influencing readings.

    11.4. If possible, shade the part of the canopy that is visible to the sensor. The more sunlit leaves the sensor can see, the larger the underestimate of LAI.

APPENDIX B

UNMANNED AERIAL VEHICLE IMAGERY

This appendix contains the aerial imagery obtained at the DOE site using an unmanned vehicle. This imagery is shown in the figure below and is saved as UnmannedImagery.jpg in the AppendixB folder.

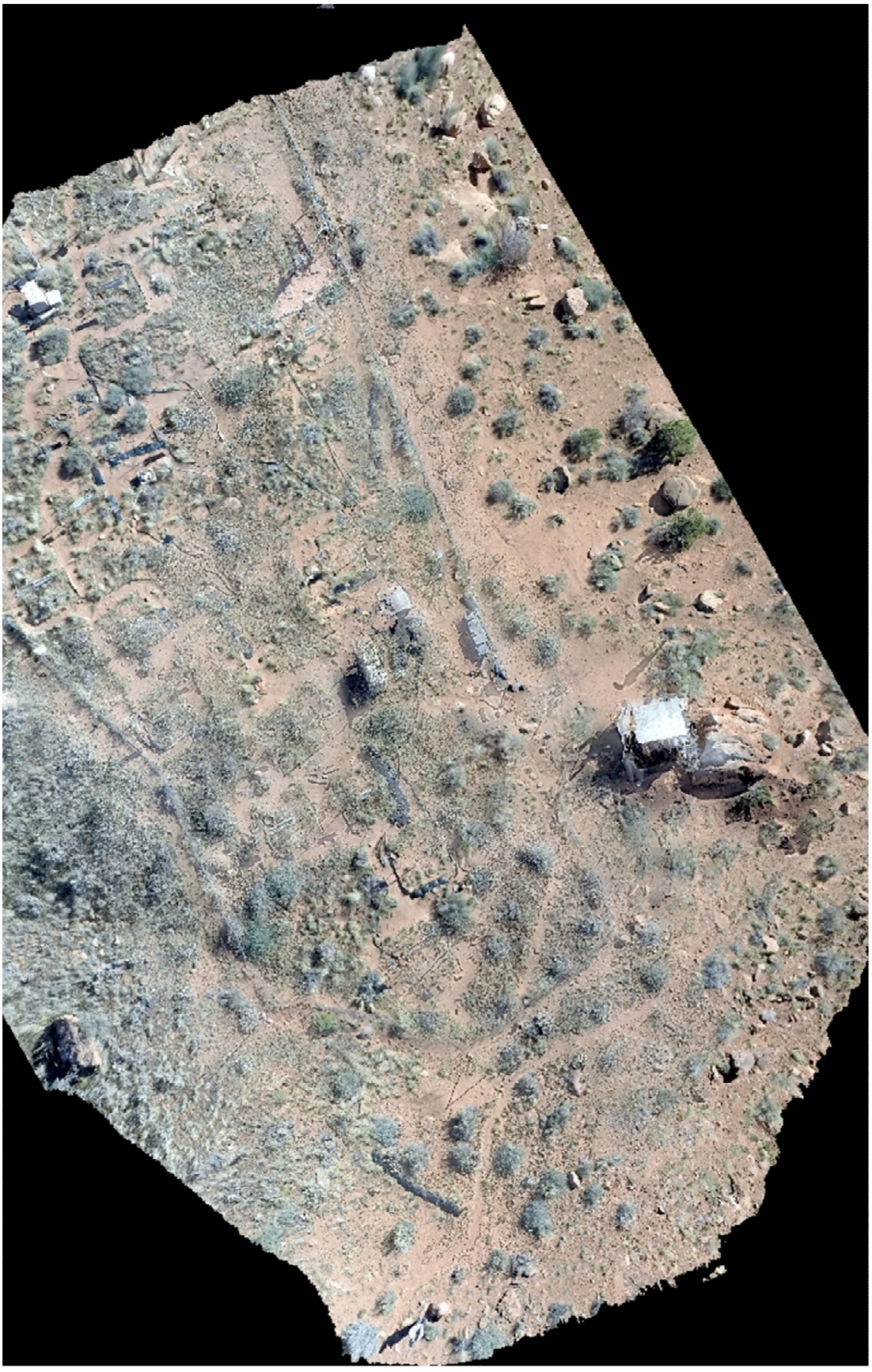

APPENDIX C

SOIL MOISTURE AND METEROLOGICAL DATA

This appendix describes the scripts and files used to process the soil moisture and meteorological observations for use with the model. All files and scripts used for this processing are contained on the external hard drive under the file AppendixC.The processed files used for the model are output to the AppendixC/ProcessedData. The processing of the soil moisture and meteorological observations are discussed in two separate sections below.

C.1 **Processing Soil Moisture Observations**

The raw soil moisture observations contained in the file sm_hourly.csv were first averaged to the daily time step, re-arranged and parsed into .txt files for each of the DOE quads using the script DailyParsing.m. This script first computes the daily average for each of the sensor measurements for each depth of each profile rep of each quad (see A.2). Then the script creates a separate matrix for each of the quads organized such that each rows contains all measurements from each rep and depth taken on a given day and the date information all separated by a comma. Each matrix is output to the folder AppendixC/Parsed and saved as a .txt file entitled M_X_entire_VWCT where X is the given block (B1, B2, B3, B4, B5, C1, C2, C3, C4, or C5).

Next, the depth-weighted average of each profile was estimated in the script DepthWeightedAve.m. This script pulls each quad matrix contained in the AppendixC/Parsed folder and estimates the depth-weighted average of each profile rep using the equation and general approach outlined in section 2.2. (eq. 3, Figure 6). For each day, the script estimates and consecrates the depth-weighted averages to each row of the given day of each individual quad matrix. Each matrix is output to the folder

AppendixC/DepthAve and saved as a .txt file entitled M_X_daily_DepthAve.txt (X is the name of the block, B1 through B5, or C1 through C5).

In the final processing step, the spatial average of all three reps of each quad was estimated next using the script AveragingReps.m. For each quad, the script pulls the corresponding file contained in the AppendixC/DepthAve folder and computes the average of the three rep measurements across each depth of measurement and across the depth-weighted average estimates. The script creates a matrix for each quad organized such that each row contains the date information and the average rep measurement value for each of the depths of measurement and the depth-weighted average estimate. Each matrix is output to the folder AppendixC/Processed and saved as a .txt file entitled M_X_AveRep.txt (X is the name of the block, B1 through B5, or C1 through C5).

C.2 **Processing Meteorological Observations**

Whitney_Thesis/AppendixC/Meteorology.xlsx contains the data collected from Uhura and used in this study. This file contains the raw data and worksheets used to process the raw data for use with the model (see A.3 for description of the raw data contained on the *raw* worksheet). The second worksheet *PivotAve* contains a pivot table, linked to the data of the *raw* worksheet, which computes the average relative humidity and air temperature of the day. The third worksheet *PivotPrecip* computes the sum of the total precipitation of the day (P_T). The third worksheet *PET* is linked to the data of the *PivotAve* worksheet and computes the daily PET according the approach and equations outlined in section 2.2 (eqs. 1-2).

The fourth worksheet *WRCC_data* contains the data obtained and used to estimate the fraction of snow (f_s) and rain (f_r) from a nearby site to aid in partitioning P_T , as described in section 2.3.1 (eqs. 12-18). The last column of this worksheet contains these f_s and f_r estimates. The data contained in this worksheet was obtained from the WRCC website (http://www.wrcc.dri.edu/summary/Climsmut.html). Daily snowfall data was obtained for the Moab station (425733) from the WRCC website (http://www.wrcc.dri.edu/summary/Climsmut.html).

The next worksheet *Irrigation* contains a summary of all experimental watering events taking place during the time period. The first four columns contain the date and depth of water added for the B-w, B-x, and C-x treatments obtained from the DOE watering schedule archives. The next here columns contains the year, month, and day of the event. The last three columns contain the estimates of the depth of watering in mm over the fractional area of the quad that is assumed sensed by the three rep sensor profiles (0.34272). All conversion factors for units and for estimating the fractional area are contained in a subsection of cells at the top of the worksheet above the main data columns. The last worksheet *met_entire* contains all of the meteorological estimations made in the previous worksheets for use in the model where each row contains all values for a given day organized under the following column headers in bold (units described here in parentheses):

DOY (day of year),

Year,

Month,

Day,

Ave_Air_Temp_C (^{o}C)

Ave_RH_perc (%)

Total_Precip_mm (mm)

Bw (B-w treatment in mm)

Bx (B-x treatment in mm)

Cx (C-x treatment in mm)

PET (Potential evapotranspiration in mm)

D (Julian day of year used for DDF measurement eq. 8)

Fs_near (f_s estimated from the nearby snow data)

Pt_dur (duration of total precipitation in hours, *h*, estimated from hourly precipitation data and used in eq. 33 for estimation of partitioned precipitation duration)

day_dur (duration of daylight, D_d, estimated in worksheet *PET* and used in eq. 33 for estimation of partitioned precipitation duration)

This last worksheet *met_entire* was saved as the excel file AppendixD/met_entire.xls and used as the meteorology input for the model described below.

APPENDIX D

ECOHYDROLOGY MODEL SCRIPTS

This appendix describes the MATLAB scripts built to run the ecohydrology model and output the verification figures, comparison metrics (Table 7), and experiments used in this study. All scripts are in the AppendixD folder and are initialized by running a main.m function. Four sections are included below to describe the scripts for creating the verification figures, for computing the comparison metrics, and for conducting the experiment and creating the appropriate figures, and for fitting lines to the calibrated parameters. A fifth section also discusses the script used to plot and visualize an observation time series as shown in the example of Figure 7.

D.1 **Verification Figures**

All scripts and files necessary to re-create the verification figures provided in this thesis (Figures 16-17) are positioned within the AppendixD/Verificaton folder to allow for plotting through the execution of a main_VerFig_X.m function, where X corresponds to the figure number and letter (X = 16a, 16b, 17a, or 17b for Figures 16a, 16b, 17a, and 17b, respectively) from the MATLAB terminal. The MATLAB figure versions (.fig), 600-dpi compressed TIFF versions, and processed and edited versions of these figures are also available as .ai files in the Whitney_Thesis/AppendixH folder described in Appendix H.

Prior to running the script, the user should specify the following variables in bold (descriptions provided below after the colon):

Ew_toCrust: An argument to specify whether to trap and condense a portion of bare soil evaporation (E_w) within the BSC layer rather than evaporating all of E_w. Specify 1 for yes and 0 for no. This variable has been pre-set in the script to 1.

k_yes: An argument to specify whether to use the PET weighting factor, k_v. Specify 1 for year and 0 for no. This variable has been pre-set in the script to 1.

crust_yes: An argument to specify whether to turn the crust layer on or off. Specify 1 for on and 0 for off. This variable has been pre-set in the script to 1.

SnowModel: An argument to specify whether to turn the snow model and precipitation partitioning on or off. Specify 1 for on and 0 for no. This variable has been pre-set in the script to 1.

SnowNear: An argument to specify whether to use f_s and f_r for the partitioning of snow, as estimated from the nearby snow data (eqs. 17a, 18a). Specify 1 for yes and 0 for no. If this variable is set to 0, the model will utilize the alternative method for estimating f_s and f_r (eqs. 17b, 18b). This variable has been pre-set in the script to 1.

plottingTimeseries: An argument to specify whether to create a timeseries plot of the observed and simulated soil moisture values, and total water inputs (X) after the simulated values have been estimated. Specify 1 for yes and 0 for no. This variable has been pre-set to 1.

plottingPDF: An argument to specify whether to create a probability distribution function (PDF) of the observed and simulated soil moisture values (e.g. insets in Figure 16). Specify 1 for yes and 0 for no. This variable has been pre-set to 1.

BSC_analysis: An argument specifying the method of obtaining the BSC parameter, either from the discrete calibration parameter sets for each RI class (BSC_analysis = 1), from the continuous parameters estimated as a function of RI under the calibrated DOE conditions (i.e. Experiment 0; BSC_analysis = 2), or from the continuous parameters estimated as a function of RI under the conditions of Experiments 1 through 3

(BSC_analysis = 3, 4, or 5, respectively). Multiple BSC_analysis types can be analyzed by specifying the smaller and larger BSC_analysis numbers, separated by a colon (i.e. to specify analyzing BSC_analysis 1 through 3, set BSC_analysis = 1:3).

plt_no: The number corresponding the block plot type (1 for B or 2 for C)

blk_no: The block number, 1-5. Multiple block locations can be plotted by specifying the smaller block number and the larger block number, separated by a colon (i.e. to loop from block 1 to 5, insert 1:5 after blk_no =)

timeperiod: The number corresponding to a time period of analysis. The list of cases below this the specification of this variable can be used for reference (i.e. refer to each case under the line that specifies "switch timeperiod"). Multiple time periods can be analyzed by specifying the smaller and larger timeperiod values separated by a colon (i.e. to loop from timperiod 1 to 2, insert 1:2, after trt=). The variable has been pre-set in the script provided to analyze the entire study period.

trt: The treatment of the quad to be analyzed (1 for control, 2 for x, 3 for w). Note that since only B plots have the w-treatment, setting a value of trt equal to 3 when the plt_no equals 2 (C plot) will produce an error. Multiple treatments can be analyzed by specifying the smaller trt number and the larger trt number, separated by a colon (i.e. to loop from trt 1 to 2, insert 1:2 after trt =)

veg_type: A variable for assuming the vegetation type and associated parameters. This value is always set to 1 in this study, since the vegetation related parameters for the soil are assumed constant across the plateau. With the current set-up, any value other than 1 will produce an error unless the user opens the get_vegetation_par.m function (described below) and adds additional cases with unique parameter values.

soil_type: A variable for assuming the soil type and associated parameters. This value is always set to 1 in this study, since the soil parameters are assumed constant across the plateau. With the current set-up, any value other than 1 will produce an error unless the user opens the get_soil_par.m function (described below) and adds additional cases with unique parameter values.

Additionally, there are a number of prescribed constants related to the precipitation partitioning, snowmelt module, and infiltration excess scheme that are pre-set in this script and can be altered for another environment accordingly. The following lists the variables in bold and a variable description after the colon:

TSF: The surface temperature factor used in equation 11 and pre-set to 1.

Tcrit: The critical air temperature where partial freezing commences (T_c; ^{o}C) and pre-set to 4.

Tb: The freezing temperature (T_b; ^{o}C) and pre-set to 0.

F_WHC: The maximum fraction of PT added to the snowpack (f_{WHC}) and pre-set to 3 for 0.3.

Ps_crit: The critical snow depth that produces a snowpack temperature equal to air temperature ($P_{s\text{-}c}$; mm; eq. 19) and pre-set to 10.

Cmin: The minimum degree-day factor value (DDF_{min}; mm per ^{o}C per day) and pre-set to 2.2.

Cmax: The maximum degree-day factor value (DDF_{max}; mm per ^{o}C per day) and pre-set to 4.5.

CCF_fraction: The fraction of DDF that is the cold content factor (CCF; eq. 9) and is pre-set to 1/10.

SWE_crit: The depth of SWE at which ET shuts off (mm) and is pre-set to 100.

I_rate: The average rate of irrigation input to sensed area (i_I; mm/hr) and is pre-set to 1.32. This value was estimated from the 2014 DOE watering schedule where 50 L was added to all C-x quads over 2.5 hr, and thus, an estimated 3.8 mm of water was added to each quad per hour. Given the fractional area of quad assumed sensed (0.34; see A.3), this produces an input rate of 1.32 mm per hour for the area sensed.

After these variables and constants are specified, the script can be run. This script first loads the *cover* data of all the sites, pulled from the excel spreadsheet located at AppendixD/cover_model.xls. This spreadsheet contains the plt_no, block, trt, RI, percent cover values of all species types used in the model (p_{Ac}, p_{Pj}, p_{Ah}, p_{LM}, p_{Cya}), the vegetation fraction (f_v), and the growth and non-growth vegetation coefficients (k_v; eq. 61) for all quads. All values of a given quad are organized in a row and all value types are organized in columns.

The script then calls the function get_data.m which extracts the observed soil moisture and meteorological data of the given timeperiod, partitions the precipitation, and estimates the all duration and water inputs to be sent to the BSC layer (or directly to soil if BSC is turned off by *crust_yes* set equal to 0). Next the script fetches the vegetation parameters associated with the prescribed *veg_type* variables, and the soil parameters associated with the prescribed *soil_type* variables by calling the functions get_vegetation_par.m and get_soil_par.m. The bare soil evaporation rate (E_w) is

estimated from the bare soil weighting factor (k_e) and PET. The initial relative soil moisture depth (s_0) is estimated by dividing the volumetric water content observed at time equals 0 by the soil porosity. A timeseries of the site and season specific vegetation coefficient values (k_v) are created by extracting the growth and non-growth k_v values from the *cover* data for the specific quad location. The values of the f_v and RI for the specific quad location are also extracted from the *cover* data.

The scripts then obtain the appropriate BSC parameters of the specified BSC_analysis type and the given RI from the function get_crust_par.m. The surface capacity (SC) and BSC depth (Z_c) of the given quad is estimated from equations 27 and 41, respectively. The combined water input and model parameters are then passed to the soil_loop.m function to determine the modeled soil and BSC moisture time series. The soil_loop.m function first sends the water input and BSC parameters to the crust_layer.m function, which estimates Ex_i, and L_c. The soil_loop.m function then estimates Ex_s and computes the surface water budget, and then computer E_c. The soil_loop.m function then calls the et_func.m and leak_func.m functions to determine losses to ET and leakage. After the modeled soil moisture time series is determines, the RMSE, CC, and *bias* is estimated in the main.m function. Lastly, the time series and PDF figures are created if specified to do so (*plottingTimeseries* and *plottingPDF* equal 1).

D.2 **Comparison Metrics**

The AppendixD/ComparisonMetrics contains the MATLAB function Main_ComparisonMetrics.m, which can be executed to compute the comparison metrics presented in Table 7 and for all other quad locations not listed in Table 7. All the same user specifications and constants are utilized within this function. The function is pre-set to loop between all quad locations and between two *timeperiod* values, representing the two verification periods (1.5 yr and entire study period). The function outputs the results to a .txt file AppendixD/ComparisonMetrics/Output. This output was loaded into ComparisonMetrics.xlsx which contains three formatted tables shown below that contain the three comparison metrics for all quad locations. The first table presents the comparisons metrics between observations vs. discrete BSC parameter simulations. The second contains the metrics between observations vs. continuous BSC parameter simulations. The third table contains the metrics between discrete vs continuous BSC parameter simulations. The ComparisonMetrics.xlsx file is located in AppendixH/Tables.

D.2.1. **Observations vs. Discrete BSC Parameters**

RI class	Quad	1.5 Year Verification Period			Entire Study Period		
		RMSE	*CC*	*bias*	*RMSE*	*CC*	*bias*
1	*B5-w*	0.01678	0.9233	1.0168	0.02139	0.8959	1.0313
	B3-w	0.01898	0.919	0.9265	0.02385	0.9082	0.8351
	B3-x	0.02743	0.9371	0.7224	0.02888	0.8945	0.7184
	B5-x	0.01579	0.9146	0.9112	0.02515	0.834	0.8291
	B4-w	0.02751	0.898	0.763	0.03249	0.8264	0.7411
	B4-x	0.02484	0.7867	1.2342	0.02733	0.7385	0.9025
	B3-c	0.01949	0.8803	0.9214	0.02605	0.8441	0.8724
2	*B2-w*	0.02724	0.8668	0.822	0.02532	0.8451	0.9373
	B1-w	0.02867	0.9268	0.7565	0.03345	0.8797	0.7093
	B2-c	0.02308	0.8197	1.0909	0.03309	0.8129	0.7937
	C5-c	0.01521	0.923	0.961	0.02203	0.899	0.8336
	C1-x	0.02002	0.884	0.8523	0.02412	0.8163	0.8729
3	*B1-x*	0.01777	0.8853	0.9535	0.02736	0.8294	0.8527
	B1-c	0.02043	0.8856	0.9523	0.02819	0.7918	1.0674
	C4-c	0.01894	0.9161	0.8949	0.024	0.874	0.9135
	C3-c	0.0237	0.8292	1.1158	0.02026	0.9001	0.9129
	C1-c	0.02456	0.8911	1.2906	0.02592	0.8464	1.1684
	C2-x	0.0215	0.8969	1.1624	0.02885	0.8198	1.2371
4	*B4-c*	0.02058	0.8866	1.0271	0.02742	0.8159	1.1539
	C4-x	0.02292	0.8397	1.0876	0.02939	0.7896	1.0385
	C5-x	0.02233	0.8603	0.9166	0.02529	0.8514	0.8867
	B5-c	0.02128	0.8482	1.0403	0.02916	0.8362	0.8286
	C3-x	0.02678	0.7657	1.1099	0.02433	0.8486	0.9645
	C2-c	0.03001	0.8313	0.8457	0.03797	0.8161	0.7231

D.2.2. **Observations vs. Continuous BSC Parameters**

RI class	Quad	1.5 Year Verification Period			Entire Study Period		
		RMSE	*CC*	*bias*	*RMSE*	*CC*	*bias*
1	*B5-w*	0.01671	0.9205	0.9818	0.02091	0.8975	0.9943
	B3-w	0.01935	0.9166	0.9164	0.0242	0.9073	0.8278
	B3-x	0.02553	0.9405	0.7457	0.0274	0.8984	0.7389
	B5-x	0.01471	0.9204	0.9525	0.02395	0.8397	0.8645
	B4-w	0.02526	0.8971	0.8028	0.03047	0.8343	0.7793
	B4-x	0.02775	0.775	1.3115	0.02689	0.7407	0.9599
	B3-c	0.0185	0.884	0.9826	0.02481	0.849	0.9345
2	*B2-w*	0.02452	0.8718	0.889	0.02472	0.8498	1.0186
	B1-w	0.02445	0.93	0.8241	0.02908	0.8945	0.7769
	B2-c	0.02593	0.8035	1.1941	0.03025	0.8269	0.8736
	C5-c	0.01646	0.9167	1.0639	0.01803	0.9181	0.9335
	C1-x	0.01666	0.8944	0.9669	0.0228	0.8318	1.0017
3	*B1-x*	0.02212	0.8817	0.828	0.03198	0.8273	0.7326
	B1-c	0.02537	0.8683	0.8332	0.028	0.7852	0.926
	C4-c	0.0245	0.9139	0.7909	0.02731	0.8732	0.7988
	C3-c	0.02057	0.8497	1.0284	0.02246	0.9011	0.8263
	C1-c	0.02034	0.8966	1.193	0.02358	0.8513	1.0613
	C2-x	0.01882	0.9053	1.0771	0.02577	0.8286	1.1298
4	*B4-c*	0.01992	0.8937	1.0177	0.02657	0.8258	1.151
	C4-x	0.02219	0.8502	1.0837	0.02877	0.7981	1.0419
	C5-x	0.0212	0.8663	0.9506	0.02395	0.8583	0.9278
	B5-c	0.02413	0.8465	1.164	0.02639	0.8393	0.9417
	C3-x	0.03464	0.7603	1.3618	0.02847	0.8354	1.2162
	C2-c	0.04382	0.8388	1.3795	0.04636	0.8465	1.3949

D.2.3. **Discrete BSC Parameters vs. Continuous BSC Parameters**

RI class	Quad	1.5 Year Verification Period			Entire Study Period		
		RMSE	*CC*	*bias*	*RMSE*	*CC*	*bias*
1	*B5-w*	0.00351	0.9981	0.9656	0.0032	0.9988	0.9641
	B3-w	0.0012	0.9997	0.9891	0.00086	0.9999	0.9912
	B3-x	0.00251	0.9992	1.0323	0.00212	0.9994	1.0285
	B5-x	0.00356	0.9982	1.0454	0.00299	0.999	1.0427
	B4-w	0.0041	0.9976	1.0522	0.00361	0.9983	1.0516
	B4-x	0.00478	0.997	1.0626	0.00441	0.9978	1.0635
	B3-c	0.00499	0.997	1.0665	0.00492	0.997	1.0712
2	*B2-w*	0.00579	0.9973	1.0816	0.00609	0.9957	1.0867
	B1-w	0.00621	0.9971	1.0893	0.00661	0.995	1.0954
	B2-c	0.00649	0.9968	1.0946	0.00691	0.9944	1.1008
	C5-c	0.00767	0.9954	1.1071	0.00848	0.9914	1.1199
	C1-x	0.00922	0.9938	1.1345	0.00964	0.9897	1.1476
3	*B1-x*	0.01198	0.9878	0.8683	0.01225	0.986	0.8592
	B1-c	0.01105	0.9902	0.8749	0.01085	0.9898	0.8675
	C4-c	0.01023	0.9907	0.8838	0.01035	0.9907	0.8744
	C3-c	0.00727	0.9941	0.9217	0.00782	0.9946	0.9052
	C1-c	0.00686	0.9951	0.9244	0.00745	0.9953	0.9083
	C2-x	0.0066	0.9956	0.9266	0.00712	0.9956	0.9133
4	*B4-c*	0.00174	0.9991	0.9908	0.00221	0.9988	0.9976
	C4-x	0.00152	0.9992	0.9964	0.00221	0.9987	1.0033
	C5-x	0.00351	0.9984	1.0372	0.0037	0.9987	1.0464
	B5-c	0.00979	0.9918	1.119	0.00971	0.9942	1.1366
	C3-x	0.01828	0.9735	1.227	0.01914	0.977	1.261
	C2-c	0.05144	0.7115	1.6311	0.06039	0.8117	1.9289

D.3 **Simulated Experiments**

All scripts necessary to run the simulation experiments and create the figures provided in this thesis (Figures 15, 18-24) are properly positioned within the AppendixD folder to allow for plotting by executing a main_Exp_X.m script, where X corresponds to the experiment number (X = 0-3) from the MATLAB terminal. The MATLAB figure versions (.fig), 600-dpi compressed TIFF versions, and processed and edited versions of these figures are also available as .ai files in the Whitney_Thesis/AppendixH folder described in Appendix H. These figures were created by executing a main_Exp_Figure_Y.m script, where Y corresponds to the figure number (15, 18-25). Below is a general description of the main_Exp_X.m and main_Exp_Y.m scripts, all pre-sets mentioned are in relation to the main_Exp_X.m scripts.

The simulated experiments are, thus, initialized by executing a main_Exp_X.m function. This function is an alternative version of the main.m script described above for plotting the verification figures. All the same user specifications and constants are utilized within this function in addition to the following user specifications in bold (descriptions provided after colons):

LoopRun: An argument to specify whether to run the loops for the ecohydrology model and estimation of moisture residence time (τ and/or τ_c) and change in relative moisture per storm (Δs and/or Δs_c). Specify 1 for yes and 0 for no. This variable has been pre-set in the script to 1.This variable should be set to 1 for all initial runs of the function to ensure that the simulated outputs for all simulated plots are estimated and initialized for analysis. Subsequent to the initial run, the variable can be set to 0 to increase computation

efficiency and focus the function on the creation of plots, rather than estimation of simulated values and variables.

AverageMoisture: An argument to specify whether to estimate the variables and create the plots of average and standard deviation of BSC and soil moisture for each simulation for analysis between simulated plots (i.e. Figures 19 and 23). Specify 1 for yes and 0 for no. This variable has been pre-set in the script to 1.

CompareWaterBalance: An argument to specify whether to create the plots of the water balance partitioning in the BSC and soil layers, the PET partitioning, and the average change in BSC parameters with RI for each simulation for analysis between the simulated plots (i.e. Figures 15, 18, 20-22). Specify 1 for yes and 0 for no. This variable has been pre-set in the script to 1.

InitialMoistureComparisons: An argument to specify whether to estimate the variables and create additional plots (not presented in this thesis but useful for further analysis) comparing the initial soil moisture values after inputs but prior to losses. Specify 1 for yes and 0 for no. This variable is pre-set to 0.

Tau_DeltaTheta: An argument to specify whether to estimate the variables and create the plots comparing the τ and/or τ_c and Δs and/or Δs_c metrics (i.e. Figures 24, 25). Specify 1 for yes and 0 for no. Note that when this variable is set to 1 and *LoopRun* is set to 1, the function will run the loops to estimate the metrics and create the plots. When this variable is set to 1 and *LoopRun* is set to 0, the function will only create the plots (presuming that an initial run was performed with *LoopRun* set to 1). This former case increases computation time immensely. This variable is pre-set to 0 to increase computation time.

TimeSeriesPlot: An argument to specify whether to plot the simulated time series at specific RI quads, specified with the **RI_plot** variable (described below). Specify 1 for yes and 0 for no. Note that the time series will only plot with *LoopRun* set to 1.

RI_plot: The range of RI to plot (when *TimeSeriesPlot* = 1) and is set equal to a matrix containing the lowest RI and highest RI values to plot within (e.g. RI = [1; 20] to plot all simulated time series for simulated plots with RI values between 1 and 20). This variable is pre-set to 0.

If plotting the τ and/or τ_c and Δs and/or Δs_c metrics (i.e. *Tau_DeltaTheta* = 1), the user should also specify the following variables:

Eliminate_LowRSq: An argument specifying whether or not to eliminate low confidence fits ($R^2 < 0.95$) to the decay moisture curves. Specify 1 for yes and 0 for no. This argument is pre-set with 1.

Eliminate_NegativeDelta: An argument specifying whether or not to negative Δs and/or Δs estimates. Specify 1 for yes and 0 for no. This argument is pre-set with 1.

Eliminate_HitTau: An argument specifying whether or not to negative τ and/or τ_c estimates (greater than 200 days). Specify 1 for yes and 0 for no. This argument is pre-set with 1.

layer: An argument to specify which layer to analyze. Specify 1 for BSC layer, 2 for soil, or 1:2 for both. Note that computation time is significantly increased when this argument is set equal to 1:2. This argument is pre-set to 1.

Once all variables have been set, the function can be executed. If *LoopRun* is set to 1, the function will run through a loop of RI values for each simulated plot, and in each loop call the soil_loop.function and corresponding functions described above in D.1, each time storing the output in larger arrays containing the output of all simulations. Then the function will estimate the variables and output of the specified plots. If *Tau_DeltaTheta* is set to 1, the τ and/or τ_c and Δs and/or Δs_c metrics will be estimated by calling the function get_Tau_DeltaTheta.m. This function first identifies all storm periods within the specified *timeperiod* according to the rules detailed in section 2.6. Then the get_Tau_DeltaTheta.m function estimates the corresponding metrics from each storm even according to the method and equations detailed in section 2.6 (eqs. 68,69). The main_Exp_X.m function then creates a matrix compatible for use with the R function Stats_ExpAnalysis.r, which is described in Appendix F and used to perform the statistical analyses of the metrics described in this thesis. This matrix is output to the AppendixF/ModelResults folder as a text file ModelResults_L_E.txt where L is the layer (BSC or soil) and E is the experiment (0-3). The main_Exp_X.m function then creates the appropriate plots.

D.4 **Fitting Lines to Calibrated Parameters**

The function FitLinesToCrustPars.m located directly in the AppendixD folder can be executed to fit lines to the calibrated parameters. The equations of the lines estimated from this function were added to the get_BSC_par.m function for estimation of parameters when appropriate. The calibrated parameters utilized in this function were calibrated according to the procedure in Appendix E. The function starts by initializing

arrays of RI values (x variable) and all calibrated parameter values for each RI Class (y variables). The function then estimates the exponential and linear fits, the R^2 values, and plots the fits. These R2 values were manually inserted into the excel file LineFitCorrelations.xlsx located in the AppendixH/Tables folder, and formatted to create Table 6.

D.5 **Visualizing Observation Time Series**

The soil moisture time series for the processed observations can be re-create using the MATLAB script VisualizingObservationTimeseries.m. This script requires the user to define the following variables in bold with a variable description provided after the colon:

plt_no: The number corresponding the block plot type (1 for B or 2 for C)

blk_no: The block number, 1-5. Multiple block locations can be plotted by specifying the smaller block number and the larger block number, separated by a colon (i.e. to loop from block 1 to 5, insert 1:5 after blk_no =)

timeperiod: The number corresponding to a time period of analysis. The list of cases below this the specification of this variable can be used for reference. The variable has been pre-set in the script provided to analyze the entire study period.

trt: The treatment of the quad to be analyzed (1 for control, 2 for x, 3 for w). Note that since only B plots have the w-treatment, setting a value of trt equal to 3 when the plt_no equals 2 (C plot) will produce an error. Multiple treatments can be plotted by specifying the smaller trt number and the larger trt number, separated by a colon (i.e. to loop from trt 1 to 2, insert 1:2 after trt =)

After setting these variables, the user can run the script. The script will obtain the soil moisture observations of the given quad, total precipitation (PT) measures, average air temperature (Ta) measures, and PET estimates using the function get_met.m (see Appendix D for description of this function). The script will then create three separate plots, one with the soil moisture and P_T observation, another for T_a, and another for PET. The script is pre-set to re-create Figure 7 of this report. The MATLAB figure versions (.fig), 600-dpi compressed TIFF versions, and processed and edited versions of these figures are also available as .ai files in the Whitney_Thesis/AppendixH folder described in Appendix H.

APPENDIX E

CALIBRATION PROCEDURES AND RESULTS

This appendix describes the MATLAB scripts and procedures used for the application of the Shuffled Complex Evolution algorithm, and the calibration strategy followed in this thesis for the four RI Class parameter sets. The scripts described below have been stored in the folder Whitney_Thesis/AppendixE.

E.1 **Shuffled Complex Evolution Algorithm**

The Shuffled Complex Evolution automated optimization routine by Duan *et al.* (1993), as written for MATLAB, contains two optimization scripts, plus an initializing script. The optimization scripts sceua.m and cceua.m work together to minimize an objective function in multi-dimensional parameter space. They both call a function functn.m that returns a single value that is to be minimized. In 2013, Volo first modified the optimization routine scripts for use with the moisture balance model proposed by Laio *et al.* (2001). These scripts have been further altered for use with the modified model used in this work. In the case of these model calibrations, the objective function to be minimized is the RMSE between the observed and modeled soil moisture time series. The initialization of the optimization script will be described, followed by a description of the steps utilized and results of the model calibration and testing of each parameter set (soil and RI I through IV).

The initialization script optim_em.m requires several user-specified inputs described below and identified in italics. The user specifies the parameter space within the arrays *bl* and *bu* (for lower and upper bounds), with each column representing a different variable parameter. The script will determine sets of parameter values within these bounds and pass the sets to the objective function as *x*. The routine runs in loops,

with each loop consisting of many trials to search within *ngs* complexes, or groups of sets of parameter values (multiple *x*'s) for sets that minimize the objective function within each complex. Between loops, sets of parameter values are shuffled to form new *ngs* complexes which are evolved from the last loop by utilizing optimal minimas of the previous loop. In this manner, the routine optimizes for global, as opposed to merely local, minima in the parameter space. The routine will discontinue searching the space when one of three conditions is met: the number of trials reaches the specified *maxn,* the normalized geometric range of the parameter space being search is smaller than the specified *peps*, or the objective function fails to improve by *pcento* percent in *kstop* loops. Following Volo (2013), the use of the routine was designed such that the third of these conditions was the exclusive reason for an end to an optimization run. The *iniflg* can be set to 1 to specify the use of an initial parameter set *x0.* Otherwise, a *seedflg* of zero causes the use of a random seed, or a random initial parameter set within the parameter space. Also following Volo (2013), the latter method (*seedflg* equal to 0) was used since this approach is useful when running several consecutive optimizations to test for parameter convergence and sensitivity.

An additional user-specified variable *opt_runs* is used here to specify the number of calibration runs to be performed. Furthermore, the user specifies many of the same variables and constants previously discussed under the verification and experiment initialization scripts, including: *Ew_toBSC*, *blk_no*, *trt*, *timeperiod*, *k_yes*, *BSC_BSC_yes*, *SnowModel*, *SnowNear*, *TSF*, *Tcrit*, *Tb*, *f_max*, *Ps_crit*, *Cmin*, *Cmax*, *CCF_fraction*, *SWE_crit*, and *I_rate*.

After specifying these variables and executing the optim_em.m function, the get_data.m function is called to estimate the forcing and extract the correct soil moisture observation timeseries, and the *cover* data is loaded and appropriate variables for the given quad are extracted from this *cover* data. The calibration specification parameters (i.e. *kstop*, *ngs*, *maxn*, *pcento*, *seedflg*, *iniflg*, and *opt_runs*), the parameter space *x*, the forcing, and the *cover* related variables are then passed an objective function script functn.m. This function performs the multiple calibration loops by establishing new parameter sets from *x* and passing the parameters and inputs for each loop to the soil_loop.m function to determine the simulated soil moisture time series (described in previous appendix).After the modeled soil moisture time series is determined, the RMSE between that and the observed series is computed and returned to the optimization script. After *opt_runs* optimizations are performed, the results, including the final values for the objective function and the parameter set used to reach that minimum, for each of the *opt_runs* optimizations, are exported into a .txt file.

E.2 **General Calibration Procedure**

As described in section 2.4, the parameter sets for the soil layer and each BSC RI Class (I through IV) were split into subset groups corresponding to those parameters most affect by wet conditions (s^*,s_{fc}, b, K_s, n, Z_r, $s_{fc,c}$, b_c, Ψ_1, $K_{s,c}$, sc_{max}, n_c, $Z_{c,max}$) and by dry conditions (s_h,s_w, k_e, f_r, $s_{h,c}$, k_c). Using the SCE routine, each subset group was calibrated individually in the order described in section 2.4 and Table 2. For each subset calibration, the parameter space was initially defined by upper and lower limits (*bu* and *bl*) using the values listed in the following table:

	Soil		RI Class I		RI Class IV		RI Class III		RI Class II	
	Lower Bound	*Upper Bound*	*Lower Bound*	*Upper Bound*	*Lower Bound*	*Upper Bound*	*Lower Bound*	*Upper Bound*	*Lower Bound*	*Upper Bound*
k_e	0.1	0.9	-	-	-	-	-	-	-	-
s_h	0.01	0.3	-	-	-	-	-	-	-	-
s_w	0.05	0.18	-	-	-	-	-	-	-	-
s^*	0.15	0.48	-	-	-	-	-	-	-	-
s_{fc}	0.18	0.6	-	-	-	-	-	-	-	-
b	1	5	-	-	-	-	-	-	-	-
K_s (mm/d)	100	900	-	-	-	-	-	-	-	-
n	0.3	0.46	-	-	-	-	-	-	-	-
Z_r (mm)	221	304	-	-	-	-	-	-	-	-
f_r	-	-	0.01	1	0.1	0.95	0.27	0.84	0.27	0.51
k_c	-	-	0.1	1	0.1	0.95	0.5	0.63	0.5	0.63
$s_{h,c}$	-	-	0.01	0.4	0.01	0.6	0.08	0.44	0.08	0.12
$s_{fc,c}$	-	-	0.2	0.6	0.2	0.9	0.27	0.9	0.27	0.47
b_c	-	-	1	12	1.4	4	2.3	3.1	2.5	3.1
Ψ_1 (mm/d)	-	-	120	310	131	400	131	267	131	216
$K_{s,c}$ (mm/d)	-	-	100	200	163	2000	163	506	163	263
n_c	-	-	0.25	0.6	0.1	0.33	0.27	0.33	0.29	0.33
$Z_{c,max}$ (mm)	-	-	70	400	-	-	-	-	-	-
$s_{c,max}$ (mm)	-	-	0.1	4	-	-	-	-	-	-

Each subset calibration exercise involved performing multiple sequences of 5 optimization runs (*opt_runs* = 5) using an *ngs* of 11. For each sequence of 5 optimization runs, the parameter space (ranges listed in table above) was narrowed until the optimal values determined from each of the 5 runs converged to a similar value, as indicated by low standard deviation values.

The results from the final automated optimization runs are listed in tables below under each subset group heading. These results are also provided as text files in the "calibrations/thesis_results" folder. These results can be repeated by using an *ngs* of approximately 11, entering the appropriate *timeseries* value to be evaluated for the given

parameter subset, and entering the appropriate parameter bounds from the tables listed below under each parameter subset heading. These parameter limits must be updated in the optim.em.m script by changing the values within the *x* matrix. Then, the appropriate parameters must be assigned to the respective columns of the *x* matrix in the optimization function funct.m. Finally, all pre-set values of the other parameters, not calibrated for in the given calibration exerceise, must be updated in the get_vegetation_par.m, get_crust_par.m, and get_soil_par.m scripts. Once these alterations have been made, the initialization function optim.em.m can be executed for calibration. Due to the random seed, the results will not be identical, but averages among several optimization runs should be similar. All scripts necessary for the final calibration routines of each parameter subset discussed below are contained within the AppendixE folder in a MATLAB terminal. Calibration can be run by executing an optim_em_X.m script, where X equals the "Calibration step" (1 through 9; Table 2) of the given calibrated parameter subset, or according to the following list:

1. Soil and RI I – dry parameter calibration
2. Soil- wet parameter calibration
3. RI I – wet parameter calibration
4. RI IV – wet parameter calibration
5. RI IV – dry parameter calibration
6. RI III – wet parameter calibration
7. RI III – dry parameter calibration
8. RI II – wet parameter calibration
9. RI II – dry parameter calibration

Data is pulled from the AppendixE/Data folder, which contains appropriate subsets of the data described in Appendix C. SCE results are output into the AppendixE/results folder as a .txt file. This folder contains all the results of the final SCE optimization routine of each subset in one .xlsx file. This file contains a worksheet for each subset calibration, labeled by an abbreviated version of the descriptions in the subset calibration list above (i.e. the worksheet for list item number, "Soil and RI I – dry parameter calibration", is entitled "Soil_RI_I_dry"). Each of these worksheets contains sets of two pages. The first page contains the formatted tables below that list the summary of results from the automated optimization routines, and the second page in a set contains the output from the automated SCE optimization routine used to create the tables below.

After the final SCE optimization routine of each subset, the time series simulated using the final optimized values was tested against the observations within each calibration timeperiod. In some instances, the SCE optimized for parameter values that minimized the RMSE but did not achieve optimal fit to the peaks and troughs of the observed timeseries. In these instances, a manual procedure was performed, varying each of the calibrated parameters, one-at-a-time (OAT), and visually inspecting the resulting timeseries for improved simulated fits. When an OAT adjustment was deemed necessary, the figures of the final OAT adjustment are included. These final OAT figures, as well as all figures used to inspect whether an OAT procedure was necessary can be recreated using the main_CalibrationFigures.m function with one input variable *set* which is equal to 1 through 8 and used to indicate the calibrated parameter subset according to this list:

1. Soil and RI I – dry parameter calibration

2. Soil and RI I – wet parameter calibration
3. RI IV – wet parameter calibration
4. RI IV – dry parameter calibration
5. RI III – wet parameter calibration
6. RI III – dry parameter calibration
7. RI II – wet parameter calibration
8. RI II – dry parameter calibration

This function will also output the RMSE, CC, and *bias* for the model testing period for the given subset and print this value on the figure. These final three comparison metrics for each parameter subset calibration procedure are listed in the following table, which can be found in CalibrationSubsetComparisonMetrics.xlsx file found in the AppendixE/results folder:

Representative Observation Quad	Calibration Timeperiod	Calibrated Parameter Set	RMSE	CC	Bias
B5-w	Dry	RI I & Soil (Dry)	0.0026	0.939	0.9779
	Wet	RI I & Soil (Wet)	0.0269	0.876	1.0521
C5-x	Wet	RI IV (Wet)	0.0247	0.889	1.1062
	Dry	RI IV (Dry)	0.0028	0.976	0.9927
C3-c	Wet	RI III (Wet)	0.0167	0.944	1.0062
	Dry	RI III (Dry)	0.0038	0.977	1.0252
C5-c	Wet	RI II (Wet)	0.0199	0.933	0.9893
	Dry	RI II (Dry)	0.0079	0.847	1.2783

Following the calibration of all subsets of a given parameter set, the calibrated parameters were verified temporally and spatially through comparisons of the three metrics (RMSE, CC, *bias*) and the visual fit to the observed time series in the plotted time

series comparison, as described in sections 2.4.1, 3.1, and D.1. The final calibrated values are listed in Table 5, which is also available in the CalibratedParameters.xlsx file located in the AppendixE/results folder.

E.3 **Soil and BSC RI Class I – Dry Parameter Calibration**

The values of the dry parameters for the soil and BSC RI Class I subsets were calibrated against the observations of the representative RI Class I quad (B5w) during the dry timeperiod (4/1/2012-9/30/2012). Since there are only six dry parameters total for both soil and RI Class I, these parameters were calibrated together. During this dry parameter calibration, the wet soil and RI Class I parameters were set equal to the initial assumed values as discussed in section 2.4, (values also listed in first table under E.2). The final SCE exercise utilized the limit values and produced the output listed in the following table:

	Pre-Set Value	Lower Bound	Minimum	Average	Maximum	Upper Bound	Standard Deviation
RMSE	-	-	0.00255	0.00255	0.00255	-	0
k_e	-	0.2	0.65265	0.67511	0.69748	0.78	0.019061
s_h	-	0.01	0.016641	0.01665	0.016654	0.25	6.53E-06
s_w	-	0.1	0.13853	0.14753	0.156359	0.18	0.007534
s^*	0.46	-	-	-	-	-	-
s_{fc}	0.56	-	-	-	-	-	-
b	4.9	-	-	-	-	-	-
K_s (mm/d)	800	-	-	-	-	-	-
n	0.43	-	-	-	-	-	-
Z_r (mm)	303	-	-	-	-	-	-
f_r	-	0.1	0.495344	0.51197	0.529602	1	0.014403
k_c	-	0.1	0.941759	0.948	0.951111	0.99	0.003812
$s_{h,c}$	-	0.01	0.079587	0.07959	0.0796	0.4	6.11E-06
$s_{fc,c}$	0.56	-	-	-	-	-	-
b_c	4.9	-	-	-	-	-	-
Ψ_1 (mm/d)	132	-	-	-	-	-	-
$K_{s,c}$ (mm/d)	362	-	-	-	-	-	-
n_c	0.43	-	-	-	-	-	-
$Z_{c,max}$ (mm	221	-	-	-	-	-	-
$s_{c,max}$ (mm)	2	-	-	-	-	-	-

This final calibration can be run by executing the optim_em_1.m function.

After this convergence was achieved, the soil moisture timeseries was simulated using the average of the parameter values (listed in table above) and plotted against the observations of the dry timeperiod. An OAT procedure was performed to improve the fit of the simulated timeseries to the observed peaks. This OAT procedure revealed that although the RMSE does not change, the simulation is better able to meet the dry period peaks when changing the crust PET weighting factor (k_c) from the automated calibration

value (0.95) to a decreased value (0.5). This increase in peak values of moisture could be due to the fact that by decreasing the percentage of PET demand met by the crust layer, more moisture is left in the crust system to infiltrate into soil below. The simulated fit using the final SCE output is plotted in the figure below as "Simulation 1" against the observations ("Observed"). The improved fit using the OAT adjustment (k_c = 0.95 and average values of all other dry parameters listed in the table above) is also plotted below as "Simulation 2". The RMSE of each simulation is also printed on the figure:

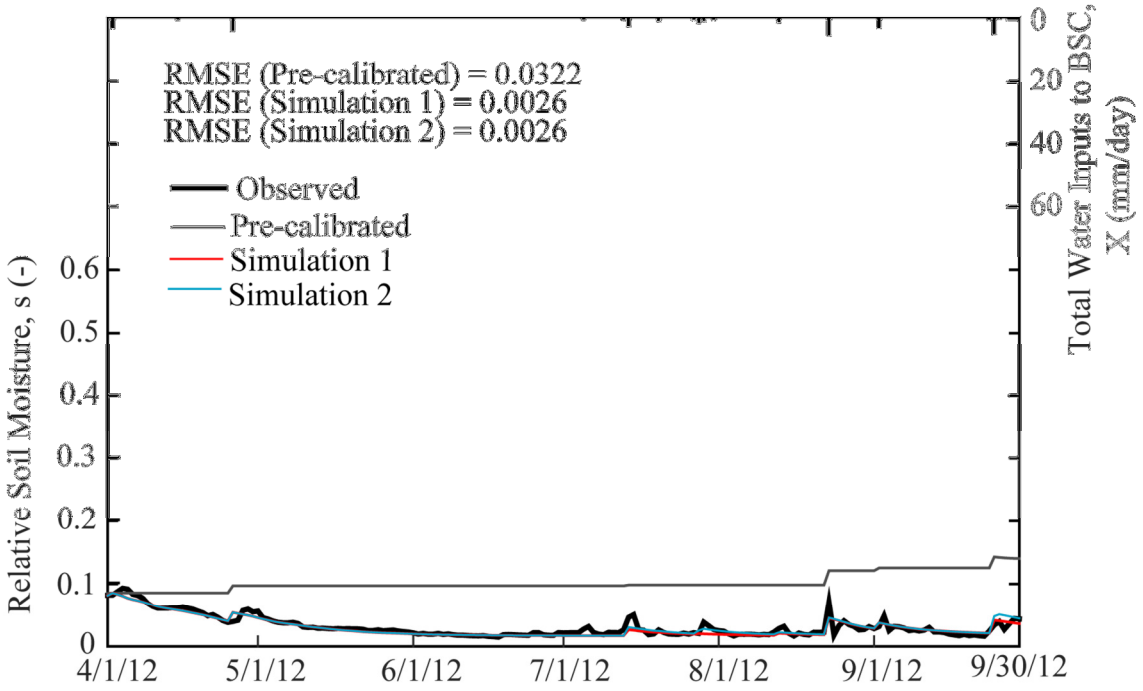

This figure can be created using the function AppendixE/calibrations/main_CalibrationFigures.m with *set* equal to 1 (Soil and BSC RI Class I dry parameters). Due to the improved fit of "Simulation 2", the final results of this thesis utilize the average SCE output for all soil and RI Class I dry parameters except for k_c (listed in table above) and a k_c value of 0.95.

E.4 **Soil and BSC RI Class I – Wet Parameter Calibration**

The values of the wet parameters for the soil and BSC RI Class I subsets were calibrated against the observations of the representative RI Class I quad (B5w) during the dry timeperiod (10/1/2009-3/31/2010). The wet soil parameters and wet BSC RI Class I parameters were first calibrated separately using a separate sequence of SCE optimization runs, calibrating for the wet soil parameters first and the wet RI I parameters second. During this wet parameter calibration, the dry soil and RI Class I parameters were set equal to the calibrated values determined from the previous calibration step (E.3; Table 5). The wet RI Class parameters were set equal to the values in the table listed below (discussed in section 2.4). After an initial wet soil calibration exercise, the parameter spaces were narrowed to ranges close to the minimum and maximum outputted parameter values in order achieve greater convergence. This second SCE exercise utilized the limit values and produced the output listed in the following table:

	Pre-Set Value	Lower Bound	Minimum	Average	Maximum	Upper Bound	Standard Deviation
RMSE	-	-	0.027227	0.02723	0.027228	-	5.48E-07
k_e	0.68	-	-	-	-	-	-
s_h	0.017	-	-	-	-	-	-
s_w	0.15	-	-	-	-	-	-
s^*	-	0.15	0.162225	0.16425	0.167375	0.18	0.002073
s_{fc}	-	0.18	0.180001	0.18001	0.180011	0.6	3.91E-06
b	-	1	1.337791	1.40338	1.432489	5	0.037802
K_s (mm/d)	-	120	124.5595	134.612	138.9331	200	5.769079
n	-	0.25	0.449634	0.44984	0.449962	0.45	0.000144
Z_r (mm)	-	303	303.0004	303.008	303.014	849	0.006147
f_r	0.51	-	-	-	-	-	-
k_c	0.5	-	-	-	-	-	-
$s_{h,c}$	0.08	-	-	-	-	-	-
$s_{fc,c}$	$= s_{fc}$	-	-	-	-	-	-
b_c	$= b$	-	-	-	-	-	-
Ψ_1 (mm/d)	132	-	-	-	-	-	-
$K_{s,c}$ (mm/d)	362	-	-	-	-	-	-
n_c	$= n$	-	-	-	-	-	-
$Z_{c,max}$ (mm)	221	-	-	-	-	-	-
$s_{c,max}$ (mm)	2	-	-	-	-	-	-

Another calibration exercise was run, setting Z_r equal to the converged value from the table above (303) and narrowing the ranges of other parameters even more. This SCE exercise utilized the limit values and produced the output listed in the following table:

	Pre-Set Value	Lower Bound	Minimum	Average	Maximum	Upper Bound	Standard Deviation
RMSE	-	-	0.027227	0.02723	0.027228	-	4.47E-07
k_e	0.68	-	-	-	-	-	-
s_h	0.017	-	-	-	-	-	-
s_w	0.15	-	-	-	-	-	-
s^*	-	0.15	0.163037	0.16525	0.166093	0.17	0.001258
s_{fc}	-	0.18	0.180002	0.18001	0.18003	0.6	1.13E-05
b	-	1	1.320071	1.37013	1.392237	1.5	0.028565
K_s (mm/d)	-	120	121.5752	125.492	131.359	140	3.760358
n	-	0.25	0.449649	0.44991	0.449992	0.45	0.000147
Z_r (mm)	-	303	303.0042	303.005	303.0078	303.01	0.001491
f_r	0.51	-	-	-	-	-	-
k_c	0.5	-	-	-	-	-	-
$s_{h,c}$	0.08	-	-	-	-	-	-
$s_{fc,c}$	$= s_{fc}$	-	-	-	-	-	-
b_c	$= b$	-	-	-	-	-	-
Ψ_1 (mm/d)	132	-	-	-	-	-	-
$K_{s,c}$ (mm/d)	362	-	-	-	-	-	-
n_c	$= n$	-	-	-	-	-	-
$Z_{c,max}$ (mm)	221	-	-	-	-	-	-
$s_{c,max}$ (mm)	2	-	-	-	-	-	-

A final calibration was run to re-calibrate for the value of *n*, setting all other parameter values to the converged values listed in the table above. This final calibration can be repeated by executing the optim_em_2.m function. The final SCE exercise utilized the limit values and produced the output listed in the following table:

	Pre-Set Value	Lower Bound	Minimum	Average	Maximum	Upper Bound	Standard Deviation
RMSE	-	-	0.027238	0.02724	0.027238	-	3.88E-18
k_e	0.68	-	-	-	-	-	-
s_h	0.017	-	-	-	-	-	-
s_w	0.15	-	-	-	-	-	-
s^*	-	0.15	0.170042	0.17006	0.170075	0.17	1.25E-05
s_{fc}	-	0.18	0.18	0.18	0.180005	0.6	2.07E-06
b	-	1	1.400195	1.40045	1.400566	1.5	0.000146
K_s (mm/d)	-	120	125.0046	125.005	125.006	140	0.000658
n	-	0.25	0.442121	0.44233	0.442627	0.45	0.000216
Z_r (mm)	-	303	303.0023	303.004	303.0067	303.01	0.001622
f_r	0.51	-	-	-	-	-	-
k_c	0.5	-	-	-	-	-	-
$s_{h,c}$	0.08	-	-	-	-	-	-
$s_{fc,c}$	$= s_{fc}$	-	-	-	-	-	-
b_c	$= b$	-	-	-	-	-	-
Ψ_1 (mm/d)	132	-	-	-	-	-	-
$K_{s,c}$ (mm/d)	362	-	-	-	-	-	-
n_c	$= n$	-	-	-	-	-	-
$Z_{c,max}$ (mm)	221	-	-	-	-	-	-
$s_{c,max}$ (mm)	2	-	-	-	-	-	-

Next, the wet BSC RI Class I parameters were calibrated setting the dry soil and RI Class I parameters equal to the calibrated values determined from the calibration step described in E.3, and the wet soil parameters equal to the average values of the output in the previous calibration steps (see table above) The final SCE exercise utilized the limit values and produced the output listed in the following table:

	Pre-Set Value	Lower Bound	Minimum	Average	Maximum	Upper Bound	Standard Deviation
RMSE	-	-	0.026151	0.02615	0.026159	-	3.35E-06
k_e	0.68	-	-	-	-	-	-
s_h	0.017	-	-	-	-	-	-
s_w	0.15	-	-	-	-	-	-
s^*	0.17	-	-	-	-	-	-
s_{fc}	0.2	-	-	-	-	-	-
b	1.4	-	-	-	-	-	-
K_s (mm/d)	125	-	-	-	-	-	-
n	0.44	-	-	-	-	-	-
Z_r (mm)	303	-	-	-	-	-	-
f_r	0.51	-	-	-	-	-	-
k_c	0.5	-	-	-	-	-	-
$s_{h,c}$	0.08	-	-	-	-	-	-
$s_{fc,c}$	-	0.2	0.268479	0.27154	0.276481	0.6	0.003502
b_c	-	3	3.052479	3.13838	3.211598	12	0.064472
Ψ_1 (mm/d)	-	120	130.5476	131.412	132.5314	310	0.871249
$K_{s,c}$ (mm/d)	-	100	154.0404	163.447	170.4475	200	6.142798
n_c	-	0.25	0.315812	0.32867	0.341012	0.6	0.009066
$Z_{c,max}$ (mm	-	70	77.8302	79.0096	80.97166	400	1.251901
$s_{c,max}$ (mm)	-	0.1	0.802045	1.67282	2.341006	3	0.599917

After this convergence was achieved, the soil moisture timeseries was simulated using the converged parameter values (listed in table above) and plotted against the observations of the wet timeperiod. An OAT procedure was performed to improve the fit of the simulated timeseries to the observed peaks. This OAT procedure revealed that although the RMSE is somewhat higher, the simulation is better able to meet the wet period peaks when changing the s_{fc} from 0.18 to 0.2. This higher value of s_{fc} is also closer to values previously calibrated for sandy loams (Laio *et al*. 2001). The simulated fit using

the final SCE output is plotted in the figure below as "Simulation 1" against the observations ("Observed"). The improved fit using the OAT adjustment (s_{fc} = 0.2 and converged values of all other parameters listed in the table above) is also plotted below as "Simulation 2". The RMSE of each simulation is also printed on the figure:

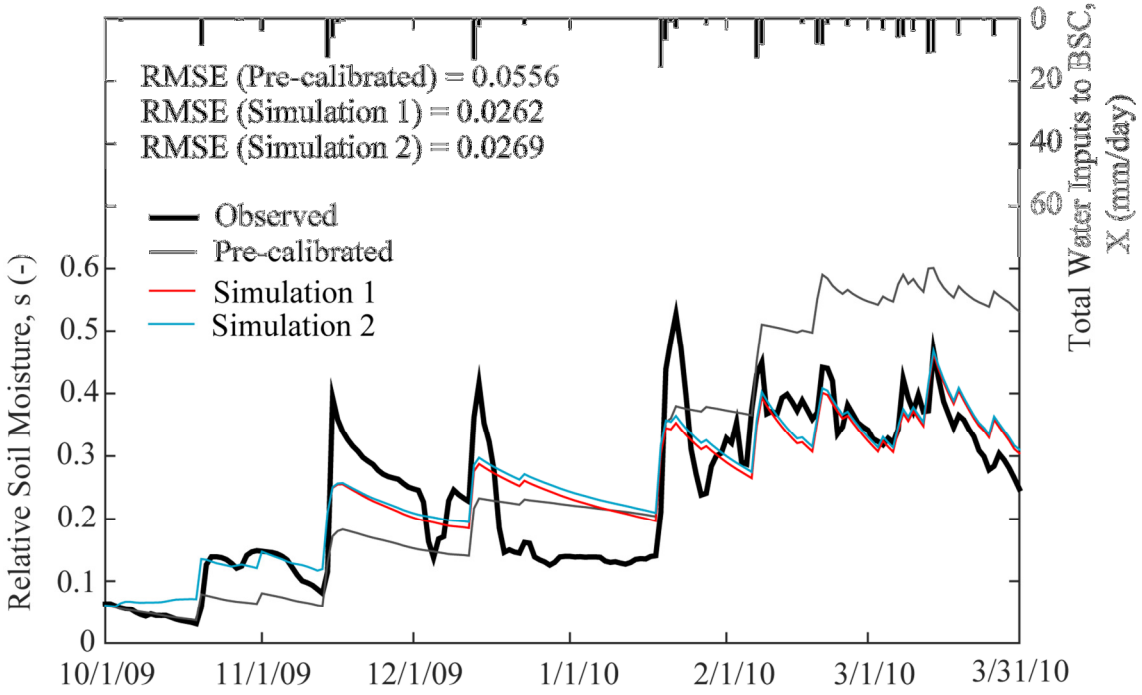

This figure can be created using the function AppendixE/calibrations/main_CalibrationFigures.m with *set* equal to 2 (Soil and BSC RI Class I wet parameters). Due to the improved fit of "Simulation 2", the final results of this thesis utilize the average SCE output for all soil and RI Class I wet parameters except for s_{fc} (listed in table above) and a s_{fc} value of 0.2 (all calibrated values listed in Table 5). The values of the calibrated $Z_{c,max}$, SC_{max}, and the calibrated soil parameters were utilized for the soil parameter values for the remainder of all analyses.

E.5 BSC RI Class IV – Wet Parameter Calibration

The values of the BSC RI Class IV parameter subsets were calibrated next to obtain the upper limit of all BSC parameters. Since there are more wet-type parameters than dry, the RI Class IV wet parameters were calibration first against the observations of the representative RI Class IV quad (C5x) during the wet time period. During this wet parameter calibration, the dry RI Class IV parameters were set equal to the initial assumed values as discussed in section 2.4, (values also listed in first table under E.2). The final SCE exercise utilized the limit values and produced the output listed in the following table:

	Pre-Set Value	Lower Bound	Minimum	Average	Maximum	Upper Bound	Standard Deviation
RMSE	-	-	0.024669	0.02467	0.024669	-	0
f_r	0.75	-	-	-	-	-	-
k_c	0.5	-	-	-	-	-	-
$s_{h,c}$	0.4	-	-	-	-	-	-
$s_{fc,c}$	-	0.27	0.820261	0.84122	0.858812	0.9	0.01427
b_c	-	1.4	1.973601	2.31202	2.68509	3.1	0.339396
Ψ_1 *(mm/d)*	-	131	234.053	266.554	306.4632	400	26.27782
$K_{s,c}$ *(mm/d)*	-	163	431.0189	505.945	617.3518	800	76.30585
n_c	-	0.1	0.260257	0.27087	0.284135	0.33	0.008858

After this convergence was achieved, the soil moisture timeseries was simulated using the converged parameter values (listed in table above) and plotted against the observations of the wet timeperiod, revealing optimal fits, and thus rendering an OAT procedure unnecessary. This figure can be created using the function AppendixE/calibrations/main_CalibrationFigures.m with *set* equal to 3 (BSC RI Class IV

wet parameters). Due to this optimal fit, the final results of this thesis utilize the above average SCE output for all RI Class IV wet parameters (calibrated values listed in Table 5).

E.6 **BSC RI Class IV – Dry Parameter Calibration**

The values of the BSC RI Class IV dry parameter subsets were calibrated next against the observations of the representative RI Class IV quad (C5x) during the dry time period. During this dry parameter calibration, the wet RI Class IV parameters were set equal to the calibrated values determined from the previous calibration step (Table 5). The final SCE exercise utilized the limit values and produced the output listed in the following table:

	Pre-Set Value	Lower Bound	Minimum	Average	Maximum	Upper Bound	Standard Deviation
RMSE	-	-	0.002829	0.00283	0.002829	-	0
f_r	-	0.1	0.720526	0.72056	0.720573	0.95	1.89E-05
k_c	-	0.3	0.625971	0.62599	0.626003	0.95	1.24E-05
$s_{h,c}$	-	0.01	0.437163	0.43718	0.437209	0.6	1.73E-05
$s_{fc,c}$	0.84	-	-	-	-	-	-
b_c	2.3	-	-	-	-	-	-
Ψ_1 *(mm/d)*	267	-	-	-	-	-	-
$K_{s,c}$ *(mm/d)*	506	-	-	-	-	-	-
n_c	0.27	-	-	-	-	-	-

After this convergence was achieved, the soil moisture timeseries was simulated using the converged parameter values (listed in table above) and plotted against the observations of the dry timeperiod, revealing optimal fits, and thus rendering an OAT

procedure unnecessary. This figure can be created using the function AppendixE/calibrations/main_CalibrationFigures.m with *set* equal to 4 (BSC RI Class IV dry parameters). Due to this optimal fit, the final results of this thesis utilize the above average SCE output for all RI Class IV dry parameters (calibrated values listed in Table 5).

E.7 **BSC RI Class III – Wet Parameter Calibration**

The values of the BSC RI Class III parameter subsets were calibrated next against the observations of the representative RI Class III quad (C3c) during the wet time period. During this wet parameter calibration, the dry RI Class III parameters were set equal to initial assumed values between those values of RI Class I and IV (as discussed in section 2.4; values also listed in first table under E.2). These pre-set dry parameter values were computed by first dividing the difference in the value of the RI Class I (v_1) and Class IV (v_4) parameters into increments (*inc*):

$$inc = \frac{v_4 - v_1}{3} \tag{E.1}$$

Next the initial values of the RI III parameters (v_3) were assumed equal to the second incremental value after v_1:

$$v_3 = v_1 + 2inc \tag{E.1}$$

The final SCE exercise utilized the limit values and produced the output listed in the following table:

	Pre-Set Value	Lower Bound	Minimum	Average	Maximum	Upper Bound	Standard Deviation
RMSE	-	-	0.016144	0.01614	0.016145	-	4.47E-07
f_r	0.65	-	-	-	-	-	-
k_c	0.59	-	-	-	-	-	-
$s_{h,c}$	0.32	-	-	-	-	-	-
$s_{fc,c}$	-	0.27	0.471823	0.47203	0.472111	0.9	0.000122
b_c	-	2.3	2.338212	2.5284	2.871732	3.1	0.20836
Ψ_1 *(mm/d)*	-	131	210.2885	216.14	222.391	267	4.282808
$K_{s,c}$ *(mm/d)*	-	163	261.7209	263.876	268.4458	506	2.622059
n_c	-	0.27	0.278965	0.28993	0.310211	0.33	0.012684

After this convergence was achieved, the soil moisture timeseries was simulated using the converged parameter values (listed in table above) and plotted against the observations of the wet timeperiod, revealing optimal fits, and thus rendering an OAT procedure unnecessary. This figure can be created using the function AppendixE/calibrations/main_CalibrationFigures.m with *set* equal to 5 (BSC RI Class III wet parameters). Due to this optimal fit, the final results of this thesis utilize the above average SCE output for all RI Class III wet parameters (calibrated values listed in Table 5).

E.8 **BSC RI Class III – Dry Parameter Calibration**

The values of the BSC RI Class III dry parameter subsets were calibrated next against the observations of the representative RI Class III quad (C3c) during the dry time period. During this dry parameter calibration, the wet RI Class III parameters were set equal to the calibrated values determined from the previous calibration step (Table 5).

The final SCE exercise utilized the limit values and produced the output listed in the following table:

	Pre-Set Value	Lower Bound	Minimum	Average	Maximum	Upper Bound	Standard Deviation
RMSE	-	-	0.003775	0.00378	0.003775	-	4.85E-19
f_r	-	0.68	0.69052	0.69598	0.699601	0.72	7.78E-06
k_c	-	0.57	0.589978	0.58999	0.589999	0.59	0.003514
$s_{h,c}$	-	0.12	0.12	0.12	0.120006	0.44	2.61E-06
$s_{fc,c}$	0.47	-	-	-	-	-	-
b_c	2.5	-	-	-	-	-	-
Ψ_1 *(mm/d)*	216	-	-	-	-	-	-
$K_{s,c}$ *(mm/d)*	263	-	-	-	-	-	-
n_c	0.29	-	-	-	-	-	-

After this convergence was achieved, the soil moisture timeseries was simulated using the converged parameter values (listed in table above) and plotted against the observations of the dry timeperiod, revealing optimal fits, and thus rendering an OAT procedure unnecessary. This figure can be created using the function AppendixE/calibrations/main_CalibrationFigures.m with *set* equal to 6 (BSC RI Class III dry parameters). Due to this optimal fit, the final results of this thesis utilize the above average SCE output for all RI Class III dry parameters (calibrated values listed in Table 5).

E.9 **BSC RI Class II – Wet Parameter Calibration**

The values of the BSC RI Class II parameter subsets were calibrated next against the observations of the representative RI Class II quad (C5c) during the wet time period.

During this wet parameter calibration, the dry RI Class II parameters were set equal to initial assumed values between those values of RI Class I and IV (as discussed in section 2.4; values also listed in first table under E.2), following the same procedure as discusses in E.7. The final SCE exercise utilized the limit values and produced the output listed in the following table:

	Pre-Set Value	Lower Bound	Minimum	Average	Maximum	Upper Bound	Standard Deviation
RMSE	-	-				-	
f_r	0.61	-	-	-	-	-	-
k_c	0.55	-	-	-	-	-	-
$s_{h,c}$	0.1	-	-	-	-	-	-
$s_{fc,c}$	-	0.28	0.280013	0.28004	0.280083	0.47	2.99E-05
b_c	-	2.5	2.795122	2.84657	2.976496	3.1	0.073909
Ψ_1 *(mm/d)*	-	131	147.2713	175.887	199.7248	216	20.84158
$K_{s,c}$ *(mm/d)*	-	163	163.0838	175.971	192.7369	263	10.98471
n_c	-	0.3	0.300012	0.30007	0.300162	0.33	5.57E-05

After this convergence was achieved, the soil moisture timeseries was simulated using the converged parameter values (listed in table above) and plotted against the observations of the wet timeperiod, revealing optimal fits, and thus rendering an OAT procedure unnecessary. This figure can be created using the function AppendixE/calibrations/main_CalibrationFigures.m with *set* equal to 7 (BSC RI Class II wet parameters). Due to this optimal fit, the final results of this thesis utilize the above average SCE output for all RI Class II wet parameters (calibrated values listed in Table 5).

E.10 **BSC RI Class II – Dry Parameter Calibration**

The values of the BSC RI Class II dry parameter subsets were calibrated next against the observations of the representative RI Class II quad (C3c) during the dry time period. During this dry parameter calibration, the wet RI Class II parameters were set equal to the calibrated values determined from the previous calibration step (Table 5). The final SCE exercise utilized the limit values and produced the output listed in the following table:

	Pre-Set Value	Lower Bound	Minimum	Average	Maximum	Upper Bound	Standard Deviation
RMSE	-	-	0.007869	0.00787	0.007869	-	0
f_r	-	0.27	0.50801	0.50936	0.51	0.51	0.000841
k_c	-	0.54	0.54003	0.54005	0.540074	0.56	1.99E-05
$s_{h,c}$	-	0.09	0.09001	0.09096	0.093	0.12	0.001243
$s_{fc,c}$	0.28	-	-	-	-	-	-
b_c	2.8	-	-	-	-	-	-
Ψ_1 *(mm/d)*	176	-	-	-	-	-	-
$K_{s,c}$ *(mm/d)*	176	-	-	-	-	-	-
n_c	0.3	-	-	-	-	-	-

After this convergence was achieved, the soil moisture timeseries was simulated using the converged parameter values (listed in table above) and plotted against the observations of the dry timeperiod, revealing optimal fits, and thus rendering an OAT procedure unnecessary. This figure can be created using the function AppendixE/calibrations/main_CalibrationFigures.m with *set* equal to 8 (BSC RI Class II dry parameters). Due to this optimal fit, the final results of this thesis utilize the above

average SCE output for all RI Class II dry parameters (calibrated values listed in Table 5).

APPENDIX F

MOISTURE INPUT RATE PER STORM AND RESIDENCE TIME SCRIPTS

This appendix has two sections. The first section, "Model Metric Analysis" describes the R functions used to perform the statistical analysis of the simulated the τ and/or τ_c and Δs and/or Δs_c metrics estimated from the output of the simulation experiments. The second section, "Observation Metrics and Analysis", describes the MATLAB function used to estimate the volumetric water content residence time τ_θ and change in volumetric water content from the observations $\Delta\theta$, as well as the R functions used to perform a statistical analysis on these metrics. The results of that can be obtained from the scripts described in this second section were not utilized in this thesis since it was determined that more measures of field site predictor variables (besides RI) were necessary to properly analyze the results.

E.1 **Model Metric Analysis**

The functions used to analyze the estimated metrics are contained in AppendixF and analyze the text files from the AppendixF/ModelResults folder (text files output from AppendixD/main_Exp_X.m function). The analysis involves the execution of two versions of essentially the same function. The first function version MetricAnalysis_BetweenRI.r performs the analysis between the average metric of RI Classes within each experiment, and the second function version MetricAnalysis_BetweenExp.r performs the analysis to between the average metric of experiments within each RI Class. In the first version, the user specifies which experiment simulations to analyze by changing the value of *sim.* When *sim* = 1, experiment 0 average metrics are compared between RI Classes, and so forth (2 for experiment 1, 3 for experiment 2, and 4 for experiment 3). In the second version, the user

specifies which RI Class to analyze by changing the value of the variable *cl.* For example, when *cl* = 1, RI Class I average metrics are compared between experiments.

The function first performs the assumptions checks of the raw datasets outlined in section 2.6. Two plots are also created to aid in visualizing these assumptions tests (qqplot for normality and boxplot for equal variance). These assumptions tests are located under the section "ANOVA ASSUMPTIONS CHECK" segregated by a line of comment symbols (#).

The next segregated section, "TRANSFORMATION ATTEMPTS" can be utilized to perform various transformations and re-test the assumptions. The transformation is specified by changing the equations listed under the sub-section "##transform data (define transformation type)". The various transformation attempts have been described in section 2.6 and reveal that the transformed datasets still do not meet the assumptions.

After attempting these transformations, the user can either run the entire script again or proceed by highlighting and executing portions of the scripts. The subsequent segregated section, "##ANOVA AND PARAMETRIC POST-HOCS" creates the ANOVA model and performs a non-parametric test for significance (Kruskal-Wallace) as well as a parametric for reference. In this section, a parametric post-hoc can also be performed for reference.

The next section contains the non-parametric post-hoc tests. The Mann-Whitney test is called by the name "wilcox.test". A loop is performed to compare the p-value results to the Bonferoni corrected significant p-value (0.05/6).

The final section plots the mean bar plots with standard error, for visual reference. The final section contains the call names for the assumptions tests, Kruskal-Wallace significance tests, and multiple comparison post-hoc tests. These names can be highlighted and executed (After the execution of the previous portions of the script), and the result of the given test will output in the command box. The assumptions tests and Kruskal-Wallace results were manually printed in the excel file AppendixH/Tables/StatsResults/MetricsResults.xlsx containing Tables 8,9,12, and 13 of this thesis. The Wilcox (or Mann-Whitney) results are output into the AppendixD/StatsResults folder. These results were then loaded and formatted in the AppendixH/Tables/StatsResults/MetricsResults.xlsx file to create Tables 10, 11, 14, and 15 of this thesis. This excel file contains one worksheet per table, each sheet labeled by the given table name (i.e. worksheet "Table8" contains Table 8 of this thesis).

E.2 **Observation Metrics and Analysis**

The functions used to estimate and analyze τ_θ and $\Delta\theta$ are contained in AppendixF/ObservationAnalysis folder. The ObservationMetrics.m function was used to estimate the metrics from the processed soil moisture observation files contained in theAppendixC/ProcessedData folder. The script operates much like the get_Tau_DeltaTheta.m function described in D.3, except the storm periods were manually identified using the same automated criteria as a starting point and then modifying the start and end dates to correspond more tightly with the general maximum and minimum soil moisture observations of each event. The script also estimates the metric for the observations from each senor in a given quad profile and the metrics from

the depth-weighted average profile. Due to the variable nature of soil moisture decays for a given quad location under the natural field conditions, the moisture profiles of each quad and sensor location are not uniformly distributed in time. Thus, the script contains a lot of arguments to search for the local maximum and minimum moisture observation of a given time series of a given event. This automated search increases the computation time substantially.

The output of the script MasterTable.txt is placed in the AppendixF/ObservationAnalysis folder. The R script CreatingRTable.r was then used to re-arrange this table to a format more easily used in R. This table is stored as MasterTable.r in the AppendixF/ObservationAnalysis folder. The R script AnalyzingObservationResults.r was then used to perform various statistical analyses on the results. The function first loads the MasterTable.r, and subsamples the observations according the RI Class. The script then performs the Shapiro-Wilks test for normality, and Bartlett's test for equal variance. The next section was used for attempting transformations and re-testing the assumptions. The final sections perform the non-parameter ANOVA (Kruskal-Wallace) and multiple-comparison post-hoc tests (non-parametric analogue of Tukey's Honest Significant Difference) on the data.

APPENDIX G

MOISTURE BALANCE AND EVAPORATIVE DEMAND PARTITIONING

This appendix contains the roughness index (RI), total inputs, and partitioning of inputs in the surface, BSC, and soil layers for each simulated plot for each experiment in tabular form. The partitioning of the total potential evapotranspiration (*PET*) between evaporative losses from the three layers for each experiment is also represented in tabular form. Partitions are represented as fractions of the total moisture input or total *PET*. Thesse results are provided in an excel file under the filename AppendixG/ExperimentPartitioning. There are four worksheets, one for each of the sections below, each named accordingly as *Surface*, *BSC*, *Soil*, and *PET*.

G.1 **Surface Moisture Balance Inputs and Partitioning**

The two tables below contain the surface moisture balance partitioning in fractional form. The fractional partitioning for experiments 0 and 1 are listed as a group of columns in the first table, and for experiments 2 and 3 in the second table. Each row corresponds to the total fraction estimated across the entire experiment simulation period for each simulated plot. The first column lists the RI of the given simulated plot. The first column of each experimental group contains the total depth in mm of surface inputs, or the total excess infiltration ($Ex_T = Ex_i + Ex_s$) across each simulated timeperiod. The next two columns of each experimental group contain the fraction of Ex_T occurring as the total ponded evaporation (E_p) and as the total runoff (Q). Total ponded (*pond*) is not shown since none occurred for any experiment.

RI	Experiment 0			Experiment 1		
	Ex_T (mm)	E_p [L/L]	Q [L/L]	Ex_T (mm)	E_p [L/L]	Q [L/L]
1	**6.333**	0.015	0.985	8.895	0.031	0.969
1.23	**4.829**	0.023	0.977	7.014	0.022	0.978
1.46	**3.823**	0.035	0.965	6.109	0.023	0.977
1.69	**3.068**	0.051	0.949	5.512	0.028	0.972
1.92	**2.466**	0.072	0.928	5.076	0.035	0.965
2.15	**1.966**	0.101	0.899	4.737	0.042	0.958
2.38	**1.541**	0.142	0.858	4.462	0.049	0.951
2.61	**1.176**	0.204	0.796	4.231	0.057	0.943
2.84	**0.862**	0.303	0.697	4.032	0.065	0.935
3.07	**0.595**	0.474	0.526	3.858	0.073	0.927
3.3	**0.374**	0.810	0.190	3.701	0.082	0.918
3.53	**0.201**	1.000	0.000	3.559	0.091	0.909
3.76	**0.077**	1.000	0.000	3.427	0.101	0.899
3.99	**0.010**	1.000	0.000	3.303	0.111	0.889
4.22	**0.000**	0.000	0.000	3.187	0.122	0.878
4.45	**0.000**	0.000	0.000	3.075	0.133	0.867
4.68	**0.000**	0.000	0.000	2.968	0.145	0.855
4.91	**0.000**	0.000	0.000	2.864	0.158	0.842
5.14	**0.000**	0.000	0.000	2.763	0.171	0.829
5.37	**0.000**	0.000	0.000	2.664	0.185	0.815
5.6	**0.000**	0.000	0.000	2.566	0.201	0.799
5.6	**0.000**	0.000	0.000	2.566	0.201	0.799
5.685	**0.000**	0.000	0.000	2.530	0.207	0.793
5.77	**0.000**	0.000	0.000	2.494	0.213	0.787
5.855	**0.000**	0.000	0.000	2.459	0.219	0.781
5.94	**0.000**	0.000	0.000	2.424	0.225	0.775
6.025	**0.000**	0.000	0.000	2.388	0.232	0.768
6.11	**0.000**	0.000	0.000	2.353	0.239	0.761
6.195	**0.000**	0.000	0.000	2.318	0.246	0.754
6.28	**0.000**	0.000	0.000	2.283	0.253	0.747
6.365	**0.000**	0.000	0.000	2.249	0.260	0.740
6.45	**0.000**	0.000	0.000	2.214	0.268	0.732
6.535	**0.000**	0.000	0.000	2.179	0.276	0.724
6.62	**0.000**	0.000	0.000	2.145	0.284	0.716
6.705	**0.000**	0.000	0.000	2.111	0.292	0.708
6.79	**0.000**	0.000	0.000	2.076	0.301	0.699
6.875	**0.000**	0.000	0.000	2.042	0.310	0.690
6.96	**0.000**	0.000	0.000	2.008	0.319	0.681

7.045	**0.000**	0.000	0.000	1.974	0.328	0.672
7.13	**0.000**	0.000	0.000	1.941	0.338	0.662
7.215	**0.000**	0.000	0.000	1.907	0.348	0.652
7.3	**0.000**	0.000	0.000	1.874	0.358	0.642
7.3	**0.000**	0.000	0.000	1.874	0.358	0.642
7.48	**0.000**	0.000	0.000	1.804	0.381	0.619
7.66	**0.000**	0.000	0.000	1.735	0.406	0.594
7.84	**0.000**	0.000	0.000	1.668	0.432	0.568
8.02	**0.000**	0.000	0.000	1.603	0.460	0.540
8.2	**0.000**	0.000	0.000	1.539	0.490	0.510
8.38	**0.000**	0.000	0.000	1.479	0.521	0.479
8.56	**0.000**	0.000	0.000	1.421	0.554	0.446
8.74	**0.000**	0.000	0.000	1.368	0.588	0.413
8.92	**0.000**	0.000	0.000	1.319	0.622	0.378
9.1	**0.000**	0.000	0.000	1.277	0.656	0.345
9.28	**0.000**	0.000	0.000	1.241	0.688	0.312
9.46	**0.000**	0.000	0.000	1.213	0.717	0.283
9.64	**0.000**	0.000	0.000	1.196	0.741	0.259
9.82	**0.000**	0.000	0.000	1.190	0.759	0.241
10	**0.000**	0.000	0.000	1.199	0.767	0.233
10.18	**0.000**	0.000	0.000	1.226	0.764	0.236
10.36	**0.000**	0.000	0.000	1.274	0.748	0.252
10.54	**0.000**	0.000	0.000	1.348	0.719	0.281
10.72	**0.000**	0.000	0.000	1.454	0.678	0.322
10.9	**0.000**	0.000	0.000	1.599	0.627	0.373
10.9	**0.000**	0.000	0.000	1.599	0.627	0.373
11.443	**0.000**	0.000	0.000	2.362	0.446	0.554
11.985	**0.000**	0.000	0.000	3.857	0.286	0.714
12.527	**0.000**	0.000	0.000	6.480	0.178	0.822
13.07	**0.000**	0.000	0.000	13.584	0.203	0.797
13.613	**0.000**	0.000	0.000	26.210	0.143	0.857
14.155	**0.000**	0.000	0.000	17.903	0.299	0.701
14.697	**0.000**	0.000	0.000	12.300	0.347	0.653
15.24	**0.000**	0.000	0.000	32.145	0.788	0.212
15.783	**0.000**	0.000	0.000	57.491	0.506	0.494
16.325	**0.000**	0.000	0.000	42.226	0.802	0.193
16.867	**0.000**	0.000	0.000	49.631	0.722	0.278
17.41	**0.000**	0.000	0.000	37.123	0.912	0.088
17.953	**0.000**	0.000	0.000	29.150	0.910	0.090
18.495	**0.000**	0.000	0.000	24.132	0.922	0.078
19.038	**0.000**	0.000	0.000	23.069	0.875	0.121

19.58	**0.000**	0.000	0.000	34.238	0.611	0.363
20.123	**0.000**	0.000	0.000	22.383	0.844	0.089
20.665	**0.000**	0.000	0.000	17.913	0.911	0.061
21.207	**0.000**	0.000	0.000	21.644	0.794	0.065
21.75	**0.000**	0.000	0.000	15.035	0.921	0.020

RI	**Experiment 2**			**Experiment 3**		
	Ex_T	E_p	Q	Ex_T	E_p	Q
	(mm)	[L/L]	[L/L]	(mm)	[L/L]	[L/L]
1	**7.286**	0.021	0.979	10.071	0.027	0.973
1.23	**5.988**	0.020	0.980	8.190	0.041	0.959
1.46	**5.215**	0.026	0.974	7.379	0.037	0.963
1.69	**4.684**	0.033	0.967	6.972	0.045	0.955
1.92	**4.291**	0.041	0.959	6.735	0.052	0.948
2.15	**3.987**	0.050	0.950	6.603	0.059	0.941
2.38	**3.743**	0.058	0.942	6.542	0.065	0.935
2.61	**3.541**	0.068	0.932	6.531	0.072	0.928
2.84	**3.372**	0.077	0.923	6.559	0.078	0.922
3.07	**3.227**	0.087	0.913	6.616	0.085	0.915
3.3	**3.100**	0.098	0.902	6.697	0.091	0.909
3.53	**2.989**	0.109	0.891	6.797	0.096	0.904
3.76	**2.890**	0.120	0.880	6.913	0.100	0.900
3.99	**2.801**	0.131	0.869	7.042	0.104	0.896
4.22	**2.721**	0.143	0.857	7.184	0.108	0.892
4.45	**2.648**	0.155	0.845	7.344	0.111	0.889
4.68	**2.581**	0.167	0.833	7.526	0.114	0.886
4.91	**2.520**	0.179	0.821	7.716	0.117	0.883
5.14	**2.464**	0.192	0.808	7.918	0.120	0.880
5.37	**2.412**	0.205	0.795	8.132	0.124	0.876
5.6	**2.364**	0.218	0.782	8.358	0.128	0.872
5.6	**2.364**	0.218	0.782	8.358	0.128	0.872
5.685	**2.347**	0.223	0.777	8.444	0.129	0.871
5.77	**2.331**	0.228	0.772	8.531	0.131	0.869
5.855	**2.315**	0.233	0.767	8.620	0.133	0.867
5.94	**2.300**	0.238	0.763	8.711	0.134	0.866
6.025	**2.285**	0.242	0.758	8.802	0.136	0.864
6.11	**2.270**	0.247	0.753	8.896	0.138	0.862
6.195	**2.256**	0.253	0.748	8.990	0.140	0.860

6.28	**2.242**	0.258	0.742	9.086	0.142	0.858
6.365	**2.229**	0.263	0.737	9.183	0.144	0.856
6.45	**2.216**	0.268	0.732	9.282	0.145	0.855
6.535	**2.203**	0.273	0.727	9.382	0.147	0.853
6.62	**2.191**	0.278	0.722	9.483	0.149	0.851
6.705	**2.179**	0.283	0.717	9.585	0.151	0.849
6.79	**2.168**	0.288	0.712	9.688	0.154	0.846
6.875	**2.157**	0.293	0.707	9.793	0.156	0.844
6.96	**2.146**	0.298	0.702	9.899	0.158	0.842
7.045	**2.135**	0.303	0.697	10.006	0.160	0.840
7.13	**2.125**	0.309	0.691	10.115	0.162	0.838
7.215	**2.115**	0.314	0.686	10.224	0.164	0.836
7.3	**2.106**	0.319	0.681	10.335	0.166	0.834
7.3	**2.106**	0.319	0.681	10.335	0.166	0.834
7.48	**2.088**	0.330	0.670	10.574	0.171	0.829
7.66	**2.072**	0.341	0.659	10.817	0.176	0.824
7.84	**2.057**	0.353	0.647	11.066	0.181	0.820
8.02	**2.045**	0.364	0.636	11.320	0.185	0.815
8.2	**2.034**	0.376	0.624	11.581	0.190	0.810
8.38	**2.025**	0.388	0.612	11.850	0.195	0.805
8.56	**2.018**	0.399	0.601	12.128	0.196	0.804
8.74	**2.013**	0.411	0.589	12.415	0.196	0.804
8.92	**2.010**	0.423	0.577	12.710	0.197	0.803
9.1	**2.009**	0.434	0.566	13.015	0.197	0.803
9.28	**2.010**	0.446	0.554	13.327	0.198	0.802
9.46	**2.012**	0.457	0.543	13.649	0.198	0.802
9.64	**2.017**	0.468	0.532	13.981	0.199	0.801
9.82	**2.024**	0.479	0.521	14.322	0.199	0.801
10	**2.033**	0.490	0.510	14.675	0.200	0.800
10.18	**2.044**	0.501	0.499	15.039	0.200	0.800
10.36	**2.057**	0.511	0.489	15.416	0.200	0.800
10.54	**2.072**	0.521	0.479	15.808	0.200	0.800
10.72	**2.090**	0.531	0.469	16.217	0.200	0.800
10.9	**2.110**	0.540	0.460	16.653	0.201	0.799
10.9	**2.110**	0.540	0.460	16.653	0.201	0.799
11.443	**2.186**	0.567	0.434	18.120	0.201	0.799
11.985	**2.285**	0.589	0.411	19.932	0.199	0.801
12.527	**2.411**	0.607	0.393	23.181	0.223	0.777
13.07	**2.567**	0.621	0.379	32.617	0.263	0.737
13.613	**2.754**	0.630	0.370	41.865	0.289	0.711
14.155	**2.979**	0.636	0.364	53.273	0.330	0.670

14.697	**3.244**	0.637	0.363	61.659	0.367	0.633
15.24	**3.555**	0.635	0.365	52.353	0.399	0.601
15.783	**3.919**	0.630	0.370	84.694	0.303	0.697
16.325	**4.344**	0.622	0.378	73.715	0.464	0.532
16.867	**4.837**	0.611	0.389	87.612	0.386	0.614
17.41	**5.419**	0.591	0.409	88.930	0.510	0.490
17.953	**6.181**	0.534	0.466	76.662	0.501	0.491
18.495	**7.071**	0.481	0.519	74.890	0.542	0.438
19.038	**8.118**	0.431	0.569	95.883	0.463	0.500
19.58	**9.363**	0.385	0.615	109.690	0.462	0.495
20.123	**11.153**	0.361	0.639	104.780	0.489	0.438
20.665	**13.669**	0.393	0.602	99.854	0.511	0.411
21.207	**20.543**	0.457	0.501	133.230	0.419	0.477
21.75	**47.910**	0.529	0.409	102.150	0.495	0.432

G.2 **BSC Moisture Balance Inputs and Partitioning**

The two tables below contain the BSC moisture balance partitioning in fractional form, as show as percentages in Figure 20. The fractional partitioning for experiments 0 and 1 are listed as a group of columns in the first table, and for experiments 2 and 3 in the second table. Each row corresponds to the total fraction estimated across the entire experiment simulation period for each simulated plot. The first column of each table lists the RI of the given simulated plot. The first column of each experimental group contains the total depth in mm of BSC inputs to each plot (*X;* eq. 36) across each simulated timeperiod. The next three columns of each experimental group contain the fraction of *X* occurring as the total BSC excess infiltration (Ex_i), the total BSC evaporation (E_c), and the total BSC leakage (L_c).

RI	Experiment 0				Experiment 1			
	X_c (mm)	Ex_{inf} [L/L]	E_c [L/L]	L_c [L/L]	X_c (mm)	Ex_{inf} [L/L]	E_c [L/L]	L_c [L/L]
1	**2701**	0.002	0.355	0.643	**2701**	0.003	0.289	0.708
1.23	**2715**	0.002	0.454	0.545	**2715**	0.003	0.344	0.654
1.46	**2728**	0.001	0.527	0.471	**2728**	0.002	0.396	0.602
1.69	**2741**	0.001	0.570	0.429	**2741**	0.002	0.442	0.557
1.92	**2755**	0.001	0.599	0.400	**2755**	0.002	0.477	0.522
2.15	**2769**	0.001	0.622	0.378	**2769**	0.002	0.504	0.495
2.38	**2782**	0.001	0.639	0.361	**2782**	0.002	0.524	0.475
2.61	**2796**	0.000	0.654	0.346	**2796**	0.002	0.539	0.460
2.84	**2810**	0.000	0.668	0.333	**2810**	0.001	0.552	0.448
3.07	**2824**	0.000	0.680	0.321	**2824**	0.001	0.561	0.438
3.3	**2839**	0.000	0.690	0.311	**2839**	0.001	0.570	0.430
3.53	**2853**	0.000	0.699	0.302	**2853**	0.001	0.576	0.424
3.76	**2868**	0.000	0.706	0.295	**2868**	0.001	0.582	0.418
3.99	**2882**	0.000	0.712	0.289	**2882**	0.001	0.587	0.414
4.22	**2897**	0.000	0.718	0.283	**2897**	0.001	0.591	0.409
4.45	**2912**	0.000	0.724	0.277	**2912**	0.001	0.595	0.405
4.68	**2927**	0.000	0.729	0.272	**2927**	0.001	0.600	0.400
4.91	**2942**	0.000	0.734	0.267	**2942**	0.001	0.605	0.395
5.14	**2957**	0.000	0.739	0.262	**2957**	0.001	0.612	0.389
5.37	**2972**	0.000	0.744	0.258	**2972**	0.001	0.618	0.383
5.6	**2988**	0.000	0.748	0.253	**2988**	0.001	0.624	0.377
5.6	**2988**	0.000	0.748	0.253	**2988**	0.001	0.624	0.377
5.685	**2994**	0.000	0.749	0.252	**2994**	0.001	0.626	0.375
5.77	**2999**	0.000	0.751	0.250	**2999**	0.001	0.628	0.373
5.855	**3005**	0.000	0.752	0.249	**3005**	0.001	0.630	0.371
5.94	**3011**	0.000	0.754	0.247	**3011**	0.001	0.632	0.369
6.025	**3017**	0.000	0.755	0.246	**3017**	0.001	0.634	0.367
6.11	**3023**	0.000	0.757	0.245	**3023**	0.001	0.635	0.366
6.195	**3028**	0.000	0.758	0.243	**3028**	0.001	0.637	0.364
6.28	**3034**	0.000	0.759	0.242	**3034**	0.001	0.638	0.363
6.365	**3040**	0.000	0.761	0.241	**3040**	0.001	0.640	0.362
6.45	**3046**	0.000	0.762	0.239	**3046**	0.001	0.641	0.360
6.535	**3052**	0.000	0.763	0.238	**3052**	0.001	0.642	0.359
6.62	**3058**	0.000	0.765	0.237	**3058**	0.001	0.643	0.358
6.705	**3064**	0.000	0.766	0.235	**3064**	0.001	0.644	0.357
6.79	**3070**	0.000	0.767	0.234	**3070**	0.001	0.645	0.356
6.875	**3076**	0.000	0.768	0.233	**3076**	0.001	0.646	0.355

6.96	**3082**	0.000	0.769	0.232	**3082**	0.001	0.647	0.354
7.045	**3088**	0.000	0.771	0.231	**3088**	0.001	0.648	0.354
7.13	**3094**	0.000	0.772	0.229	**3094**	0.001	0.649	0.353
7.215	**3100**	0.000	0.773	0.228	**3100**	0.001	0.649	0.352
7.3	**3106**	0.000	0.774	0.227	**3106**	0.001	0.650	0.352
7.3	**3106**	0.000	0.774	0.227	**3106**	0.001	0.650	0.352
7.48	**3119**	0.000	0.776	0.225	**3119**	0.001	0.651	0.351
7.66	**3132**	0.000	0.778	0.222	**3132**	0.001	0.652	0.350
7.84	**3145**	0.000	0.781	0.220	**3145**	0.001	0.652	0.350
8.02	**3159**	0.000	0.783	0.218	**3159**	0.001	0.653	0.349
8.2	**3172**	0.000	0.785	0.216	**3172**	0.000	0.653	0.349
8.38	**3185**	0.000	0.787	0.214	**3185**	0.000	0.652	0.350
8.56	**3199**	0.000	0.789	0.212	**3199**	0.000	0.652	0.350
8.74	**3212**	0.000	0.791	0.210	**3212**	0.000	0.651	0.351
8.92	**3226**	0.000	0.792	0.208	**3226**	0.000	0.650	0.352
9.1	**3240**	0.000	0.794	0.206	**3240**	0.000	0.649	0.353
9.28	**3254**	0.000	0.796	0.205	**3254**	0.000	0.648	0.355
9.46	**3268**	0.000	0.797	0.203	**3268**	0.000	0.646	0.357
9.64	**3282**	0.000	0.799	0.201	**3282**	0.000	0.644	0.359
9.82	**3296**	0.000	0.800	0.200	**3296**	0.000	0.642	0.361
10	**3310**	0.000	0.802	0.198	**3310**	0.000	0.640	0.363
10.18	**3324**	0.000	0.803	0.197	**3324**	0.000	0.637	0.366
10.36	**3339**	0.000	0.805	0.195	**3339**	0.000	0.634	0.369
10.54	**3353**	0.000	0.806	0.194	**3353**	0.000	0.631	0.372
10.72	**3368**	0.000	0.807	0.193	**3368**	0.000	0.628	0.375
10.9	**3382**	0.000	0.808	0.192	**3382**	0.000	0.625	0.378
10.9	**3382**	0.000	0.808	0.192	**3382**	0.000	0.625	0.378
11.443	**3427**	0.000	0.812	0.188	**3427**	0.001	0.613	0.390
11.985	**3473**	0.000	0.815	0.185	**3473**	0.001	0.599	0.404
12.527	**3519**	0.000	0.817	0.182	**3519**	0.002	0.583	0.419
13.07	**3567**	0.000	0.819	0.180	**3567**	0.004	0.565	0.435
13.613	**3615**	0.000	0.820	0.179	**3615**	0.007	0.545	0.452
14.155	**3665**	0.000	0.822	0.177	**3665**	0.005	0.523	0.476
14.697	**3715**	0.000	0.823	0.176	**3715**	0.003	0.500	0.501
15.24	**3766**	0.000	0.824	0.175	**3766**	0.009	0.476	0.520
15.783	**3819**	0.000	0.824	0.174	**3819**	0.015	0.451	0.538
16.325	**3872**	0.000	0.825	0.173	**3872**	0.011	0.424	0.570
16.867	**3926**	0.000	0.825	0.173	**3926**	0.013	0.396	0.596
17.41	**3982**	0.000	0.825	0.173	**3982**	0.009	0.368	0.628
17.953	**4038**	0.000	0.824	0.173	**4038**	0.007	0.339	0.659
18.495	**4096**	0.000	0.823	0.173	**4096**	0.006	0.309	0.690

19.038	**4155**	0.000	0.822	0.174	**4155**	0.006	0.278	0.721
19.58	**4215**	0.000	0.821	0.176	**4217**	0.008	0.247	0.750
20.123	**4276**	0.000	0.819	0.177	**4279**	0.005	0.215	0.785
20.665	**4339**	0.000	0.816	0.179	**4340**	0.004	0.182	0.819
21.207	**4402**	0.000	0.814	0.182	**4410**	0.005	0.148	0.851
21.75	**4467**	0.000	0.809	0.186	**4470**	0.003	0.116	0.886

RI	**Experiment 2**				**Experiment 3**			
	X_c **(mm)**	Ex_{inf} [L/L]	E_c [L/L]	L_c [L/L]	X_c **(mm)**	Ex_{inf} [L/L]	E_c [L/L]	L_c [L/L]
1	**2701**	0.003	0.365	0.632	**2701**	0.004	0.305	0.692
1.23	**2715**	0.002	0.469	0.529	**2715**	0.003	0.371	0.626
1.46	**2728**	0.002	0.540	0.458	**2728**	0.003	0.436	0.561
1.69	**2741**	0.002	0.580	0.418	**2741**	0.003	0.489	0.509
1.92	**2755**	0.002	0.608	0.391	**2755**	0.002	0.527	0.471
2.15	**2769**	0.001	0.630	0.370	**2769**	0.002	0.553	0.445
2.38	**2782**	0.001	0.646	0.353	**2782**	0.002	0.572	0.427
2.61	**2796**	0.001	0.662	0.338	**2796**	0.002	0.586	0.412
2.84	**2810**	0.001	0.675	0.324	**2810**	0.002	0.598	0.400
3.07	**2824**	0.001	0.687	0.313	**2824**	0.002	0.608	0.390
3.3	**2839**	0.001	0.696	0.304	**2839**	0.002	0.617	0.382
3.53	**2853**	0.001	0.704	0.296	**2853**	0.002	0.624	0.375
3.76	**2868**	0.001	0.711	0.289	**2868**	0.002	0.630	0.369
3.99	**2882**	0.001	0.718	0.282	**2882**	0.002	0.636	0.363
4.22	**2897**	0.001	0.725	0.275	**2897**	0.002	0.640	0.359
4.45	**2912**	0.001	0.731	0.270	**2912**	0.003	0.644	0.355
4.68	**2927**	0.001	0.736	0.264	**2927**	0.003	0.648	0.351
4.91	**2942**	0.001	0.741	0.259	**2942**	0.003	0.651	0.348
5.14	**2957**	0.001	0.746	0.254	**2957**	0.003	0.653	0.346
5.37	**2972**	0.001	0.751	0.249	**2972**	0.003	0.655	0.344
5.6	**2988**	0.001	0.755	0.245	**2988**	0.003	0.656	0.343
5.6	**2988**	0.001	0.755	0.245	**2988**	0.003	0.656	0.343
5.685	**2994**	0.001	0.757	0.243	**2994**	0.003	0.657	0.342
5.77	**2999**	0.001	0.758	0.242	**2999**	0.003	0.657	0.342
5.855	**3005**	0.001	0.760	0.240	**3005**	0.003	0.658	0.341
5.94	**3011**	0.001	0.761	0.239	**3011**	0.003	0.658	0.341
6.025	**3017**	0.001	0.763	0.238	**3017**	0.003	0.659	0.340
6.11	**3023**	0.001	0.764	0.236	**3023**	0.003	0.659	0.340

6.195	**3028**	0.001	0.765	0.235	**3028**	0.003	0.659	0.340
6.28	**3034**	0.001	0.766	0.234	**3034**	0.003	0.659	0.340
6.365	**3040**	0.001	0.767	0.233	**3040**	0.003	0.659	0.340
6.45	**3046**	0.001	0.769	0.232	**3046**	0.003	0.659	0.340
6.535	**3052**	0.001	0.770	0.230	**3052**	0.003	0.659	0.340
6.62	**3058**	0.001	0.771	0.229	**3058**	0.003	0.659	0.340
6.705	**3064**	0.001	0.772	0.228	**3064**	0.003	0.659	0.340
6.79	**3070**	0.001	0.773	0.227	**3070**	0.003	0.659	0.340
6.875	**3076**	0.001	0.774	0.226	**3076**	0.003	0.658	0.341
6.96	**3082**	0.001	0.775	0.225	**3082**	0.003	0.658	0.341
7.045	**3088**	0.001	0.776	0.224	**3088**	0.003	0.658	0.341
7.13	**3094**	0.001	0.777	0.223	**3094**	0.003	0.657	0.342
7.215	**3100**	0.001	0.778	0.222	**3100**	0.003	0.657	0.342
7.3	**3106**	0.001	0.779	0.221	**3106**	0.003	0.656	0.343
7.3	**3106**	0.001	0.779	0.221	**3106**	0.003	0.656	0.343
7.48	**3119**	0.001	0.782	0.218	**3119**	0.003	0.656	0.344
7.66	**3132**	0.001	0.784	0.216	**3132**	0.003	0.655	0.344
7.84	**3145**	0.001	0.786	0.214	**3145**	0.004	0.654	0.345
8.02	**3159**	0.001	0.787	0.212	**3159**	0.004	0.653	0.346
8.2	**3172**	0.001	0.789	0.211	**3172**	0.004	0.653	0.346
8.38	**3185**	0.001	0.791	0.209	**3185**	0.004	0.652	0.347
8.56	**3199**	0.001	0.792	0.207	**3199**	0.004	0.652	0.347
8.74	**3212**	0.001	0.794	0.206	**3212**	0.004	0.651	0.348
8.92	**3226**	0.001	0.795	0.204	**3226**	0.004	0.650	0.349
9.1	**3240**	0.001	0.797	0.203	**3240**	0.004	0.649	0.350
9.28	**3254**	0.001	0.798	0.201	**3254**	0.004	0.648	0.351
9.46	**3268**	0.001	0.799	0.200	**3268**	0.004	0.646	0.353
9.64	**3282**	0.001	0.801	0.199	**3282**	0.004	0.644	0.355
9.82	**3296**	0.001	0.802	0.198	**3296**	0.004	0.642	0.357
10	**3310**	0.001	0.803	0.196	**3310**	0.004	0.640	0.359
10.18	**3324**	0.001	0.804	0.195	**3324**	0.005	0.637	0.362
10.36	**3339**	0.001	0.806	0.194	**3339**	0.005	0.634	0.365
10.54	**3353**	0.001	0.807	0.193	**3353**	0.005	0.631	0.368
10.72	**3368**	0.001	0.808	0.191	**3368**	0.005	0.628	0.371
10.9	**3382**	0.001	0.809	0.190	**3382**	0.005	0.624	0.374
10.9	**3382**	0.001	0.809	0.190	**3382**	0.005	0.624	0.374
11.443	**3427**	0.001	0.812	0.187	**3427**	0.005	0.612	0.386
11.985	**3473**	0.001	0.814	0.184	**3473**	0.006	0.598	0.400
12.527	**3519**	0.001	0.816	0.182	**3519**	0.007	0.582	0.415
13.07	**3567**	0.001	0.818	0.180	**3567**	0.009	0.564	0.430
13.613	**3615**	0.001	0.820	0.178	**3615**	0.012	0.545	0.448

14.155	**3665**	0.001	0.821	0.177	**3665**	0.015	0.523	0.467
14.697	**3715**	0.001	0.822	0.175	**3715**	0.017	0.500	0.488
15.24	**3766**	0.001	0.823	0.174	**3766**	0.014	0.476	0.515
15.783	**3819**	0.001	0.824	0.173	**3819**	0.022	0.451	0.532
16.325	**3872**	0.001	0.824	0.172	**3872**	0.019	0.424	0.562
16.867	**3926**	0.001	0.824	0.172	**3926**	0.022	0.397	0.586
17.41	**3982**	0.001	0.824	0.172	**3982**	0.022	0.367	0.615
17.953	**4038**	0.002	0.823	0.172	**4040**	0.019	0.339	0.647
18.495	**4096**	0.002	0.823	0.172	**4099**	0.018	0.308	0.678
19.038	**4155**	0.002	0.822	0.173	**4162**	0.023	0.277	0.705
19.58	**4215**	0.002	0.820	0.174	**4225**	0.026	0.245	0.733
20.123	**4276**	0.003	0.818	0.175	**4292**	0.024	0.213	0.766
20.665	**4339**	0.003	0.816	0.177	**4354**	0.023	0.180	0.800
21.207	**4404**	0.005	0.812	0.179	**4430**	0.030	0.146	0.826
21.75	**4473**	0.011	0.804	0.180	**4482**	0.023	0.115	0.866

G.3 **Soil Moisture Balance Inputs and Partitioning**

The two tables below contain the soil water balance partitioning in fractional form, as shown as percentages in Figures 21. The fractional partitioning for experiments 0 and 1 are listed as a group of columns in the first table, and for experiments 2 and 3 in the second table. Each row corresponds to the total fraction estimated across the entire experiment simulation period for each simulated plot. The first column of each table lists the RI of the given simulated plot. The first column of each experimental group contains the total depth in mm of soil inputs, or BSC leakage (L_c), to each plot across each simulated timeperiod. The next four columns of each experimental group contain the fraction of L_c occurring as the total bare soil evaporation ($E_{s,b}$; $s \leq s_w$), the total stressed soil evapotranspiration ($ET_{s,s}$; $s_w < s \leq s^*$), the total unstressed soil evapotranspiration ($ETs_{,u}$; $s^* < s \leq s_{fc}$), and the total is leakage from the soil layer (L_s). The fraction occurring as saturation excess (Ex_s) is not shown since none occurred for any experiment.

RI	Experiment 0					Experiment 1				
	L_c (mm)	$E_{s,b}$ [L/L]	$ET_{s,s}$ [L/L]	$ET_{s,u}$ [L/L]	L_s [L/L]	L_c (mm)	$E_{s,b}$ [L/L]	$ET_{s,s}$ [L/L]	$ET_{s,u}$ [L/L]	L_s [L/L]
1.00	**1737**	0.510	0.073	0.298	0.127	**1912**	0.474	0.092	0.316	0.125
1.23	**1478**	0.512	0.058	0.304	0.136	**1776**	0.501	0.081	0.299	0.126
1.46	**1286**	0.493	0.054	0.318	0.146	**1643**	0.514	0.071	0.294	0.130
1.69	**1177**	0.478	0.056	0.327	0.152	**1527**	0.514	0.066	0.296	0.134
1.92	**1102**	0.463	0.064	0.330	0.156	**1437**	0.515	0.058	0.298	0.138
2.15	**1047**	0.454	0.070	0.330	0.159	**1371**	0.509	0.058	0.302	0.141
2.38	**1004**	0.449	0.066	0.337	0.162	**1322**	0.507	0.055	0.304	0.144
2.61	**969**	0.442	0.069	0.340	0.164	**1286**	0.503	0.053	0.308	0.147
2.84	**936**	0.437	0.074	0.337	0.167	**1259**	0.501	0.051	0.310	0.149
3.07	**907**	0.431	0.077	0.339	0.170	**1238**	0.498	0.051	0.312	0.150
3.30	**882**	0.427	0.082	0.336	0.173	**1221**	0.498	0.051	0.311	0.152
3.53	**862**	0.421	0.086	0.335	0.175	**1209**	0.495	0.053	0.311	0.153
3.76	**846**	0.418	0.091	0.331	0.177	**1199**	0.494	0.053	0.311	0.154
3.99	**832**	0.417	0.093	0.328	0.179	**1192**	0.491	0.054	0.311	0.155
4.22	**819**	0.416	0.093	0.328	0.181	**1186**	0.488	0.056	0.310	0.157
4.45	**807**	0.414	0.096	0.326	0.182	**1180**	0.487	0.055	0.311	0.158
4.68	**796**	0.412	0.094	0.328	0.185	**1172**	0.486	0.055	0.310	0.160
4.91	**785**	0.408	0.094	0.330	0.187	**1163**	0.484	0.054	0.311	0.162
5.14	**775**	0.404	0.094	0.331	0.190	**1150**	0.478	0.057	0.312	0.165
5.37	**766**	0.402	0.090	0.334	0.193	**1137**	0.473	0.055	0.315	0.168
5.60	**757**	0.400	0.087	0.336	0.196	**1125**	0.469	0.052	0.320	0.171
5.60	**757**	0.400	0.087	0.336	0.196	**1125**	0.469	0.052	0.320	0.171
5.69	**754**	0.401	0.084	0.338	0.197	**1121**	0.466	0.053	0.320	0.172
5.77	**751**	0.398	0.085	0.338	0.198	**1118**	0.465	0.053	0.321	0.174
5.86	**748**	0.396	0.087	0.337	0.199	**1114**	0.464	0.051	0.322	0.175
5.94	**745**	0.394	0.085	0.340	0.200	**1111**	0.462	0.052	0.323	0.176
6.03	**742**	0.393	0.082	0.342	0.201	**1108**	0.461	0.051	0.323	0.177
6.11	**739**	0.392	0.082	0.342	0.203	**1106**	0.459	0.051	0.323	0.178
6.20	**737**	0.390	0.082	0.343	0.204	**1103**	0.458	0.050	0.325	0.179
6.28	**734**	0.389	0.081	0.344	0.205	**1101**	0.455	0.052	0.324	0.180
6.37	**731**	0.388	0.080	0.344	0.206	**1099**	0.454	0.053	0.324	0.181
6.45	**729**	0.385	0.082	0.344	0.207	**1098**	0.452	0.054	0.323	0.182
6.54	**726**	0.384	0.081	0.345	0.209	**1096**	0.451	0.054	0.323	0.183
6.62	**723**	0.383	0.081	0.345	0.210	**1095**	0.450	0.053	0.324	0.184
6.71	**721**	0.380	0.081	0.347	0.211	**1094**	0.450	0.052	0.325	0.185
6.79	**719**	0.380	0.080	0.347	0.212	**1093**	0.446	0.052	0.327	0.186

6.88	**716**	0.379	0.078	0.348	0.213	**1093**	0.445	0.052	0.327	0.187
6.96	**714**	0.377	0.079	0.347	0.215	**1092**	0.444	0.052	0.327	0.188
7.05	**712**	0.376	0.077	0.349	0.216	**1092**	0.440	0.056	0.327	0.189
7.13	**710**	0.374	0.076	0.351	0.217	**1092**	0.438	0.056	0.327	0.190
7.22	**708**	0.372	0.073	0.355	0.218	**1092**	0.438	0.057	0.326	0.191
7.30	**705**	0.369	0.076	0.354	0.219	**1093**	0.438	0.057	0.325	0.192
7.30	**705**	0.369	0.076	0.354	0.219	**1093**	0.438	0.057	0.325	0.192
7.48	**701**	0.367	0.071	0.358	0.222	**1094**	0.436	0.058	0.324	0.194
7.66	**697**	0.362	0.073	0.358	0.225	**1096**	0.436	0.054	0.325	0.196
7.84	**693**	0.358	0.072	0.360	0.228	**1100**	0.434	0.055	0.324	0.198
8.02	**689**	0.352	0.072	0.363	0.231	**1104**	0.433	0.055	0.322	0.200
8.20	**685**	0.345	0.072	0.367	0.233	**1109**	0.432	0.048	0.329	0.202
8.38	**681**	0.342	0.067	0.371	0.236	**1114**	0.432	0.050	0.325	0.203
8.56	**678**	0.340	0.066	0.372	0.239	**1121**	0.429	0.052	0.325	0.205
8.74	**675**	0.335	0.067	0.373	0.242	**1128**	0.429	0.051	0.324	0.207
8.92	**672**	0.326	0.068	0.378	0.246	**1136**	0.430	0.049	0.322	0.209
9.10	**669**	0.321	0.064	0.383	0.249	**1145**	0.431	0.044	0.324	0.210
9.28	**666**	0.318	0.063	0.383	0.252	**1155**	0.429	0.044	0.325	0.212
9.46	**664**	0.312	0.066	0.384	0.255	**1165**	0.427	0.044	0.324	0.214
9.64	**661**	0.305	0.068	0.386	0.259	**1177**	0.429	0.046	0.319	0.215
9.82	**659**	0.301	0.066	0.388	0.262	**1189**	0.426	0.048	0.318	0.217
10.00	**656**	0.294	0.067	0.390	0.266	**1202**	0.423	0.048	0.320	0.218
10.18	**654**	0.292	0.062	0.393	0.269	**1216**	0.419	0.051	0.318	0.220
10.36	**653**	0.285	0.065	0.393	0.273	**1230**	0.414	0.058	0.315	0.221
10.54	**651**	0.279	0.068	0.393	0.277	**1246**	0.409	0.062	0.314	0.223
10.72	**649**	0.275	0.064	0.396	0.280	**1263**	0.407	0.061	0.316	0.224
10.90	**648**	0.271	0.062	0.398	0.284	**1280**	0.396	0.068	0.318	0.226
10.90	**648**	0.271	0.062	0.398	0.284	**1280**	0.396	0.068	0.318	0.226
11.44	**644**	0.255	0.061	0.403	0.296	**1337**	0.356	0.090	0.331	0.229
11.99	**642**	0.245	0.056	0.405	0.309	**1403**	0.264	0.154	0.355	0.233
12.53	**642**	0.236	0.052	0.405	0.322	**1476**	0.155	0.230	0.384	0.237
13.07	**643**	0.226	0.044	0.407	0.337	**1553**	0.075	0.246	0.442	0.242
13.61	**645**	0.217	0.042	0.403	0.352	**1634**	0.036	0.208	0.512	0.250
14.16	**649**	0.210	0.040	0.394	0.369	**1745**	0.018	0.130	0.579	0.277
14.70	**653**	0.205	0.036	0.385	0.387	**1860**	0.006	0.024	0.652	0.323
15.24	**657**	0.198	0.033	0.375	0.405	**1957**	0.000	0.023	0.608	0.373
15.78	**663**	0.193	0.027	0.365	0.426	**2056**	0.000	0.012	0.572	0.419
16.33	**670**	0.183	0.026	0.353	0.447	**2206**	0.000	0.000	0.528	0.474
16.87	**678**	0.179	0.026	0.334	0.470	**2340**	0.000	0.000	0.482	0.521
17.41	**687**	0.174	0.022	0.318	0.496	**2500**	0.000	0.000	0.435	0.567
17.95	**698**	0.169	0.019	0.297	0.523	**2659**	0.000	0.000	0.394	0.607

18.50	**710**	0.155	0.025	0.274	0.552	**2825**	0.000	0.000	0.357	0.644
19.04	**724**	0.132	0.034	0.256	0.584	**2996**	0.000	0.000	0.322	0.678
19.58	**740**	0.109	0.033	0.246	0.617	**3162**	0.000	0.000	0.292	0.708
20.12	**758**	0.080	0.032	0.238	0.655	**3359**	0.000	0.000	0.262	0.737
20.67	**778**	0.048	0.027	0.231	0.698	**3554**	0.000	0.000	0.235	0.764
21.21	**801**	0.018	0.029	0.206	0.751	**3754**	0.000	0.000	0.210	0.788
21.75	**831**	0.000	0.022	0.180	0.801	**3959**	0.000	0.000	0.187	0.811

RI	**Experiment 0**					**Experiment 1**				
	L_c **(mm)**	$E_{s,b}$ [L/L]	$ET_{s,s}$ [L/L]	$ET_{s,u}$ [L/L]	L_s [L/L]	L_c **(mm)**	$E_{s,b}$ [L/L]	$ET_{s,s}$ [L/L]	$ET_{s,u}$ [L/L]	L_s [L/L]
1.00	**1708**	0.514	0.075	0.291	0.128	**1868**	0.489	0.090	0.304	0.125
1.23	**1436**	0.509	0.059	0.303	0.138	**1701**	0.512	0.075	0.292	0.128
1.46	**1250**	0.486	0.056	0.321	0.149	**1532**	0.513	0.064	0.297	0.134
1.69	**1147**	0.471	0.061	0.326	0.154	**1396**	0.505	0.060	0.303	0.141
1.92	**1076**	0.459	0.066	0.329	0.158	**1298**	0.496	0.054	0.314	0.147
2.15	**1023**	0.448	0.071	0.333	0.161	**1233**	0.486	0.059	0.315	0.151
2.38	**982**	0.443	0.071	0.336	0.164	**1187**	0.478	0.058	0.321	0.154
2.61	**944**	0.436	0.076	0.336	0.167	**1152**	0.472	0.057	0.325	0.157
2.84	**911**	0.435	0.075	0.337	0.170	**1125**	0.466	0.059	0.327	0.160
3.07	**883**	0.431	0.080	0.333	0.173	**1102**	0.461	0.061	0.329	0.162
3.30	**862**	0.426	0.086	0.331	0.175	**1084**	0.457	0.063	0.328	0.164
3.53	**844**	0.428	0.085	0.328	0.176	**1069**	0.457	0.062	0.327	0.166
3.76	**828**	0.425	0.092	0.324	0.178	**1057**	0.455	0.061	0.329	0.168
3.99	**812**	0.423	0.092	0.326	0.179	**1047**	0.455	0.059	0.329	0.170
4.22	**797**	0.422	0.089	0.327	0.181	**1039**	0.454	0.054	0.333	0.172
4.45	**785**	0.417	0.093	0.326	0.183	**1033**	0.451	0.056	0.333	0.174
4.68	**774**	0.414	0.091	0.329	0.186	**1028**	0.448	0.058	0.332	0.175
4.91	**763**	0.409	0.096	0.326	0.188	**1025**	0.446	0.059	0.331	0.177
5.14	**752**	0.405	0.096	0.327	0.191	**1023**	0.446	0.058	0.330	0.179
5.37	**741**	0.402	0.094	0.330	0.194	**1023**	0.443	0.060	0.329	0.181
5.60	**732**	0.397	0.091	0.335	0.197	**1024**	0.441	0.060	0.329	0.183
5.60	**732**	0.397	0.091	0.335	0.197	**1024**	0.441	0.060	0.329	0.183
5.69	**729**	0.397	0.088	0.337	0.198	**1024**	0.439	0.061	0.329	0.183
5.77	**726**	0.394	0.088	0.338	0.199	**1025**	0.439	0.061	0.329	0.184
5.86	**722**	0.396	0.084	0.340	0.200	**1025**	0.439	0.058	0.330	0.185
5.94	**720**	0.394	0.084	0.341	0.201	**1026**	0.439	0.057	0.332	0.185

6.03	**717**	0.393	0.084	0.340	0.203	**1027**	0.438	0.056	0.332	0.186
6.11	**714**	0.390	0.084	0.341	0.204	**1028**	0.439	0.056	0.331	0.187
6.20	**712**	0.389	0.083	0.342	0.205	**1030**	0.440	0.054	0.331	0.187
6.28	**710**	0.387	0.084	0.343	0.206	**1031**	0.439	0.052	0.333	0.188
6.37	**708**	0.385	0.081	0.346	0.207	**1033**	0.438	0.055	0.331	0.189
6.45	**705**	0.383	0.080	0.348	0.209	**1035**	0.438	0.055	0.330	0.189
6.54	**703**	0.382	0.079	0.349	0.210	**1037**	0.436	0.058	0.328	0.190
6.62	**701**	0.381	0.078	0.350	0.211	**1040**	0.437	0.058	0.327	0.190
6.71	**699**	0.379	0.077	0.351	0.212	**1042**	0.437	0.057	0.326	0.191
6.79	**697**	0.375	0.077	0.353	0.214	**1045**	0.437	0.057	0.327	0.192
6.88	**695**	0.374	0.077	0.353	0.215	**1048**	0.437	0.053	0.329	0.192
6.96	**693**	0.371	0.077	0.355	0.216	**1051**	0.438	0.054	0.327	0.193
7.05	**691**	0.370	0.078	0.355	0.217	**1054**	0.437	0.054	0.328	0.193
7.13	**689**	0.368	0.075	0.358	0.219	**1057**	0.438	0.053	0.327	0.194
7.22	**687**	0.365	0.076	0.358	0.220	**1061**	0.438	0.054	0.325	0.194
7.30	**685**	0.363	0.073	0.361	0.221	**1064**	0.438	0.055	0.324	0.195
7.30	**685**	0.363	0.073	0.361	0.221	**1064**	0.438	0.055	0.324	0.195
7.48	**681**	0.360	0.070	0.364	0.224	**1072**	0.436	0.058	0.322	0.196
7.66	**678**	0.354	0.071	0.366	0.227	**1079**	0.438	0.057	0.320	0.197
7.84	**674**	0.352	0.067	0.371	0.230	**1086**	0.438	0.057	0.317	0.198
8.02	**671**	0.345	0.067	0.374	0.233	**1092**	0.440	0.058	0.314	0.200
8.20	**668**	0.340	0.066	0.377	0.236	**1098**	0.439	0.049	0.321	0.201
8.38	**665**	0.335	0.066	0.378	0.239	**1104**	0.440	0.050	0.317	0.203
8.56	**663**	0.329	0.064	0.383	0.242	**1110**	0.437	0.054	0.315	0.205
8.74	**661**	0.322	0.067	0.385	0.245	**1117**	0.437	0.053	0.314	0.207
8.92	**659**	0.315	0.067	0.388	0.248	**1125**	0.437	0.052	0.313	0.208
9.10	**657**	0.311	0.066	0.390	0.251	**1134**	0.438	0.049	0.314	0.210
9.28	**656**	0.308	0.067	0.388	0.254	**1143**	0.437	0.045	0.316	0.211
9.46	**654**	0.305	0.066	0.390	0.258	**1153**	0.436	0.045	0.316	0.213
9.64	**652**	0.300	0.065	0.392	0.261	**1164**	0.437	0.046	0.312	0.214
9.82	**651**	0.292	0.069	0.392	0.264	**1176**	0.434	0.049	0.310	0.216
10.00	**649**	0.290	0.067	0.393	0.268	**1189**	0.431	0.049	0.312	0.217
10.18	**648**	0.289	0.062	0.394	0.271	**1203**	0.430	0.049	0.311	0.219
10.36	**647**	0.280	0.066	0.395	0.275	**1217**	0.424	0.057	0.307	0.220
10.54	**646**	0.274	0.069	0.395	0.278	**1232**	0.420	0.060	0.307	0.221
10.72	**645**	0.272	0.063	0.399	0.282	**1248**	0.415	0.062	0.308	0.223
10.90	**644**	0.269	0.061	0.400	0.286	**1266**	0.406	0.070	0.309	0.224
10.90	**644**	0.269	0.061	0.400	0.286	**1266**	0.406	0.070	0.309	0.224
11.44	**641**	0.254	0.058	0.406	0.298	**1322**	0.368	0.090	0.322	0.228
11.99	**640**	0.243	0.056	0.406	0.310	**1387**	0.276	0.157	0.343	0.231
12.53	**641**	0.234	0.052	0.406	0.323	**1460**	0.161	0.238	0.372	0.235

13.07	**642**	0.224	0.044	0.408	0.337	**1535**	0.076	0.271	0.417	0.241
13.61	**644**	0.215	0.042	0.404	0.352	**1619**	0.036	0.228	0.493	0.248
14.16	**647**	0.208	0.040	0.395	0.369	**1710**	0.019	0.159	0.559	0.267
14.70	**651**	0.203	0.036	0.386	0.387	**1812**	0.006	0.027	0.664	0.307
15.24	**655**	0.196	0.033	0.376	0.406	**1939**	0.000	0.023	0.614	0.366
15.78	**661**	0.191	0.027	0.366	0.426	**2030**	0.000	0.014	0.578	0.411
16.33	**667**	0.181	0.026	0.355	0.448	**2176**	0.000	0.000	0.536	0.467
16.87	**675**	0.177	0.027	0.335	0.471	**2299**	0.000	0.000	0.490	0.512
17.41	**684**	0.172	0.022	0.319	0.496	**2450**	0.000	0.000	0.443	0.559
17.95	**694**	0.167	0.019	0.298	0.523	**2615**	0.000	0.000	0.400	0.601
18.50	**706**	0.155	0.023	0.276	0.553	**2780**	0.000	0.000	0.362	0.639
19.04	**718**	0.136	0.029	0.257	0.585	**2932**	0.000	0.000	0.329	0.672
19.58	**734**	0.113	0.032	0.241	0.619	**3098**	0.000	0.000	0.297	0.703
20.12	**750**	0.085	0.033	0.230	0.658	**3289**	0.000	0.000	0.266	0.733
20.67	**768**	0.049	0.031	0.225	0.699	**3485**	0.000	0.000	0.239	0.760
21.21	**788**	0.018	0.032	0.206	0.748	**3658**	0.000	0.000	0.215	0.784
21.75	**805**	0.000	0.023	0.184	0.796	**3881**	0.000	0.000	0.190	0.808

G.4 **Total Evaporative Demand and Partitioning**

The two tables below contain the partitioning of the total evaporative demand, or of the total potential evapotranspiration (*PET*) in fractional form, as show as percentages in Figure 22. Each row corresponds to the total fraction estimated across the entire experiment simulation period for each simulated plot. The first column lists the RI of the given simulated plot. The second column contains the total depth in mm of total *PET* across each simulated timeperiod. The fractional partitioning for each experiment is listed as a group of columns. The three columns of each experimental group contain the fraction of *PET* occurring as the total ponded evaporation (E_p), the total evaporation from the BSC (E_c), and the total soil evapotranspiration ($ET_{s,T}$). The unmet *PET* demand is not shown but can be extracted from each column by subtracting the sum of the fractions from 1 $\left(1-(E_p+E_c+ET_{s,T})\right)$.

RI	*PET* (mm)	Experiment 0			Experiment 1		
		E_p [L/L]	E_C [L/L]	ET_s [L/L]	E_p [L/L]	E_C [L/L]	ET_s [L/L]
1.00	**4941**	0.000	0.194	0.310	0.000	0.158	0.341
1.23	**4941**	0.000	0.249	0.261	0.000	0.189	0.317
1.46	**4941**	0.000	0.291	0.225	0.000	0.219	0.292
1.69	**4941**	0.000	0.316	0.205	0.000	0.245	0.270
1.92	**4941**	0.000	0.334	0.191	0.000	0.266	0.254
2.15	**4941**	0.000	0.348	0.181	0.000	0.282	0.241
2.38	**4941**	0.000	0.360	0.173	0.000	0.295	0.232
2.61	**4941**	0.000	0.370	0.167	0.000	0.305	0.225
2.84	**4941**	0.000	0.380	0.161	0.000	0.314	0.220
3.07	**4941**	0.000	0.389	0.155	0.000	0.321	0.216
3.30	**4941**	0.000	0.397	0.151	0.000	0.327	0.212
3.53	**4941**	0.000	0.403	0.147	0.000	0.333	0.210
3.76	**4941**	0.000	0.410	0.144	0.000	0.338	0.208
3.99	**4941**	0.000	0.416	0.141	0.000	0.342	0.206
4.22	**4941**	0.000	0.421	0.139	0.000	0.346	0.205
4.45	**4941**	0.000	0.427	0.137	0.000	0.351	0.204
4.68	**4941**	0.000	0.432	0.134	0.000	0.355	0.202
4.91	**4941**	0.000	0.437	0.132	0.000	0.360	0.200
5.14	**4941**	0.000	0.442	0.130	0.000	0.366	0.197
5.37	**4941**	0.000	0.447	0.128	0.000	0.372	0.194
5.60	**4941**	0.000	0.452	0.126	0.000	0.378	0.191
5.60	**4941**	0.000	0.452	0.126	0.000	0.378	0.191
5.69	**4941**	0.000	0.454	0.125	0.000	0.380	0.190
5.77	**4941**	0.000	0.456	0.125	0.000	0.382	0.190
5.86	**4941**	0.000	0.458	0.124	0.000	0.383	0.189
5.94	**4941**	0.000	0.459	0.123	0.000	0.385	0.188
6.03	**4941**	0.000	0.461	0.123	0.000	0.387	0.187
6.11	**4941**	0.000	0.463	0.122	0.000	0.389	0.187
6.20	**4941**	0.000	0.465	0.122	0.000	0.390	0.186
6.28	**4941**	0.000	0.466	0.121	0.000	0.392	0.185
6.37	**4941**	0.000	0.468	0.120	0.000	0.394	0.185
6.45	**4941**	0.000	0.470	0.120	0.000	0.395	0.184
6.54	**4941**	0.000	0.472	0.119	0.000	0.397	0.184
6.62	**4941**	0.000	0.473	0.118	0.000	0.398	0.183
6.71	**4941**	0.000	0.475	0.118	0.000	0.400	0.183
6.79	**4941**	0.000	0.477	0.117	0.000	0.401	0.183
6.88	**4941**	0.000	0.478	0.117	0.000	0.402	0.182

6.96	**4941**	0.000	0.480	0.116	0.000	0.404	0.182
7.05	**4941**	0.000	0.482	0.116	0.000	0.405	0.182
7.13	**4941**	0.000	0.483	0.115	0.000	0.406	0.181
7.22	**4941**	0.000	0.485	0.115	0.000	0.408	0.181
7.30	**4941**	0.000	0.487	0.114	0.000	0.409	0.181
7.30	**4941**	0.000	0.487	0.114	0.000	0.409	0.181
7.48	**4941**	0.000	0.490	0.113	0.000	0.411	0.181
7.66	**4941**	0.000	0.494	0.112	0.000	0.413	0.181
7.84	**4941**	0.000	0.497	0.111	0.000	0.415	0.181
8.02	**4941**	0.000	0.500	0.110	0.000	0.417	0.181
8.20	**4941**	0.000	0.504	0.109	0.000	0.419	0.181
8.38	**4941**	0.000	0.507	0.108	0.000	0.421	0.182
8.56	**4941**	0.000	0.511	0.107	0.000	0.422	0.183
8.74	**4941**	0.000	0.514	0.106	0.000	0.423	0.183
8.92	**4941**	0.000	0.517	0.105	0.000	0.425	0.184
9.10	**4941**	0.000	0.521	0.104	0.000	0.426	0.185
9.28	**4941**	0.000	0.524	0.103	0.000	0.427	0.186
9.46	**4941**	0.000	0.527	0.102	0.000	0.427	0.188
9.64	**4941**	0.000	0.531	0.101	0.000	0.428	0.189
9.82	**4941**	0.000	0.534	0.101	0.000	0.428	0.191
10.00	**4941**	0.000	0.537	0.100	0.000	0.429	0.192
10.18	**4941**	0.000	0.540	0.099	0.000	0.429	0.194
10.36	**4941**	0.000	0.544	0.098	0.000	0.429	0.196
10.54	**4941**	0.000	0.547	0.097	0.000	0.428	0.198
10.72	**4941**	0.000	0.550	0.097	0.000	0.428	0.200
10.90	**4941**	0.000	0.553	0.096	0.000	0.428	0.203
10.90	**4941**	0.000	0.553	0.096	0.000	0.428	0.203
11.44	**4941**	0.000	0.563	0.094	0.000	0.425	0.210
11.99	**4941**	0.000	0.573	0.092	0.000	0.421	0.220
12.53	**4941**	0.000	0.582	0.090	0.000	0.415	0.230
13.07	**4941**	0.000	0.591	0.088	0.001	0.408	0.240
13.61	**4941**	0.000	0.600	0.086	0.001	0.399	0.250
14.16	**4941**	0.000	0.609	0.085	0.001	0.388	0.257
14.70	**4941**	0.000	0.619	0.083	0.001	0.376	0.256
15.24	**4941**	0.000	0.628	0.081	0.005	0.363	0.250
15.78	**4941**	0.000	0.637	0.078	0.006	0.349	0.243
16.33	**4941**	0.000	0.646	0.076	0.007	0.332	0.236
16.87	**4941**	0.000	0.655	0.074	0.007	0.315	0.228
17.41	**4941**	0.000	0.665	0.071	0.007	0.296	0.220
17.95	**4941**	0.000	0.674	0.069	0.006	0.277	0.212
18.50	**4941**	0.000	0.683	0.065	0.005	0.257	0.204

19.04	**4941**	0.000	0.691	0.062	0.004	0.234	0.196
19.58	**4941**	0.000	0.700	0.058	0.004	0.211	0.187
20.12	**4941**	0.000	0.709	0.054	0.004	0.186	0.178
20.67	**4941**	0.000	0.717	0.048	0.003	0.160	0.169
21.21	**4941**	0.000	0.725	0.041	0.004	0.132	0.160
21.75	**4941**	0.000	0.732	0.034	0.003	0.105	0.150

RI	***PET*** **(mm)**	**Experiment 2**			**Experiment 3**		
		E_p [L/L]	E_C [L/L]	ET_s [L/L]	E_p [L/L]	E_C [L/L]	ET_s [L/L]
1.00	**4941**	0.000	0.200	0.304	0.000	0.167	0.334
1.23	**4941**	0.000	0.258	0.253	0.000	0.204	0.303
1.46	**4941**	0.000	0.298	0.218	0.000	0.241	0.271
1.69	**4941**	0.000	0.322	0.199	0.000	0.271	0.245
1.92	**4941**	0.000	0.339	0.186	0.000	0.294	0.227
2.15	**4941**	0.000	0.353	0.177	0.000	0.310	0.215
2.38	**4941**	0.000	0.364	0.169	0.000	0.322	0.206
2.61	**4941**	0.000	0.375	0.162	0.000	0.332	0.199
2.84	**4941**	0.000	0.384	0.156	0.000	0.340	0.194
3.07	**4941**	0.000	0.393	0.151	0.000	0.348	0.190
3.30	**4941**	0.000	0.400	0.147	0.000	0.354	0.186
3.53	**4941**	0.000	0.407	0.144	0.000	0.360	0.183
3.76	**4941**	0.000	0.413	0.141	0.000	0.366	0.181
3.99	**4941**	0.000	0.419	0.138	0.000	0.371	0.179
4.22	**4941**	0.000	0.425	0.135	0.000	0.375	0.177
4.45	**4941**	0.000	0.431	0.133	0.000	0.380	0.175
4.68	**4941**	0.000	0.436	0.131	0.000	0.384	0.174
4.91	**4941**	0.000	0.441	0.128	0.000	0.387	0.173
5.14	**4941**	0.000	0.447	0.126	0.000	0.391	0.173
5.37	**4941**	0.000	0.452	0.124	0.000	0.394	0.172
5.60	**4941**	0.000	0.457	0.122	0.000	0.397	0.172
5.60	**4941**	0.000	0.457	0.122	0.000	0.397	0.172
5.69	**4941**	0.000	0.459	0.121	0.000	0.398	0.172
5.77	**4941**	0.000	0.460	0.121	0.000	0.399	0.172
5.86	**4941**	0.000	0.462	0.120	0.000	0.400	0.172
5.94	**4941**	0.000	0.464	0.119	0.000	0.401	0.172
6.03	**4941**	0.000	0.466	0.119	0.000	0.402	0.172
6.11	**4941**	0.000	0.467	0.118	0.000	0.403	0.172
6.20	**4941**	0.000	0.469	0.117	0.000	0.404	0.172

6.28	**4941**	0.000	0.471	0.117	0.000	0.405	0.172
6.37	**4941**	0.000	0.472	0.116	0.000	0.406	0.172
6.45	**4941**	0.000	0.474	0.116	0.000	0.406	0.172
6.54	**4941**	0.000	0.475	0.115	0.000	0.407	0.173
6.62	**4941**	0.000	0.477	0.115	0.000	0.408	0.173
6.71	**4941**	0.000	0.479	0.114	0.000	0.409	0.173
6.79	**4941**	0.000	0.480	0.114	0.000	0.409	0.173
6.88	**4941**	0.000	0.482	0.113	0.000	0.410	0.174
6.96	**4941**	0.000	0.484	0.113	0.000	0.411	0.174
7.05	**4941**	0.000	0.485	0.112	0.000	0.411	0.175
7.13	**4941**	0.000	0.487	0.112	0.000	0.412	0.175
7.22	**4941**	0.000	0.488	0.111	0.000	0.412	0.176
7.30	**4941**	0.000	0.490	0.111	0.000	0.413	0.176
7.30	**4941**	0.000	0.490	0.111	0.000	0.413	0.176
7.48	**4941**	0.000	0.493	0.110	0.000	0.414	0.177
7.66	**4941**	0.000	0.497	0.109	0.000	0.415	0.178
7.84	**4941**	0.000	0.500	0.108	0.000	0.416	0.179
8.02	**4941**	0.000	0.503	0.107	0.000	0.418	0.179
8.20	**4941**	0.000	0.507	0.106	0.000	0.419	0.180
8.38	**4941**	0.000	0.510	0.105	0.000	0.421	0.180
8.56	**4941**	0.000	0.513	0.104	0.000	0.422	0.181
8.74	**4941**	0.000	0.516	0.103	0.000	0.423	0.182
8.92	**4941**	0.000	0.519	0.103	0.001	0.425	0.183
9.10	**4941**	0.000	0.522	0.102	0.001	0.426	0.184
9.28	**4941**	0.000	0.526	0.101	0.001	0.426	0.185
9.46	**4941**	0.000	0.529	0.101	0.001	0.427	0.186
9.64	**4941**	0.000	0.532	0.100	0.001	0.428	0.187
9.82	**4941**	0.000	0.535	0.099	0.001	0.428	0.189
10.00	**4941**	0.000	0.538	0.098	0.001	0.428	0.190
10.18	**4941**	0.000	0.541	0.098	0.001	0.429	0.192
10.36	**4941**	0.000	0.544	0.097	0.001	0.429	0.194
10.54	**4941**	0.000	0.548	0.096	0.001	0.428	0.196
10.72	**4941**	0.000	0.551	0.096	0.001	0.428	0.198
10.90	**4941**	0.000	0.554	0.095	0.001	0.427	0.201
10.90	**4941**	0.000	0.554	0.095	0.001	0.427	0.201
11.44	**4941**	0.000	0.563	0.093	0.001	0.425	0.209
11.99	**4941**	0.000	0.572	0.091	0.001	0.421	0.218
12.53	**4941**	0.000	0.582	0.090	0.001	0.415	0.228
13.07	**4941**	0.000	0.591	0.088	0.002	0.408	0.238
13.61	**4941**	0.000	0.600	0.086	0.002	0.398	0.248
14.16	**4941**	0.000	0.609	0.084	0.004	0.388	0.255

14.70	**4941**	0.000	0.618	0.082	0.005	0.376	0.256
15.24	**4941**	0.000	0.627	0.080	0.004	0.363	0.250
15.78	**4941**	0.000	0.637	0.078	0.005	0.348	0.243
16.33	**4941**	0.001	0.646	0.076	0.007	0.332	0.236
16.87	**4941**	0.001	0.655	0.074	0.007	0.315	0.228
17.41	**4941**	0.001	0.664	0.071	0.009	0.296	0.220
17.95	**4941**	0.001	0.673	0.068	0.008	0.277	0.212
18.50	**4941**	0.001	0.682	0.065	0.008	0.256	0.204
19.04	**4941**	0.001	0.691	0.061	0.009	0.233	0.195
19.58	**4941**	0.001	0.700	0.057	0.010	0.209	0.186
20.12	**4941**	0.001	0.708	0.053	0.010	0.185	0.177
20.67	**4941**	0.001	0.716	0.047	0.010	0.159	0.168
21.21	**4941**	0.002	0.724	0.041	0.011	0.131	0.159
21.75	**4941**	0.005	0.728	0.034	0.010	0.104	0.149

APPENDIX H

TABLES, FIGURES AND PHOTOGRAPHS

This appendix describes the contents of the AppendixH folder which contains three main folders: Figures, Tables, and Photographs. The Tables folder contains excel files each containing a table presented in this report and each saved as "Table#" where # corresponds to the number of the given table. The Photographs folder contains photographs of the study site (instrumentation, landscape, field activities) that have been taken over different periods of time. The organization and label of the photographs are described in a document PhotographContents.pdf placed in the Photographs folder. The Figures folder contains the following folders listed below in fold. Each figure folder content and any steps necessary to re-create the figures are described in order of figures.

Figure1to4:

This folder contains four 600-dpi compressed TIFF versions of Figures 1 through 4, each labeled as Figure#.tif.tar.gz, where # corresponds to the number of the given figure.

Figure5:

This folder contains seven 600-dpi compressed TIFF versions of Figures 5a, 5b, 5c, 5d, 5e, 5f, and 5g, each labeled as Figure5X, where X corresponds to the letter of the given sub-figure. This folder also contains Figure5.ai which can be opened in Adobe Illustrator to view and edit the final version of Figure 5 shown in this thesis. A folder Figure5a contains a repository of GIS data used in the creation of Figure 5a. The following shapefiles in itallics are stored in this folder and were used to create Figure 5a:

- *FS.shp*: The point location of the field site using the coordinate system GCS_WGS_1984.

- *states_clip.shp*: The outline of US states clipped to the map area, designated by *map_outline.shp,* clipped from the geodatabase feature class *dtl_st_ln.gdb,* which contains all US state boundaries. The coordinate system is GCS_WGS_1984.
- *Mx_clip.shp*: The outline of the Mexico boundaries clipped to the map area from the geodatabase feature class *country.gdb,* which contains all country outlines. The coordinate system is GCS_WGS_1984.
- *physio_dis.shp*: The outline of the Colorado Plateau clipped to the map area from the *physio.shp,* which contains the Colorado Plateau outline, discretized by counties. The coordinate system is NAD_1983_Albers.

Figure5c of the field map was created from a Google Earth screenshot and not georeferenced. Adobe Illustrator was used to outline the estimated block and plot locations, and can be edited in the Figure5.ai file from Adobe Illustrator.

Figure6:

Figure 6 was created using Adobe Illustrator in the file Figure6.ai. This version is provided in the Figure6 folder for viewing and editing, as well as a 600-dpi compressed TIFF version saved as Figure6.tif.tar.gz.

Figure7:

Figure 7 was created in Adobe Illustrator by combining the.eps versions of the three figures created by executing AppendixD/VisualizingObservationTimeseries.m (Described in section D.5). These three figure outputs contain the soil moisture (and total

precipitation), air temperature, and PET time series output for the given quad and time period. The output used to create Figure 7 is saved in the AppendixH/Figure7 folder as Figure7_sm_Pt.eps, Figure7_Ta.eps, and Figure7_PET.eps. The MATLAB .fig versions of these figures are also saved in the Figure7 folder. The file Figure7.ai is saved in the Figure7 folder and can be viewed and edited in Adobe Illustrator and serve as a template for the creation of any other observation time series figures. The final edited figure is also saved as a 600-dpi compressed TIFF version (Figure7.tif.tar.gz).

Figure8:

This folder contains three 600-dpi compressed TIFF versions of Figures 8a, 8b, and 8c as Figure8X.tif.tar.gz, where X corresponds to the letter of the given sub-figure. This folder also contains Figure8.ai which can be opened in Adobe Illustrator to view and edit the final version of Figure 8 shown in this thesis.

Figure9:

Figure 9 was first plot in the Excel file RI_Plot.xlsx and then edited in the Adobe Illustrator file RI_Plot.ai. Both of these are provided in the Figure9 folder, as well as the final edited figure saved as a 600-dpi compressed TIFF version (Figure9.tif.tar.gz).

Figure10to11:

Figures 10 and 11 were first created in Power Point files Figure10.pptx and Figure11.pptx and edited in Adobe Illustrator files Figure10.ai and Figure11.ai. All four

files are contained in the Figure10to11 file, as well as the final edited figures saved as 600-dpi compressed TIFF versions (Figure10.tif.tar.gz and Figure11.tif.tar.gz).

Figures12to14:

The Adobe Illustrator files used to edit Figures 12-14 are saved in this folder as Figure#.ai (# = number of figure).The final edited figures are saved as 600-dpi compressed TIFF versions (Figure#.tif.tar.gz).

Figure15:

Figure 15 was created in Adobe Illustrator by combining the.eps versions of four figures created by executing AppendixD/ main_Exp_Figure_15.m (Described in section D.3). These four figure outputs are identified by text prints on the figure corresponding the sub-figure lettering scheme in Figure 15 (i.e. Figure 15a will have "(a)" printed in the plot area). The output used to create Figure 15 are saved in the AppendixH/Figure15 folder as Figure15X.eps, where X corresponds to the sub-figure letter. The MATLAB .fig versions of these figures are also saved in the Figure 15 folder. The file Figure15.ai is saved in the Figure15 folder and can be viewed and edited in Adobe Illustrator. The final edited figure is also saved as a 600-dpi compressed TIFF version (Figure15.tif.tar.gz).

Figures16to17:

Figures 16 and 17 were created in Adobe Illustrator by combining the.eps versions of four figures created by executing AppendixD/Verificaton/main_VerFig_X.m, where X corresponds to the figure number and letter (X = 16a, 16b, 17a, or 17b for

Figures 16a, 16b, 17a, and 17b, respectively). These four figure outputs are identified by text prints on the figure corresponding the sub-figure lettering scheme in Figure 16 and 17 (i.e. Figure 16a will have "(16a)" printed in the plot area). The output used to create Figure 16 and 17 are saved in the AppendixH/Figure16to17 folder as FigureX.eps, where X corresponds to the figure number and sub-figure letter. The MATLAB .fig versions of these figures are also saved in the Figure16to17 folder. The files Figure16.ai and Figure17.ai are saved in the Figure16to17 folder and can be viewed and edited in Adobe Illustrator and serve as a template for the creation of any other verification time series figures. The final edited figures are also saved as a 600-dpi compressed TIFF version (Figure16.tif.tar.gz and Figure17.tif.tar.gz).

Figure18, Figure19, Figure20, Figure21, Figure22, Figure23:

Figures 18-23 were created in Adobe Illustrator by combining the.eps versions of four figures created by executing AppendixD/ main_Exp_Figure_X.m, where X corresponds to the figure number (Described in section D.3). These four figure outputs are identified by text prints on the figure corresponding the sub-figure lettering scheme in Figures 18-23 (i.e. Figure 18a will have "(a)" printed in the plot area). The output used to create Figures 18-23 are saved in the AppendixH/FigureX folder as FigureXy.eps, where X corresponds to the given figure number and y corresponds to the sub-figure letter. The MATLAB .fig versions of these figures are also saved in their respecive folders, as well as a file FigureX.ai (X = figure number), which can be viewed and edited in Adobe Illustrator. The final edited figures are also saved as a 600-dpi compressed TIFF version (FigureX.tif.tar.gz).

Figure24 and **Figure25**:

Figures 24 and 25 were created in Adobe Illustrator by combining the.eps versions of eight bar plots, one for each experiment and each metric, created by executing AppendixD/ main_Exp_Figure_X.m, where X corresponds to the figure number (described in section D.3). Each of these bar plots contains the average of a given metric of each RI Class for the given experiment. The experiment of a given output can be identified by text prints on the figure corresponding to the experiment number (i.e. Experiment 0 will have a "0" printed in the plot area). The eight output figures used to create Figures 24 and 25 are saved in the AppendixH/FigureX folder as FigureXy_E.eps, where X corresponds to the given figure number (24 or 25), y corresponds to the sub-figure letter (a or b), and E corresponds to the experiment number (0-4). The MATLAB .fig versions of these figures are also saved in their respective folders, as well as a file FigureX.ai (X = figure number), which can be viewed and edited in Adobe Illustrator. In this .ai figures, the lower case and capital letters, denoting significant differences, were manually printed and referenced from the results shown in Tables 10, 11, 14, and 15. The final edited figures are also saved as a 600-dpi compressed TIFF version (FigureX.tif.tar.gz).